2015

Synthesis, Characterization, and Evaluation of Small Molecule-based Fluorogenic Probes for the Detection of Cellular Thiols

Rasika Ranatunga Nawimanage
Louisiana State University and Agricultural and Mechanical College, rranat1@tigers.lsu.edu

SYNTHESIS, CHARACTERIZATION, AND EVALUATION OF SMALL MOLECULE-BASED FLUOROGENIC PROBES FOR THE DETECTION OF CELLULAR THIOLS

A Dissertation

Submitted to the Graduate Faculty of the
Louisiana State University and
Agricultural and Mechanical College
in partial fulfillment of the
requirements for the degree of
Doctor of Philosophy

in

The Department of Chemistry

by
Rasika Ranatunga Nawimanage
B.S., University of Colombo, 2008
May 2015

This dissertation is dedicated

to the memory of my grandfather Daniel Ranatunga

who listened, believed, and taught me to be strong

and

with love to my family

my husband Suraj U Hettiarachchi

my beautiful son Nivain….!

ACKNOWLEDGEMENTS

It is my immense pleasure to offer my heartfelt gratitude for all who have supported, encouraged and guided me over the past five years during my doctoral studies and during the completion of this dissertation.

First I would like to express my deepest appreciation to my research advisor, Professor Robin L. McCarley. Without his guidance and persistent help this dissertation would not have been possible. I consider it as a great honor to complete my doctoral studies under your guidance. Your advices on both research as well as building up my future career have been invaluable.

I would also like to thank Dr. Andrew Maverick, Dr. Carol M. Taylor, Dr. Justin Ragains, and my Dean's representative Dr. Terry Bricker for your brilliant comments and suggestions, and valuable time taken to serve on my advisory committee.

Also, a special thank goes to all the wonderful group of scientists both past and present in the McCarley group and especial thanks goes to Bijeta Prasai for helping with cellular studies. I cannot imagine a better collection of people with such willingness to give a helping hand whenever needed.

I would also like to express my gratitude to the Department of Chemistry at LSU and special thank goes out to Dr. Connie David for her prompt support in mass spectrometry efforts, Dr. Frank R. Fronczek for the crystallographic data and Dr. Thomas Weldgheorghis and late Dr. W. Dale Treleaven for their NMR training and expertise.

I also like to extend my deepest gratitude to my parents, my two sisters and my brother for their love, support and sacrifices they made on behalf of me. I love you all so much and would not have made it this far without having you all by my side. I express all my gratitude and love to my husband Suraj for all support and understanding throughout this time. Thank you for the multiple roles you played in my life as my best friend, husband, lab mate and above all, a wonderful dad. Without you in my side most of these things would not have been possible.

Last but not least I like to thank my son Nivain, the little wonder of my life. You have made the biggest impact on my life. I would ask for nothing else in life but to share each and every moment I can with you. Giving you a better life has always been my motivation to work hard. Although you are only 2 years old when I write this, you mean world to me. Mommy loves you more than words can express that I offer you in this dissertation.

TABLE OF CONTENTS

LIST OF ABBREVIATIONS AND SYMBOLS

Ac_2O	Acetic anhydride
AcCN	Acetonitrile
AcOH	Acetic acid
ATP	Adenosine Triphosphate
BSA	Bovine serum albumin
Cys	Cysteine
CV	Cyclic voltammetry
^{13}C NMR	Carbon 13 Nuclear magnetic resonance
d	Doublet
DBTL	Dibutyl tin dilaurate
DCM	Dicyanomethylene-4*H*-pyran
DIC	Differential interference contrast
DIEA	*N*,*N*-Di-isopropylethylamine
DMF	Dimethylformamide
DMSO	Dimethyl sulfoxide
DT	Sodium dithionite
ESI-TOF	Electrospray ionization–time-of-flight
EtOAc	Ethyl acetate
EtOH	Ethanol
FBS	Fetal bovine serum
GSH	Glutathione
GC	Gas chromatography

Hcy	Homocysteine
Hex	*n*-Hexane
HPLC	High-performance liquid chromatography
HMTA	Hexamethylenetetramine
hNQO1	Human NAD(P)H:quinone oxidoreductase-1
^{1}H NMR	Proton nuclear magnetic resonance
ICT	Internal charge transfer
*i*PrOH	Isopropanol
J	Coupling constant
k_{cat}	Catalytic constant
k_{cat}/K_m	Enzyme catalytic efficiency
K_m	Michalis constant; substrate affinity
LOD	Limit of detection
LOQ	Limit of quantification
m/z	Mass-to-charge ratio
MeOH	Methanol
NADH	Reduced nicotinamide adenine dinucleotide
NADPH	Reduced nicotinamide adenine dinucleotide phosphate
NEM	*N*-ethylmaleimide
NIR	Near-infrared
OeT	Oxidative electron transfer
PBS	Phosphate-buffered saline
PeT	Photo-induced electron transfer

ppm	Parts per million
q	Quartet
QD	Quantum dot
ReT	Reductive electron transfer
RFU	Relative fluorescence unit
ROS	Reactive-oxygen species
RNS	Reactive-nitrogen species
RT	Room temperature
SBR	Signal-to-background ratio
SHE	Standard hydrogen electrode
SOD	Super oxide dismutase
t	Triplet
TBAF	Tetrabutylammonium fluoride
Trx	Thiredoxin enzyme
THF	Tetrahydrofuran
TLC	Thin-layer chromatography
V_{max}	Maximum theoretical turnover rate

ABSTRACT

Fluorescence methods for disease diagnosis and detection of important analytes are becoming popular route as a technique, as they offer a simple non-invasive approach. Recently, many novel fluorophores and probes have been reported for selectively and sensitively detecting low abundance biological species in disease pathways.

Biological thiols, such as glutathione, cysteine, and homocysteine, along with the smallest member hydrogen sulfide, are key thiol analytes in biological environments, and they play a vital role in living systems by maintaining the redox homeostasis of cells. Alteration of their ratios can cause cellular dysfunction and cell death. Furthermore, thiol levels in cells and biological fluids act as biomarkers of several diseases, including neurodegenerative disorders, liver disease, cystic fibrosis, pulmonary and cardiovascular diseases, and Alzheimer's disease. Thus, the development of efficacious methods for detection and quantification of biological thiols has received significant attention in recent years. Although many traditional thiol detection methods are available, fluorescent methods hold more promise for simple, non-invasive detection with simple instrumentation.

The work presented in this dissertation discusses the successful fluorescent detection of biologically important thiols with two probes HMBQ-Nap 1 and DCM-Cys. The HMBQ-Nap 1 probe consists of a hydroxymethyl benzoquinone trigger group (HMBQ) and 4-amino-9-(*n*-butyl)-1,8-naphthalimide (Nap 2) as the reporter dye. This probe led to excellent class selective detection of the free thiols glutathione, cysteine, and homocysteine versus other analytes found in the body. The second probe, DCM-Cys, is composed of a cysteine-selective acrylate moiety attached to dicyanomethylene-4*H*-pyran (DCM) reporter dye via a benzyl alcohol linker. DCM-Cys exhibited a remarkable ability to detect free cysteine in media versus other thiols and various potent analytes found in biological environments. Both HMBQ-Nap 1 and DCM-Cys offer nM in vitro detection, and successful in cyto imaging of thiols. Selectivity, a relative low limit of detection (nM), the ability to function under physiological conditions and a high signal-to-background ratio of these methods as well as low thiol-to-probe ratios for the qualitative and quantitative detection, and relatively short response time make these probes excellent systems for thiol analysis.

CHAPTER 1
INTRODUCTION

1.1 Research Goal and Aims

Precise understanding and monitoring of the molecular causes, effect, and signature of a disease are essential for increasing the advancement of modern medicine. Personalized treatments directed at highly specific disease sub-states now influence insight into the molecular origin and signature of these disorders.[1] The ever-growing demand on advanced treatment options puts more burden on the development of advanced, easy-to-operate early diagnostic techniques. The objective of small molecule-based reporter systems is to assist specific detection of biochemical signatures in living cells or organisms with minimal interruption to native physiological processes. The expression levels of target molecules, such as a protein receptor or the activity of a disease-related specific analyte, or in other words "biomarkers", can be used diagnostically to give information about a disease state, such as disease staging or predicting responses to specific therapies.[2] Small molecule-based fluorescent reporters such as thiol detecting agents, possess superior advantages over other traditional methods in that they facilitate non-invasive live cell detection and provide cost-effective simple instrumentation. Therefore, the main goal of my research is to build a reliable set of small-molecule fluorescent probe systems that can detect and quantify cellular thiols in vivo and in cyto with a relative short analysis time.

In living systems, thiols are found as cysteine and derived molecules of cysteine possessing low and high molecular weights. Specifically they can be divided into two main categories: protein-based thiols with high molecular weights and small molecular weight non protein thiols.[3] There is a growing interest in the importance of thiol physiology, and in the number of physiological functions involved these small but crucial molecules. Given their effective redox capabilities, and their high intracellular concentration and prevalent distribution, the role of thiols as a potent defense agent against oxidative and electrophilic stress is well established.[4] *γ-L*-glutamyl-*L*-cysteinylglycine (glutathione or GSH), cysteine (Cys) and homocysteine (Hcy) are the main non-protein thiols found in the body. In proteins, cysteine accounts for 3% or less of the its amino acid composition, and cysteine is responsible for almost all the protein thiols found in mammalian cells.[4]

The main thiol/disulfide couples in cells are glutathione/glutathione disulfide (GSH/GSSG), cysteine/cystine (Cys/CySS), and the thioredoxins (Trx) enzyme systems. Out of these, GSH is the most abundant non-protein thiol present in all mammalian tissues at 1–10 mM concentrations intra-cellularly, and it acts as the main defense against oxidative stress. In addition, GSH plays a key role in many other regulatory pathways, including cellular proliferation and apoptosis, and the post-transcriptional modification of proteins through *S*-glutathionylation.[5] Furthermore GSH's are also important in the detoxification of hydroperoxides and diverse xenobiotic compounds.[5] Also, GSH has been proven to be vital to mitochondrial function and maintenance of mitochondrial DNA and may be relevant to DNA methylation.[6] Given the diverse roles of GSH in cellular physiology, the clinical importance of altered glutathione homeostasis is gaining significant attention. GSH homeostasis variations have been implicated in neurodegenerative disorders, liver disease, cystic fibrosis, pulmonary and cardiovascular diseases, as well as chronic age-related disorders such as Alzheimer's disease.[6] On the other hand, homocysteine and cysteine are both precursors of glutathione, and they play a crucial physiological role in the body. Bioavailability of cysteine limits the rate of GSH synthesis in cells.[6] Abnormal levels of Cys are associated with many diseases, including slow growth, hair depigmentation, skin lesions,[7] and cystinuria, the latter being a common heritable disorder of amino acid transport.[8] Moreover, the cysteine residue plays a major role in protein functionality in cells, although it is one of the least abundant amino acids incorporated into proteins in many organisms. It is found to concentrate in functionally important positions of protein backbones, such as the active site of enzymes.[9] Importantly, redox-active enzymes, such as thioredoxins (Trx), have catalytic activities that depend on the reactivity of the Cys residue in their active site. Homocysteine, on the other hand, is a well-known risk factor for atherosclerosis and premature cardiovascular diseases, birth defects, and hyperhomocysteinemia.[7-8]

Given the importance of small molecule-based reporter systems, the first aim of this research is to invent the properties of novel redox active moiety—hydroxymethyl benzoquinone (HMBQ) as potential trigger for targeted delivery of molecules. The kinetics of quinone methide formation by HMBQ and self-immolation ability of the attached probe releasing the reporter was investigated using absorption and NMR spectroscopies. As the next aim of this project, two different fluorescent probes were synthesized and characterized to selectively detect and quantify non protein cellular thiols. In Figure 1.1 it shows the basic design strategy of the thiol-reporter

system. It basically consists of a reporter dye whose fluorescence is quenched by thiol-reactive moiety that is attached to the reporter dye. Upon reacting the thiol-targeted trigger group (reactive moiety) with thiols, chemical alteration of the thiol-reactive moiety causes unmasking of the fluorescence, giving rise to a bright reporter signal. The fluorophore choices for the thiol reporter systems were 4-amino-9-(*n*-butyl)-1,8-naphthalimide and dicyanomethylene-4*H*-pyran due to their excellent photo-physical properties. The first probe I synthesized contains 4-amino-9-(*n*-butyl)-1,8-naphthalimide reporter (Nap 2) attached to a hydroxymethyl benzoquinone (HMBQ) trigger group, which is a potential reactive site for thiols. The 4-amino-1,8-napthalimide and its derivatives are conventional fluorescent dyes used in fiber materials and polymers, and they have recently become well-known in the development of biological sensing and imaging probes.[10] They have interesting optical properties, such as strong absorption and emission in the visible region (green), and large Stokes shifts (difference in absorption and emission energies). Their fluorescence can be modulated through intramolecular charge transfer (ICT) events. The latter feature is important for the design of the probe in my work. [11] As a result of the ICT nature of the dye once the HMBQ trigger group is attached, the thiol probe should have its fluorescence completely quenched.

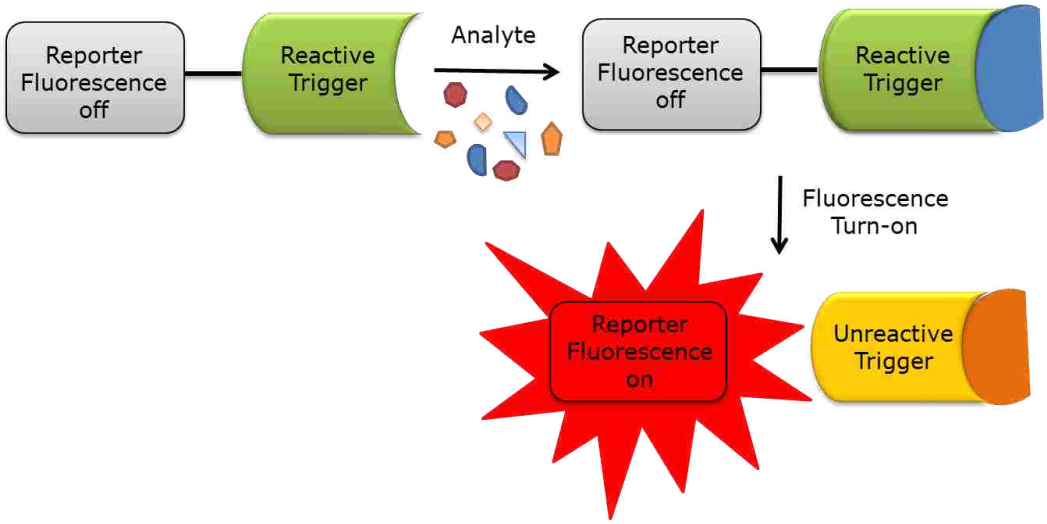

Figure 1.1 Schematic representation of the basic concept of thiol detection with a triggarable probe.

The next probe I synthesized has a dicyanomethylene-4*H*-pyran (DCM) as the reporter fluorophore. Similar to Nap, DCM is also an ICT dye with remarkably large Stoke shift (> 100

nm). Therefore, once attached to the potential reactive site, the initial fluorescence will be altered. Unmasking of the fluorescence will happen only with the elimination of the reactive moiety, thereby resulting in a lower background signal. DCM also has good fluorescence brightness, with its emission in the red region, and it also has a very high photostability in comparison to other NIR dyes that are being used in the literature.[12-13] The cysteine selective probe has a DCM dye attached to an acrylate moiety via a short benzyl alcohol spacer. The probe is designed to utilize both the sulfhydryl group and the amine group of Cys in a nucleophilic addition and subsequent cyclization reactions. Upon cyclization, the benzyl alcohol linker undergoes elimination, leading to release of the reporter dye DCM.[14]

The second aim of this project is characterization of the optical properties of each of the probes synthesized and determination of the effectiveness of these probes to act as potential thiol sensors. The quantum yields of the free reporters and probes are determined in order to assess the efficiency of PeT quenching. To determine the quantum yield of the free dye and the probe, the fluorescence signal was compared to known standards. To check the thiol sensing ability of these probes, solution-phase, fluorescence-based analysis with each thiol was conducted. For the quantitative determination of thiols, the necessary calibration curves were constructed. To determine the potential cross reactivity with other analytes, the fluorescence change of the probes were tested in the presence of excess of other commonly found interferrents (e.g. NADH, amino acids, ascorbic acid, enzymes, etc.). The solution-phase stability of these probes were also tested by incubating aqueous solutions of theses probes at 25 $^{\circ}$C/ 37 $^{\circ}$C. Finally, in order to produce evidence for the elimination mechanisms, NMR kinetic experiments and mass spectral data after reacting with each of the corresponding analytes was examined.

The ultimate objective of this research is the determination of the capability of these probes to detect thiol levels in cellular media. To achieve this objective, suitable cancer cell lines with up-regulated thiol levels were incubated with each probe, and probe ability to image these cells were determined using confocal microscopy. As a control experiment, thiols in the cells were scavenged by incubating the cells with a known thiol capturing agent *N*-ethylmaleimide, then the fluorescence change was monitored by incubating these cells with the corresponding thiol probe.

The collective information obtained through this work demonstrates the potential ability of two novel fluorescent probes to detect thiols in a cellular environment, with high selectivity and sensitivity. In the long run, I believe that these two probes will diversify the pool of growing

research aimed at developing new methods, probes, and tools to image specific molecular targets that can act as biomarkers of disease conditions in the body.

1.2 Biosynthesis of Glutathione and the Metabolic Relationship with Other Thiols

Methionine (Met) and cysteine (Cys) are the main precursors for the synthesis of glutathione (GSH) in the body (Figure 1.2).[15] The first step involves converting methionine to an intermediate compound named as *S*-adenosylmethionine (AdoMet); a universal methyl donor in transmethylation reactions in the presence of adenosine triphosphate (ATP). This process is catalyzed by the enzyme methionine adenosyltransferase (MAT). The transfer of the methyl group from AdoMet by a variety of methyltransferases (MTs) yields the intermediate compound *S*-adenosylhomocysteine (AdoHcy) that is rapidly hydrolyzed to adenosine and homocysteine via the enzyme SAHH (*S*-adenosylhomocysteinehydrolase). The generation of Hcy is a critical juncture in the sulfur cycle, because it can either be methylated to regenerate methionine, or it yields cysteine and H_2S in the transsulfuration pathway. The transsulfuration pathway is composed of two enzymatic steps. In the first step, Hcy (Figure 1.2, compound 2) is condensed with serine to form cystathionine in a reaction catalyzed by cystathionine β-synthase (CBS). This is followed by the cleavage of cystathionine to α-ketobutyrate, ammonia, and cysteine (Figure 1.2, compound 1) in a reaction catalyzed by γ-cystathionase (CSE). In mammalian tissues, the transsulfuration pathway is irreversible, and as a result, Cys cannot be converted back to methionine. Finally, GSH (Figure 1.2, compound 3) is synthesized from cysteine in two ATP-dependent enzymatic steps.

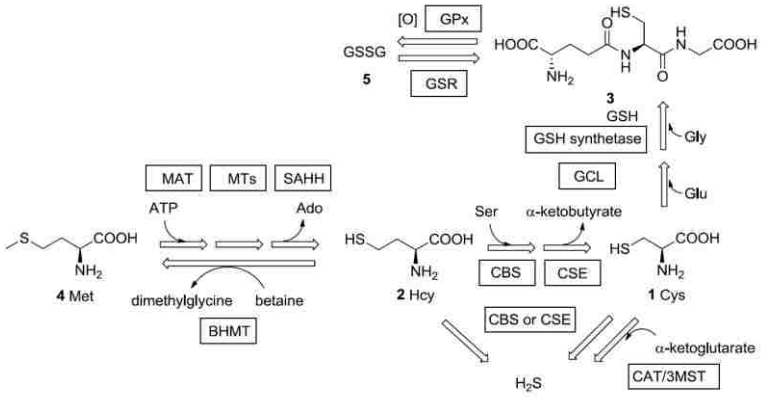

Figure 1.2 Schematic representation of GSH biosynthesis and the metabolic relationships of sulfur analytes in the GSH biosynthesis pathway.[4]

In the first step, γ-glutamylcysteine is produced from glutamate and cysteine, catalysed by the enzyme γ-glutamate-cysteine ligase (GCL), this is considered to be the rate-limiting step in GSH synthesis. In the final step, GSH is produced by combining γ-glutamylcysteine and glycine in a reaction catalyzed by the enzyme GSH synthetase. The reactivity of GCL is subject to feedback inhibition by GSH which controls the bioavailability of GSH.[16-20]

1.3 Antioxidant Function and Redox Signaling of GSH

1.3.1 Reactive-oxygen and Reactive-nitrogen Species (ROS/RNS)

ROS and RNS are often small molecules responsible for mediating redox modifications of various biomolecules, and thus they play a lead role in many diseases, including cancer, neurodegenerative diseases, and diabetes.[21] The overproduction and/or mismanagement of ROS in cells lead to the general phenomenon of oxidative stress that is implicated in many diseases. Superoxide ($[O_2]^{-\cdot}$), hydrogen peroxide (H_2O_2), hypochlorous acid (HOCl), singlet oxygen ($^1O_2$), lipid peroxides (ROOH), ozone (O_3), and hydroxyl radical ($[OH]^{\cdot}$) are some of the major ROS in living systems.[22] Although less common than ROS, reactive nitrogen species (RNS), such as nitric oxide ([NO]), are also important to human physiology. These RNS can react with ROS to form oxidants such as peroxynitrites ($ONOO^-$), known for their cytotoxic function.[22-24]

The organelles with localized ROS generation for physiology include phagosomes within specified cells of the immune system for killing pathogens and peroxisomes that mediate catabolic oxidation reactions for energy metabolism. In addition, the three other major locations for ROS generation are the mitochondria, endoplasmic reticulum (ER), and cell membranes.[22] The electron-transfer chain (ETC) in mitochondria results in electron transfer from NADH and succinate along a controlled redox path that results in the four-electron reduction of O_2 to H_2O during ATP synthesis. Nevertheless, the flow of electrons through the ETC is an imperfect process, and occasionally oxygen molecules undergo one or two-electron reduction reactions to form ROS, especially H_2O_2 and $[O_2]^{-\cdot}$ (Figure 1.3).[25] The major source of ROS from the ER results from oxidative protein folding. Folding proteins often undergo enzyme-catalyzed disulfide formation using O_2 as a two-electron acceptor to form one equivalent of H_2O_2 for each disulfide bond formed, creating a strong flux of ROS inside the ER. In addition, the ER can also house an isoform of NADPH oxidase (NOX4)[26-27] that generates H_2O_2 from O_2. Another source of ROS is cell membrane-localized NOX and their dual oxidase relatives (Duox), that are

localized in various cellular membranes.[22, 28] In order to keep these ROS/RNS below the toxic threshold and maintain a healthy environment inside cells, they implement an antioxidant defense mechanism. This is composed of two main systems that play a leading role, including GSH/GSSG thiol system and the Trx/TrxR enzyme system.[5, 9]

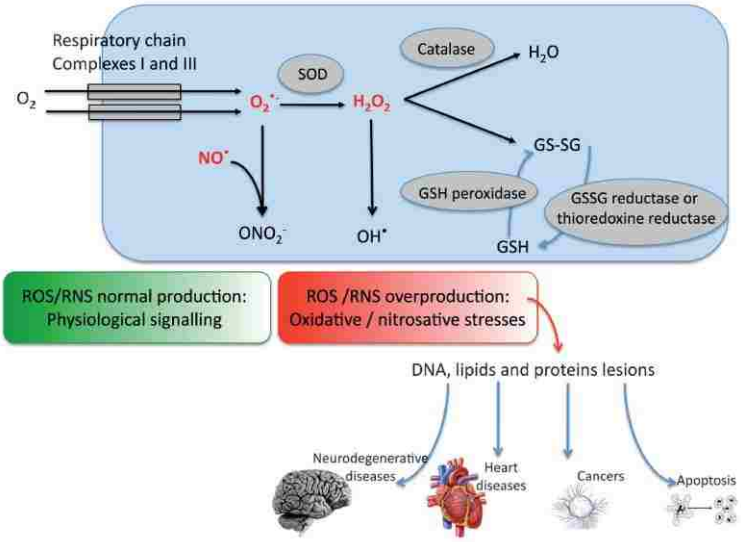

Figure 1.3 Generation of ROS and RNS during the mitochondrial respiratory chain and their physiological effect in normal and pathological conditions.[25]

1.3.2 Antioxidant Function of GSH

The antioxidant function of GSH is facilitated by GSH peroxidase (GPx)-catalyzed reactions. As a result, hydrogen peroxide radicals and lipid peroxides are reduced, while GSH is oxidized to GSSG (Figure 1.4). Then the oxidized GSSG, in turn, is reduced back to GSH by GSSG reductase through NADPH consumption to make $NADP^+$. This mechanism is particularly important in the mitochondria as a defense against both physiologically– and pathologically–generated oxidative stress.[29-31]

The GSH to GSSG ratio largely determines the intracellular redox potential (proportional to the log of $[GSH]^2/[GSSG]$). Therefore to prevent a major shift in the redox equilibrium when oxidative stress overcomes the ability of the cell to reduce GSSG back to GSH, the GSSG can be actively exported out of the cell or react with a protein sulfhydryl group, leading to the formation of a mixed disulfide. Hence, severe oxidative stress depletes cellular GSH as it oxidized to GSSG (Figure 1.4).[3, 5]

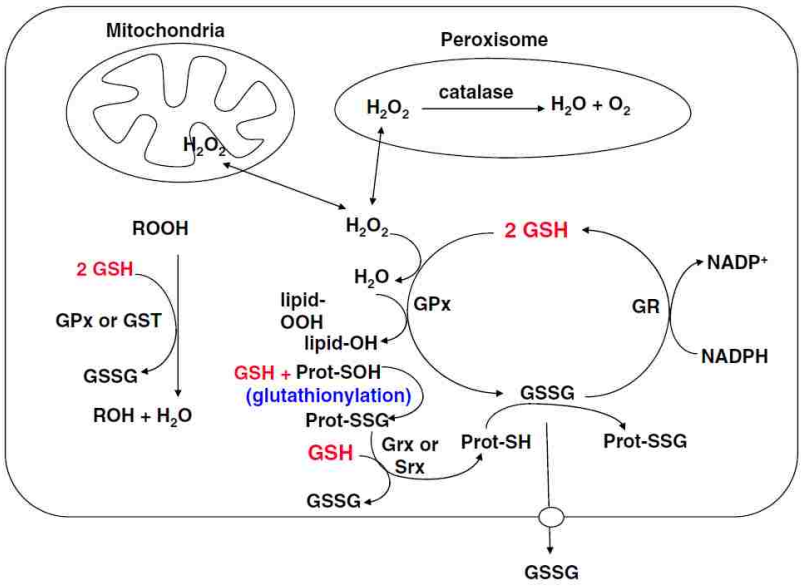

Figure 1.4 Antioxidant and redox signaling function of GSH inside the cell.[5]

1.3.3 Role of GSH for Redox Signaling in Cells

The effect of reactive species (e.g. ROS or RNS) can range from cellular damage to subtle effects on cell metabolism, morphology, or signaling pathways. Especially at lower concentrations, these reactive species act more as function regulators than damaging species. The overall impact of a reactive species on a cellular function varies greatly with the type of reactive species, cell type, level of endogenous antioxidant, or antioxidant enzymes present, as well as extracellular environment.[32] For example, reactive species, such as NO and H_2O_2, are known to activate several transcription factors and protein kinases. As shown in Figure 1.4 GSH regulates redox-dependent cell signaling. [33-34] GSH can reversibly bind to the free –SH groups of protein cysteinyl residues (Prot-SH) by a process called glutathionylation, generating glutathionylated proteins (Prot-SSG). This process can either activate or inactivate the corresponding protein, which can be responsible for several downstream processes in cells. These cellular proteins that are constantly undergoing thiol modification are an important part of cellular housekeeping, and they are involved in key cellular signaling cascades.[35] Also, these mechanisms protect sensitive protein thiols from irreversible oxidation and also serve to prevent depletion of GSH under oxidative conditions.[32] Once the cellular conditions are back to normal deglutathionylation can occur through glutaredoxin and sulfredoxin enzyme-catalyzed reactions using GSH as a reductant. As mentioned earlier, many transcription factors and signaling

proteins have critical cysteine residues that can be oxidized by ROS and RNS. These reactive species regulate protein function and cell signaling that can be modulated by GSH.[5, 35-36]

1.4 Functional Role of Cysteine in Biological Systems

In addition to free cysteine being a crucial intermediate in GSH biosynthesis, and the regulation of redox function in cells and disease biomarkers, protein-bound cysteines also play a diverse and yet prominent role in the body. As shown in Figure 1.5, cysteines contribute to the regulatory activity of several protein kinases, by forming structural disulfides, acting as nucleophilic catalysts, and binding to metal ions in detoxifications as well as structural stabilization of the proteins.[9, 37-38]

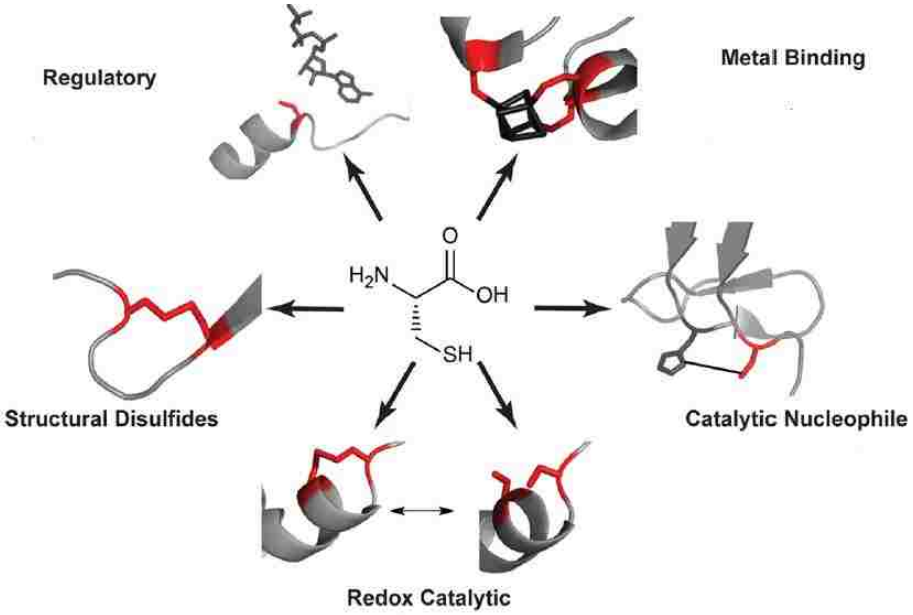

Figure 1.5 Diverse role of protein-bound cysteine in biological systems.[9]

The anionic thiolate form of cysteine acts as a ligand and binds strongly to several metal ions, including $Fe^{2+/3+}$, Zn^{2+}, Cd^{2+} and Cu^{+}. Due to its ability to adopt a wide range of oxidation states (−2 to +6),[9] sulfur is able to accommodate a large number of bonds and geometries, leading to a very diverse set of metal-protein complexes.[23] These metal-bound cysteines are generally unreactive, as the cysteine is tightly coordinated to the metal, but they are usually reactive in the unbound state in the protein. This has been utilized as a regulatory pathway of

enzyme activity. As another function, cysteines are involved in regulatory activity of catalytic reactions. However, regulatory cysteines are not directly involved in catalysis, due to their proximity to the active site or surfaces involved in essential protein-protein interactions. Moreover Cys-containing proteins can act as redox catalytic enzymes, and they are called oxidoreductases. Thioredoxin, a typical member of the thiol oxidoreductase family plays a vast role in conjunction with GSH, to maintain the redox balance in cells. As shown in Figure 1.6, the thioredoxin system is composed of thioredoxin (Trx) together with thioredoxin reductase (TrxR) and NADPH. The active site of human Trx contains two cysteine residues at positions 32 and 35, and it acts as the hub for many redox catalysis reactions. Upon reduction of a disulfide bond in a substrate protein, the two redox-active cysteines in Trx undergo reversible oxidation to form an intramolecular disulfide bond. When TrX is oxidized, it is then recycled to the reduced state through the simultaneous action of TrxR and NADPH (Figure 1.6).[9]

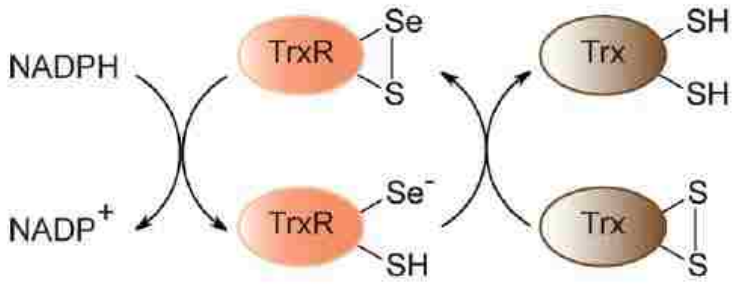

Figure 1.6 Thioredoxin (Trx)/Thioredoxin reductase (TrxR) system in redox modulation.[9]

Not only the Trx/TrxR system, but many enzyme active sites contain cysteine residues that serve as catalytic nucleophiles. This is mainly due to the reversible oxidation, and reduction ability of these motifs; however, the overall oxidation state of these units remains unchanged during the catalytic cycle. Most of these cysteine residues tend to be highly conserved across related species, and they are found in a variety of enzyme classes.[9, 23]

1.5 Functional role of H_2S in Biological System

1.5.1 Gasotransmitters in Cells

Gasotransmitters are important gaseous small molecules synthesized in cells that are involved in regulating physiological functions and cellular signaling. Among them—NO, CO,

and H_2S—are the most important known gasotransmitters, and they have attracted a great amount of research interest.[39] However, it is important to note, that until very recently, these molecules were known only as toxic molecules or environmental pollutants until their physiological and pathological role was revealed. Gasotransmitters have inverted the traditional concept of intercellular communication. For instance, unlike other signaling molecules, gaseous substances are not readily stored in vesicular structures or cells, and they must necessarily be synthesized as needed. [40]. Instead of binding to plasma membrane receptors these gaseous molecules are cell membrane-permeable; therefore they diffuse freely through the plasma membrane to adjacent cells and interact with their targets.[40]

1.5.2 Gasotransmitter Characteristics

Nitric Oxide (NO)—NO was first identified as a mediator of two processes: i) relaxation of blood vessels and macrophages and ii) activation of anti-inflammatory responses. Macrophages that elicited tumorcidal and bactericidal activities involved a production of NO inside the cells. The reaction of NO with superoxide generates peroxynitrites that kill bacteria and tumor cells.[40] The second most important function is relaxation of blood vessels, involving activation of the secondary messenger cGMP. NO activates the cGMP by forming an enzyme guanylcyclase by binding to iron in the active site of the enzyme. In a similar fashion, NO also activates several mitochondrial heme proteins and may also interfere with cellular energetics. NO also serves as an intermediate in several other functions, *S*-nitrosylation of cysteine residues in proteins, and modification of several ion channels.[40]

Carbon monoxide (CO)—CO is a colorless and odorless gas and is typically produced in nature when carbon-containing compounds are only partially oxidized.[41] The major source of CO in the body is from the breakdown of heme by the enzyme hemeoxygenase. At high concentrations, CO is toxic to animals, as it binds to hemoglobin about 200-times more strongly than O_2, and the resulting carboxyhemoglobin is no longer available for oxygen transport.[41] Despite the toxicity at even lower concentrations, CO also has a similar reactivity as NO. CO plays an important role as a cell signaling molecule and neurotransmitter, hormone release, also as a cytoprotective agent, and in the regulation of vascular tone.[42-43] CO is involved in several important anti-inflammatory pathways by upregulating anti-inflammatory cytokines, and it prevents arteriosclerotic lesions by inhibiting smooth muscle cell proliferation. [44-45]

Hydrogen Sulfide (H_2S)—H_2S is the most recently identified high-valued major gasotransmitter, and it joins CO and NO as important signaling molecules in the body. Similar to CO and NO, at high concentrations H_2S is toxic; about five times more than CO.[46] Though only recently recognized as being formed under physiological conditions in mammalian cells, H_2S has been known to exist in animal tissues for many years. H_2S is also known as the smallest member of the thiol family, and it is produced as a byproduct of glutathione synthesis.[47] Being the smallest member of the thiol family, the importance of H_2S and its physiological role will be briefly discussed below.

1.6 H_2S Metabolism in Cells

As shown in Figure 1.7, the major sources of H_2S are from cysteine via the GSH metabolism pathway, methionine and dietary cysteine/cystines. These precursor molecules enter cells via specific transporters and go through a biochemical pathway that leads to the synthesis of H_2S as a byproduct.

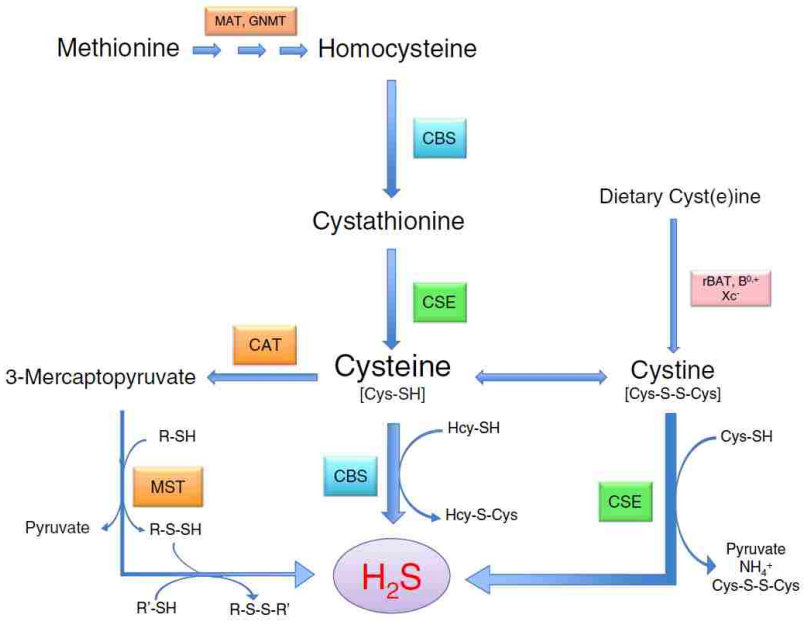

Figure 1.7 Pathways of H_2S metabolism. Cysteine metabolism from methionine, and dietary cyst (e)ine that enter cells via transporters, leads to H_2S production.[47]

H_2S is basically derived from three main sulfur sources in the pathway. This includes cysteine, cystine, and 3-mercaptopyruvate. The enzyme 3-mercaptopyruvate sulfurtransferase

(Figure 1.7, MST) and 2-cysteine aminotransferase (Figure 1.7, CAT) produce H_2S from 3MP. One of the two important H_2S enzymes—cystathionine-β-synthase (Figure 1.7, CBS) catalyzes the β-replacement of cysteine with homocysteine (Hcy) to generate H_2S and the corresponding thiol ether (Hcy-S-Cys). A second enzyme cystathionine-γ-lyase (Figure 1.7, CSE), catalyzes β-disulfide elimination on cystine, the product of this reaction reacts with available thiols (e.g. Cys) to generate H_2S and a disulfide.[47-48]

1.7 Functional Role of H_2S in Cells

1.7.1 H_2S as a Signaling Molecule

H_2S participates in cellular signaling pathways[49] by modifying proteins through a process called protein persulfidation.[50-52] Due to the strong nucleophilic properties of H_2S, persulfidation can occur by direct nucleophilic attack of the sulfide anion on an oxidized cysteine. Depending on the type of protein and the site where it is persulfidated, the activity of proteins is up regulated or down regulated. For example, persulfidation of the active site cysteine in protein tyrosine phosphatase inhibits its activity, resulting in a buildup of phosphorylating endoplasmic reticulum kinases, which enhance the cellular response to endoplasmic reticulum (ER) stress.[53] Persulfidation of ATP-sensitive potassium channels results in channel opening and hyperpolarization of endothelial smooth muscle cells, leading to vasodilation.[16, 46, 54] Sulfhydration of various electrophiles, including 8-nitro-cyclic GMP (nitro derivatives of unsaturated fatty acids and cyclopentenone prostaglandin) provides an additional molecular mechanism for H_2S signaling. Another mechanism for H_2S-mediated signaling is through its interactions with metal centers in the active sites of proteins. Depending on the stereo electronic characteristics of these centers, H_2S can be reduced or it will coordinate to the metal and modify the activity of the protein.

1.7.2 Physiological Effect of H_2S

H_2S shows its effect on several important sites in the body, including the cardiovascular system, central nervous system (CNS), and endoplasmic reticulum (ER) of cells, and it also plays a role in anti-inflammatory action, as shown in Figure 1.8.[48] Similar to other members of the gasotransmitter family, H_2S also dilates blood vessels in the body. H_2S vasodilation largely depends on hyperpolarization elicited by opening ATP-sensitive potassium channels (K_{ATP}).[42]

Due to the promising cardiovascular action of H_2S, a variety of drugs have been developed based on this gasotransmitter. Some are simple H_2S donors, although some structures are combined with anti-inflammatory drugs or classic vasodilators.[49] H_2S can affect the synaptic potential and concentration of neurotransmitters, like epinephrine, norepinephrine, and serotonin in the central nervous system.[55] In particular, H_2S can act as a neuro protectant in the central nervous system by increasing production of GSH and suppressing mitochondrial oxidative stress.[16] The beneficial effect of H_2S on the ER is alleviating the stress response[56-57] induced during the special protein folding taking place in ER. H_2S inhibits specific protein kinases that govern this process, by changing the oxidative potential in the ER lumen.[53, 58] The anti-inflammatory influences of H_2S have led to discoveries of new therapeutic agents. Classic non-steroidal anti-inflammatory drugs (NSAIDs) often cause gastric irritation in patients by inhibiting prostaglandin formation, which is the cyto-protectant of gastric mucosa.[47] H_2S reduces mucosal inflammation and protects the gastrointestinal mucosa from injury and also enhances tissue repair.[59-60] Upon comparison of naproxen and its H_2S-linked derivative, the latter exhibits comparable therapeutic efficacy with reduced gastric damage;[61-62] similarly, several other NSAIDs have also been combined with H_2S donors to improve therapeutic effects.[62]

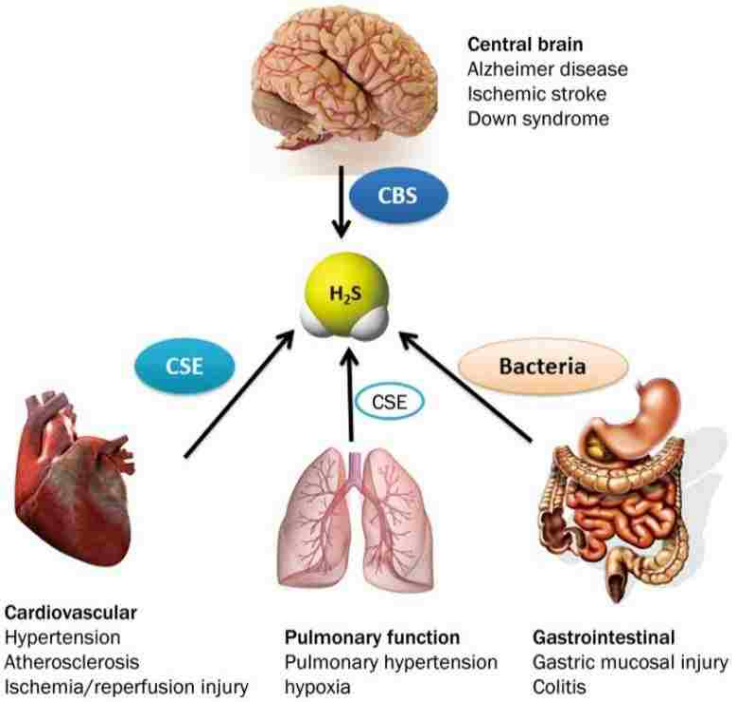

Figure 1.8 Involvement of H_2S in various physiological and pathological functions.[48]

1.8 Fluorescence Technologies for Biochemical Sensing

The platform is diverse for molecular imaging capabilities available via small molecules, fluorescence proteins, and polymeric nanoparticles for the detection of low-abundance biomarkers of a disease pathway.[63] The effort continues toward improving traditional imaging and detecting technologies in order to obtain advanced capacity for rapid identification of chronic conditions that require continuous monitoring. Molecules functionalized with fluorescence moieties remain one of the best methods for analyte detection due to their simple architecture. As shown in Figure 1.9, molecules including glycosides, peptides, aptamers, antibodies and nanoparticles bound to fluorescent dyes can be used to design "smart probes".[64] Each of these diagnostic techniques has their own specific application and specific design that are promising for clinical and biomedical applications; hence, a short description of each of the methods follows below.

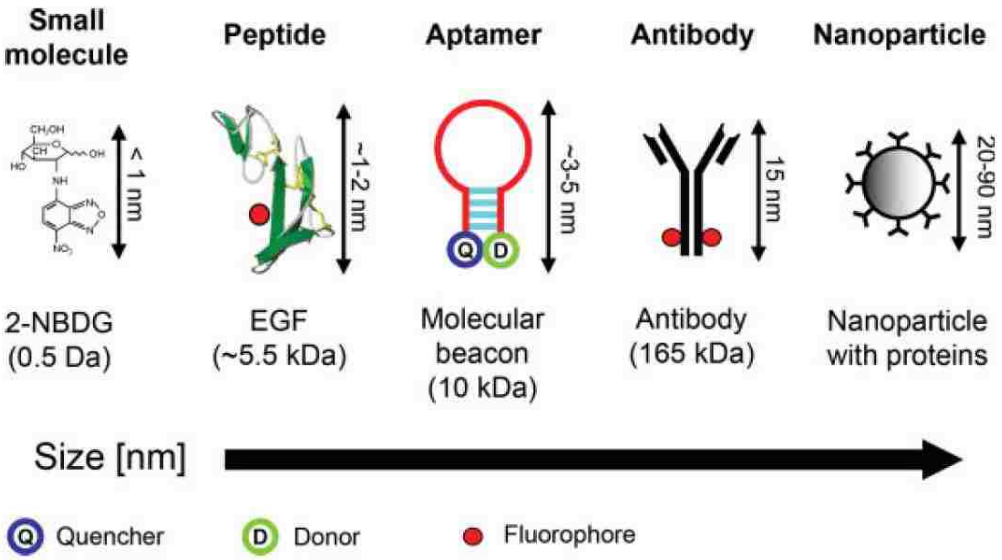

Figure 1.9 Five classes of molecular-specific optical contrast agents in the order of increasing size.[64]

1.8.1 Peptide and Protein Based Fluorescence Sensing

Peptides are particularly useful as surrogates of whole proteins, especially when site-specific modification of or purification of a particular protein is impractical. Peptides are small enough to be easily manipulated on the bench top using standard laboratory protocols and solid-phase techniques.[65] The polymeric nature of peptides facilitates the ability to add a select amino acid

sequence with high affinity for a particular target. Peptide scaffolds, being intrinsically modular, allow for the introduction of multiple fluorophores into their backbone while they retain the same or virtually the same biological activity.[66] A wide variety of sensors, such as proteins and enzyme sensors, ion sensors and nucleic acid sensors, have been developed using peptide scaffolds. An interesting approach to detect HIV antibodies using the peptide beacon (PB) concept has been reported by Plaxco[67] and coworkers. They attached a ruthenium(II) *bis*pyridine-phenanthroline to one end of the peptide as a fluorophore and methyl viologen as a quencher to the other end. Similar to any unbound, unstructured polypeptide, the two labelled ends collided with each other leading to quenching of the Ru(II) fluorophore. However when it is bound to its target antibody, the peptide epitope adopts a rigid extended conformation. Due to this binding-induced segregation of fluorophore and the quencher, the possibility of electron transfer is decreased, leading to a 6-fold fluorescence enhancement that allows for the detection of the targeted antibody (Figure 1.10).[67]

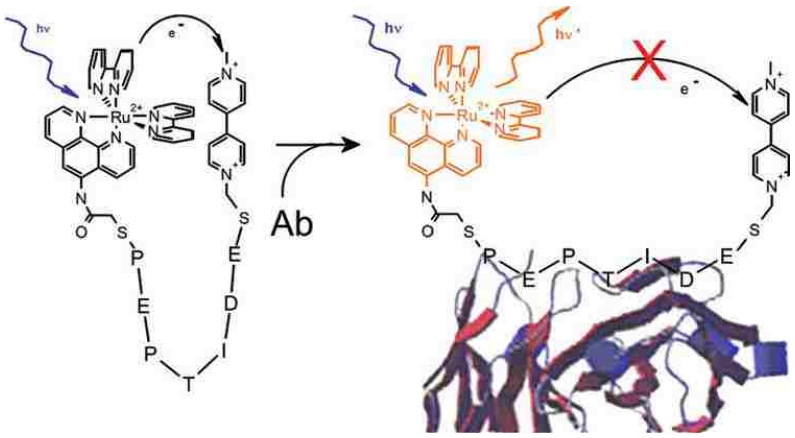

Figure 1.10 Schematic of PB architecture comprises a long-lived fluorophore, an electron accepting quencher, and a recognition peptide.[67]

As a another peptide-based strategy; to detect collagenase protease activity in cells, Mattoussi et al. connected quantum dots and a rhodamine dye by a short tetrapeptide that can be cleaved by the effects of collagenase, giving rise to a different fluorescent output.[68] This probe showed remarkable selectivity towards the collagen protease versus other proteolytic enzymes, such as thrombin, and chymotrypsin. Zhang's group has used peptides modified with the NBD (7-nitrobenz-2-oxa-1,3-diazol-4-yl) fluorogenic unit at the *N*-terminus to determine the natural

binding location of a transcription factor (GCN4).[69] Peptides can also be used as ion sensors; Nitz and coworkers have used the 6-methoxyquinolinium fluorophore to detect chloride ions in their cellular assays.[70] Certain disadvantages of peptide probes are difficulty in cell internalization, sensitivity toward vast amounts of proteases present in cells, and the need for longer sequences to fold into stable three-dimensional structures limit their use in analyte detecting probes.[66]

The discovery of proteins with strong visual fluorescence ("Fluorescent protein", FP)[71-72] have revolutionized protein labelling and in vivo detection. FPs are naturally occurring in marine coelenterates, such as jelly fish and corals.[71] The advantage of FPs for molecular imaging is, that cells can be forced to express the gene encoding for a particular FP, which make the cells fluorescent. Because these proteins are being made inside the cells in their natural environment, toxicity issues are much diminished. The fluorescence of the FP can be modulated depending on the cell environment or the presence of a special target. Tsien and coworkers were the first to discover green fluorescent proteins, and his group has performed a great deal of work on FP as a cellular probe. As shown in Figure 1.11[72] the Tsien group has built up an entire library of FP ranging from short wavelength emission to longer red emission derived from modified green fluorescent protein (GFP) and red fluorescent protein (RFP).[66, 71, 73] Lately many other groups have attempted to use FPs for various analyte detections. For example recently Zhang et al. used enhanced green florescent proteins to detect cancer cells (Ramos cells/human Burkitt lymphoma cells) using a triplex molecular beacon. Plasmids[74] with the specific gene code for expression of GFP was transferred to cells, and cancer cells were identified depending on the expression level of the protein.[74]

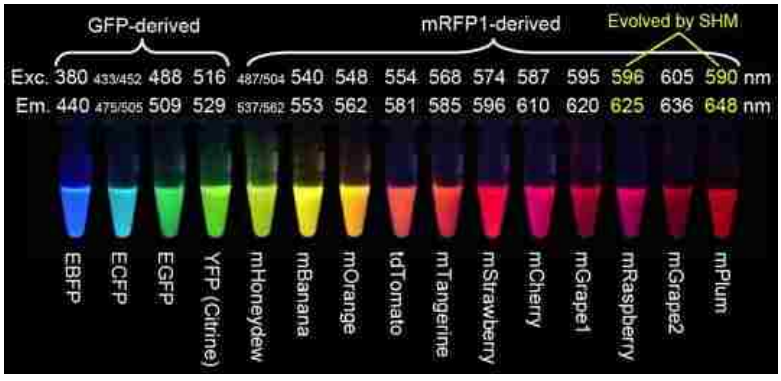

Figure 1.11 Emission color pallet of fluorescent proteins (FPs), ranging from the shortest wavelength to the longest emission wavelength.[72]

To investigate the specificity of this system, other cells were also incubated with plasmid, and expression of GFP (eGFP) was measured. However eGFP fluorescent signal was only observed in the target cells providing a promising route to detect cancer cells.[75] As another approach for GFP-mediated analyte detection, Ai and coworkers developed a modified GFP probe, hs-GFP, for H_2S detection by incorporating an H_2S-reactive moiety in the GFP backbone.[76] The probe exhibits good selectivity toward H_2S versus other commonly found oxidants in the body.[77] The major disadvantages of fluorescence proteins include difficulty of protein modification for specific chemical labelling, narrow wavelength range of proteins, poor photo-stability, and the large time consumption required for expression in cells.[66]

1.8.2 Aptamer-based Fluorescence Sensing

Aptamers[78] are single-stranded nucleic acids that can fold into 3-dimenssional structures so as to bind to target molecules. Aptamers have attracted the attention of molecular-targeted researchers due to their small size, high binding affinity for target molecules, and ease of modification.[79-82] Most aptamers are obtained through a combinatorial selection process called systematic evolution of ligands by exponential enrichment (SELEX).[83] As shown in Figure 1.12, [79] this SELEX process is a rather time-consuming process, it needs specialized

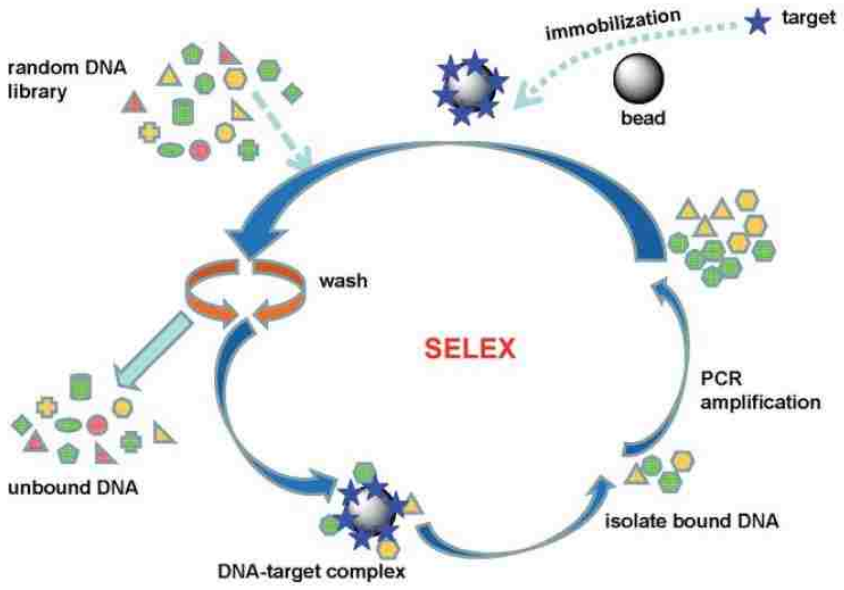

Figure 1.12 Schematic representation of isolation of aptamers using SELEX process. In this example, the target molecule is immobilized on a bead to achieve separation.[79]

instrumentation like PCR amplification and it involves tedious separation strategies. Hence, these complex preparation steps are the main disadvantage of aptamer sensors. In addition, aptamers can be the target of degradation by enzymes like RNAses[84] and DNAses[85-86] that are commonly found in the body. Also the pH, ionic strength, and temperature, of the system and the presence of matrix molecules greatly affect the success of the target binding.[79] However, there is a broad range of aptameric fluorescence sensors to detect analytes, such as peptides, small molecules, proteins, and metal ions and also more complex targets, such as whole cells and material surfaces.[79] As reported by Lu and coworkers, a new DNA-based aptamer (Figure 1.13) can be used for a label-free detection of analytes.[87] A selected DNA aptamer with the appropriate sequence was coupled to an additional sequence that served as a binding site for the fluorophore (2-amino-5,6,7-trimethyl-1,8-naphthyridine).[88] In the absence of the targeted analyte, the binding site sequence was stabilized by intramolecular forces and fluorescence was suppressed.[83, 87, 89]

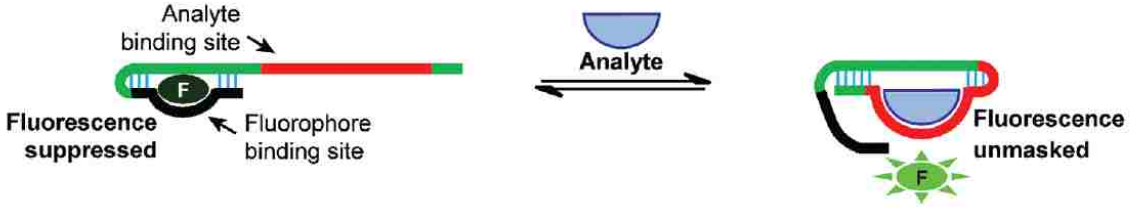

Figure 1.13 Target-oriented, label-free aptamer probe with fluorophore binding sequence minimizes fluorescence in the absence of analyte.[83]

Upon binding the analyte, the aptamer underwent a structural change that resulted in florescence emission. They have utilized this approach to synthesize several fluorescent probes for metal ions (Pb^{2+}, Hg^{2+}, UO_2^{+}) and adenosine.[89] Tan et al. reported an aptamer-based fluorescence complex for protein detection in biological fluids. They have molecular engineered a light-switching excimer aptamer for protein monitoring both in steady-state and time-resolved fluorescence microscopy. The aptamer sequence that binds with high affinity to the target protein (platelet-derived growth factor, PDGF-BB) is labeled with a pyrene molecule at both ends. Binding of the aptamer to its target protein induces a conformational change in the probe, resulting in two pyrene molecules in close proximity to form an excimer. This excimer formation shifts the fluorescence, an event that can be easily detected. This method facilitates the direct detection of target protein without any need for sample clean-up process.[90]

1.8.3 Antibody-based Fluorescence Sensors

Antibodies can be easily modified covalently so as to be attached to a wide variety of substrates without losing their antigen effect. Due to their high affinity, variability in target binding, and remarkable biocompatibility, antibodies are an ideal candidate for bio-molecular imaging and analyte detection.[91-92] One of the first labelling techniques for antibodies were iodine and other radioactive isotopes, and for non-radiative labeling, biotin was used. More recently labelling with small-molecule fluorophores like fluorescein, cyanine 5/7, and Alexafluor, and bioluminescence, has emerged for cellular and in vivo detection of targets. There are many variants of antibody assays available; however, two main types are "label-based" assays and "sandwich-based" assays. In label-based assays, target proteins are labeled with a fluorescent tag that allows detection after capture by an immobilized antibody. The sandwich assay involves immobilized antibodies, that capture unlabeled proteins, and the captured proteins are detected by a secondary antibody possessing a fluorescent tag. Sandwich assays are more specific and sensitive because two antibodies target the same analyte.[93] Antibody-based probes are particularly useful for cancer-targeted diagnosis, especially in vivo cancer imaging.[94-95] Rosenthal and coworkers used an anti-EGFR (epidermal growth factor receptor) antibody labelled with Cy 5.5 fluorophore for in vivo detection of tumors in mice. The analysis of images showed the probe selectively accumulates in the tumor region.[96-97] Due to increased deep-tissue penetration and low autofluorescence, Zou et al. used Cy 7 dye conjugated to both murine and human CC49 (anti TAG-72) antibodies to image tumor-associated glycoprotein (TAG-72) in colorectal cancer in mice. The data showed successful tumor-specific accumulation and longer retention times at the tumor site than that for previously reported probes.[98] Although widely used in cancer therapies and other analyte detection there are a few drawbacks, such as loss of recognition after conjugation with the fluorophore, lack of stability due to attack by the body's immune system, the loss of fluorescence signal after a dye conjugation needs to be addressed to make antibody probes more beneficial.[64]

1.8.4 Nanoparticle-based Fluorescence Sensors

Recent advances with nanotechnology and nanomaterials have successfully contributed to the development of many nanomaterial-based probes for medical and analytical purposes. Out of numerous diagnostic techniques that are associated with nanomaterials, fluorescent nanoparticles

(NPs) have advantages over traditional techniques in relation to sensitivity, stability, and the ability to be multiplexed[99-100] in cellular imaging and analyte detection. Compared to the traditional use of single organic dye probes, fluorescent NPs have been made by encapsulating organic dyes in a particle matrix. These particles are much brighter than a single dye, and therefore more photostable because the dye entrapment enhances its stability and biocompatibility. In addition to the dye entrapment route, NPs such as quantum dots (QDs) are intrinsically fluorescent with excellent optical properties. Nano particles can also be made out of organic matrices such as polymers (polystyrene,[101] acrylate derivatives[102-103]) or dendrimers. But the majority of NPs are synthesized with inorganic materials like silica,[104] semiconductor quantum dots,[105-106] magnetite,[107] and noble metals such as gold, silver, and platinum. In addition, carbon and silicon NPs have been used to make NPs.[100] Wen et al. used peptide-templated Au NPs to develop a real-time, label-free sensing approach for the detection of post-translationally modified enzymes (PTM) and peptidases. Enzyme modification of the peptidase causes significant fluorescence quenching, as shown in Figure 1.14. The chemical modification destroys the peptide coating on Au NPs, and as a result, oxygen-mediated quenching and oxidation of the fluorescent Au NPs took place more easily. The fluorescence decrease is a linear function of enzyme concentration, allowing quantitative determination of the enzyme.[108-110]

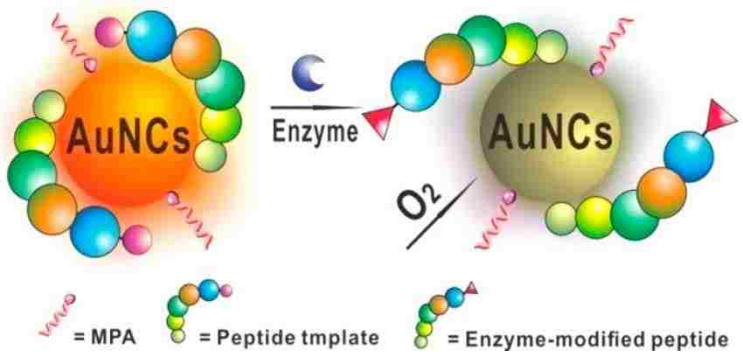

Figure 1.14 Mechanism for peptide-templated Au NPs as a label-free sensor for post-translationally modified enzyme.[108]

Both Frangioni and Prasad with their coworkers used Cd/Se/Te-based quantum dots with NIR emission to facilitate cancer surgery via sentinel lymph node mapping. Frangioni's group used a polydentate phosphine coating to make the QDs soluble, dispersed, and stable in serum. Injection of only 400 pmol of NIR QDs facilitated easy imaging of 1-cm deep sentinel lymph

nodes in real time using 500-nm excitation and low power density.[111] Lysine cross-linked mercaptoundecanoic acid was used by Prasad and coworkers to coat their Cd quantum dots, and they also successfully demonstrated the in vivo distribution of NPs in tumors, their clearance, and the cytotoxicity of these quantum dots.[112]

One of the major disadvantages of NPs and quantum dots are their cytotoxicity. Toxicity of NPs are closely associated with surface chemistries, size, dose, and the administration route of the NPs. Frangioni and coworkers reported that in vivo behavior of QDs greatly depend on their hydrodynamic size, and according to their observations, QDs smaller than 5.5 nm can be rapidly cleared through renal excretion, whereas QDS larger than 15 nm accumulate in the liver and spleen.[113] Another concern with NPs, especially for in vivo applications, is their interaction with matrix protein and other bio-macromolecules. Protein binding to NPs may induce conformational changes and concomitantly alter NPs intended function. Dawson and coworkers reported the loss of function of transferring receptor targeted silica NPs due to the binding of serum protein (Figure 1.15).[114]

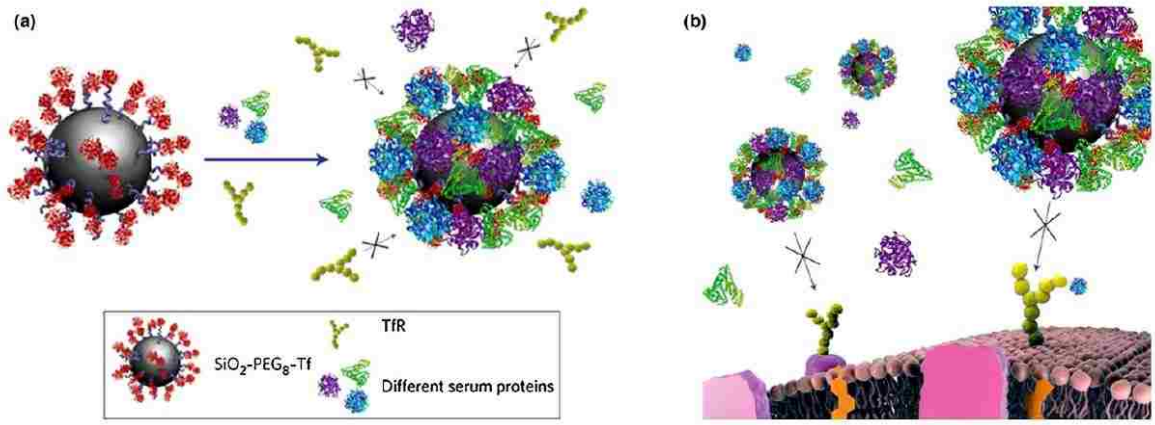

Figure 1.15 a) Schematic depiction of blocked transferrin-transferrin receptor interaction in the solution phase in the presence of serum protein. b) Schematic representation of the loss of targeting capability of transferring-conjugated NPs towards transferring receptor on the cell surface in the presence of serum protein.[114]

1.8.5 Small-molecule-based Fluorescence Probes

Small molecule probes are one of the most indispensable tools in chemical biology and medicine. Simple architecture and ubiquitous role they play as cellular stains, enzyme substrates, bimolecular labels and environmental indicators are the greatest advantages of small molecular

probes.[115-117] When compared to other detection techniques, small molecules with organic fluorophores have extreme modularity. They facilitate the attachment of various reactive functional groups, substrate moieties, chelating components, and other chemical entities, to a small number of "core" fluorophores to generate a diverse set of new molecular probes with unique properties.[118] As stability, fluorescence characteristics, and design of these "core fluorophore" are well established, selection and design of a new class of probes are quiet simplified. There are several endogenous molecules like quinine, certain amino acids,[119] and NADH[120] that can act as natural fluorophores, especially at short wavelengths (UV region, Figure 1.16).[118] These natural fluorophores can sometime be useful, but most of the time, they can be interfering with the emission of other synthetic fluorophores that give rise to tissue auto-fluorescence.[121] The synthetic classes of fluorophores which are being synthesized and are inspired by naturally fluorescent molecules, can be classified into several categories, such as polycyclic aromatics, coumarins, quinolines, indoles and imidazoles, rhodamines, naphthoxanthenes, bodipys, cyanines and phthalocyanines (Figure 1.16).[118]

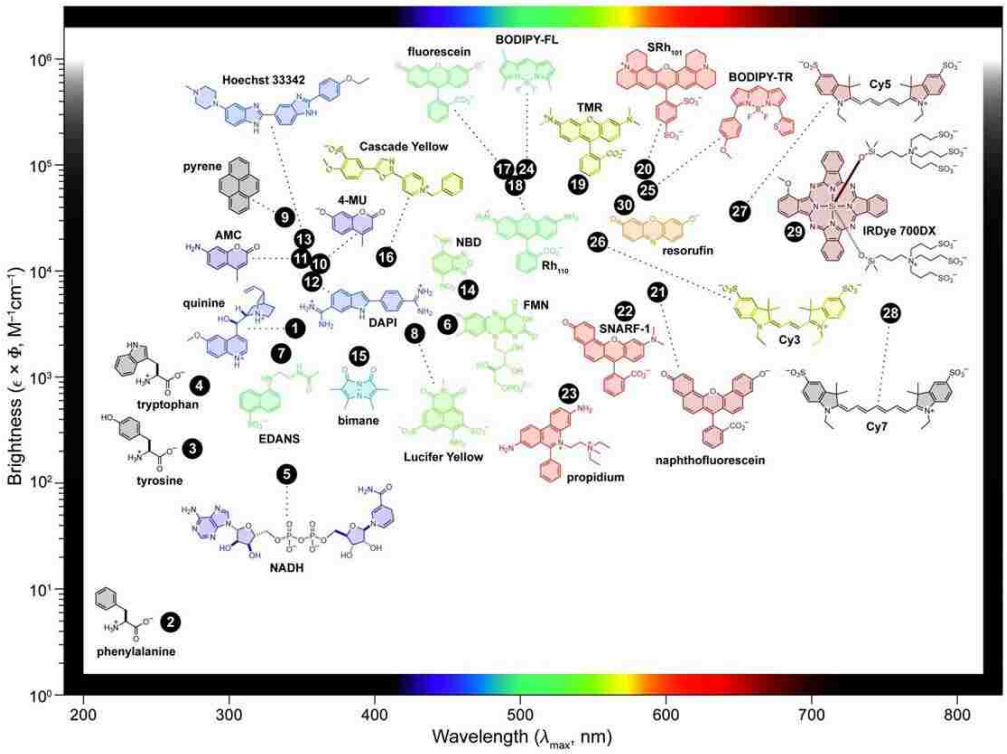

Figure 1.16 Commonly used organic fluorophores for probe synthesis with fluorophore brightness ($\epsilon \times \Phi$) vs the wavelength of maximum absorption (λ_{max}); the color of the structure indicates its wavelength of maximum emission (λ_{em}).[118]

Fluorescence probes used for analyte detection primarily fall into two categories: "always-on" probes and "off-on" (activatable) probes. Always-on probes have a constant fluorescence signal, and as a result yield high background signals and limited signal contrast, especially in cellular environments and in vivo. However, "off-on" probes are activated only at specific site or only in the presence of specific analyte. These probes can offer significantly reduced background signal, and improved contrast and sensitivity.[122] The main routes towards development of "off-on" activated probes are as shown in Figure 1.17—photoinduced electron transfer (PeT) and Foster (or fluorescence) resonance energy transfer (FRET).[123] PeT is electron transfer to (or from) the fluorophore in the excited state from (or to) an electron donor (or acceptor) moiety that is introduced in close proximity to the fluorophore. When PeT occurs, the excited state of the fluorescent molecule is quenched, thereby decreasing the fluorescence intensity.

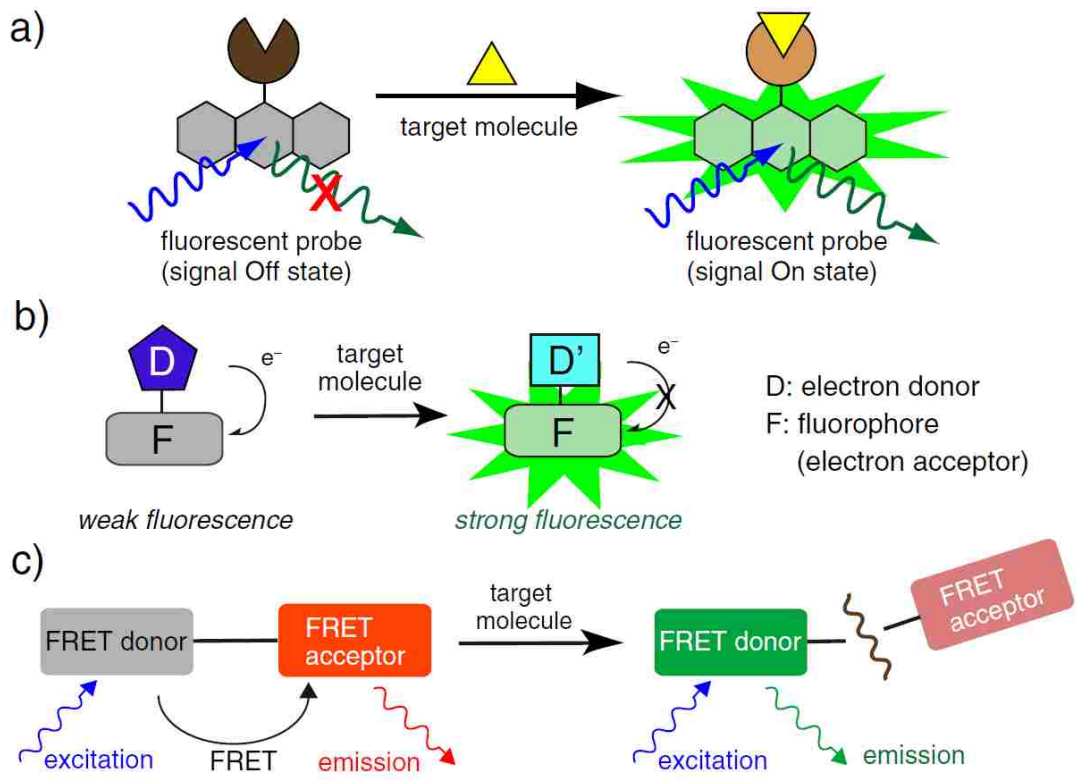

Figure 1.17 Design strategies for fluorescence probes: a) General concept of activatable fluorescence probes; b) Design concept for PeT-based fluorescence probes; and C) Design concept for FRET-based fluorescence probes.[123]

In the case of activatable fluorescent probes, the PeT mechanism is made inactive by chemical reactions of the probe with target molecule, thereby unmasking the highly intense fluorescence of the reporter dye (Figure 1.17 b). The second method, FRET, is a non-radiative transfer of energy between two fluorescent molecules, with one molecule being a donor and the second being the acceptor (Figure 1.17 c). When this process occurs, fluorescence of the donor is weakened, allowing fluorescence from the acceptor to be prominent, even though the donor is the one being irradiated. For efficient FRET, factors like spectral overlap of the donor and acceptor and distance between the two fluorophores are important. As in the example in Figure 1.16 c, if the bond between the donor and the acceptor is disrupted, FRET is cancelled, thereby restoring donor fluorescence.[122-124] Both PeT and FRET mechanisms have been greatly exploited by many researchers to develop activatable probes for different analytes, such as enzymes, metal ions, and thiols, as well their application in cancer imaging.

As described before, the disadvantages of organic fluorophores are tissue absorbance and interference from biological autofluorescence. Sometimes adverse side reactions of the probe or the fluorophore with other biological analytes, and cellular toxicity, can also be an issue.

1.9 Fluorescence-based Detection of Important Analytes in the Body

Living organisms are composed of a diverse set of cells that are morphologically and functionally different depending on the location, function, and organ in which they are located. Each of these cells, regardless of what function they perform, contains an enormous variety of biomolecules. The concentrations, chemical modification, and interaction of these molecules are generally precisely controlled, both spatially and temporally. Alteration of these analytes can be an indicator of disease state or a change in an important biological process in the body.[125] Conventional clinical chemistry relies on the detection and measurement of a wide range of body substances, including gases, electrolytes, hemoglobin, hydrogen ions, enzymes, metabolites, hormones, vitamins, proteins, and therapeutic drugs. Monitoring of these disease biomarkers provides an idea of disease progression, and the effect of therapeutic drugs, including the assessment of eventual drug resistance effects.[126] Compared to other detection methods, such as radioisotope labelling, MRI, ESR, electrochemical methods, HPLC and GC/MS that are currently used in clinical diagnosis, fluorescence imaging has many advantages. It enables highly sensitive, noninvasive, and safe detection using simple instrumentation.[125] As a result, there is a

huge interest in developing fluorescence based sensors for the detection of various analytes found in the body. In the following section, several important analytes, such as metal ions, enzymes, NADH, glucose, pH, and ROS/RNS, and methods for their fluorescent detection will be discussed.

1.9.1 Fluorescent Probes for Metal Ions

Metal ions play a critical role in fundamental processes of cells, including osmotic regulation, catalysis, metabolism, and signal transduction.[127] Group I and II metals, such as sodium, potassium, calcium and magnesium, are highly abundant in most biological systems. Transition metal ions, including copper, manganese, cobalt, nickel, and chromium, are often found in trace quantities compared to group I and II metals but still play a critical role in body.[128-129] Out of many attempts reported in the literature, Zhu and coworker have developed the 6-hydroxyindole BODIPY-based fluorescent probe (1-OH) for the detection of Zn^{2+} ions.[130] The sensing mechanism of the probe is based on chelation-enhanced fluorescence upon Zn^{2+} binding to the Schiff-base ligand, where it deprotonates the phenol group to yield a chelate that exhibits high fluorescence at wavelength around 680 nm. This sensor was used to locate Zn^{2+} in the perinuclear area of the cytosol in living cells.[130] Tang and coworkers[131] developed a NIR-fluorescent probe Cy-Cu, composed of a tricarbocyanine fluorophore and 2,2′-azanediyl-bis(*N*-hydroxyacetamide) as the Cu^{+} receptor ligand. When Cu^{+} binds to the receptor, the PET mechanism is blocked, resulting in a fluorescent enhancement. The cell membrane-permeable analog of Cy-Cu was used to detect labile Cu^{+} in living cells and mice. Tian et al. developed a tricarbocyanine-based probe [132] for Hg^{2+} and CH_3Hg^{+} ions. The response of these probes to Hg^{2+} depends on the strong thiophilic affinity of mercury. Release of the free dye by mercury presence results in a large shift in absorption and emission maxima from 664 nm to 840 nm.[129]

1.9.2 Fluorescent Probes for pH Changes

Measuring intracellular or extracellular pH changes provides important information about the nature of physiological or pathological processes.[129] As acidic environments are generally associated with inflammation and tumor progression, sensing even slight changes in pH is important to build therapeutic targets.[133] Achilefu and coworkers synthesized indolium cyanine probe 1 as a pH indicator.[134] The probe is non-fluorescent when unprotonated, but the probe

becomes strongly fluorescent at 800 nm when an acidic environment is present. As another strategy, Nagano and coworkers developed a cyanine dye attached to ethylene diamine and a piperazine conjugate. This strategy involving tuning of the pK_a values of the diamine moiety, to provide an effective method to design and predict the ratiometric measurement of pH changes over a wide range of pH, both in vitro and in vivo.[135]

1.9.3 Fluorescent Probes for the Detection of Enzymes

Fluorescence-based probes for the detection of enzyme activity are particularly attractive for the easy, sensitive, and selective monitoring of enzymes behavior, that alter their expression level as a result of a disease conditions. Numerous fluorescent probes have been developed for determining the functional role of enzymes in the physiological environment.[136-137] Nagano and coworkers[138] reported a glutathione-*S*-transferase (GST)[139-140] activatable fluorescent probe (DNAF) based on 3,4-dinitrobenzanilide and the 5– and 6– isomers of amino fluorescein. DNAFs have shown excellent kinetic parameters on yielding fluorescence upon activation by GST. In order to detect intracellular distribution of GST, the authors have synthesized DNAT-Me, which exhibited a dramatic fluorescence increase once exposed to cells with upregulated GST.[138] Peng et al. recently reported a novel "off/on" fluorescent probe targeting cyclooxygenase-2 (COX-2) localized in the Golgi apparatus of cancer cells.[141] The probe ANQ-IMC-6 consists of a green fluorescent dye at 560 nm (ANQ) as fluorophore and indomethacin (IMC) as the recognition moiety. The probe yields a high selectivity toward COX-2[142-143] and has successfully been used to image COX-2 in the Golgi apparatus.[136] The contribution from the McCarley group towards detection of human NAD(P)H quinone oxidoreductase 1 (NQO1)[144-145] used a quinone propionic acid trigger group attached to the fluorophore 1,8 naphthalimide.[146-147] Upon reduction of the quinone propionic acid moiety by NQO1, the cloaked probe undergoes a rearrangement, thereby releasing the highly fluorescent naphthalimide reporter. These reporter probes have successfully demonstrated the ability to detect cellular NQO1 with high selectivity. As another successful strategy, the probe TG-βGal was reported by Urano and coworkers for detection of the β-galactosidase[148-149] activity in living cells.[150-151] The probe TG-βGal is composed of β-galactoside as the enzyme activatable group and *O*-alkylated xanthene as the fluorophore. Upon hydrolysis, the β-galactoside group was released, and fluorescence is turned

on. Due to the reasonable membrane permeability of the probe, Urano was able to detect the β-galactosidase enzyme activity in a real-time manner.[136]

1.9.4 Fluorescent Probes for the Detection of Reactive-oxygen Species (ROS) and Reactive-nitrogen Species (RNS)

ROS and RNS play an important role in cellular health and function. Therefore, to understand the chemistry of these very small and transient species in living systems, it is important to monitor their concentration precisely, especially in the cellular environment.[152] As a major ROS in living systems, H_2O_2 plays a key role as a secondary messenger in cellular signal transduction. Developing fluorescent probes for H_2O_2 gives a unique opportunity for real-time noninvasive detection of H_2O_2. Shabat and coworkers recently developed a cyanine-based NIR-probe,[153] composed of a boronate moiety as a specific reaction site for H_2O_2. Upon reaction the boronate group is chemically modified to a phenol group that results in generation of an extensive π-conguated NIR fluorophore, which gives a fluorescence signal around 720 nm. Chang and coworkers[154] developed a ratiometric fluorescent probe RPF1 for H_2O_2 detection that contains a coumarin donor and a boronate-protected fluorescein acceptor linked through a spacer.[155] In the absence of oxidant, only coumarin emission is observed; whereas, with the addition of H_2O_2, the intensity of the green fluorescence associated with the fluorescein acceptor increases via a FRET process, when excite at the coumarin wavelength. The concentration changes of H_2O_2 are readily determined by measuring the ratio of the intensities of the two wavelengths.[156] As another strategy, Yang et al. developed a BODIPY-based peroxynitrite probe HK-green 2, which does not have emission in the absence of peroxynitrite. In the presence of excess peroxynitrite, the probe exhibits a 69-fold fluorescence enhancement, and the fluorescence-intensity increases linearly, proportionate with the concentration in the range of 0–15 μM.[157] Tang and coworkers developed a BODIPY-based probe, TEMPO-BDP, for the detection of hydroxyl radicals. The probe itself shows weak fluorescence in the absence of the hydroxyl radical, but in the presence of hydroxyl radicals and with the addition of DMSO, a significant fluorescence enhancement was observed.[158]

1.9.5 Fluorescent Probes for the Detection of Anions

Anions also play a crucial part in physiology, just like their cation counterparts. Anions, such as CN^- (important analyte in cystic fibrosis), and PPi (inorganic pyrophosphate, generated from ATP hydrolysis)[159-160] play an important role in the body. Yoon et al. reported a probe for CN^- ions designed with tricarbocyanine dye and a copper receptor moiety; when the probe binds to Cu^{2+} to form the probe-Cu^{2+} complex the absorption maximum at 718 nm shifts to 743 nm and fluorescence at 748 nm is quenched. When CN^- was added to a solution of copper-bound probe, the fluorescence intensity at 748 nm increased rapidly, giving rise to a copper cyanide complex. Using this probe, they were able to detect CN^- selectively without an effect from other anions. Zhu and coworkers developed a fluorescent probe, DCEA, which acts on PPi anion in aqueous solution. The precursor probe consists of dicyanomethylene-4-*H*-chromene as a fluorophore and the iminodiacetate group as Cu^{2+} receptor ligand. Fluorescence is decreased by Cu^{2+} addition with chelation to the diacetate group in the ligand moiety. Once the anion PPi was added, fluorescence at 675 nm increased due to interaction between Cu^{2+} and the PPi anion. However, its intensity did not completely return to that of a free reporter, suggesting that the coordination of PPi anion is not strong enough to cause complete removal of Cu^{2+} from the DCEA-Cu^{2+} probe.[133, 161]

1.10 Traditional Thiol Detection Methods

Conventional techniques for the determination of thiols, such as high-performance liquid chromatography[162] and capillary electrophoresis (CE) separations, can be coupled with different detection methods like ultraviolet absorbance (UV), fluorescence, and electrochemical detection to provide superior resolution. Typically for amino acids thiols, UV and fluorescence detection methods are based on derivatization of the thiol either at the amino end or thiol moiety. However, some of these derivatives are not stable, or accurate measurement of that are hampered by the presence of excess reagents and products from side reactions in the system.[163] HPLC-linked electrochemical detection of thiols first introduced by Kahn et al.,[164] using a glassy-carbon working electrode during chromatographic separations to analyze thiols in human plasma.[165] D'Eramo and co-workers also used HPLC with an electrochemical detection protocol by using a glassy carbon electrode, total homocysteine levels were detected with a low limit of detection.[166]

Due to simple instrumentation and quick analysis with relatively small amounts of sample, CE has become a popular route in thiol analysis.[167-168] UV-vis and electrochemical approaches are the most commonly used detection methods to date for CE. However, spectroscopic detection has drawbacks due to the small path length across the capillary, yielding the limitation of lower sensitivity. Electrochemical detection in CE has the advantage of simplicity, ease of miniaturization, high sensitivity, and relatively low cost. Both HPLC and CE methods have their own benefits including good selectivity and low detection limits; however, they often require extensive, time-consuming sample preparation (both pre- and post-column) and derivatization steps prior to sample analysis.[164, 169]

Direct electrochemical approaches for thiol detection and quantification have offered potential simplicity among other traditional techniques. However, direct electro-oxidation of thiol compounds on common solid electrodes limits its selectivity because of the similarity in oxidation potential for most biological reducing substances in comparison to thiols Also, methods based on direct oxidation of thiols at solid electrodes are time consuming and usually require a large overpotential.[170] Although this can be alleviated by indirect detection on mercury amalgam electrodes the toxicity associated with mercury hinders further use of these methods for live sample analysis. According to the literature, some other organic and inorganic electroactive indicators as electron mediators have also been used, yet the necessity of delicate and finely tuned experimental conditions for the success of the electro-catalytic reaction between the thiol compounds and the indicator limits their wide application especially live monitoring of samples.[170-172]

Mass spectrometric-based assays are also another widely used method for thiol detection. Mass methods, such as trap-and-release membrane introduction mass spectrometry (T&R-MMS),[173] gas chromatography and liquid chromatography coupled to mass spectrometry (GC-MS, LC-MS)[174] are applied to thiol detection.[175] Mass spectrometry provides specificity in that it is able to monitor select mass ions from fragment parent ions; it provides enhanced signal-to-noise ratio, and decreased time due to minimal sample cleanup and derivatization. Each of these methods has their drawbacks, such as extensive sample processing, complexity, high equipment cost, long run time, and limited number of samples processed at a given time and/or validation parameters assessed; these issues make them impractical for high-throughput routine clinical or research purposes.[176]

In addition, other techniques, such as nuclear magnetic resonance spectroscopy (NMR) methods,[177-178] are being used for GSH and GSSG detection in brain cells in vivo and intact cells in cyto. Trabesinger and coworkers pioneered a method applicable to the human brain wherein they used ^{1}H NMR with double quantum coherence filtering in combination with point-resolved spectroscopy volume selection with a relatively low strength field.[178] The GSH concentration can also be assayed in blood through ^{19}F NMR, as reported by Potapenko et al. by measuring the product of the exchange reactions of thiols with a newly synthesized fluorinated disulfide 2,3,5,6-tetrafluoro-4-mercaptobenzoic acid.[179] Another important route of NMR measurement is investigation of thiol content in intact cells. Kenett et al. used ^{1}H spin-echo NMR and ^{13}C NMR to measure the intracellular and extracellular GSH redox status of cells while keeping the cells alive.[180]

Among these various thiol detection methods, optical techniques, including florescence or colorimetric approaches have proven to be some of the most convenient. Fluorescence techniques especially have a number of advantages, including simplicity, low detection limits, and ease of handling. Above all, the most beneficial use of fluorescent probes is the ability to monitor live cells and intracellular analytes. With this purpose in mind, during the last couple of decades, a great effort has been devoted to the development of fluorescent and colorimetric sensors that can selectively sense biological thiols.[7]

1.11 Fluorescence Probes for Bio-Thiol Detection

Most of the fluorescent probes reported in the literature for the detection of thiols are based on one of the two basic qualities observed for thiols. These methods have utilized either the high nucleophilicity of thiols toward a reporter system or the high binding affinity of thiols toward metal centers.[176, 181] The probes take advantage of high nucleophilicity can be sub-divided depending on their reactivity as—Michael addition,[182-184] cyclization with aldehydes,[185-186] conjugate addition-cyclization reactions,[187-188] cleavage of sulfonamide and sulfonate esters,[189-190] thiol-halogen nucleophilic substitution,[191] and disulfide exchange.[181, 192-193] The potential capabilities of a few of the recently reported thiol probes are discussed here below.

Lee and coworkers reported a single galactose-appended naphthalimide probe for hepatic thiol determination. According to the authors, the galactose subunit in their probe acts as a guide for the probe to reach hepatocytes by targeting asialoglycoprotein receptors (ASGP-R). When

bound to the receptor, the probe was internalized by receptor-mediated endocytosis. Inside the cell, the disulfide bond of the probe undergoes disulfide cleavage by reaction with targeted intracellular thiols; this releases the naphthalimide reporter leading to a fluorescence change. The authors were able to image cellular thiol levels with a minimum 20-min incubation time using a 5000:1 thiol to probe ratio.[194]

Guan et al. reported a benzofurazan sulfide-based probe; by changing the substituent in the benzofurazan ring, they were able to tune the reactivity of the probe. By incubating for 90 min, they were able image cellular thiols; however, any solution- phase kinetics or comment about thiol to probe ratio required for an efficient signal was not reported.[192] Zhang reported a coumarin-based thiol probe designed with 7-hydroxyl-coumarin dye as the fluorophore and an α,β-unsaturated ketone in the 8-position of the dye as the Michael acceptor. The initial non fluorescent probe became fluorescent upon Michael addition of thiols to the ketone, followed by a cleavage of the hemiketal, which resulted in the formation of a fluorescent 7-hydroxyl coumarine derivative. This probe was applied to thiol detection in human blood, serum, and living cells, with a 70:1 thiol-to-probe ratio. A good fluorescence signal was obtained within a relatively short time (about 10-min incubation) leading to rapid release.[195]

Kim et al. also reported another thiol probe using a coumarin dye as the reporter. The probe was designed with three active units: a coumarin moiety acts as the signaling unit; the conjugated enone is the reactive unit, and the *O*-hydroxyl group serves as an activation unit through resonance-assisted hydrogen bonding. When incubated with bio-thiols, a ratiometric response was observed. The authors were able to detect cellular thiols by incubating the sample for 60 min using 1000:1thiol-to-probe ratio.[196] As another approach, Cho and coworkers developed a ratiometric two-photon probe (SSH-mito) for mitochondrial thiol detection. They used 6-(benzo[*d*]thiazol-2'-yl)-2-(*N*,*N*-dimethylamino) naphthalene (BTDN) as the reporter dye, a disulfide group as the thiol reaction site, and triphenylphosphonium salt (TPP) as the mitochondrial targeting site. According to the authors, the cationic TPP group facilitates the probe's ability to accumulate in mitochondria. Once the disulfide group was cleaved off by replacement with mitochondrial thiols, subsequent cyclization caused release of the free fluorophore, offering a probe and reporter with a different fluorescence. They were able to detect mitochondrial thiols with quite a long incubation time (120 min for fluorescence increase) with a 2000:1 thiol-to-probe ratio.[197] Guo and coworkers developed a bodipy-based TMPAB-*O*-M

probe (1,3,5,7-tetramethyl-8-phenyl-(2-maleimide)difluoroboradiaza-*S*-indacene) to detect thiols in live cells. Initially, the fluorescence of the probe was quenched and reaction of the maleimide group, with cellular thiols facilitated a fluorescence increase. The probe was incubated with live cells, and the fluorescence increase was monitored overtime. A very rapid (90 s) fluorescence turn-on effect was observed, with relatively low thiol to probe ratio (1:1).[198]

While most of these literature-reported probes are rather successful in achieving their goal, most of them still suffer from excessively long reaction time, requirement of high analyte, and lower selectivity in biological media. None of the above-discussed probes have commented on their signal to background ratios; reporting such values would be an excellent way to prove their success in cellular imaging. As a result, there remains a great demand for a new class of thiol detecting probes that would increase both selectivity and sensitivity, alone with a shorter reaction time, higher analyte signal and lower background fluorescence.

1.12 References

1. Kelley, S. O.; Mirkin, C. A.; Walt, D. R.; Ismagilov, R. F.; Toner, M.; Sargent, E. H., Advancing the Speed, Sensitivity and Accuracy of Biomolecular Detection Using Multi-Length-Scale Engineering. *Nat. Nanotechnol.,* **2014**, *9*, 969-980.

2. Akers, W. J.; Achilefu, S. In *Molecular Reporter Systems for Optical Imaging*, CRC Press: **2011**; pp 673-696.

3. Turell, L.; Radi, R.; Alvarez, B., The Thiol Pool in Human Plasma: The Central Contribution of Albumin to Redox Processes. *Free Radical Biol. Med.,* **2013**, *65*, 244-253.

4. Hanjing P., W. C., Yunfeng C.,Lovemore H., Strongin R., Wang B., Thiol Reactive Probes and Chemosensors. *Sensors,* **2012**, *12*, 15907-15946.

5. Lu, S. C., Glutathione Synthesis. *Biochimica. et. Biophysica. Acta,* **2013**, *1830*, 3143-3153.

6. Townsend, D. M.; Tew, K. D.; Tapiero, H., The Importance of Glutathione in Human Disease. *Biomed. Pharmacother.*, **2003**, *57*, 145-155.

7. Jung, H. S.; Chen, X.; Kim, J. S.; Yoon, J., Recent Progress in Luminescent and Colorimetric Chemosensors for Detection of Thiols. *Chem. Soc. Rev.*, **2013**, *42*, 6019-6031.

8. Pastore, A.; Massoud, R.; Motti, C.; Lo Russo, A.; Fucci, G.; Cortese, C.; Federici, G., Fully Automated Assay for Total Homocysteine, Cysteine, Cysteinylglycine, Glutathione,

Cysteamine, and 2-Mercaptopropionylglycine in Plasma and Urine. *Clin. Chem.*, **1998**, *44*, 825-832.

9. Pace, N. J.; Weerapana, E., Diverse Functional Roles of Reactive Cysteines. *ACS Chem. Biol.*, **2013**, *8*, 283-96.

10. Grabchev, I.; Moneva, I.; Bojinov, V.; Guittonneau, S., Synthesis and Properties of Fluorescent 1,8-Naphthalimide Dyes for Application in Liquid Crystal Displays. *J. Mater. Chem.*, **2000**, *10*, 1291-1296.

11. Qian, X.; Xiao, Y.; Xu, Y.; Guo, X.; Qian, J.; Zhu, W., "Alive" Dyes as Fluorescent Sensors: Fluorophore, Mechanism, Receptor and Images in Living Cells. *Chem. Commun.*, **2010**, *46*, 6418-6436.

12. Sun, W.; Fan, J.; Hu, C.; Cao, J.; Zhang, H.; Xiong, X.; Wang, J.; Cui, S.; Sun, S.; Peng, X., A Two-Photon Fluorescent Probe with near-Infrared Emission for Hydrogen Sulfide Imaging in Biosystems. *Chem. Commun.*, **2013**, *49*, 3890-3892.

13. Wu, X.; Sun, X.; Guo, Z.; Tang, J.; Shen, Y.; James, T. D.; Tian, H.; Zhu, W., In Vivo and in Situ Tracking Cancer Chemotherapy by Highly Photostable Nir Fluorescent Theranostic Prodrug. *J. Am. Chem. Soc.*, **2014**, *136*, 3579-3588.

14. Yang, X.; Guo, Y.; Strongin, R. M., Conjugate Addition/Cyclization Sequence Enables Selective and Simultaneous Fluorescence Detection of Cysteine and Homocysteine. *Angew.Chem. Int. Ed.*, **2011**, *50*, 10690-10693.

15. Forman, H. J.; Zhang, H.; Rinna, A., Glutathione: Overview of Its Protective Roles, Measurement, and Biosynthesis. *Mol. Aspect. Med.*, **2009**, *30*, 1-12.

16. Kabil, O.; Vitvitsky, V.; Banerjee, R., Sulfur as a Signaling Nutrient through Hydrogen Sulfide. *Annu. Rev. Nutr.*, **2014**, *34*, 171-205.

17. Mosharov, E.; Cranford, M. R.; Banerjee, R., The Quantitatively Important Relationship between Homocysteine Metabolism and Glutathione Synthesis by the Transsulfuration Pathway and Its Regulation by Redox Changes. *Biochemistry*, **2000**, *39*, 13005-13011.

18. Vitvitsky, V.; Mosharov, E.; Tritt, M.; Ataullakhanov, F.; Banerjee, R., Redox Regulation of Homocysteine-Dependent Glutathione Synthesis. *Redox Rep.*, **2003**, *8*, 57-63.

19. Brosnan, J. T.; Brosnan, M. E., The Sulfur-Containing Amino Acids: An Overview. *J. Nutr.*, **2006**, *136*, 1636S-1640S.

20. Moriarty-Craige, S. E.; Jones, D. P., Extracellular Thiols and Thiol/Disulfide Redox in Metabolism. *Annu. Rev. Nutr.,* **2004**, *24*, 481-509.

21. Ray, P. D.; Huang, B.-W.; Tsuji, Y., Reactive Oxygen Species (Ros) Homeostasis and Redox Regulation in Cellular Signaling. *Cell. Signal.,* **2012**, *24*, 981-990.

22. Dickinson, B. C.; Chang, C. J., Chemistry and Biology of Reactive Oxygen Species in Signaling or Stress Responses. *Nat. Chem. Biol.*, **2011**, *7*, 504-511.

23. Paulsen, C. E.; Carroll, K. S., Cysteine-Mediated Redox Signaling: Chemistry, Biology, and Tools for Discovery. *Chem. Rev.*, **2013**, *113*, 4633-4679.

24. Kowaltowski, A. J.; de Souza-Pinto, N. C.; Castilho, R. F.; Vercesi, A. E., Mitochondria and Reactive Oxygen Species. *Free Radical Biol. Med.,* **2009**, *47*, 333-343.

25. Calas-Blanchard, C.; Catanante, G.; Noguer, T., Electrochemical Sensor and Biosensor Strategies for Ros/Rns Detection in Biological Systems. *Electroanalysis,* **2014**, *26*, 1277-1286.

26. Lambeth, J. D.; Krause, K.-H.; Clark, R. A., Nox Enzymes as Novel Targets for Drug Development. *Semin. Immunopathol.,* **2008**, *30*, 339-363.

27. Lambeth, J. D., Nox Enzymes, Ros, and Chronic Disease: An Example of Antagonistic Pleiotropy. *Free Radical. Biol. Med.,* **2007**, *43*, 332-347.

28. Nauseef, W. M., Biological Roles for the Nox Family Nadph Oxidases. *J. Biol. Chem.,* **2008**, *283*, 16961-16965.

29. Borges-Santos, M. D.; Moreto, F.; Pereira, P. C. M.; Ming-Yu, Y.; Burini, R. C., Plasma Glutathione of Hiv+ Patients Responded Positively and Differently to Dietary Supplementation with Cysteine or Glutamine. *Nutrition,* **2012**, *28*, 753-756.

30. Jones, D. P.; Carlson, J. L.; Mody, V. C.; Cai, J.; Lynn, M. J.; Sternberg, P., Redox State of Glutathione in Human Plasma. *Free Radical. Biol. Med.,* **2000**, *28*, 625-35.

31. Groitl, B.; Jakob, U., Thiol-Based Redox Switches. *Biochim. Biophys. Acta, Proteins Proteomics,* **2014**, *1844*, 1335-1343.

32. Wall, S. B.; Oh, J.-Y.; Diers, A. R.; Landar, A., Oxidative Modification of Proteins: An Emerging Mechanism of Cell Signaling. *Frontiers in Physiology,* **2012**, *3, 369, 1-9.*

33. Finkel, T., Oxygen Radicals and Signaling. *Curr. Opin. Cell Biol.,* **1998**, *10*, 248-253.

34. Circu, M. L.; Aw, T. Y., Reactive Oxygen Species, Cellular Redox Systems, and Apoptosis. *Free Radical Biol. Med.,* **2010**, *48*, 749-762.

35. Biswas, S.; Chida, A. S.; Rahman, I., Redox Modifications of Protein–Thiols: Emerging Roles in Cell Signaling. *Biochem. Pharmacol.,* **2006**, *71*, 551-564.

36. Forman, H. J.; Ursini, F.; Maiorino, M., An Overview of Mechanisms of Redox Signaling. *J. Mol. Cell. Cardiol.,* **2014**, *73*, 2-9.

37. Nagumo, K.; Tanaka, M.; Chuang, V. T. G.; Setoyama, H.; Watanabe, H.; Yamada, N.; Kubota, K.; Tanaka, M.; Matsushita, K.; Yoshida, A.; Jinnouchi, H.; Anraku, M.; Kadowaki, D.; Ishima, Y.; Sasaki, Y.; Otagiri, M.; Maruyama, T., Cys34-Cysteinylated Human Serum Albumin Is a Sensitive Plasma Marker in Oxidative Stress-Related Chronic Diseases. *Plos One,* **2014**, *9*, 9.

38. Grigoryan, H.; Li, H.; Iavarone, A. T.; Williams, E. R.; Rappaport, S. M., Cys34 Adducts of Reactive Oxygen Species in Human Serum Albumin. *Chem. Res. Toxicol.,* **2012**, *25*, 1633-1642.

39. Hermann, H., Sitdikova, G., Weiger, T., *Gasotranmitters:Physiology and Pathology*. Springer Berlin Heidelberg: **2012**.

40. Mustafa, A. K.; Gadalla, M. M.; Snyder, S. H., *Signaling by Gasotransmitters*. **2009**; Vol. 2, p re2-re2.

41. Heinemann, S. H.; Hoshi, T.; Westerhausen, M.; Schiller, A., Carbon Monoxide - Physiology, Detection and Controlled Release. *Chem. Commn.,* **2014**, *50*, 3644-3660.

42. Olas, B., Carbon Monoxide Is Not Always a Poison Gas for Human Organism: Physiological and Pharmacological Features of Co. *Chem. Biol. Interact.,* **2014**, *222*, 37-43.

43. Farrugia, G.; Lei, S.; Lin, X.; Miller, S. M.; Nath, K. A.; Ferris, C. D.; Levitt, M.; Szurszewski, J. H., A Major Role for Carbon Monoxide as an Endogenous Hyperpolarizing Factor in the Gastrointestinal Tract. *Proc. Natl. Acad. Sci.,* **2003**, *100*, 8567-8570.

44. Kim, H. P.; Ryter, S. W.; Choi, A. M. K., Co as a Cellular Signaling Molecule. *Annu. Rev. Pharmacol. Toxicol.,* **2006**, *46*, 411-449.

45. Carrington, S. J.; Chakraborty, I.; Bernard, J. M. L.; Mascharak, P. K., Synthesis and Characterization of a "Turn-on" Photocorm for Trackable Co Delivery to Biological Targets. *ACS Med. Chem. Lett.,* **2014**, *5*, 1324-1328.

46. Mustafa, A. K.; Sikka, G.; Gazi, S. K.; Steppan, J.; Jung, S. M.; Bhunia, A. K.; Barodka, V. M.; Gazi, F. K.; Barrow, R. K.; Wang, R.; Amzel, L. M.; Berkowitz, D. E.; Snyder, S. H., Hydrogen Sulfide as Endothelium-Derived Hyperpolarizing Factor Sulfhydrates Potassium Channels. *Circ. Res.*, **2011**, *109*, 1259-1268.

47. Vandiver, M. S.; Snyder, S., Hydrogen Sulfide: A Gasotransmitter of Clinical Relevance. *J. Mol. Med.*, **2012**, *90*, 255-263.

48. Guo, W.; Cheng, Z.-y.; Zhu, Y.-z., Hydrogen Sulfide and Translational Medicine. *Acta. Pharmacol. Sin.*, **2013**, *34*, 1284-1291.

49. Mustafa, A. K.; Gadalla, M. M.; Sen, N.; Kim, S.; Mu, W.; Gazi, S. K.; Barrow, R. K.; Yang, G.; Wang, R.; Snyder, S. H., H2s Signals through Protein S-Sulfhydration. *Sci. Signaling*, **2009**, *2*, No pp. given.

50. Hargrove, J. L., Persulfide Generated from L-Cysteine Inactivates Tyrosine Aminotransferase. Requirement for a Protein with Cysteine Oxidase Activity and Γ-Cystathionase. *J. Biol. Chem.*, **1988**, *263*, 17262-9.

51. Bian, J.-S.; Yong, Q. C.; Pan, T.-T.; Feng, Z.-N.; Ali, M. Y.; Zhou, S.; Moore, P. K., Role of Hydrogen Sulfide in the Cardioprotection Caused by Ischemic Preconditioning in the Rat Heart and Cardiac Myocytes. *J. Pharmacol. Exp. Ther.*, **2006**, *316*, 670-678.

52. Elrod, J. W.; Calvert, J. W.; Morrison, J.; Doeller, J. E.; Kraus, D. W.; Tao, L.; Jiao, X.; Scalia, R.; Kiss, L.; Szabo, C.; Kimura, H.; Chow, C.-W.; Lefer, D. J., Hydrogen Sulfide Attenuates Myocardial Ischemia-Reperfusion Injury by Preservation of Mitochondrial Function. *Proc. Natl. Acad. Sci.*, **2007**, *104*, 15560-15565.

53. Krishnan, N.; Fu, C.; Pappin, D. J.; Tonks, N. K., H_2S-Induced Sulfhydration of the Phosphatase Ptp1b and Its Role in the Endoplasmic Reticulum Stress Response. *Sci. Signaling*, **2011**, *4*, ra86, 12 pp.

54. Zhao, W.; Zhang, J.; Lu, Y.; Wang, R., The Vasorelaxant Effect of H2s as a Novel Endogenous Gaseous Katp Channel Opener. *EMBO J.*, **2001**, *20*, 6008-6016.

55. Chen, C.-q.; Xin, H.; Zhu, Y.-z., Hydrogen Sulfide: Third Gaseous Transmitter, but with Great Pharmacological Potential. *Acta Pharmacol. Sin.*, **2007**, *28*, 1709-1716.

56. Breder, I.; Coope, A.; Arruda, A. P.; Razolli, D.; Milanski, M.; Dorighello, G. d. G.; de Oliveira, H. C. F.; Velloso, L. A., Reduction of Endoplasmic Reticulum Stress-a Novel Mechanism of Action of Statins in the Protection against Atherosclerosis. *Atherosclerosis*, **2010**, *212*, 30-31.

57. Hotamisligil, G. S., Endoplasmic Reticulum Stress and Atherosclerosis. *Nat. Med.*, **2010**, *16*, 396-399.

58. Dickhout, J. G.; Carlisle, R. E.; Jerome, D. E.; Mohammed-Ali, Z.; Jiang, H.; Yang, G.; Mani, S.; Garg, S. K.; Banerjee, R.; Kaufman, R. J.; Maclean, K. N.; Wang, R.; Austin, R. C., Integrated Stress Response Modulates Cellular Redox State Via Induction of Cystathionine Γ-Lyase: Cross-Talk between Integrated Stress Response and Thiol Metabolism. *J. Biol. Chem.*, **2012**, *287*, 7603-7614.

59. Fiorucci, S.; Antonelli, E.; Distrutti, E.; Rizzo, G.; Mencarelli, A.; Orlandi, S.; Zanardo, R.; Renga, B.; Di Sante, M.; Morelli, A.; Cirino, G.; Wallace, J. L., Inhibition of Hydrogen Sulfide Generation Contributes to Gastric Injury Caused by Anti-Inflammatory Nonsteroidal Drugs. *Gastroenterology*, **2005**, *129*, 1210-1224.

60. Li, L.; Rossoni, G.; Sparatore, A.; Lee, L. C.; Del Soldato, P.; Moore, P. K., Anti-Inflammatory and Gastrointestinal Effects of a Novel Diclofenac Derivative. *Free Radical Biol. Med.*, **2007**, *42*, 706-719.

61. Wallace, J. L.; Caliendo, G.; Santagada, V.; Cirino, G., Markedly Reduced Toxicity of a Hydrogen Sulphide-Releasing Derivative of Naproxen (Atb-346). *Br. J. Pharmacol.*, **2010**, *159*, 1236-1246.

62. Wallace, J. L.; Caliendo, G.; Santagada, V.; Cirino, G.; Fiorucci, S., Gastrointestinal Safety and Anti-Inflammatory Effects of a Hydrogen Sulfide-Releasing Diclofenac Derivative in the Rat. *Gastroenterology*, **2007**, *132*, 261-271.

63. Woolley, C. F.; Hayes, M. A., Emerging Technologies for Biomedical Analysis. *Analyst*, **2014**, *139*, 2277-88.

64. Pierce, M. C.; Javier, D. J.; Richards-Kortum, R., Optical Contrast Agents and Imaging Systems for Detection and Diagnosis of Cancer. *Int. J. Cancer*, **2008**, *123*, 1979-1990.

65. Vazquez, M. E.; Rothman, D. M.; Imperiali, B., A New Environment-Sensitive Fluorescent Amino Acid for Fmoc-Based Solid Phase Peptide Synthesis. *Org. Biomol. Chem.*, **2004**, *2*, 1965-1966.

66. Pazos, E.; Vazquez, O.; Mascarenas, J. L.; Eugenio Vazquez, M., Peptide-Based Fluorescent Biosensors. *Chem. Soc. Rev.*, **2009**, *38*, 3348-3359.

67. Oh, K. J.; Cash, K. J.; Hugenberg, V.; Plaxco, K. W., Peptide Beacons: A New Design for Polypeptide-Based Optical Biosensors. *Bioconjugate Chem.*, **2007**, *18*, 607-609.

68. Medintz, I. L.; Clapp, A. R.; Brunel, F. M.; Tiefenbrunn, T.; Tetsuo Uyeda, H.; Chang, E. L.; Deschamps, J. R.; Dawson, P. E.; Mattoussi, H., Proteolytic Activity Monitored by Fluorescence Resonance Energy Transfer through Quantum-Dot-Peptide Conjugates. *Nat. Mater.,* **2006**, *5*, 581-589.

69. Zhang, M.; Wu, B.; Zhao, H.; Taylo, J. W., The Effect of C-Terminal Helix Stabilization on Specific DNA Binding by Monomeric Gcn4 Peptides. *J. Pept Sci.,* **2002**, *8*, 125-36.

70. Jagt, R. B. C.; Gómez-Biagi, R. F.; Nitz, M., Pattern-Based Recognition of Heparin Contaminants by an Array of Self-Assembling Fluorescent Receptors. *Angew. Chem. In. Ed.,* **2009**, *48*, 1995-1997.

71. Weissleder, R., *Molecular Imaging: Principles and Practice*. People's Medical Publishing House: **2010**.

72. Tsien, R. Y., Nobel Lecture: Constructing and Exploiting the Fluorescent Protein Paintbox. *Integr. Biol.,* **2010**, *2*, 77-93.

73. Shaner, N. C.; Campbell, R. E.; Steinbach, P. A.; Giepmans, B. N. G.; Palmer, A. E.; Tsien, R. Y., Improved Monomeric Red, Orange and Yellow Fluorescent Proteins Derived from Discosoma Sp. Red Fluorescent Protein. *Nat. Biotechnol.,* **2004**, *22*, 1567-1572.

74. Verma, I. M., Gene Therapy That Works. *Science,* **2013**, *341*, 853-855.

75. Xi, D.; Wang, X.; Ai, S.; Zhang, S., Detection of Cancer Cells Using Triplex DNA Molecular Beacons Based on Expression of Enhanced Green Fluorescent Protein (Egfp). *Chem. Commun.,* **2014**, *50*, 9547-9549.

76. Chen, Z.-j.; Ai, H.-w., A Highly Responsive and Selective Fluorescent Probe for Imaging Physiological Hydrogen Sulfide. *Biochemistry,* **2014**, *53*, 5966-5974.

77. Heger, Z.; Kominkova, M.; Cernei, N.; Krejcova, L.; Kopel, P.; Zitka, O.; Adam, V.; Kizek, R., Fluorescence Resonance Energy Transfer between Green Fluorescent Protein and Doxorubicin Enabled by DNA Nanotechnology. *Electrophoresis,* **2014**, *35*, 3290-3301.

78. Lee, J. H.; Yigit, M. V.; Mazumdar, D.; Lu, Y., Molecular Diagnostic and Drug Delivery Agents Based on Aptamer-Nanomaterial Conjugates. *Adv. Drug Delivery Rev.,* **2010**, *62*, 592-605.

79. Zhou, W.; Huang, P.-J. J.; Ding, J.; Liu, J., Aptamer-Based Biosensors for Biomedical Diagnostics. *Analyst,* **2014**, *139*, 2627-2640.

80. Chang, C.-C.; Chen, C.-P.; Lee, C.-H.; Chen, C.-Y.; Lin, C.-W., Colorimetric Detection of Human Chorionic Gonadotropin Using Catalytic Gold Nanoparticles and a Peptide Aptamer. *Chem. Commun.,* **2014**, *50,* 14443-14446.

81. Raina, M.; Sharma, R.; Deacon, S. E.; Tiede, C.; Tomlinson, D.; Davies, A. G.; McPherson, M. J.; Walti, C., Antibody Mimetic Receptor Proteins for Label-Free Biosensors. *Analyst,* **2014**, Ahead of Print.

82. Szeto, K.; Craighead, H. G., Devices and Approaches for Generating Specific High-Affinity Nucleic Acid Aptamers. *Appl. Phys. Rev.,* **2014**, *1*, 031103/1-031103/17.

83. Vendrell, M.; Zhai, D.; Er, J. C.; Chang, Y.-T., Combinatorial Strategies in Fluorescent Probe Development. *Chem. Rev.*, **2012**, *112*, 4391-4420.

84. Eller, C. H.; Lomax, J. E.; Raines, R. T., Bovine Brain Ribonuclease Is the Functional Homolog of Human Ribonuclease 1. *J. Biol. Chem.,* **2014**, *289,* 25996-26006.

85. Vogel, B.; Frantz, S., Determination of Dnase Activity by Degradation of Ethidium Bromide-DNA Complexes Using a Fluorescence Plate Reader. *Anal. Biochem.,* **2015**, Ahead of Print.

86. Sen, D.; Geyer, C. R., DNA Enzymes. *Curr. Opin.Chem.Biol.,* **1998**, *2*, 680-687.

87. Xu, W.; Lu, Y., Label-Free Fluorescent Aptamer Sensor Based on Regulation of Malachite Green Fluorescence. *Anal. Chem.,* **2009**, *82*, 574-578.

88. Li, N.; Mei, L.; Xiang, Y.; Tong, A.; Nishizawa, S.; Teramae, N., Fluorescence Detection of Single-Nucleotide Polymorphisms with Two Simple and Low Cost Methods: A Double-DNA-Probe Method and a Bulge Form Method. *Anal. Chim. Acta,* **2007**, *597,* 97-102.

89. Xiang, Y.; Wang, Z.; Xing, H.; Wong, N. Y.; Lu, Y., Label-Free Fluorescent Functional DNA Sensors Using Unmodified DNA: A Vacant Site Approach. *Anal. Chem.,* **2010**, *82*, 4122-4129.

90. Yang, C. J.; Jockusch, S.; Vicens, M.; Turro, N. J.; Tan, W., Light-Switching Excimer Probes for Rapid Protein Monitoring in Complex Biological Fluids. *Proc. Natl. Acad. Sci.,* **2005**, *102*, 17278-17283.

91. Corley, R. B., *A Guide to Methods in the Biomedical Sciences*. Springer: **2006**.

92. Warram, J. M.; de Boer, E.; Sorace, A. G.; Chung, T. K.; Kim, H.; Pleijhuis, R. G.; van Dam, G. M.; Rosenthal, E. L., Antibody-Based Imaging Strategies for Cancer. *Cancer Metastasis Rev.,* **2014**, *33*, 809-822.

93. Haab, B. B., Antibody Arrays in Cancer Research. *Mol. Cell. Proteomics*, **2005**, *4*, 377-383.

94. Ogawa, M.; Kosaka, N.; Longmire, M. R.; Urano, Y.; Choyke, P. L.; Kobayashi, H., Fluorophore-Quencher Based Activatable Targeted Optical Probes for Detecting in Vivo Cancer Metastases. *Mol. Pharmaceutics,* **2009**, *6*, 386-395.

95. Luo, S.; Zhang, E.; Su, Y.; Cheng, T.; Shi, C., A Review of Nir Dyes in Cancer Targeting and Imaging. *Biomaterials,* **2011**, *32*, 7127-7138.

96. Rosenthal, E. L.; Kulbersh, B. D.; Duncan, R. D.; Zhang, W.; Magnuson, J. S.; Carroll, W. R.; Zinn, K., In Vivo Detection of Head and Neck Cancer Orthotopic Xenografts by Immunofluorescence. *Laryngoscope,* **2006**, *116*, 1636-41.

97. Kaur, S.; Venktaraman, G.; Jain, M.; Senapati, S.; Garg, P. K.; Batra, S. K., Recent Trends in Antibody-Based Oncologic Imaging. *Cancer Lett.*, **2012**, *315*, 97-111.

98. Zou, P.; Xu, S.; Povoski, S. P.; Wang, A.; Johnson, M. A.; Martin, E. W.; Subramaniam, V.; Xu, R.; Sun, D., Near-Infrared Fluorescence Labeled Anti-Tag-72 Monoclonal Antibodies for Tumor Imaging in Colorectal Cancer Xenograft Mice. *Mol. Pharm.*, **2009**, *6*, 428-440.

99. Goesmann, H.; Feldmann, C., Nanoparticulate Functional Materials. *Angew. Chem., Int. Ed.*, **2010**, *49*, 1362-1395.

100. Ruedas-Rama, M. J.; Walters, J. D.; Orte, A.; Hall, E. A. H., Fluorescent Nanoparticles for Intracellular Sensing: A Review. *Anal.Chim.Acta.*, **2012**, *751*, 1-23.

101. Schmälzlin, E.; Van Dongen, J. T.; Klimant, I.; Marmodée, B.; Steup, M.; Fisahn, J.; Geigenberger, P.; Löhmannsröben, H. G., An Optical Multifrequency Phase-Modulation Method Using Microbeads for Measuring Intracellular Oxygen Concentrations in Plants. *Biophy. J.*, **2005**, *89*, 1339-1345.

102. Cao, Y.; Koo, Y. E. L.; Kopelman, R., Poly(Decyl Methacrylate)-Based Fluorescent Pebble Swarm Nanosensors for Measuring Dissolved Oxygen in Biosamples. *Analyst,* **2004**, *129*, 745-750.

103. Ruedas-Rama, M. J.; Hall, E. A. H., K+-Selective Nanospheres: Maximising Response Range and Minimising Response Time. *Analyst,* **2006**, *131*, 1282-1291.

104. Shi, H.; He, X.; Wang, K.; Yuan, Y.; Deng, K.; Chen, J.; Tan, W., Rhodamine B Isothiocyanate Doped Silica-Coated Fluorescent Nanoparticles (Rbitc-Dsfnps)-Based Bioprobes Conjugated to Annexin V for Apoptosis Detection and Imaging. *Nanomed. Nanotechnol. Biol. Med.*, **2007**, *3*, 266-272.

105. Yue, Z.; Lisdat, F.; Parak, W. J.; Hickey, S. G.; Tu, L.; Sabir, N.; Dorfs, D.; Bigall, N. C., Quantum-Dot-Based Photoelectrochemical Sensors for Chemical and Biological Detection. *ACS Appl. Mater. Interfaces*, **2013**, *5*, 2800-2814.

106. Medintz, I. L.; Stewart, M. H.; Trammell, S. A.; Susumu, K.; Delehanty, J. B.; Mei, B. C.; Melinger, J. S.; Blanco-Canosa, J. B.; Dawson, P. E.; Mattoussi, H., Quantum-Dot/Dopamine Bioconjugates Function as Redox Coupled Assemblies for in Vitro and Intracellular Ph Sensing. *Nat. Mat.*, **2010**, *9*, 676-684.

107. Wu, Y.; Chu, M.; Shi, B.; Li, Z., A Novel Magneto-Fluorescent Nano-Bioprobe for Cancer Cell Targeting, Imaging and Collection. *Appl. Biochem. Biotechnol.*, **2011**, *163*, 813-825.

108. Wen, Q.; Gu, Y.; Tang, L.-J.; Yu, R.-Q.; Jiang, J.-H., Peptide-Templated Gold Nanocluster Beacon as a Sensitive, Label-Free Sensor for Protein Post-Translational Modification Enzymes. *Anal. Chem.*, **2013**, *85*, 11681-11685.

109. Gu, Y.; Wen, Q.; Kuang, Y.; Tang, L.; Jiang, J., Peptide-Templated Gold Nanoclusters as a Novel Label-Free Biosensor for the Detection of Protease Activity. *RSC Adv.*, **2014**, *4*, 13753-13756.

110. Chen, L.-Y.; Wang, C.-W.; Yuan, Z.; Chang, H.-T., Fluorescent Gold Nanoclusters: Recent Advances in Sensing and Imaging. *Anal. Chem.*, **2014**, *87*, 216-229.

111. Kim, S.; Lim, Y. T.; Soltesz, E. G.; De Grand, A. M.; Lee, J.; Nakayama, A.; Parker, J. A.; Mihaljevic, T.; Laurence, R. G.; Dor, D. M.; Cohn, L. H.; Bawendi, M. G.; Frangioni, J. V., Near-Infrared Fluorescent Type Ii Quantum Dots for Sentinel Lymph Node Mapping. *Nat. Biotechnol.*, **2004**, *22*, 93-97.

112. Yong, K.-T.; Roy, I.; Ding, H.; Bergey, E. J.; Prasad, P. N., Biocompatible near-Infrared Quantum Dots as Ultrasensitive Probes for Long-Term in Vivo Imaging Applications. *Small*, **2009**, *5*, 1997-2004.

113. Choi, H. S.; Liu, W.; Misra, P.; Tanaka, E.; Zimmer, J. P.; Ipe, B. I.; Bawendi, M. G.; Frangioni, J. V., Renal Clearance of Quantum Dots. *Nat. Biotechnol.*, **2007**, *25*, 1165-1170.

114. Salvati, A.; Pitek, A. S.; Monopoli, M. P.; Prapainop, K.; Bombelli, F. B.; Hristov, D. R.; Kelly, P. M.; Aberg, C.; Mahon, E.; Dawson, K. A., Transferrin-Functionalized Nanoparticles Lose Their Targeting Capabilities When a Biomolecule Corona Adsorbs on the Surface. *Nat. Nanotechnol.*, **2013**, *8*, 137-143.

115. Petit, J.-M.; Denis-Gay, M.; Ratinaud, M.-H., Assessment of Fluorochromes for Cellular Structure and Function Studies by Flow Cytometry. *Biol. Cell.*, **1993**, *78*, 1-13.

116. Waggoner, A., [15] Covalent Labeling of Proteins and Nucleic Acids with Fluorophores. In *Methods in Enzymology*, Kenneth, S., Ed. Academic Press: **1995**; Vol. Volume 246, pp 362-373.

117. Frangioni, J. V., In Vivo near-Infrared Fluorescence Imaging. *Curr. Opini. Chem. Biol.,* **2003**, *7*, 626-634.

118. Lavis, L. D.; Raines, R. T., Bright Ideas for Chemical Biology. *ACS Chem. Biol.,* **2008**, *3*, 142-155.

119. Reinert, K. C.; Dunbar, R. L.; Gao, W.; Chen, G.; Ebner, T. J., Flavoprotein Autofluorescence Imaging of Neuronal Activation in the Cerebellar Cortex in Vivo. *J. Neurophysiol.,* **2004**, *92*, 199-211.

120. Eng, J.; Lynch, R. M.; Balaban, R. S., Nicotinamide Adenine Dinucleotide Fluorescence Spectroscopy and Imaging of Isolated Cardiac Myocytes. *Biophys. J.,* **1989**, *55*, 621-30.

121. Brookner, C. K.; Follen, M.; Boiko, I.; Galvan, J.; Thomsen, S.; Malpica, A.; Suzuki, S.; Lotan, R.; Richards-Kortum, R., Autofluorescence Patterns in Short-Term Cultures of Normal Cervical Tissue. *Photochem. Photobiol.,* **2000**, *71*, 730-736.

122. Tian, R.; Li, M.; Wang, J.; Yu, M.; Kong, X.; Feng, Y.; Chen, Z.; Li, Y.; Huang, W.; Wu, W.; Hong, Z., An Intracellularly Activatable, Fluorogenic Probe for Cancer Imaging. *Org. Biomol. Chem.,* **2014**, *12*, 5365-5374.

123. Terai, T.; Nagano, T., Small-Molecule Fluorophores and Fluorescent Probes for Bioimaging. *Euro. J. Physiol.,* **2013**, *465*, 347-359.

124. Kobayashi, H.; Ogawa, M.; Alford, R.; Choyke, P. L.; Urano, Y., New Strategies for Fluorescent Probe Design in Medical Diagnostic Imaging. *Chem. Rev.,* **2010**, *110*, 2620-2640.

125. Terai, T.; Nagano, T., Fluorescent Probes for Bioimaging Applications. *Curr. Opin. Chem. Biol.,* **2008**, *12*, 515-521.

126. Teles, F. R. R., Fonseca, L. P., Th E Contribution of Smart Materials Andadvanced Clinical Diagnostic Micro Devices on the Progress and Improvement of Human Health Care. In *Adv. Healthc. Mater.,* Tiwari, A., Ed. Scrivener Publishing LLC: **2014**; pp 203-236.

127. Sharma, B.; Singh, S.; Siddiqi, N. J., Biomedical Implications of Heavy Metals Induced Imbalances in Redox Systems. *BioMed Res. Int.,* **2014**, 640754/1-640754/27, 27 pp.

128. Carter, K. P.; Young, A. M.; Palmer, A. E., Fluorescent Sensors for Measuring Metal Ions in Living Systems. *Chem. Rev.*, **2014**, *114*, 4564-4601.

129. Guo, Z. Q.; Park, S.; Yoon, J.; Shin, I., Recent Progress in the Development of near-Infrared Fluorescent Probes for Bioimaging Applications. *Chem. Soc. Rev.*, **2014**, *43*, 16-29.

130. Cao, J.; Zhao, C.; Wang, X.; Zhang, Y.; Zhu, W., Target-Triggered Deprotonation of 6-Hydroxyindole-Based Bodipy: Specially Switch on Nir Fluorescence Upon Selectively Binding to Zn2+. *Chem. Commn.*, **2012**, *48*, 9897-9899.

131. Li, P.; Duan, X.; Chen, Z.; Liu, Y.; Xie, T.; Fang, L.; Li, X.; Yin, M.; Tang, B., A near-Infrared Fluorescent Probe for Detecting Copper(Ii) with High Selectivity and Sensitivity and Its Biological Imaging Applications. *Chem. Commun.*, **2011**, *47*, 7755-7757.

132. Guo, Z.; Zhu, W.; Zhu, M.; Wu, X.; Tian, H., Near-Infrared Cell-Permeable Hg2+-Selective Ratiometric Fluorescent Chemodosimeters and Fast Indicator Paper for Mehg+ Based on Tricarbocyanines. *Chem. A Euro. J.*, **2010**, *16*, 14424-14432.

133. Guo, Z.; Park, S.; Yoon, J.; Shin, I., Recent Progress in the Development of near-Infrared Fluorescent Probes for Bioimaging Applications. *Chem. Soc. Rev.*, **2014**, *43*, 16-29.

134. Lee, H.; Akers, W.; Bhushan, K.; Bloch, S.; Sudlow, G.; Tang, R.; Achilefu, S., Near-Infrared Ph-Activatable Fluorescent Probes for Imaging Primary and Metastatic Breast Tumors. *Bioconjugate Chem.*, **2011**, *22*, 777-784.

135. Myochin, T.; Kiyose, K.; Hanaoka, K.; Kojima, H.; Terai, T.; Nagano, T., Rational Design of Ratiometric near-Infrared Fluorescent Ph Probes with Various Pka Values, Based on Aminocyanine. *J. Am. Chem. Soc.*, **2011**, *133*, 3401-3409.

136. Zhang, W.; Ma, Z.; Du, L.; Li, M., Design Strategy for Photoinduced Electron Transfer-Based Small-Molecule Fluorescent Probes of Biomacromolecules. *Analyst*, **2014**, *139*, 2641-2649.

137. Kobayashi, H.; Choyke, P. L., Target-Cancer-Cell-Specific Activatable Fluorescence Imaging Probes: Rational Design and in Vivo Applications. *Acc. Chem. Res.*, **2011**, *44*, 83-90.

138. Fujikawa, Y.; Urano, Y.; Komatsu, T.; Hanaoka, K.; Kojima, H.; Terai, T.; Inoue, H.; Nagano, T., Design and Synthesis of Highly Sensitive Fluorogenic Substrates for Glutathione S-Transferase and Application for Activity Imaging in Living Cells. *J. Am. Chem. Soc.*, **2008**, *130*, 14533-14543.

139. Armstrong, R. N., Structure, Catalytic Mechanism, and Evolution of the Glutathione Transferases. *Chem. Res. Toxicol.*, **1997**, *10*, 2-18.

140. Hayes, J. D.; Flanagan, J. U.; Jowsey, I. R., Glutathione Transferases. *Annu. Rev. Pharmacol. Toxicol.*, **2005**, *45*, 51-88, 1 plate.

141. Zhang, H.; Fan, J.; Wang, J.; Zhang, S.; Dou, B.; Peng, X., An Off-on Cox-2-Specific Fluorescent Probe: Targeting the Golgi Apparatus of Cancer Cells. *J. Am. Chem. Soc.*, **2013**, *135*, 11663-11669.

142. Dubois, R. N.; Abramson, S. B.; Crofford, L.; Gupta, R. A.; Simon, L. S.; A. Van De Putte, L. B.; Lipsky, P. E., Cyclooxygenase in Biology and Disease. *FASEB J.*, **1998**, *12*, 1063-1073.

143. Fitzpatrick, F. A., Cyclooxygenase Enzymes: Regulation and Function. *Curr. Pharm. Des.*, **2004**, *10*, 577-588.

144. Nolan, K. A.; Scott, K. A.; Barnes, J.; Doncaster, J.; Whitehead, R. C.; Stratford, I. J., Pharmacological Inhibitors of Nad(P)H Quinone Oxidoreductase, Nqo1: Structure/Activity Relationships and Functional Activity in Tumour Cells. *Biochem. Pharmacol.*, **2010**, *80*, 977-981.

145. Scott, K. A.; Barnes, J.; Whitehead, R. C.; Stratford, I. J.; Nolan, K. A., Inhibitors of Nqo1: Identification of Compounds More Potent Than Dicoumarol without Associated Off-Target Effects. *Biochem. Pharmacol.*, **2011**, *81*, 355-363.

146. Silvers, W. C.; Prasai, B.; Burk, D. H.; Brown, M. L.; McCarley, R. L., Profluorogenic Reductase Substrate for Rapid, Selective, and Sensitive Visualization and Detection of Human Cancer Cells That Overexpress Nqo1. *J. Am. Chem. Soc.*, **2013**, *135*, 309-14.

147. Hettiarachchi, S. U.; Prasai, B.; McCarley, R. L., Detection and Cellular Imaging of Human Cancer Enzyme Using a Turn-on, Wavelength-Shiftable, Self-Immolative Profluorophore. *J.Am. Chem. Soc.*, **2014**, *136*, 7575-7578.

148. Nolan, G. P.; Fiering, S.; Nicolas, J. F.; Herzenberg, L. A., Fluorescence-Activated Cell Analysis and Sorting of Viable Mammalian Cells Based on B-D-Galactosidase Activity after Transduction of Escherichia Coli Lacz. *Proc. Natl. Acad. Sci.*, **1988**, *85*, 2603-7.

149. Chilvers, K. F.; Perry, J. D.; James, A. L.; Reed, R. H., Synthesis and Evaluation of Novel Fluorogenic Substrates for the Detection of Bacterial B-Galactosidase. *J. Appl. Microbiol.*, **2001**, *91*, 1118-1130.

150. Urano, Y.; Kamiya, M.; Kanda, K.; Ueno, T.; Hirose, K.; Nagano, T., Evolution of Fluorescein as a Platform for Finely Tunable Fluorescence Probes. *J. Am. Chem. Soc.*, **2005**, *127*, 4888-4894.

151. Lee, H. W.; Heo, C. H.; Sen, D.; Byun, H.-O.; Kwak, I. H.; Yoon, G.; Kim, H. M., Ratiometric Two-Photon Fluorescent Probe for Quantitative Detection of B-Galactosidase Activity in Senescent Cells. *Anal. Chem.*, **2014**, *86*, 10001-10005.

152. Manjare, S. T.; Kim, Y.; Churchill, D. G., Selenium- and Tellurium-Containing Fluorescent Molecular Probes for the Detection of Biologically Important Analytes. *Acc. Chem. Res.*, **2014**, *47*, 2985-2998.

153. Karton-Lifshin, N.; Segal, E.; Omer, L.; Portnoy, M.; Satchi-Fainaro, R.; Shabat, D., A Unique Paradigm for a Turn-on near-Infrared Cyanine-Based Probe: Noninvasive Intravital Optical Imaging of Hydrogen Peroxide. *J. Am. Chem. Soc.*, **2011**, *133*, 10960-10965.

154. Albers, A. E.; Okreglak, V. S.; Chang, C. J., A Fret-Based Approach to Ratiometric Fluorescence Detection of Hydrogen Peroxide. *J. Am. Chem. Soc.*, **2006**, *128*, 9640-9641.

155. Chen, X.; Tian, X.; Shin, I.; Yoon, J., Fluorescent and Luminescent Probes for Detection of Reactive Oxygen and Nitrogen Species. *Chem. Soc. Rev.*, **2011**, *40*, 4783-4804.

156. Srikun, D.; Miller, E. W.; Domaille, D. W.; Chang, C. J., An Ict-Based Approach to Ratiometric Fluorescence Imaging of Hydrogen Peroxide Produced in Living Cells. *J. Am. Chem. Soc.*, **2008**, *130*, 4596-4597.

157. Sun, Z.-N.; Wang, H.-L.; Liu, F.-Q.; Chen, Y.; Tam, P. K. H.; Yang, D., Bodipy-Based Fluorescent Probe for Peroxynitrite Detection and Imaging in Living Cells. *Org. Lett.*, **2009**, *11*, 1887-1890.

158. Li, P.; Xie, T.; Duan, X.; Yu, F.; Wang, X.; Tang, B., A New Highly Selective and Sensitive Assay for Fluorescence Imaging Of .Oh in Living Cells: Effectively Avoiding the Interference of Peroxynitrite. *Chem. Eur. J.*, **2010**, *16*, 1834-1840, S1834/1-S1834/4.

159. Mertz, E. L.; Leikin, S., Interactions of Inorganic Phosphate and Sulfate Anions with Collagen. *Biochemistry*, **2004**, *43*, 14901-14912.

160. Nemeth-Csoka, M.; Tasnadi, G., The Effect of Inorganic Pyrophosphate (Ppi) Anions on the in Vitro Collagen Fibril Formation. *Exp. Pathol.*, **1981**, *20*, 58-63.

161. Zhu, W.; Huang, X.; Guo, Z.; Wu, X.; Yu, H.; Tian, H., A Novel Nir Fluorescent Turn-on Sensor for the Detection of Pyrophosphate Anion in Complete Water System. *Chem. Commun.*, **2012**, *48*, 1784-1786.

162. Santa, T., Recent Advances in Analysis of Glutathione in Biological Samples by High-Performance Liquid Chromatography: A Brief Overview. *Drug. Discov. Ther.*, **2013**, *7*, 172-177.

163. Hansen, R. E.; Roth, D.; Winther, J. R., Quantifying the Global Cellular Thiol–Disulfide Status. *Proc. Nat. Acad. Sci.*, **2009**, *106*, 422-427.

164. Eksin, E.; Erdem, A., Electrochemical Determination of Homocysteine at Disposable Graphite Electrodes. *Electroanalysis*, **2014**, *26*, 1945-1951.

165. Khan, A.; Khan, M. I.; Iqbal, Z.; Shah, Y.; Ahmad, L.; Nazir, S.; Watson, D. G.; Khan, J. A.; Nasir, F.; Khan, A.; Ismail, A New Hplc Method for the Simultaneous Determination of Ascorbic Acid and Aminothiols in Human Plasma and Erythrocytes Using Electrochemical Detection. *Talanta*, **2011**, *84*, 789-801.

166. D'Eramo, J. L.; Finkelstein, A.; Boccazzi, F.; Fridman, O., Total Homocysteine Levels in Plasma: High-Performance Liquid Chromatographic Determination with Electrochemical Detection and Glassy Carbon Electrode. *J. Chromatogr. B.*, **1998**, *720*, 205-210.

167. Inoue, T.; Kirchhoff, J. R., Determination of Thiols by Capillary Electrophoresis with Amperometric Detection at a Coenzyme Pyrroloquinoline Quinone Modified Electrode. *Anal. Chem.*, **2002**, *74*, 1349-1354.

168. Kubalczyk, P.; Bald, E.; Furmaniak, P.; Glowacki, R., Simultaneous Determination of Total Homocysteine and Cysteine in Human Plasma by Capillary Zone Electrophoresis with Ph-Mediated Sample Stacking. *Anal. Methods.*. **2014**, *6*, 4138-4143.

169. Wu, J. F.; Xu, K. R.; Landers, J. P.; Weber, S. G., An in Situ Measurement of Extracellular Cysteamine, Homocysteine, and Cysteine Concentrations in Organotypic Hippocampal Slice Cultures by Integration of Electroosmotic Sampling and Microfluidic Analysis. *Anal. Chem.*, **2013**, *85*, 3095-3103.

170. Wang, W.; Li, L.; Liu, S.; Ma, C.; Zhang, S., Determination of Physiological Thiols by Electrochemical Detection with Piazselenole and Its Application in Rat Breast Cancer Cells 4t-1. *J.Am.Chem.Soc.*, **2008**, *130*, 10846-10847.

171. Inoue, T.; Kirchhoff, J. R., Electrochemical Detection of Thiols with a Coenzyme Pyrroloquinoline Quinone Modified Electrode. *Anal. Chem.*, **2000**, *72*, 5755-5760.

172. Moore, R. R.; Banks, C. E.; Compton, R. G., Electrocatalytic Detection of Thiols Using an Edge Plane Pyrolytic Graphite Electrode. *Analyst*, **2004**, *129*, 755-758.

173. Vellasco, A. P.; Haddad, R.; Eberlin, M. N.; Hoeehr, N. F., Combined Cysteine and Homocysteine Quantitation in Plasma by Trap and Release Membrane Introduction Mass Spectrometry. *Analyst,* **2002**, *127*, 1050-1053.

174. Rafii, M.; Elango, R.; Courtney-Martin, G.; House, J. D.; Fisher, L.; Pencharz, P. B., High-Throughput and Simultaneous Measurement of Homocysteine and Cysteine in Human Plasma and Urine by Liquid Chromatography-Electrospray Tandem Mass Spectrometry. *Anal. Biochem.,* **2007**, *371*, 71-81.

175. Sass, J. O.; Endres, W., Quantitation of Total Homocysteine in Human Plasma by Derivatization to Its N(O,S)-Propoxycarbonyl Propyl Ester and Gas Chromatography-Mass Spectrometry Analysis. *J. Chromatogr. A,* **1997**, *776*, 342-347.

176. Chen, X.; Zhou, Y.; Peng, X.; Yoon, J., Fluorescent and Colorimetric Probes for Detection of Thiols. *Chem. Soc. Rev.,* **2010**, *39*, 2120-2135.

177. Rhieu, S. Y.; Urbas, A. A.; Lippa, K. A.; Reipa, V., Quantitative Measurements of Glutathione in Yeast Cell Lysate Using 1h Nmr. *Anal. Bioanal. Chem.,* **2013**, *405*, 4963-4968.

178. Monostori, P.; Wittmann, G.; Karg, E.; Turi, S., Determination of Glutathione and Glutathione Disulfide in Biological Samples: An in-Depth Review. *J. Chromatogr. B: Anal. Technol. Biomed. Life Sci.,* **2009**, *877*, 3331-3346.

179. Potapenko, D. I.; Bagryanskaya, E. G.; Grigoriev, I. A.; Maksimov, A. M.; Reznikov, V. A.; Platonov, V. E.; Clanton, T. L.; Khramtsov, V. V., Quantitative Determination of Sh Groups Using 19f Nmr Spectroscopy and Disulfide of 2,3,5,6-Tetrafluoro-4-Mercaptobenzoic Acid. *Magn. Reson. Chem.,* **2005**, *43*, 902-909.

180. Kennett, E. C.; Bubb, W. A.; Bansal, P.; Alewood, P.; Kuchel, P. W., Nmr Studies of Exchange between Intra- and Extracellular Glutathione in Human Erythrocytes. *Redox Rep.,* **2005**, *10*, 83-90.

181. Jung, H. S.; Chen, X.; Kim, J. S.; Yoon, J., Recent Progress in Luminescent and Colorimetric Chemosensors for Detection of Thiols. *Chem. Soc. Rev.,* **2013**, *42*, 6019-31.

182. Kand, D.; Kalle, A. M.; Varma, S. J.; Talukdar, P., A Chromenoquinoline-Based Fluorescent Off-Onthiol Probe for Bioimaging. *Chem. Commun.,* **2012**, *48*, 2722-2724.

183. Jung, H. S.; Ko, K. C.; Kim, G.-H.; Lee, A.-R.; Na, Y.-C.; Kang, C.; Lee, J. Y.; Kim, J. S., Coumarin-Based Thiol Chemosensor: Synthesis, Turn-on Mechanism, and Its Biological Application. *Org. Lett.,* **2011**, *13*, 1498-1501.

184. Sun, Y.-Q.; Chen, M.; Liu, J.; Lv, X.; Li, J.-f.; Guo, W., Nitroolefin-Based Coumarin as a Colorimetric and Fluorescent Dual Probe for Biothiols. *Chem. Commun.*, **2011**, *47*, 11029-11031.

185. Hu, M.; Fan, J.; Li, H.; Song, K.; Wang, S.; Cheng, G.; Peng, X., Fluorescent Chemodosimeter for Cys/Hcy with a Large Absorption Shift and Imaging in Living Cells. *Org. Biomol. Chem.*, **2011**, *9*, 980-3.

186. Wang, P.; Liu, J.; Lv, X.; Liu, Y.; Zhao, Y.; Guo, W., A Naphthalimide-Based Glyoxal Hydrazone for Selective Fluorescence Turn-on Sensing of Cys and Hcy. *Org. Lett.*, **2012**, *14*, 520-523.

187. Yang, X.; Guo, Y.; Strongin, R. M., Conjugate Addition/Cyclization Sequence Enables Selective and Simultaneous Fluorescence Detection of Cysteine and Homocysteine. *Angew. Chem. Int. Ed.*, **2011**, *50*, 10690-3.

188. Wang, H.; Zhou, G.; Gai, H.; Chen, X., A Fluorescein-Based Probe with High Selectivity to Cysteine over Homocysteine and Glutathione. *Chem. Commun.*, **2012**, *48*, 8341-8343.

189. Ji, S.; Guo, H.; Yuan, X.; Li, X.; Ding, H.; Gao, P.; Zhao, C.; Wu, W.; Wu, W.; Zhao, J., A Highly Selective Off-on Red-Emitting Phosphorescent Thiol Probe with Large Stokes Shift and Long Luminescent Lifetime. *Org. Lett.*, **2010**, *12*, 2876-2879.

190. Yuan, L.; Lin, W.; Zhao, S.; Gao, W.; Chen, B.; He, L.; Zhu, S., A Unique Approach to Development of near-Infrared Fluorescent Sensors for in Vivo Imaging. *J. Am. Chem. Soc.*, **2012**, *134*, 13510-23.

191. Niu, L. Y.; Guan, Y. S.; Chen, Y. Z.; Wu, L. Z.; Tung, C. H.; Yang, Q. Z., Bodipy-Based Ratiometric Fluorescent Sensor for Highly Selective Detection of Glutathione over Cysteine and Homocysteine. *J. Am. Chem. Soc.*, **2012**, *134*, 18928-31.

192. Li, Y.; Yang, Y.; Guan, X., Benzofurazan Sulfides for Thiol Imaging and Quantification in Live Cells through Fluorescence Microscopy. *Anal. Chem.*, **2012**, *84*, 6877-6883.

193. Lee, J. H.; Lim, C. S.; Tian, Y. S.; Han, J. H.; Cho, B. R., A Two-Photon Fluorescent Probe for Thiols in Live Cells and Tissues. *J. Am. Chem. Soc.*, **2010**, *132*, 1216-7.

194. Lee, M. H.; Han, J. H.; Kwon, P.-S.; Bhuniya, S.; Kim, J. Y.; Sessler, J. L.; Kang, C.; Kim, J. S., Hepatocyte-Targeting Single Galactose-Appended Naphthalimide: A Tool for Intracellular Thiol Imaging in Vivo. *J. Am. Chem. Soc.*, **2011**, *134*, 1316-1322.

195. Long, L.; Zhou, L.; Wang, L.; Meng, S.; Gong, A.; Du, F.; Zhang, C., A Coumarin-Based Fluorescent Probe for Biological Thiols and Its Application for Living Cell Imaging. *Org. Biomol. Chem.*, **2013**, *11*, 8214-8220.

196. Kim, G.-J.; Lee, K.; Kwon, H.; Kim, H.-J., Ratiometric Fluorescence Imaging of Cellular Glutathione. *Org. Lett.*, **2011**, *13*, 2799-2801.

197. Lim, C. S.; Masanta, G.; Kim, H. J.; Han, J. H.; Kim, H. M.; Cho, B. R., Ratiometric Detection of Mitochondrial Thiols with a Two-Photon Fluorescent Probe. *J. Am. Chem. Soc.*, **2011**, *133*, 11132-11135.

198. Guo, X.-F.; Chen, J.-B.; Wang, H.; Zhang, H.-S.; Huang, W.-H.; Guo, J., Real-Time and in-Situ Cell Imaging of Thiol Compounds in Living Cells Using Maleimide Bodipy Labeling. *Talanta*, **2012**, *99*, 1046-1050.

CHAPTER 2
KINETICS OF A REDOX-ACTIVE TRIGGER SYSTEM AS AN ACTIVATABLE GROUP FOR CARGO RELEASE

2.1 Introduction

Target–selective delivery of biologically active compounds is becoming an increasingly important tool in the diagnosis and treatment of diseases, such as cancer.[1-2] These types of selective delivery systems are particularly significant in delivery of prodrugs and selective detection of analytes at a specific target site.[3] These systems are designed in a way that the activity of a select group of compounds is masked by chemically connecting them together, and upon chemical disintegration from each other at a select target site, they provide a different chemical outcome. For example, during chemotherapeutic treatments, delivery of therapeutic parent drugs as prodrugs can offer numerous advantages over their traditional counterparts.[4] Inactive prodrugs can be tailored to be site-specifically activated to release the active drug so as to exert its biological function at the target site. This will result in higher therapeutic efficacy, as well as reduced side effects.[3, 5-6] To achieve targeted delivery, it is often required to link a specific chemical or biological reactive group to target molecules that control the activity of the system.[7-8] These systems can be designed by either directly attaching the trigger (activatable molecule) to a target molecule (Figure 2.1a) or having a linker in between to form a three-component (tripartite) system (Figure 2.1b).[9]

Three-component delivery systems generally consist of a trigger, a linker, and a targeted delivery molecule.[9] The three functionalities of such a tripartite system are illustrated in Figure 2.1b, and can be used as follows: first the system contains the trigger molecule which is responsible for the site specific activation in the presence of a specific analyte such as an enzyme;[10] second the linker in between facilitates the attachment of target molecule to active trigger. When a corresponding analyte activates the trigger, such activation will result in spontaneous reaction that releases the active molecule from the target moiety.[9]

There are two different mechanisms that are used in active delivery systems. The first one is based on a spontaneous intra-cyclization reaction to form a stable cyclic molecule. The cleavage of the activated trigger molecule generates a free nucleophilic center which will undergo an intra-cyclization to release the target molecule from the linker.[11] The second reported method in

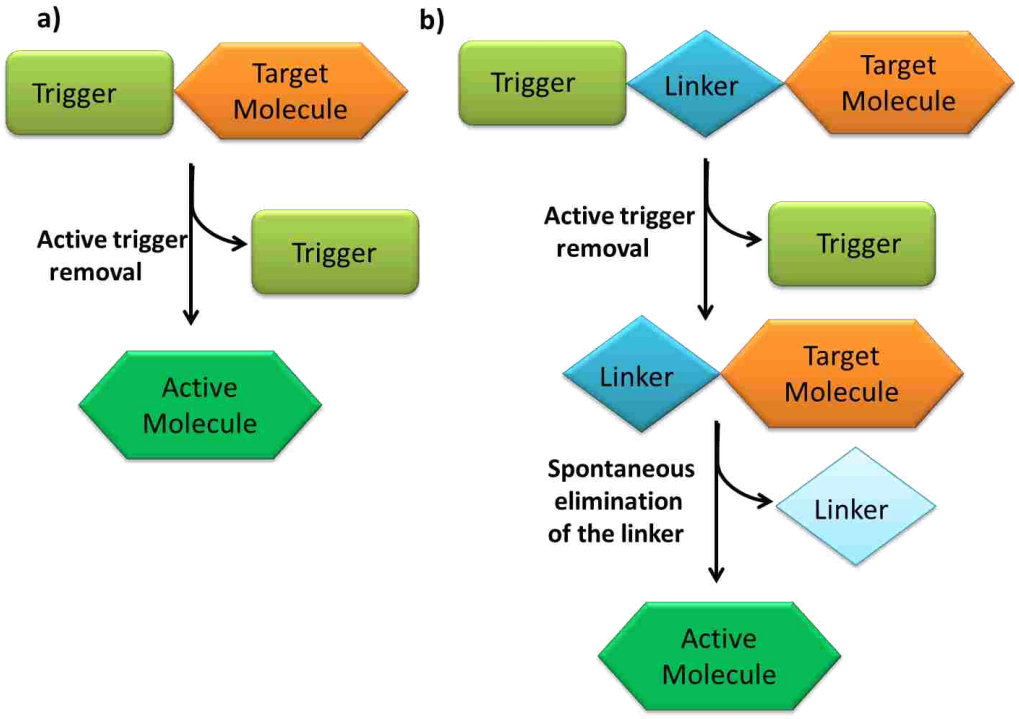

Figure 2.1 Schematic representation of design strategies used for delivery systems.

the literature is elimination based on quinone methide formation. Similar to the first system, cleavage of the trigger generates a free phenol or amine functionality that subsequently undergoes a self-immolative reaction via quinone methide rearrangement[7, 9, 12-13] to release the target molecule. As demonstrated in Figure 2.2, the elimination reactions of substituted aniline or phenol could take place via two routes. Removal of the substrate from compound 1 and 2 leads to the formation of compound 1a and 2a respectively.

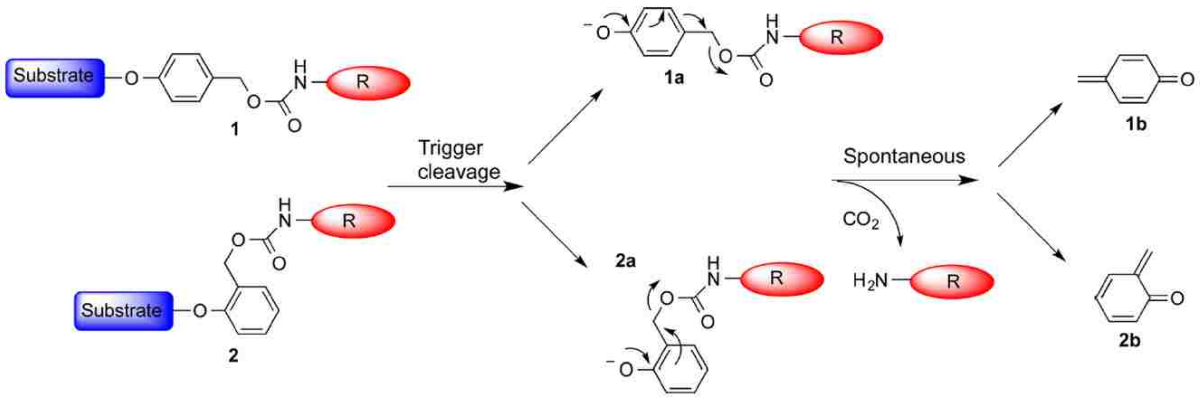

Figure 2.2 *p*-quinone methide vs *o*-quinone methide elimination mechanism.[7]

Depending on the position of the attached substrate, *o*– or *p*– quinone methide will be formed during the elimination process. Compound 1a undergoes 1,6-elimination to release the activated molecule (R) and *p*-quinone methide 1b; compound 2a undergoes 1,4 elimination to release the activated molecule (R) and *o*-quinone methide 2b.[7] The released end group (R) could be a variety of activated molecules such as a chromogenic molecule,[14-15] polymeric substance,[16-17] or a drug molecule,[18-19] depending on the purpose of the designed system. According to literature, depending on the position of the quinone methide formation, the elimination kinetics and the rate will vary.[20]

Over the past 20 years, numerous methods have been developed to address the issues related to drug encapsulation, retention, and stability of liposomal formulations. There is great attention in the science community to develop trigger systems that can control the release of contents from inside liposomes.[21-22] Mainly, the stimulus to release the drug should be specific to the target site, and the liposome must be sensitive enough to the trigger signal to yield effective release.[23-24] Therefore in an effort to invent an effective release system for liposomes,[25-26] a novel, reactive hydroxymethyl benzoquione (HMBQ)[27] group was utilized as a possible trigger for activated delivery of attached cargo. A hydroxmethyl benzoquinone (HMBQ) modified 1,2-dioleoyl-*sn*-glycero-3-phosphoethanolamine (DOPE) was synthesized to determine the ability of HMBQ-DOPE to act as a possible redox activated trigger group for liposomal drug delivery. As shown in Figure 2.3, upon applying a reductive stimulus, the reduction of the quinone moiety forms the hydroquinone.

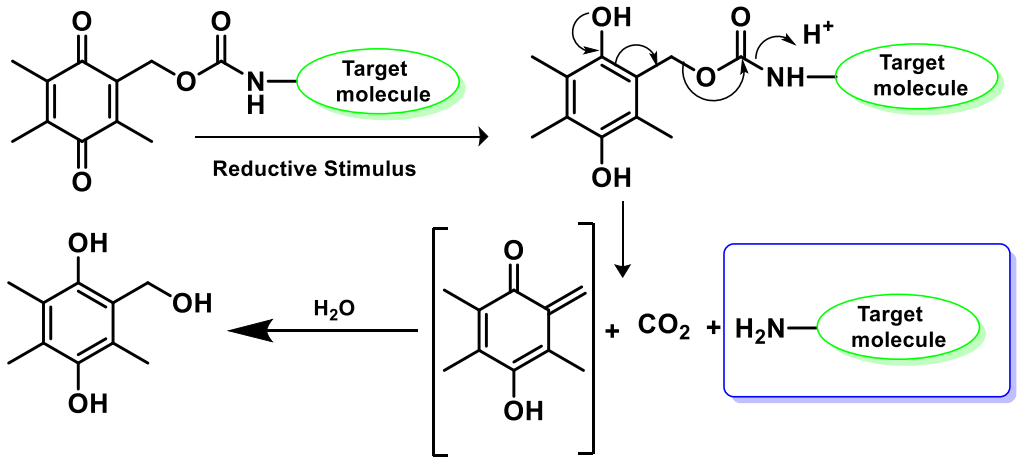

Figure 2.3 Activation mechanism of HMBQ with quinone methide formation and release of the target molecule.

The hydroquinone formed will undergo a rapid rearrangement to generate the *ortho*-quinone methide and the free target molecule, with concomitant formation of CO_2 gas. Adopting this rearrangement strategy (Figure 2.3), calcein dye-encapsulated HMBQ-DOPE liposomes were synthesized. When the HMBQ head groups are removed from the DOPE lipids, it is expected that the liposome will then undergo a conformational change from a stable lamellar phase to an unstable hexagonal phase causing the release of the encapsulated calcein dye.[28] The release of the highly fluorescent calcein dye can be monitored using fluorescence spectroscopy.

Then as the second part of this work, the *para*-nitroaniline derivative of HMBQ (HMBQ-Npc) was synthesized as a model compound to determine the release mechanism of Npc and the kinetics of quinone methide formation. In this system, HMBQ was connected to *para*-nitroaniline via a carbamate linkage to form HMBQ-Npc. HMBQ-Npc was expected to undergo a similar mechanism to that described in Figure 2.3, wherein there is release of the free *para*-nitroaniline reporter moiety and quinone methide. Using the absorbance spectral changes of the HMBQ-Npc/*p*-nitroaniline system, the kinetics of the self-immolative system can be determined.

2.2 Experimental

2.2.1 Synthetic Material and Methods

All the column purifications were performed using SNAP silica columns on a Flashmaster Personal from Biotage. Chemicals were purchased from Sigma-Aldrich or Fisher Scientific. Thin-layer chromatography was performed on aluminium-backed 60 F_{254} silica plates from EMD Chemicals Incorporated. ^{1}H NMR and ^{13}C NMR spectra were collected in chloroform-*d* or DMSO-d_6 at 25 $^{\circ}C$ on a Bruker AV-400 Spectrometer. Chemical shifts are reported in the standard δ notation of parts per million, using tetramethylsilane (TMS) as an internal reference. Absorption bands in NMR spectra are listed as singlet (s), doublet (d), triplet (t), or multiplet (m), and the coupling constants *J* are expressed in hertz (Hz). Mass spectral analyses were carried out using an Agilent 6210 ESI-TOFMS. All the solutions were prepared using Nanopure water from a Barnstead Diamond Nanopure Water System (18 MΩ-cm).

2.2.2 Synthesis

Hydroxymethylbenzoquinone (HMBQ), HMBQ-DOPE and HMBQ-Npc were synthesized by adapting literature methods. Synthesis schemes for HMBQ,[27] HMBQ-DOPE,[28-29] and HMBQ-Npc[30] are shown in Scheme 2.1, Scheme 2.2 and Scheme 2.3, respectively.

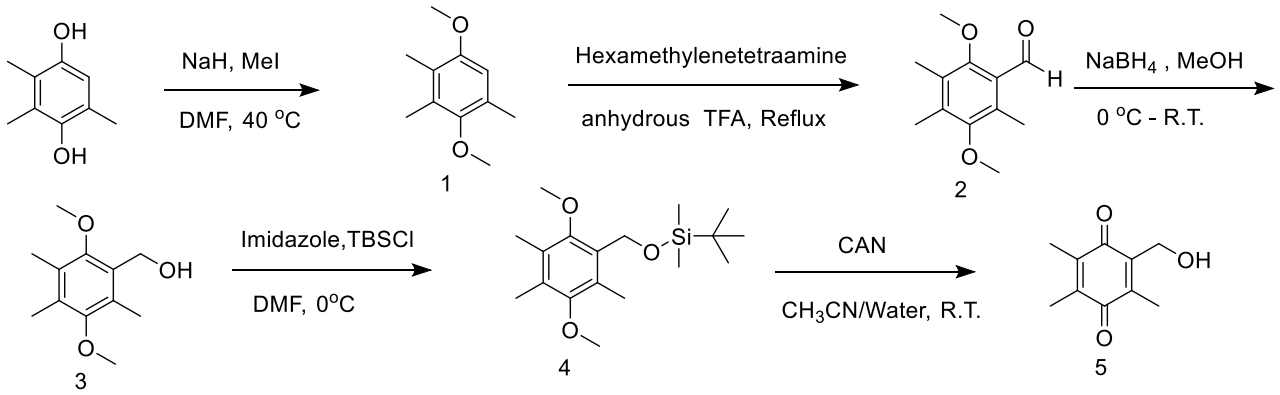

Scheme 2.1 Synthesis of HMBQ

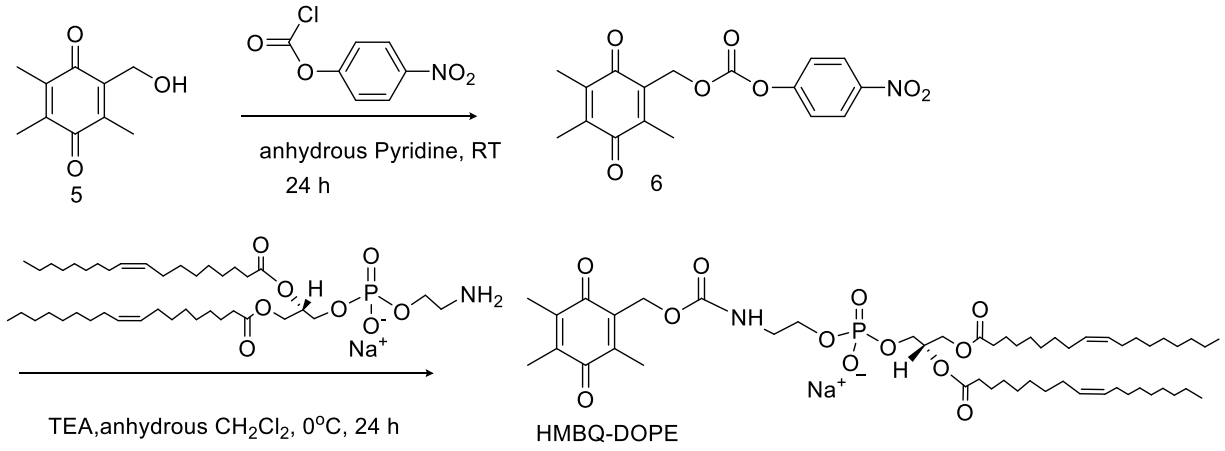

Scheme 2.2 Synthesis of HMBQ-DOPE

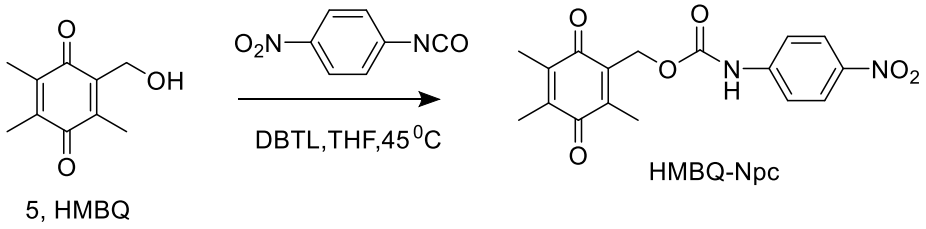

Scheme 2.3 Synthesis of HMBQ-Npc

1,4-Dimethoxy-3,5,6-trimethyl benzene (1)

In a dry, three–neck flask equipped with a condenser and a magnetic stirring bar under argon environment, sodium hydride (0.87 g, 36.14 mmol) was dissolved in a small amount of dry DMF (10 mL), and 2,3,5-trimethylhydroquinone (2.50 g, 16.43 mmol) was added in small portions (dissolved in dry DMF) over 15–20 min using an addition funnel. After evolution of H_2 gas had ceased, methyl iodide (4.1 mL, 65.72 mmol) was added dropwise over 15–20 min using an addition funnel. When the addition was finished, the reaction mixture was stirred at 40 $^{\circ}$C for 6 h. Brine (200 mL) was added to the flask, and the resulting mixture was extracted with diethyl ether (3 × 50 mL). The combined organic layers were washed with water (2 × 50 mL) and then dried over $MgSO_4$. After filtration the solvent was evaporated under reduced pressure, and the residue was purified on a flash column (4:1 Hex:EtOAc, v/v). The final product was obtained as a yellow oil in 80% yield. ^{1}H NMR (400 MHz, chloroform-*d*) δ 6.60 (s, 1H), 3.83 (s, 3H), 3.72 (s, 3H), 2.35 (s, 3H), 2.27 (s, 3H), 2.19 (s, 3H). ESI-MS: for $C_{11}H_{16}O$: expected *m/z* = 181.1230 $[M+H]^+$; found *m/z* =181.1210 $[M+H]^+$; 11.0 ppm error.

2,5-Dimethoxy-3,4,6-trimethylbenzaldehyde (2)

Anhydrous TFA (12 mL) was added to a solution of compound 1 (1.5 g, 8.5 mmol) in hexamethylenetetramine (1.19 g, 8.5 mmol). The solution was stirred at room temperature for 1 h and then heated at reflux (72.5 $^{\circ}$C) for 28 h. After cooling, the solution was poured into ice water, and then neutralized with Na_2CO_3, followed by extraction with CH_2Cl_2 (3 × 100 mL). The organic layer was washed with water, dried ($MgSO_4$), and concentrated under reduced pressure. Product was purified on a flash column (4:1 CH_2Cl_2:Hex, v/v) to obtain the final product as a yellow solid in 73% yield. ^{1}H NMR (400 MHz, chloroform-*d*) δ 10.48 (s, 1H), 3.77 (s, 3H), 3.64 (s, 3H), 2.49 (s, 3H), 2.26 (s, 3H), 2.20 (s, 3H). ESI-MS: for $C_{12}H_{16}O_3$: expected *m/z* = 209.1180 $[M+H]^+$; found *m/z* = 209.1160 $[M+H]^+$; 9.50 ppm error.

1-Hydroxymethyl-2,5-dimethoxy-3,4,6-trimethylbenzene (3)

To a stirred suspension of $NaBH_4$ (0.14 g, 3.6 mmol) in MeOH (4.0 mL) under N_2 gas at 0 $^{\circ}$C, was introduced a solution of aldehyde 2 (0.36 g, 1.7 mmol) in MeOH with a syringe within 10 min. The mixture was stirred for a further 3 h at 0 $^{\circ}$C and then allowed to warm to RT. After evaporation of MeOH, the crude product was dissolved in CH_2Cl_2 (50 mL), which

was washed with water (3 × 50 mL). The organic layer was dried ($MgSO_4$), filtered and the solvent was then evaporated under vacuum to yield a white solid. The compound was used for the next step without further purification (77% yield). ^{1}H NMR (400 MHz, chloroform-*d*) δ 4.73 (s, 2H), 3.74 (s, 3H), 3.65 (s, 3H), 2.32 (s, 3H), 2.19 (d, J = 7.4 Hz, 6H), 2.01 (d, J = 4.6 Hz, 1H). ESI-MS: for $C_{12}H_{18}O_3$: expected m/z = 233.1156 $[M+Na]^+$; found m/z = 233.1154 $[M+Na]^+$; 0.9 ppm error.

tert-Butyl[(2,5-dimethoxy-3,4,6-trimethylphenyl)methoxy]dimethylsilane (4)

Compound 3 (0.28 g, 1.33 mmol) was dissolved in DMF (3.0 mL), with the solution then cooled to 0 $^\circ$C. Imidazole (0.27 g, 3.99 mmol) and TBSCl (0.6 g, 3.99 mmol) were added. The reaction was allowed to warm to room temperature, and it was stirred for an additional 2 h. The reaction was monitored by TLC. Upon completion, the reaction was diluted with diethyl ether, and then it was washed with NH_4Cl solution. The organic layer was dried over magnesium sulfate, and the solvent was removed under reduced pressure. The resulting oil was purified on a flash column (9:1 Hex:EtOAc, v/v) to afford a yellowish-white oil in 70% yield. ^{1}H NMR (400 MHz, chloroform-*d*) δ 4.73 (s, 2H), 3.72 (s, 3H), 3.66 (s, 3H), 2.31 (s, 3H), 2.19 (d, J = 6.6 Hz, 6H), 0.93 (s, 10H), 0.14 (s, 6H). ^{13}C NMR (101 MHz, chloroform-*d*) δ 153.30, 130.76, 130.25, 129.39, 128.13, 77.54, 62.27, 60.31, 57.80, 26.20, 18.63, 13.08, 12.77, 12.04, -5.14.

2-Hydroxymethyl-3,5,6-trimethyl-1,4-benzoquinone (5, HMBQ)

To a solution of compound 4 (0.16 g, 0.51 mmol) in CH_3CN (2.0 mL) was slowly added a solution of ammonium cerium (IV) nitrate (0.7 g, 1.31 mmol) in water. The resulting mixture was stirred for 4 h at RT and then diluted with water (25 mL). The organic layer was extracted with CH_2Cl_2 (3 × 50 mL), dried, and concentrated under vacuum. The compound was purified on a flash column (100 % $CHCl_3$) to give an orange solid in 80% yield. ^{1}H NMR (400 MHz, chloroform-*d*) δ 4.52 (d, J = 6.0 Hz, 2H), 2.74 (t, J = 6.7 Hz, 1H), 2.07 (s, 3H), 2.00 (dt, J = 4.3, 1.3 Hz, 6H). ^{13}C NMR (101 MHz, chloroform-*d*) δ 188.64, 187.82, 141.72, 141.48, 140.68, 140.34, 57.83, 12.67, 12.24, 11.93. ESI-MS: for $C_{12}H_{18}O_3$: expected m/z = 179.0706 $[M-H]^-$; found m/z = 179.0722 $[M-H]^-$; −8.93 ppm error.

4-Nitrophenyl (2,4,5-trimethyl-3,6-dioxocyclohexa-1,4-dien-1-yl)methyl carbonate (6)

To a solution of 5 (41.0 mg, 23.0 mmol) in anhydrous THF (10.0 mL) under argon, 4-nitrophenyl chloroformate (99.6 mg, 49.4 mmol) was added, alone with anhydrous pyridine (55.7 μL). The mixture was stirred 24 h in RT. The resulting white solid was filtered off, and the filtrate was evaporated under vacuum. The resulting yellow residue was purified using a flash column (1:1 EtOAc:Hex, v/v) to afford compound 6 as a pale yellow solid in 85% yield. ^{1}H NMR (400 MHz, chloroform-*d*) δ 8.28 (d, J = 9.2 Hz, 2H), 7.39 (d, J = 9.2 Hz, 2H), 5.25 (s, 2H), 2.20 (s, 3H), 2.06 (d, J = 2.2 Hz, 6H). ESI-MS: for $C_{17}H_{15}O_7$: expected *m/z* = 345.0748 $[M+Na]^+$; found *m/z* = 368.0735 $[M+Na]^+$; 3.5 ppm error.(Crystal structure is shown in Figure 2.4)

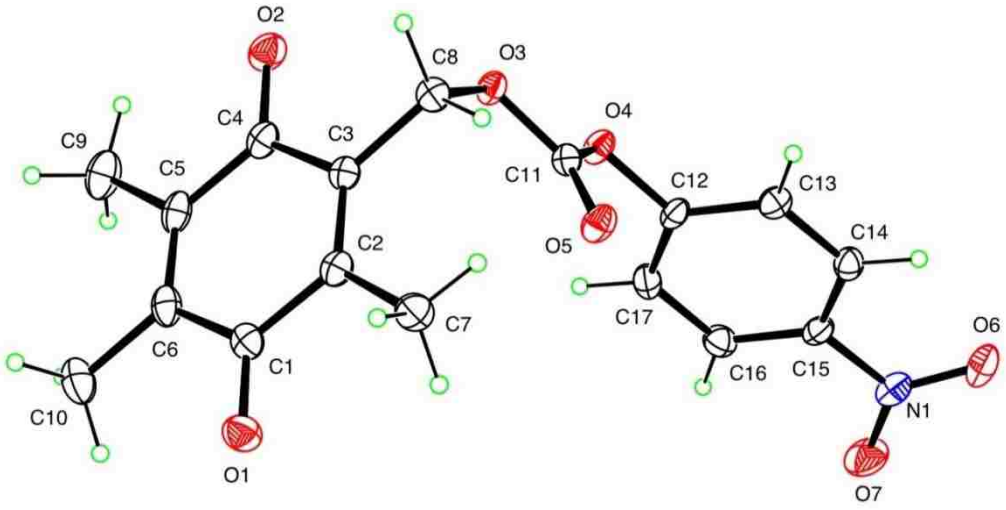

Figure 2.4 Crystal structure of compound 6

Synthesis of HMBQ-DOPE

To a cooled (0 $^\circ$C) solution of DOPE lipid (109.6 mg, 0.15 mmol) in CH_2Cl_2 (15.0 mL), triethylamine (125 μL, 0.87 mmol) and compound 6 (53.89 mg, 0.15 mmol) were added dropwise. The resulting mixture was stirred 24 h at RT. Then the reaction mixture was diluted with CH_2Cl_2 to 30 mL and washed with 5% $NaHCO_3$ (2 × 25 mL). The organic layer was dried with $MgSO_4$, filtered and concentrated under vacuum. The crude residue was purified by a flash column with gradient elution (1:1 CH_2Cl_2:EtOAc, v/v and 3:1 EtOAc:MeOH, v/v) to afford HMBQ-DOPE as a brown wax in 35% yield. ESI-MS: for $C_{52}H_{87}NO_{12}P^-$: expected *m/z* = 948.5971 $[M]^-$; found *m/z* = 984.5954 $[M]^-$; 1.8 ppm error.

Synthesis of HMBQ-Npc

HMBQ (6; 59.8 mg, 0.33 mmol) and dibutyltin dilaurate (DBTL; 20 μL, 0.03 mmol) were added to a solution of 4-nitroaniline isocyanate (65.6 mg, 0.40 mmol) in dry THF (5.0 mL). The reaction mixture was heated to 45 $^{\circ}$C and stirred for 1 h. Then the solvent was evaporated under vacuum, and the reaction mixture was purified on a flash column (1:1 EtOAc:Hex, v/v) to obtain HMBQ-Npc as a yellow solid in 70% yield. ^{1}H NMR (400 MHz, chloroform-*d*) δ 8.19 (d, J = 9.2 Hz, 2H), 7.53 (d, J = 9.2 Hz, 2H), 6.99 (s, 1H), 5.16 (s, 1H), 2.20 (s, 3H), 2.12–1.92 (m, 6H). ^{13}C NMR (101 MHz, chloroform-*d*) δ 187.22, 185.90, 152.21, 145.12, 143.51, 143.21, 141.33, 140.78, 136.06, 125.24, 117.78, 58.65, 12.53, 12.36. ESI-MS: for $C_{17}H_{16}N_2O_6$: expected *m/z* = 367.091 $[M+Na]^+$; found *m/z* = 367.100 $[M+Na]^+$; 24.5 ppm error.

2.2.3 Cyclic Voltammetry of HMBQ trigger group

Cyclic voltammetry (CV) was performed in 0.1 M, pH 7.4 phosphate–buffered saline (PBS) under anaerobic conditions with 1% ethanol to help solubilize the quinone (HMBQ). Power Suite 2.53 operating software was used with a Princeton Applied Research Model 273A Potentiostat/Galvanostat. Voltammograms were collected at scan rate of 0.1 Vs^{-1} at room temperature (25 $^{\circ}$C) after degassing the solution with nitrogen for 20 min. A three-electrode cell was used containing glassy carbon working (BAS, 3-mm diameter), platinum wire counter, and Ag reference (BAS) electrode, and the potentials were referenced versus ferrocene/ferrocenium internal standard.

2.2.4 Synthesis of Liposome-Encapsulated Calcein

HMBQ-DOPE liposomes containing calcein were prepared adopting standard liposome preparation techniques reported in the literature.[28, 31] The HMBQ-DOPE lipid mixture was thoroughly dissolved in a small amount of $CHCl_3$ to get a homogeneous lipid solution. Then a portion of the dissolved lipid was transferred to a pre–weighed culture tube, and the solvent was removed using a dry nitrogen stream in a fume hood. Next, the final lipid weight was measured to obtain usually 1–2 mg of lipids. The lipid mixture was thoroughly dried to remove residual organic solvents by placing the tube under vacuum for a few hours. Next, for the hydration of the resulting lipid cake, 40 mM calcein dye (Sigma-Aldrich, Milwaukee, WI) in degassed (purged with N_2 for 15 min) 0.1 M, pH 7.4 phosphate-buffered saline (PBS; 0.5 mL) was added to the

lipid mixture, with subsequent aging for a few hours in a refrigerator at 10 °C. Then the mixture was subjected to 6 freeze–thaw cycles by freezing the sample in a dry ice/acetone bath and warming the sample back to room temperature in a water bath with vigorous vortexing for a few seconds during each cycle. Then the lipid mixture was placed in a Lipex lipid extruder (Northern Lipids; Vancouver, BC, Canada) and passed through a 100-nm pore size polycarbonate filter (Whatman Nucleopore, track-etched) for 19 times to obtain a homogeneous size distribution of the final suspension. To remove excess calcein that is not encapsulated in liposomes, the lipid mixture was passed through a short Sephadex column. A 300 μL aliquot of liposome mixture was added on top of the Sephadex spin column and centrifuged at 500 × g for 3 min. The liposome sample was filtered through the column and it was collected to an Eppendorf tube kept at the end of the column. Finally, the suspension was characterized by dynamic light scattering (DLS) to obtain the particle size and its poly dispersity index (PDI)

2.2.5 Liposome Characterization

Dynamic light scattering measurements were obtained from backscatter intensities (173°, 633-nm red laser) at a temperature of 25 °C for calcein–loaded liposome in 0.1 M, pH 7.4 phosphate-buffered saline using a Zetasizer Nano ZS particle size analyzer (Malvern Instruments, Worcestershire, U.K.).

2.2.6 Spectroscopic Methods

All spectroscopic measurements were performed in degassed 0.1 M, pH 7.4 phosphate-buffered saline at 25 °C. Fluorescence data were collected using a Perkin Elmer LS-55 spectrometer, and absorption spectra were recorded using a Varian Cary-50 spectrophotometer. Samples for absorption and emission measurements were obtained in 1-cm × 1-cm quartz cuvettes (3.5-mL volume, Sigma-Aldrich).

2.2.7 Calcein Release Studies

The purified calcein-encapsulated liposomes (0.75 μL) were diluted with 0.1 M, pH 7.4 PBS (3 mL) to achieve to a concentration around 80–100 μM of lipids. A 50 μL aliquot of aqueous $Na_2S_2O_4$ (DT; Sigma-Aldrich) 10 equivalents or/and 7.5 μL of 30% (v/v) Triton X-100 (Sigma-Aldrich) were added to the cuvettes as appropriate. Fluorescence intensities were recorded using

the florescence spectrophotometer at 25 °C. Samples were excited at λ_{ex} = 485 nm and emission was measured at λ_{em} = 525 nm with excitation and emission slit widths of 2.5 nm, with a ND 0.5 emission filter.

2.2.8 UV-Vis Studies of HMBQ-Npc

A stock solution of 150 μM HMBQ-Npc was prepared in 60% DMSO:40% 0.1 M, pH 7.4 phosphate–buffered saline and subsequently diluted to prepare preferred concentration solutions of HMBQ-Npc in 12% DMSO:88% 0.1 M, pH 7.4 PBS. Stock solutions of aqueous $Na_2S_2O_4$ were freshly prepared prior to each experiment. Absorbance spectra were recorded at 25 °C using a Varian Cary-50 spectrophotometer, scanning from 250–800 nm. All the spectral data were blank corrected using 12%DMSO:88% 0.1 M, pH 7.4 PBS solution.

2.2.9 NMR Kinetics of Dithionite Induced Reduction of HMBQ-Npc

A HMBQ-Npc (2.0 mg) sample was dissolved in 400 μL of 6:1 DMSO:D_2O solution under argon at 25 °C and initial NMR spectra were recorded using a Bruker AV-400 spectrometer. Then a 10 μL aliquot of (2 equivalents) solution of $Na_2S_2O_4$ (DT) dissolved in D_2O was injected in to the sample tube and NMR spectra were recorded every 2 min for 4 h. NMR spectra of *para*-nitroaniline and HMBQ were also recorded using equivalent conditions for comparison purposes.

2.3 Results and Discussion

2.3.1 Reduction Potential of HMBQ Trigger Group

The standard redox potential of HMBQ reduction was measured (converted to standard hydrogen electrode by adding 0.210 V)[32] using the CV graph shown in Figure 2.5. The cathodic potential ($E_{p,c}$) was 0.007 V, and the anodic potential ($E_{p,a}$) was 0.199 V, giving a half wave potential of ($E_{1/2}$) 0.103 V vs SHE (calculated according to Equation 2.1). As implied by positive $E_{1/2}$ of HMBQ, it should be rapidly reduced by a strong reducing agent such as DT ($E_{1/2}$ = −0.66 V).[33]

$$E_{\frac{1}{2}} = \left(\frac{\Delta E_p}{2}\right) + E_{p,c} \qquad \text{Equation 2.1}$$

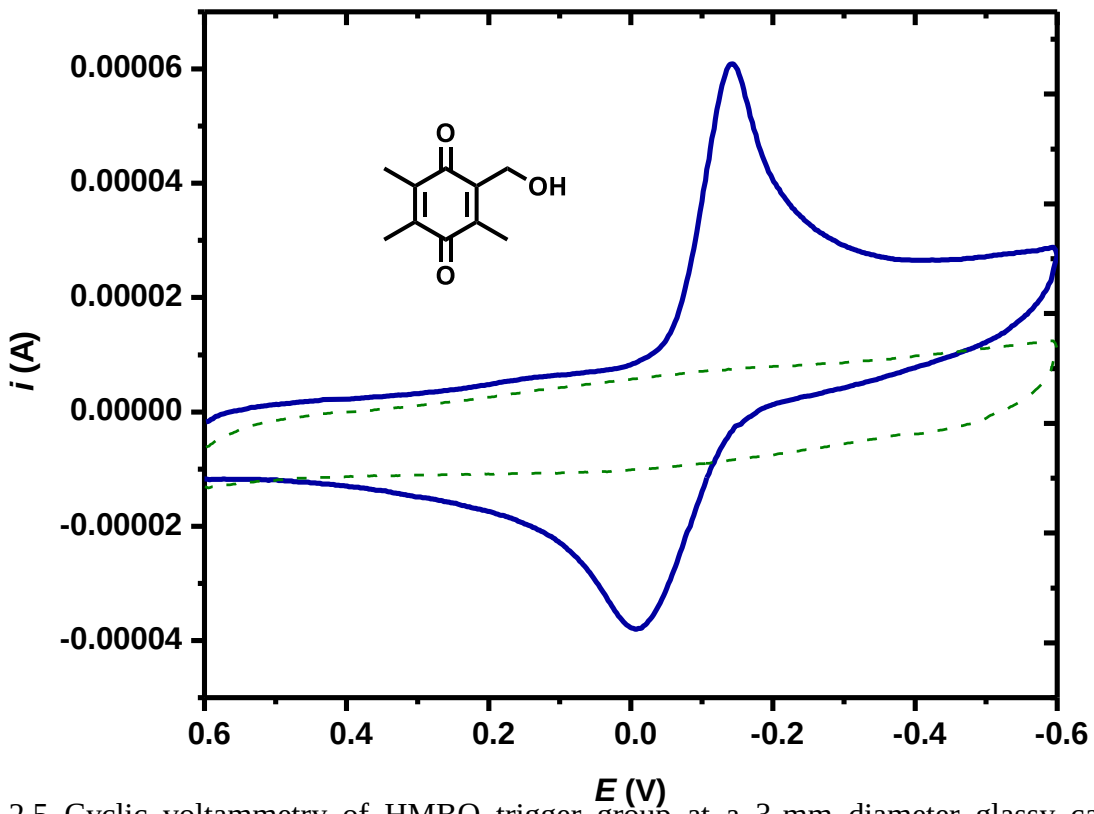

Figure 2.5 Cyclic voltammetry of HMBQ trigger group at a 3-mm diameter glassy carbon working electrode using 0.1 M, pH 7.4 PBS with 1% ethanol. Scan rate was 0.1 V s^{-1} at T = 25 °C. The blue colored line is the HMBQ and the dashed green line is background voltammogram of the buffer.

2.3.2 Characterization of HMBQ-DOPE Liposomes

In order to obtain the average size of the HMBQ-DOPE liposomes, dynamic light scattering experiments were performed in solutions of 0.1 M, pH 7.4 phosphate-buffered saline at 25 °C. As shown in Figure 2.6, the average diameter of the liposomes was determined to be 150 nm. The measurement of the size heterogeneity of the molecules in the mixture, the polydispersity index (PDI),[34] was obtained as 0.055, indicating a small variation in the diameter of the liposomes.

2.3.3 Reduction of HMBQ-DOPE Liposomes and Calcein Release Studies

According to previously reported data from the McCarley group[28] and others, a rapid increase in the fluorescence intensity was expected as soon as the reducing agent DT was added to the HMBQ-DOPE liposomes. The sample was excited at λ_{ex} = 458 nm and emission was detected at λ_{em} = 525 nm, the maximum excitation and emission wavelength range of the calcein dye. However, as shown in Figure 2.7, such an increase in the fluorescence intensity was

not observed, indicating that an inability of the DT-exposed liposomes to release the encapsulated calcein dye, even after 1000 min of DT incubation. This outcome was observed several times (>3 times) with different batches of lipid. Once Triton X-100 detergent was added to rupture the lipid bilayer,[28] a rapid increase in fluorescence was observed. This indicated the immediate release of the encapsulated calcein from HMBQ-DOPE liposomes. The possible reason for not observing release from the redox triggered liposomes is discussed in the following section.

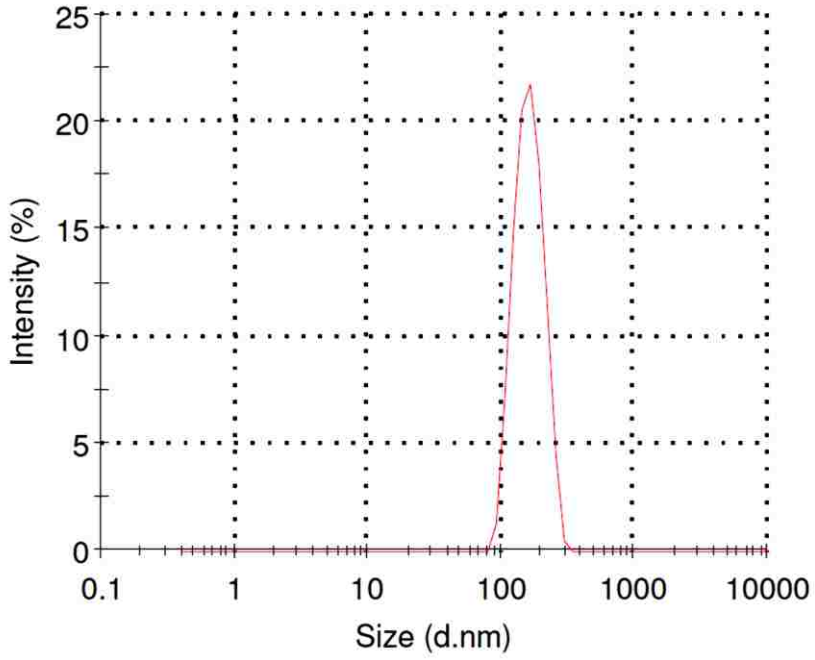

Figure 2.6 Characterization of HMBQ-DOPE liposomes using DLS to obtain their diameter and distribution of diameter (d) at $T = 25\ ^{\circ}C$

2.3.4 Mechanism of Redox-Triggered Liposomes

The proposed, anticipated reaction mechanism in Figure 2.8 implies a rapid release of contents from HMBQ-DOPE liposomes. Initially, when the quinone group is attached to the lipid, a stable lamellar phase (L_{α}) will be formed. When lipid is in a stable lamellar phase it will form the vesicular structure with lipid bilayer encapsulating the calcein dye; thus DLS and Triton induced lysing experiments support this situation. The hydroquinone formed after the reduction of the exterior quinone moieties by the strong reducing agent DT will undergo rapid quinone methide rearrangement, releasing the lipid from the quinone head group. The release of head

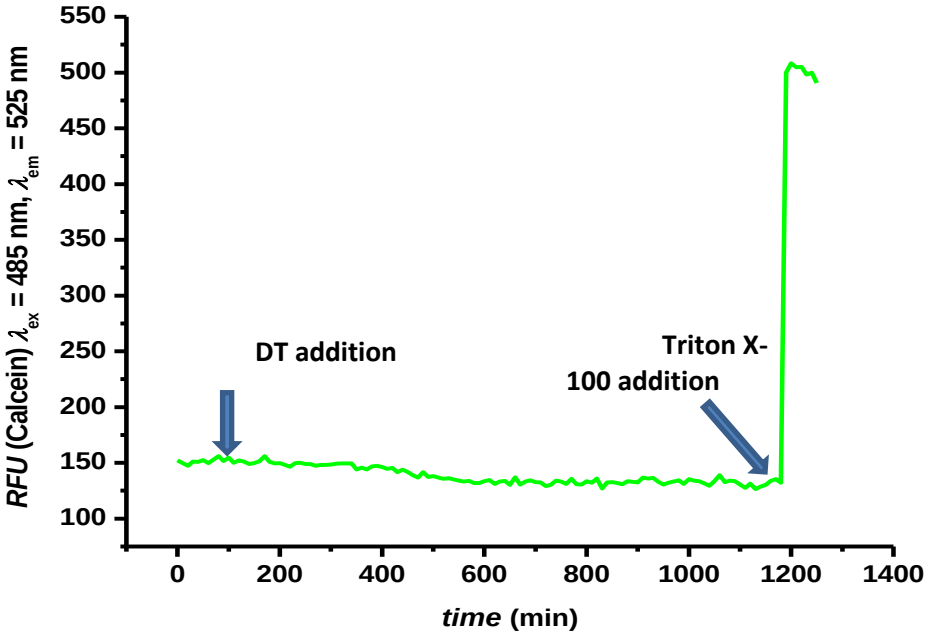

Figure 2.7 Time-dependent monitoring of the fluorescence intensity of calcein-loaded liposomes at λ_{ex} = 485 nm and λ_{em} = 525 nm in 0.1 M, pH 7.4 phosphate-buffered saline at T = 25 °C.

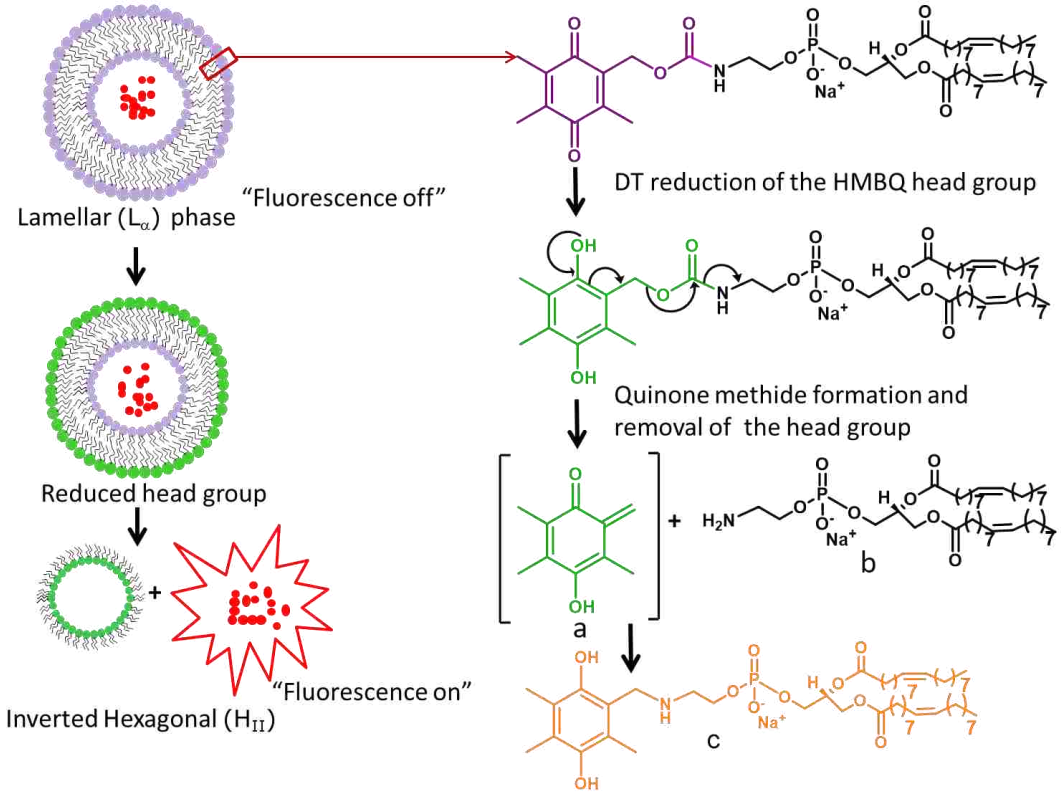

Figure 2.8 Schematic representation of proposed HMBQ-DOPE liposome releasing mechanism via quinone methide formation.

group will induce a conformation change in the lipid assembly compelling it to form an unstable inverted micelle hexagonal phase (H_{II}) resulting in breakdown of the vesicular structure and release of the encapsulated calcein dye. This proposed mechanism is based on previous observations in the McCarley group with redox–cleavable head group lipids.[28, 35] However, it is possible that the highly reactive quinone methide species (Figure 2.8, compound a) formed by the reduction is susceptible to many nucleophilic substitution reactions in the media. When there is a high local concentration of lipids with a free amine group (Figure 2.8, compound b) in close proximity, attack of the quinone methide moiety is a possibility to form compound c (Figure 2.8, compound c). If this reaction took place a stable hydroquinone attached DOPE lipid species will be formed. This formation will stabilize the lamellar (L_{α}) phase inhibiting the phase transition, to the inverted micelle hexagonal phase. However it is possible that the quinone methide species (a) does not leave the DOPE lipids. In order to further understand the mechanism of quinone methide formation and release of attached amine-bearing motifs, I synthesized the HMBQ-Npc system as a model compound.

2.3.5 Spectral Properties of HMBQ-Npc/*para*-nitroaniline System

As shown by the absorbance spectrum of HMBQ-Npc in Figure 2.9 (red line), the two bands centered at λ_{max} = 264 nm and λ_{max} = 330 nm correspond to the absorbance of the quinone moiety and the carbamate bonded nitroaniline, respectively. The main absorbance band of the compound (λ_{max} = 330 nm) is blue shifted about 60 nm from the absorbance maximum of the *para*-nitroaniline (green line, 390 nm) reporter group. This spectral difference therefore, facilitates the monitoring of free reporter release upon reduction of HMBQ-Npc by DT.

2.3.5 Reduction Triggered Self-Immolation of HMBQ-Npc

Upon incubating a 40 μM sample of HMBQ-Npc with 2 equivalents of aqueous $Na_2S_2O_4$; rapid release of *para*-nitroaniline was achieved (Figure 2.10, green arrow) along with the concomitant reduction of bands corresponds to HMBQ-NPC. This was evident by the reduction of the quinone band at λ_{max} = 260 nm (Figure 2.10, blue arrow) and the carbamate-linked nitroaniline band at λ_{max} = 330 nm (Figure 2.10, red arrow). The intensity of the signal level indicates that full release of the *para*-nitroaniline reporter occurs within about 1 hour; however,

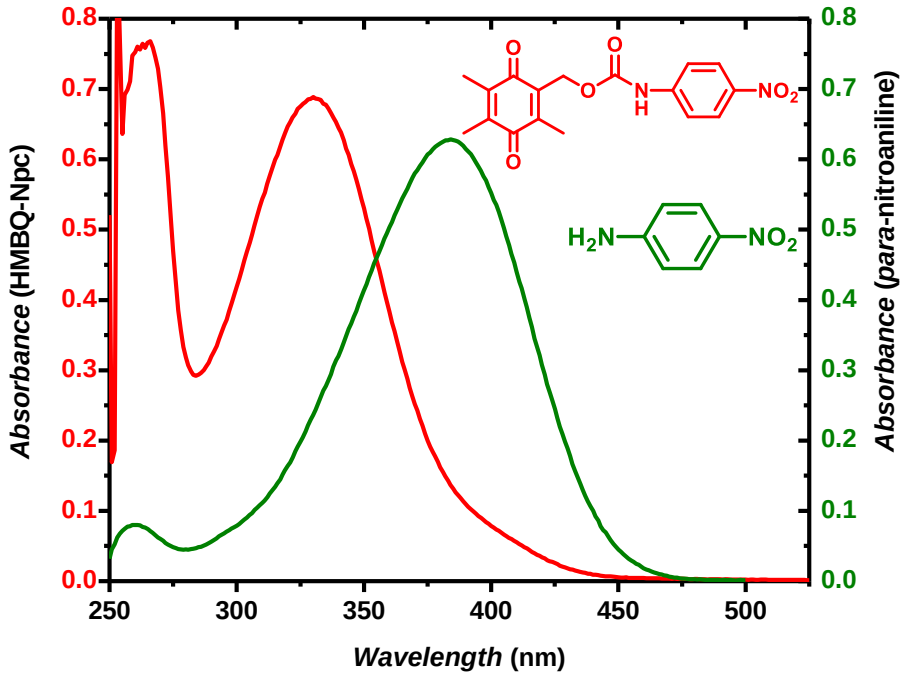

Figure 2.9 Absorbance spectra of 40 μM HMBQ-Npc (red line) and 40 μM *para*-nitroaniline (green line) in 12% DMSO:88% 0.1 M, pH 7.4 PBS at T = 25 °C.

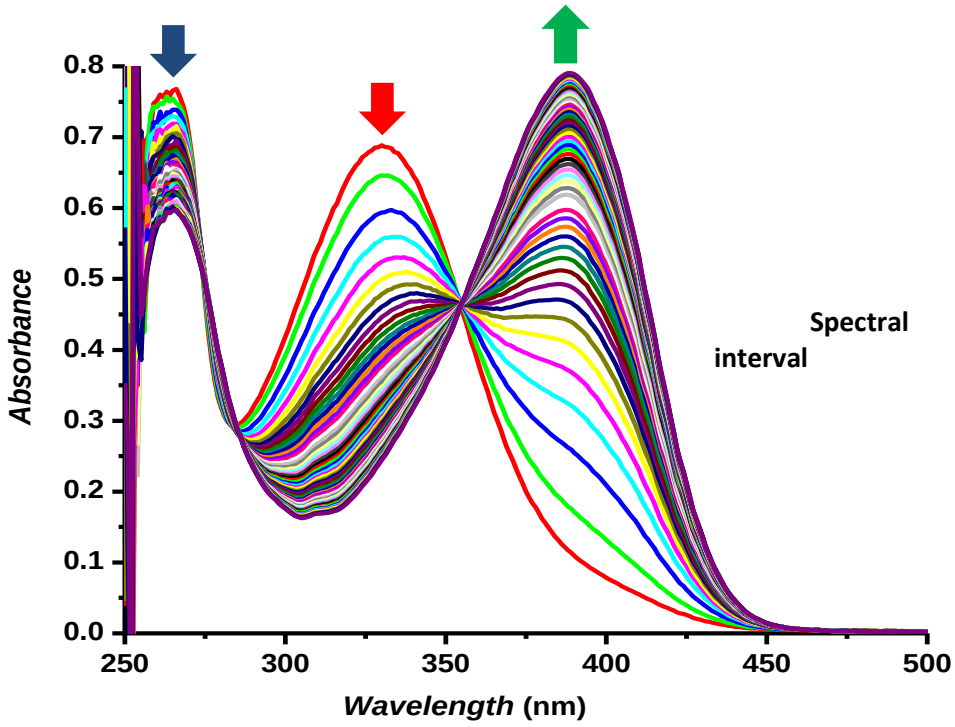

Figure 2.10 Dithionite (2 equivalents) reduction of 40 μM HMBQ-Npc in 12% DMSO:88% pH 7.4, PBS at T = 25 °C. Each spectrum was obtained by examining the sample every 2 min (Δt = 2 min) for 70 min after the addition of aqueous DT.

a significantly enhanced signal was achieved within about 20 min after addition of DT, providing evidence for the rapid nature of the reaction.

2.3.7 Kinetics of Self-Immolation of HMBQ-Npc

According to the proposed reaction mechanism for HMBQ-Npc and the observed absorbance data, it is assumed that redox activation of the HMBQ moiety results in rapid formation of the hydroquinone species (R) with elimination of the quinone methide and formation of the free *para*-nitroaniline reporter being the rate limiting step (Scheme 2.4). The kinetic constant of the system was determined as shown below.

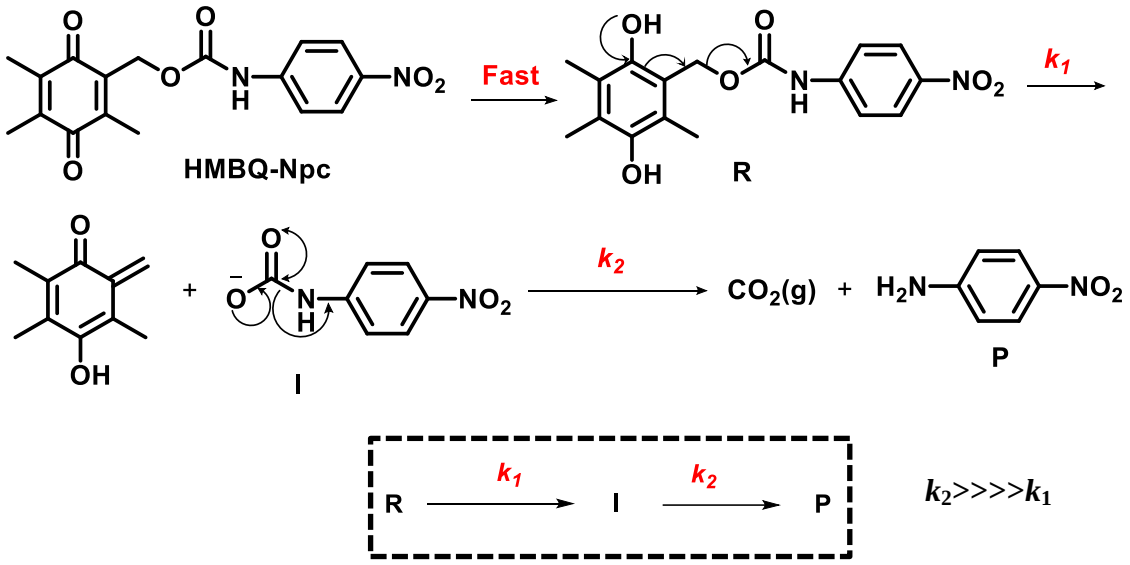

Scheme 2.4 The proposed reaction mechanism for formation of *para*-nitroaniline by quinone methide formation.

Previously published data in the McCarley group for a wide range of quinone substrates having redox potentials similar to those of HMBQ revealed that dithionite reduction of the quinone head group to a reduced hydroquinone is very rapid and complete with in 1s.[36-37] Therefore it is assumed that the initial reduction step to cause hydroquinone formation (Scheme 2.4, compound R) has no influence on the overall reaction rate. Additionally, the work reported by Johnson *et al.* has reported that zwitterionic carbamic species of *N*-arylcarbamates (Scheme 2.4, compound I) have short lifetimes (<<seconds).[38] Thus, it is assumed that a rapid decarboxylation step occurs shortly after the reduction without accumulation of the carbamic

acid species (*N*-arylcarbamate) and does not provide sufficient contribution to the overall rate change. When the initial reduction step and decarboxylation were deemed as non-rate limiting steps, the overall reaction can be simplified to a simple pseudo first–order rate equation, (Equation 2.2). Using this equation, the pseudo first order rate constant was derived as described below. The graph of extent of product disappearance measured at maximum absorbance wavelength of 330 nm, and product (P) appearance measured at 390 nm is shown in the Figure 2.11 a.

$$Rate = -\frac{d\,[R]}{d[t]} = k_1[R]$$

$$\int_{[R]_0}^{[R]} \frac{d[R]}{[R]} = -k_1 \int_0^t dt$$

$$ln([R] = [R]_0\ e^{-k_1 t})$$

$$\ln[R] = \ln[R]_0 - k_1 \times t$$

$$ln\left(\frac{[R]}{[R]_0}\right) = -k_1 t \qquad \text{Equation 2.2}$$

According to the Equation 2.2, to determine the order of the reaction, the graph of ln extent of product appearance and ln reactant disappearance was plotted as shown in Figure 2.11 b. As expected, a portion of the reactant disappearance (Figure 2.11 b, blue line) is seen to be linear (Figure 2.11, blue box). However, when the ln graph of product formation was observed, it is clear that *para*-nitroaniline product formation (green line) did not follow the linear first order kinetics because the shape of the graph is more hyperbolic than linear. Therefore, *para*-nitroaniline product formation cannot be used for the rate constant calculations. The linear portion of the HMBQ-Npc reactant disappearance curve was separately plotted in a graph, in order to do the linear fit and obtain the rate constant. As shown by Figure 2.12, the linear fit of the data demonstrates the disappearance of the HMBQ-Npc to form the quinone methide and *para*-nitroaniline species follows first order kinetics, with a rate constant of $k_1 = 0.0303\ \text{min}^{-1}$.

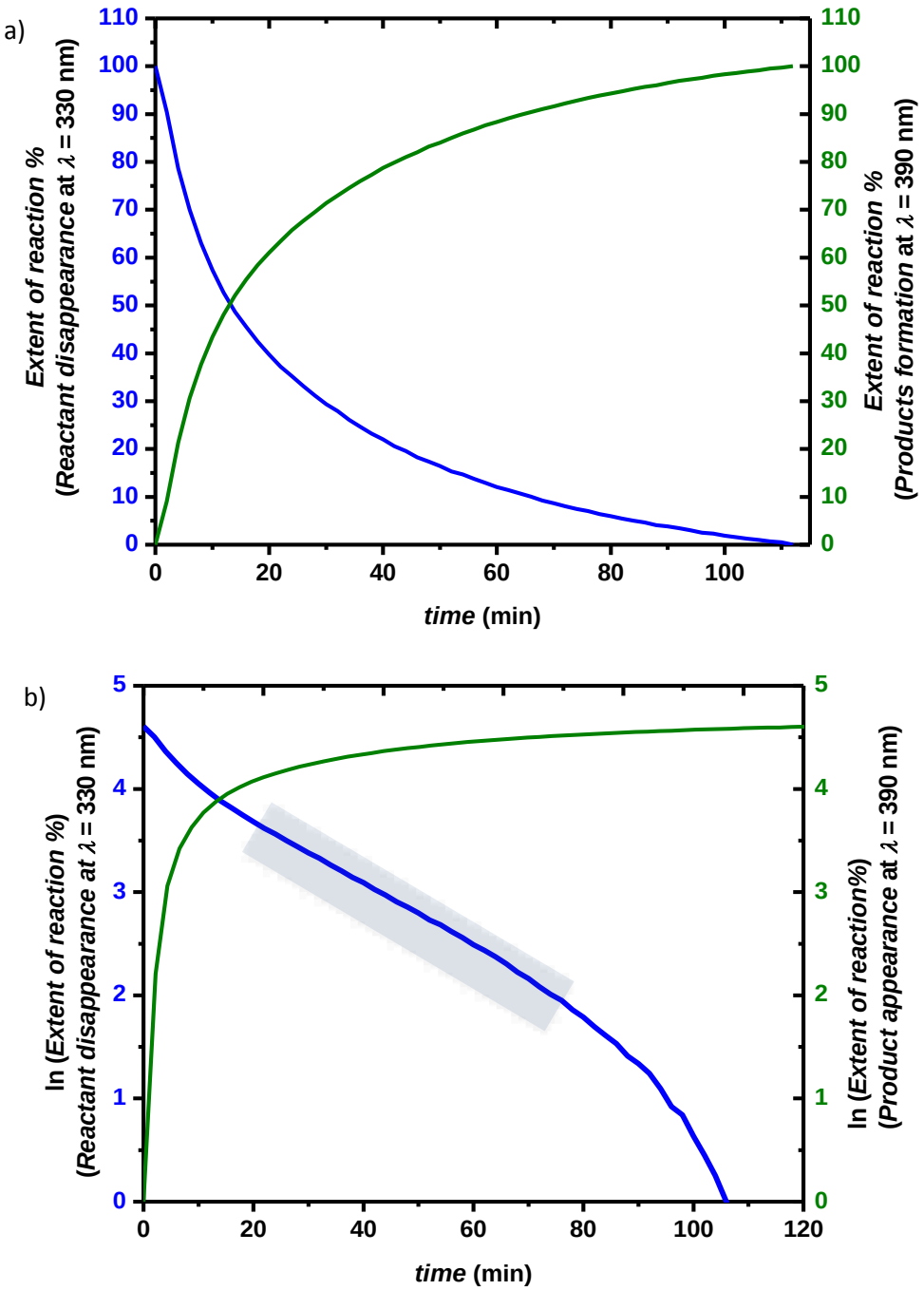

Figure 2.11 a) a plot of extent of product formation (green line, monitored at λ_{max} = 330 nm) and product disappearance (blue line, monitored at λ_{max} = 390 nm) vs time from Figure 2.10, b) a plot of ln (extent of reaction) disappearance (blue line) and product formation (green line). The linear region of the ln graph (first order kinetics) is marked with a blue box.

2.3.8 NMR Assessment of Kinetics of the HMBQ-Npc Reduction

As another piece of evidence for the mechanism of *para*-nitroaniline formation from reduced HMBQ-Npc, NMR kinetic experiments were conducted. The HMBQ-Npc sample was dissolved in 6:1 DMSO:D_2O to obtain a final concentration of 15 mM and an initial spectrum was recorded (Figure 2.13, panel a). Then 2 equivalents (10 μL of 1.0 M DT sample) of DT dissolved in D_2O was injected under argon, and spectra were recorded every 2 min for 4 hours.

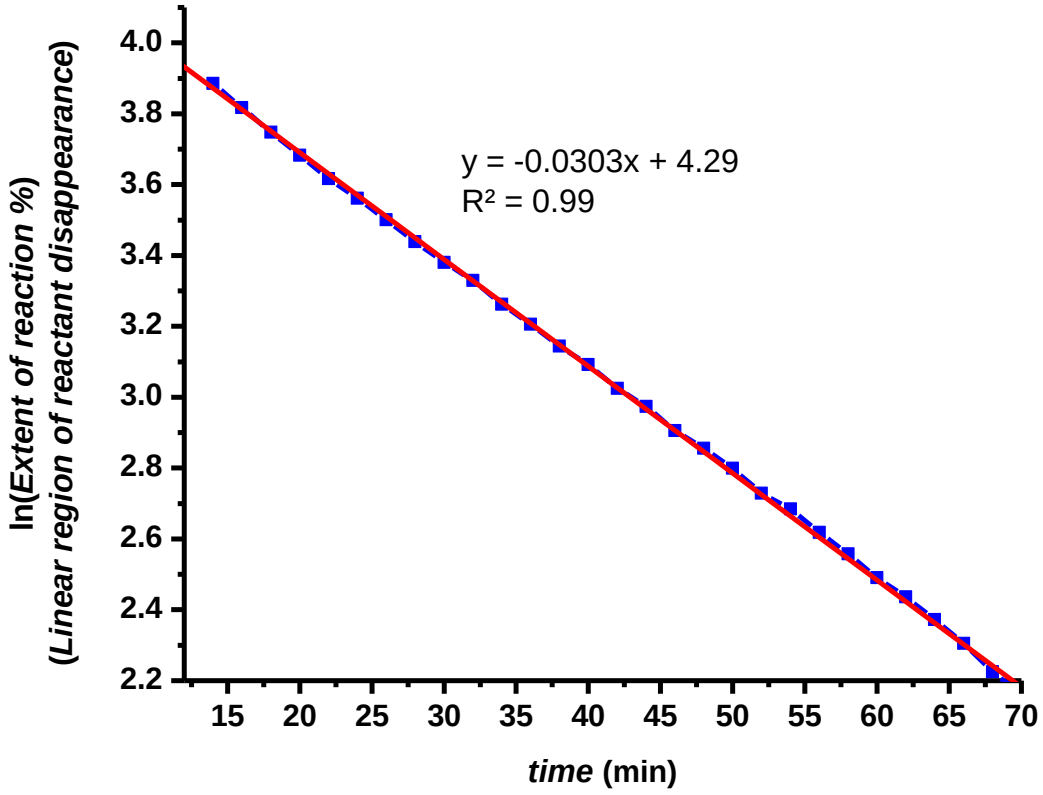

Figure 2.12 Linear region of the ln(extent of the reactant disappearance) vs time plot from Figure 2.11 b, exhibiting apparent first-order kinetics.

Shortly after DT was added, peaks corresponding to *para*-nitroaniline started to appear around 7.9 ppm and 6.6 ppm (Figure 2.13, panels b and c). Prominent *para*-nitroaniline peaks were observed about 15 min after DT addition that matches with the data observed for the spectroscopic monitoring of HMBQ-Npc reduction by DT, (Figure 2.13, panel b). The two aromatic hydrogen peaks corresponding to the HMBQ-Npc are located around 8.2 ppm and 7.6 ppm, and they gradually decreased as the reaction progressed (Figure 2.13, panels b and c). After

about 90 min, the reaction was completed. The peaks corresponding to the starting compound HMBQ-Npc, were completely absent (Figure 2.13, Panel d, blue arrow), while peaks corresponding to *para*-nitroaniline were clearly prominent (Figure 2.13, panel d, red arrow). Remarkably, two other peaks around 5.9 ppm and 5.4 ppm (panels b and c, denoted by *) appeared soon after DT addition and these two peaks diminished as the reaction reached completion. Because peaks around this region usually correspond to alkene hydrogens, these two peaks are speculated to be the two alkene protons of the quinone methide intermediate. Furthermore, the peak at 5.1 ppm that corresponds to the two methylene protons of HMBQ-Npc also diminished with time (panels b and c, green arrow), and it was virtually non-existent when the reaction was complete after 90 min (panel d, green arrow).

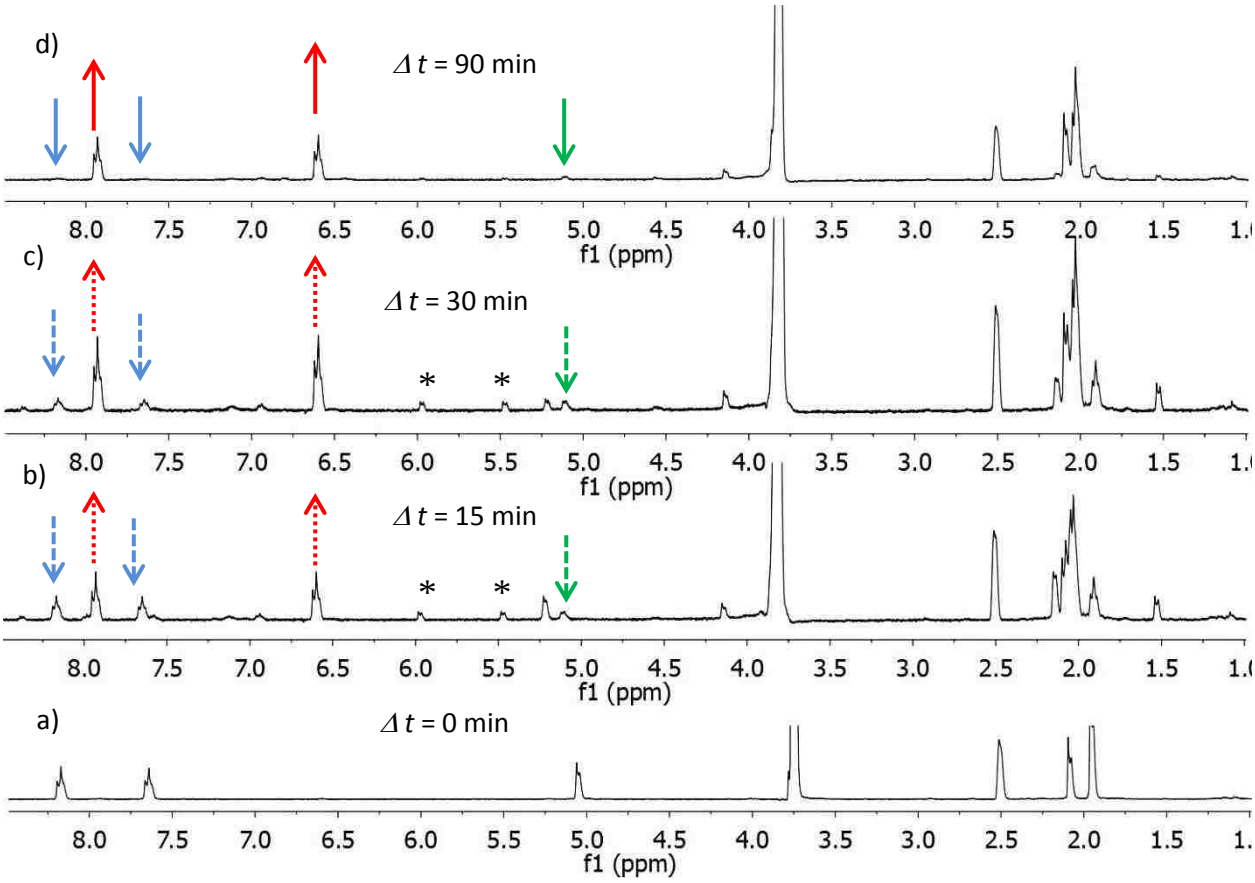

Figure 2.13 NMR spectra of HMBQ-Npc in 6:1 DMSO:D_2O; a) Initial NMR spectrum of HMBQ-Npc at Δt = 0 min before addition of DT, b) NMR spectrum of HMBQ-Npc at Δt = 15 min after addition of DT, c) NMR spectrum of HMBQ-Npc at Δt = 30 min after addition of DT, and d) NMR spectrum of HMBQ-Npc at Δt = 90 min after addition of DT. * Proposed quinone methide intermediate. Colored arrows indicate the appearance or disappearance of a peak.

2.4 Conclusions

According to cyclic voltammetric data and other spectroscopic data obtained, it is clear that the redox activity of the novel HMBQ trigger group is quite promising. It has the capability to undergo rapid reduction by potent reducing agents with subsequent efficient elimination to form the *para*-nitroaniline product. This was proven by the HMBQ-Npc system where rapid elimination of the attached group (*para*-nitroaniline) was observed by both absorbance data and NMR kinetics. However, from the HMBQ-DOPE calcein release studies it is concluded that the efficiency of elimination depends on the property of the leaving group as well. When there is a more electron-rich leaving group, such as an alkyl chain, nucleophilic re-attack of the quinone methide is a possible reaction. It is proposed that this is especially possible in a crowded environment, like liposomes where molecules in close proximity of each other can undergo rapid reactions. Although expected release from these redox-responsive liposomes could not be achieved using the HMBQ trigger system, the rapid nature of HMBQ elimination observed by absorption and NMR spectroscopies hold promise for other triggerable approaches, such as delivery of prodrugs and possible application as imaging agents.

2.5 References

1. Warnecke, A. In *Site-Specific Prodrug Activation and the Concept of Self Immolation*, Wiley-VCH Verlag GmbH & Co. KGaA: **2012**; pp 553-589.

2. Mo, R.; Jiang, T.; DiSanto, R.; Tai, W.; Gu, Z., Atp-Triggered Anticancer Drug Delivery. *Nat. Commun.,* **2014**, *5*.

3. de Groot, F. M. H.; Loos, W. J.; Koekkoek, R.; van Berkom, L. W. A.; Busscher, G. F.; Seelen, A. E.; Albrecht, C.; de Bruijn, P.; Scheeren, H. W., Elongated Multiple Electronic Cascade and Cyclization Spacer Systems in Activatible Anticancer Prodrugs for Enhanced Drug Release. *J. Org. Chem.,* **2001**, *66*, 8815-8830.

4. Bildstein, L.; Dubernet, C.; Couvreur, P., Prodrug-Based Intracellular Delivery of Anticancer Agents. *Adv. Drug Deliv. Rev.,* **2011**, *63*, 3-23.

5. Huang, P. S.; Oliff, A., Drug-Targeting Strategies in Cancer Therapy. *Curr. Opin. Gen. Dev.,* **2001**, *11*, 104-110.

6. Dubowchik, G. M.; Walker, M. A., Receptor-Mediated and Enzyme-Dependent Targeting of Cytotoxic Anticancer Drugs. *Pharmacol. Ther.,* **1999**, *83*, 67-123.

7. Gnaim, S.; Shabat, D., Quinone-Methide Species, a Gateway to Functional Molecular Systems: From Self-Immolative Dendrimers to Long-Wavelength Fluorescent Dyes. *Acc. Chem. Res.,* **2014**, *47*, 2970-2984.

8. Kudgus, R. A.; Walden, C. A.; McGovern, R. M.; Reid, J. M.; Robertson, J. D.; Mukherjee, P., Tuning Pharmacokinetics and Biodistribution of a Targeted Drug Delivery System through Incorporation of a Passive Targeting Component. *Sci. Rep.,* **2014**, *4*.

9. Shabat, D.; Amir, R. J.; Gopin, A.; Pessah, N.; Shamis, M., Chemical Adaptor Systems. *Chem. Eur. J.,* **2004**, *10*, 2626-2634.

10. Niculescu-Duvaz, D.; Negoita-Giras, G.; Niculescu-Duvaz, I.; Hedley, D.; Springer, C. J., Directed Enzyme Prodrug Therapies. *Methods Princ. Med. Chem.,* **2011**, *47*, 271-344.

11. Shan, D.; Nicolaou, M. G.; Borchardt, R. T.; Wang, B., Prodrug Strategies Based on Intramolecular Cyclization Reactions. *J. Pharm. Sci.,* **1997**, *86*, 765-767.

12. Erez, R.; Shabat, D., The Azaquinone-Methide Elimination: Comparison Study of 1,6- and 1,4-Eliminations under Physiological Conditions. *Org. Biomol. Chem.,* **2008**, *6*, 2669-2672.

13. Weinstain, R.; Segal, E.; Satchi-Fainaro, R.; Shabat, D., Real-Time Monitoring of Drug Release. *Chem. Commun.,* **2010**, *46*, 553-555.

14. Zhou, W.; Leippe, D.; Duellman, S.; Sobol, M.; Vidugiriene, J.; O'Brien, M.; Shultz, J. W.; Kimball, J. J.; Di Bernardo, C.; Moothart, L.; Bernad, L.; Cali, J.; Klaubert, D. H.; Meisenheimer, P., Self-Immolative Bioluminogenic Quinone Luciferins for Nad(P)H Assays and Reducing Capacity-Based Cell Viability Assays. *Chem. BioChem.,* **2014**, *15*, 670-675.

15. Kisin-Finfer, E.; Ferber, S.; Blau, R.; Satchi-Fainaro, R.; Shabat, D., Synthesis and Evaluation of New Nir-Fluorescent Probes for Cathepsin B: Ict Versus Fret as a Turn-on Mode-of-Action. *Bioorg. Med. Chem. Lett.,* **2014**, *24*, 2453-2458.

16. Li, Y.; Zhao, L.; Cheng, Y. In *Improving the Biocompatibility of Dendrimers in Drug Delivery*, John Wiley & Sons, Inc.: **2012**; pp 207-237.

17. Avital-Shmilovici, M.; Shabat, D., Self-Immolative Dendrimers: A Distinctive Approach to Molecular Amplification. *Soft Matter,* **2010**, *6*, 1073-1080.

18. Greenwald, R. B.; Pendri, A.; Conover, C. D.; Zhao, H.; Choe, Y. H.; Martinez, A.; Shum, K.; Guan, S., Drug Delivery Systems Employing 1,4- or 1,6-Elimination: Poly(Ethylene Glycol) Prodrugs of Amine-Containing Compounds. *J. Med. Chem.,* **1999**, *42*, 3657-3667.

19. Lee, M.-R.; Baek, K.-H.; Jin, H. J.; Jung, Y.-G.; Shin, I., Targeted Enzyme-Responsive Drug Carriers: Studies on the Delivery of a Combination of Drugs. *Angew. Chem. Int. Ed.*, **2004**, *43*, 1675-1678.

20. Lee, H. Y.; Jiang, X.; Lee, D., Kinetics of Self-Immolation: Faster Signal Relay over a Longer Linear Distance? *Org Lett*, **2009**, *11*, 2065-8.

21. Guo, X.; Szoka, F. C., Jr., Chemical Approaches to Triggerable Lipid Vesicles for Drug and Gene Delivery. *Acc. Chem. Res.*, **2003**, *36*, 335-341.

22. Dan, N., Drug Release through Liposome Pores. *Colloids. Surf., B*, **2015**, *126*, 80-86.

23. Yu, S.; He, C.; Ding, J.; Cheng, Y.; Song, W.; Zhuang, X.; Chen, X., Ph and Reduction Dual Responsive Polyurethane Triblock Copolymers for Efficient Intracellular Drug Delivery. *Soft Matter*, **2013**, *9*, 2637-2645.

24. Sudimack, J.; Lee, R. J., Targeted Drug Delivery Via the Folate Receptor. *Adv. Drug Deliv. Rev.*, **2000**, *41*, 147-162.

25. Samad, A.; Sultana, Y.; Aqil, M., Liposomal Drug Delivery Systems: An Update Review. *Current Drug Delivery*, **2007**, *4*, 297-305.

26. Chonn, A.; Cullis, P. R., Recent Advances in Liposomal Drug-Delivery Systems. *Curr. Opini. Biotechnol.*, **1995**, *6*, 698-708.

27. Giraud, L.; Giraud, A., Diels-Alder Trapping of Ortho-Quinone Methides. A New Entry to Substituted Xanthene-1,4-Diones. *Synthesis*, **1998**, 1153-1160.

28. Ong, W.; Yang, Y.; Cruciano, A. C.; McCarley, R. L., Redox-Triggered Contents Release from Liposomes. *J. Am. Chem. Soc.*, **2008**, *130*, 14739-14744.

29. Zalipsky, S.; Qazen, M.; Walker, J. A., II; Mullah, N.; Quinn, Y. P.; Huang, S. K., New Detachable Poly(Ethylene Glycol) Conjugates: Cysteine-Cleavable Lipopolymers Regenerating Natural Phospholipid, Diacyl Phosphatidylethanolamine. *Bioconjugate Chem.*, **1999**, *10*, 703-707.

30. Sella, E.; Weinstain, R.; Erez, R.; Burns, N. Z.; Baran, P. S.; Shabat, D., Sulfhydryl-Based Dendritic Chain Reaction. *Chem. Commun.*, **2010**, *46*, 6575-6577.

31. Lasic, D. D., *Liposomes in Gene Delivery*. Taylor & Francis: **1997**.

32. Friis, E. P.; Andersen, J. E. T.; Madsen, L. L.; Bonander, N.; Møller, P.; Ulstrup, J., Dynamics of Pseudomonas Aeruginosa Azurin and Its Cys3ser Mutant at Single-Crystal

Gold Surfaces Investigated by Cyclic Voltammetry and Atomic Force Microscopy. *Electrochimi. Acta*, **1998**, *43*, 1114-1122.

33. Mayhew, S. G., The Redox Potential of Dithionite and Sulfur Dioxide(1-) from Equilibrium Reactions with Flavodoxins, Methyl Viologen and Hydrogen Plus Hydrogenase. *Eur. J. Biochem.*, **1978**, *85*, 535-47.

34. Gilbert, R. G.; Hess, M.; Jenkins, A. D.; Jones, R. G.; Kratochvil, P.; Stepto, R. F. T.; Baron, M.; Kitayama, T.; Allegra, G.; Chang, T.; dos Santos, C.; Fradet, A.; Hatada, K.; He, J.; Hellwich, K. H.; Hiorns, R. C.; Hodge, P.; Horie, K.; Jin, J. I.; Kahovec, J.; Kubisa, P.; Meisel, I.; Metanomski, W. V.; Meille, V.; Mita, I.; Moad, G.; Mormann, W.; Ober, C.; Penczek, S.; Rebelo, L. P.; Rinaudo, M.; Schopov, I.; Schubert, M.; Schue, F.; Shibaev, V. P.; Slomkowski, S.; Tabak, D.; Vairon, J. P.; Vert, M.; Vohlidal, J.; Wilks, E. S.; Work, W. J., Dispersity in Polymer Science (Iupac Recommendations 2009). *Pure Appl. Chem.*, **2009**, *81*, 351-353.

35. McCarley, R. L.; Forsythe, J. C.; Loew, M.; Mendoza, M. F.; Hollabaugh, N. M.; Winter, J. E., Release Rates of Liposomal Contents Are Controlled by Kosmotropes and Chaotropes. *Langmuir*, **2013**, *29*, 13991-13995.

36. Mendoza, M. F.; Hollabaugh, N. M.; Hettiarachchi, S. U.; McCarley, R. L., Human Nad(P)H:Quinone Oxidoreductase Type I (Hnqo1) Activation of Quinone Propionic Acid Trigger Groups. *Biochemistry*, **2012**, *51*, 8014-8026.

37. Balasubramanian, S. M., McCarley, R. L., Unpublished Work, Louisiana State University.

38. Johnson, S. L.; Morrison, D. L., Kinetics and Mechanism of Decarboxylation of N-Arylcarbamates. Evidence for Kinetically Important Zwitterionic Carbamic Acid Species of Short Lifetime. *J. Am. Chem. Soc.*, **1972**, *94*, 1323-34.

CHAPTER 3
A RAPID, SELECTIVE, AND SENSITIVE FLUORESCENT PROBE FOR THE DETECTION AND CELLULAR IMAGING OF PHYSIOLOGICALLY SIGNIFICANT THIOLS*

3.1 Introduction

Biologically relevant thiol compounds (bio-thiols)—such as glutathione (GSH), cysteine (Cys), and homocysteine (Hcy)—play a crucial role in living systems.[1] They are the most abundant low-molecular mass sulfhydryls (LMM-SHs) occurring in the extracellular milieu. Together with albumin, GSH, Cys, and Hcy, these species represent almost all the thiols in mammalian plasma.[2]

Variations in cellular bio-thiol levels are intimately linked to a wide collection of diseases, such as cancer, HIV, cystic fibrosis, Parkinson's disease, and diabetes.[3] Monitoring the ratio of GSH to its corresponding disulfide is a key route for assessing cellular oxidative stress levels associated with these diseases. As an example, in diabetic patients chronic exposure to hyperglycemic conditions that can lead to cellular dysfunction become irreversible over time; this process is termed glucose toxicity. As a result, elevated glutathione levels are observed in the pancreatic β-cells of diabetic patients because reactive oxygen species are produced via oxidative phosphorylation during anaerobic glycolysis. According to recent findings, aging is also correlated with a decrease in plasma GSH and other main sulfhydryl compounds, with a concomitant rise in most oxidized forms of LMM-SHs.[4] Furthermore, GSH metabolism has an intricate and significant role in both cancer and antineoplastic therapy.[5] As good scavenger of reactive species, thiols are important in detoxification of harmful chemicals, such as epoxides, alkenes, halides, heavy metals, and various oxygen– and nitrogen–centered radicals. But on the other hand, elevated levels of thiols in many types of tumors may also increase resistance to chemotherapy and radiotherapy.[5]

---

*Portions of this chapter previously appeared as Nawimanage, R. R.; Prasai, B.; Hettiarachchi, S. U.; McCarley, R. L., Rapid, Photoinduced Electron Transfer-Modulated, Turn-on Fluorescent Probe for Detection and Cellular Imaging of Biologically Significant Thiols. *Anal.Chem.*, **2014**, 86, 12266-12271. (Featured article "*ACS Editor's Choice"*). It is reprinted by permission of copyright (2014) from the American Chemical Society.

Increased total Hcy level in blood is denoted as hyperhomocysteinemia, and it is emerging as a strong risk factor for atherosclerotic vascular diseases. Moreover, Hcy levels in plasma and serum are also valuable indicators of pregnancy complications, vitamin B12 and folate deficiencies, and mental disorders.[6]

In cells, bio-thiols exist mostly in their reduced thiol form, with total LMM thiol concentration being 2–17 mM; glutathione makes up approximately 90% of intracellular LMM bio-thiols.[2, 7] In stark contrast, cysteine, homocysteine, and glutathione are present in the extracellular (plasma) environment at very low concentrations, roughly 12–20 μM.[7] In the cytosolic compartment, protein thiols are more abundant (10–50 mM) than free LMM thiols, and they are over whelmingly in the reduced from (90%). Human serum albumin is the most abundant plasma protein, and it accounts for 55–60% of the measured serum protein.[8] Although most of the previously reported probes are sensitive to millimolar levels of thiols, there are few extant methods that can detect LMM thiols at low micromolar concentrations with good selectivity and sensitivity.[9-10]

Thus, the development of efficacious methods for detection and quantification of bio-thiols has received significant attention in recent years.[7] Many instrumental methods for the detection of thiols have been reported, such as high performance liquid chromatography, capillary electrophoresis, mass spectrometry, and electrochemical methods. However, these methods have certain limitations, such as complex sample processing and high equipment cost, which make them impractical for routine clinical analysis. Owing to their simplicity, low cost, and selectivity, a variety of colorimetric and fluorescent probes have gathered much attention during the last decade, particularly those probes that take advantage of either the high nucleophilicity of thiols or their affinity for transition metals.[1] Presently, there is a small group of environmentally stable probes whose fluorescence is turned on in the complex media of mammalian cells only by the collective presence of the biologically relevant thiol compounds. Fluorescence ensues from these probes upon their activation by thiol reactions of varying selectivity; for example, cleavage,[11] cyclization,[12] or metal-complex displacement,[13] to name a few. Recent approaches that make use of Michael addition reactions for probe activation include those employing Michael acceptors, such as maleimide,[14-15] squarine,[15] oxa-norbornadiene,[16] chromane,[17] propiolate,[18] acrylic acid,[19] unsaturated aldehydes/ketones,[19-21] and malonitrile,[22] as well as quinones.[23-24]

To date, most of these probes that respond to thiol presence are limited in bio-analysis and cellular imaging applications, as a result of slow response time and decreased water solubility of probe, the large fluorescence background response of the probe in comparison to the signal of the reporter (caused by spectral overlap of probe and reporter absorption/emission), and the requirement of highly concentrated analyte to elicit significant reporter response (leads to high limits of detection). Furthermore, the GSH/Cys/Hcy selectivity of these previously reported probes with regard to presence of H_2S or protein thiols is either not known or is quite poor.

Thus, due to the crucial role that GSH, Cys, and Hcy play in biological systems, particularly within cells, it is important to develop probes that are passively taken up by cells in a quick fashion; whose fluorescence signal is rapidly turned on in the presence of these three biological thiols, while remaining fluorescently silent upon exposure to other biologically important analytes; and whose fluorescence background response in comparison to the signal of the reporter is exceedingly small (minimal spectral overlap of probe and reporter absorption/emission), so as to allow for cellular imaging with high contrast (large signal-to-background ratio).

The work here presents the design, synthesis, and evaluation of a quinone–based, turn on probe HMBQ-Nap 1 (Figure 3.1) that offers rapid and selective detection of physiological thiols at the sub-micromolar level, and yields quick (<5 min) and selective imaging of bio-thiols within human cancer cells. The general design rationale of the photoinduced-electron

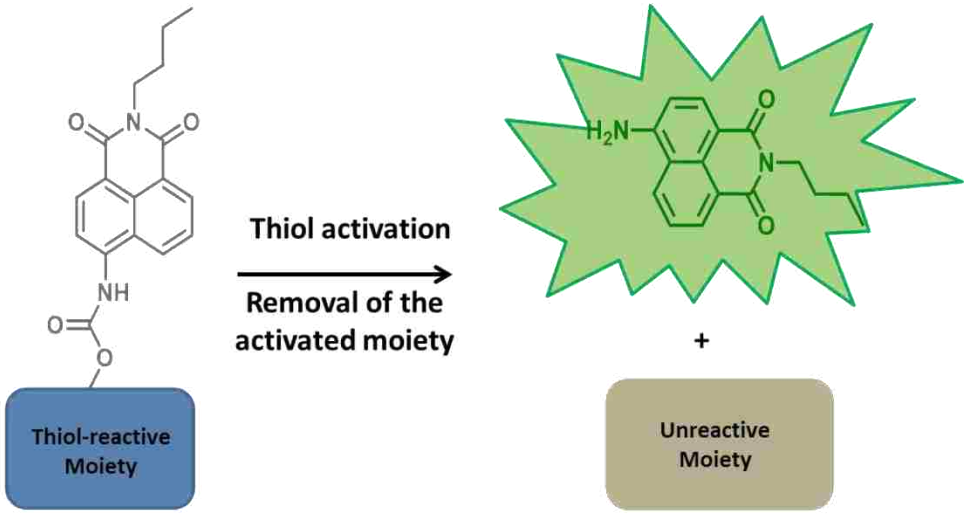

Figure 3.1 Design concept of thiol–activated fluorescence probe HMBQ-Nap 1.

transfer (PeT) quenched fluorescence probe HMBQ-Nap 1 is as follows. HMBQ-Nap 1 contains 4-amino-9-(*n*-butyl)-1,8-naphthalimide (Nap 2) as the reporter dye and hydroxymethyl benzoquinone (HMBQ) as the PeT quencher and potential reaction site for thiols. Thus, upon successful thiol–probe interaction (elimination of thiol-HMBQ product and CO_2), a highly intense fluorescence signal is expected. Furthermore, the electrically neutral HMBQ-Nap 1 should enter cells readily[25] and report the presence of bio-thiols.

3.2 Experimental

3.2.1 Synthetic Material and Methods

All the column purifications were performed using SNAP silica columns on a Flashmaster Personal from Biotage. Chemicals were purchased from Sigma-Aldrich or Fisher Scientific. Thin-layer chromatography was performed on aluminium-backed 60 F_{254} silica plates from EMD Chemicals Incorporated. All the ^{1}H NMR and ^{13}C NMR spectra were collected in D_2O or DMSO-d_6 at 25 $^{\circ}C$ on a Bruker AV-400 Spectrometer. Chemical shifts are reported in the standard δ notation of parts per million, using tetramethylsilane (TMS) as an internal reference. Absorption bands in NMR spectra are listed as singlet (s), doublet (d), triplet (t), or multiplet (m), and the coupling constants *J* are expressed in hertz (Hz). Mass spectral analyses were carried out using an Agilent 6210 ESI-TOFMS. All the solutions were prepared using Nanopure water from a Barnstead Diamond Nanopure water System (18 MΩ-cm).

3.2.2 Synthesis

The synthesis of hydroxymethyl benzoquinone (HMBQ) was described in the previous chapter, 4-amino-9-(*n*-butyl)-1,8-naphthalimide (Nap 2) and HMBQ-Nap 1 were synthesized by adapting literature methods. A synthesis scheme for the synthesis of HMBQ-Nap 1 is shown in the Scheme 3.1. [26]

4-Amino-9-(*n*-butyl)-1,8-naphthalimide (Nap 2)

Under nitrogen atmosphere, 4-amino-1,8-napthalic anhydride 4 (1.14 g, 4.6 mmol) was dissolved in 250 mL ethanol and brought to reflux. Upon addition of the *n*-butylamine (2.0 mL, 20.23 mmol) the mixture was refluxed for 14 h. After cooling, the solvent was removed under

reduced pressure, and the crude material was purified on a flash column (20:1 DCM: EtOAc) to yield the product Nap 2 as a yellow solid in 75% yield.

^{1}H NMR (400 MHz, DMSO-d_6) δ 8.61 (d, J = 8.4 Hz, 1H), 8.43 (d, J = 7.3 Hz, 1H), 8.24 – 8.13 (m, 1H), 7.66 (t, J = 7.9 Hz, 1H), 7.43 (s, 2H), 6.85 (d, J = 8.6 Hz, 1H), 4.01 (t, J = 7.5 Hz, 2H), 1.58 (p, J = 7.5 Hz, 2H), 1.33 (h, J = 7.7 Hz, 2H), 0.95 – 0.89 (m, 3H). ^{13}C NMR (126 MHz, DMSO-d_6) δ 14.22, 20.30, 30.31, 108.04, 108.62, 119.83, 122.27, 124.45, 129.73, 130.14, 131.45, 134.40, 153.14, 163.36, 164.23. ESI-MS: for $C_{16}H_{16}$: N_2O_2: expected m/z = 269.1292 $[M+H]^+$; found m/z = 269.1288 $[M+H]^+$; 1.5 ppm error.

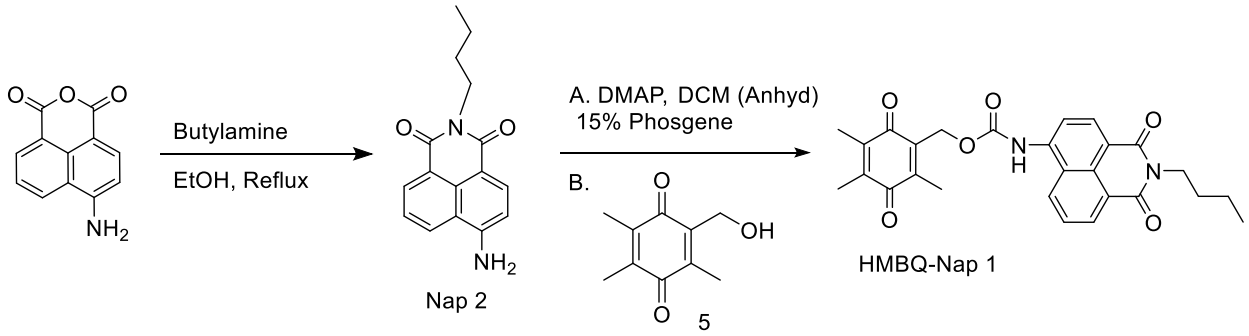

Scheme 3.1 Synthesis of HMBQ-Nap.

Synthesis of HMBQ-Nap 1

4-Dimethylaminopyridine (DMAP; 32.92 mg, 0.27 mmol) was added to a solution of Nap 2 (36.39 mg, 0.14 mmol) in anhydrous DCM, then to the mixture was added a solution of phosgene (15% toluene, 1 mL) at −10 °C and stirred under argon for 3 h. The excess phosgene was removed by bubbling argon gas through the solution for 30 min. To this resulting solution was added compound 5 (70.39 mg, 0.39 mmol), and the solution was stirred at 0 °C for an additional 12 h. The reaction mixture was quenched with water (30 mL) and extracted with CH_2Cl_2 (3 × 50 mL). The organic phase was dried over Na_2SO_4, subsequently filtered, and the solvent was evaporated. The crude product was purified by silica gel flash column using CH_2Cl_2/EtOAc (10:1, v/v). The final product was obtained as a yellow solid. ^{1}H NMR (400 MHz, DMSO-d_6) δ 10.30 (s, 1H), 8.65 (dd, J = 8.8, 3.7 Hz, 1H), 8.57–8.43 (m, 2H), 8.16 (dd, J = 8.3, 3.7 Hz, 1H), 7.82 (td, J = 8.2, 3.6 Hz, 1H), 5.14 (d, J = 3.5 Hz, 2H), 4.03 (q, J = 6.0, 4.4 Hz, 2H), 2.15 (d, J = 3.7 Hz, 3H), 1.99 (d, J = 3.5 Hz, 6H), 1.61 (p, J = 7.4 Hz, 2H), 1.42–1.30 (m, 2H), 0.97–0.87 (m, 3H). ^{13}C NMR (100

MHz, DMSO-d_6) δ 12.56, 12.72, 14.18, 20.26, 30.14, 58.52, 117.70, 118.89, 122.70, 124.40, 126.86, 128.78, 129.76, 131.37, 132.11, 136.80, 140.48, 141.14, 144.82, 154.19, 163.38, 163.92, 185.92, 187.42 ESI-MS: for $C_{27}H_{26}N_2O$: expected *m/z* 475.188 $[M+H]^+$; found *m/z* = 475.1864 $[M+H]^+$; 1.5 ppm error.

3.2.3 Spectroscopic Methods

All spectroscopic measurements were performed in phosphate buffer/0.1 M KCl solutions, pH 7.4. Fluorescence data were collected using a Perkin Elmer LS-55 spectrometer, and absorption spectra were recorded using a Varian Cary-50 spectrophotometer. Samples for absorption and emission measurements were obtained in 1-cm × 1-cm quartz cuvettes (3.5 mL volume, Sigma-Aldrich).

3.2.4 Voltammetric Measurements

Cyclic voltammetry was performed in 0.1 M (*n*-butyl)$_4$NClO$_4$/dry acetonitrile under anaerobic conditions. Power Suite 2.53 operating software was used with a Princeton Applied Research Model 273A Potentiostat/Galvanostat. Voltammograms were collected at scan rate of 0.1 Vs^{-1} at room temperature (25 $^{\circ}$C) after degassing the solution with nitrogen for 20 min. Glassy carbon working (BAS, 3-mm diameter), platinum wire counter, and Ag/AgCl reference (BAS) electrodes were used, and the potentials were referenced versus ferrocene/ferrocenium internal standard.

3.2.5 Procedure for Thiol Sensing

A stock solution of 100 μM HMBQ-Nap 1 was prepared in 100% DMSO and was subsequently diluted to prepare preferred concentration solutions of HMBQ-Nap **1** in pH 7.4 DMSO/PBS buffer (10% DMSO:90% 0.1 M PBS buffer). Stock solutions of thiol were freshly prepared prior to each experiment. For the calibration curve, the solution of HMBQ-Nap **1** was incubated with different concentrations of thiols at 25 $^{\circ}$C for 15 min, and spectral data were recorded. Excitation was performed at 432 nm, and emission was detected at 540 nm. The excitation and emission slit widths were set at 2.5 nm.

3.2.6 NQO1 Enzyme Kinetics

All fluorescence measurements (λ_{ex} = 432 nm, λ_{em} = 540 nm) were obtained at 25 °C, using a Fluorostar Optima plate reader with solutions made in pH 7.4, 0.1 M PBS/0.1 M KCl/0.007% BSA. A stock solution of 400 μM β-nicotinamide adenine dinucleotide reduced disodium salt (NADH, Sigma-Aldrich) was prepared in pH 7.4, 0.1 M PBS/0.1 M KCl/0.007% BSA so the subsequent assay solutions possessed a final concentration of 1×10^{-4} M β-NADH in each well. A stock solution of HMBQ-Nap 1 in 100% DMSO was made and then diluted to obtain a concentration series from 5×10^{-7} to 11.5×10^{-6} M probe in pH 7.4, 0.1 M PBS/0.1 M KCl/0.007% BSA 2×10^{-3}g mL^{-1} stock solution of recombinant hNQO1 (Sigma-Aldrich) was prepared using the same buffer/BSA system as above so as to give 2.0×10^{-6} g hNQO1 per assay. Assays were performed in a quartz 96-well plate containing an appropriate amount of HMBQ-Nap 1 stock solution to obtain the preferred concentrations, 50 μL of enzyme solution, and an amount of BSA solution to make a total volume of 150 μL in a well. Measurements were initiated by the addition of 50 μL NADH solution. Measurements were collected every 30 s for 10 min. Fluorescence units were converted to concentration by relating the signal increase to a fluorescence signal derived from a known concentration of Nap 2 reporter. The linear portion of the plots of velocity versus HMBQ-Nap 1 concentration were used to obtain apparent K_m and V_{max} values from nonlinear least-squares analysis employing algorithms developed by Cleland for Michaelis−Menten kinetics.

3.2.7 Cell Culture

Human non-small cell lung cancer cells H596, cell culture base media, and fetal bovine serum (FBS) were purchased from American Type Cell Culture (ATCC, Manassas, VA). All cell culture procedures were performed as suggested by ATCC. H596 cells were cultured in RPMI-1640 with 10% FBS and 100 IU/ml penicillin-streptomycin. Cells were incubated at 37 °C in a humidified incubator containing 5% wt/vol CO_2.

3.2.8 Cell Imaging via Scanning Laser Confocal Microscopy

H596 cells were cultured overnight on 22-mm × 22-mm glass cover slips on a treated tissue culture 6-well plate purchased from Fisher Scientific. The existing growth medium was replaced with 2 mL of fresh medium and then incubated at 37 °C. Solutions of HMBQ-Nap **1** dissolved in

DMSO were added to the cells to give final concentration of 2×10^{-5} M of HMBQ-Nap **1**, keeping the DMSO concentration at < 1%. Then cells were incubated with HMBQ-Nap **1** at 37 °C for 10 min. Cells were then treated with 3.0×10^{-6} M DRAQ5 (nuclear stain obtained from Thermo Scientific) for 1 min. Next, the medium was removed, and the cells were fixed in 2 mL of 4% paraformaldehyde for 15 min with shaking. After fixing, the cells were rinsed with Nanopure water, and the cover slips were mounted to glass slides with Immumount (obtained from Fisher Scientific). Glass slides were left in the dark overnight to allow the Immumount to dry. Confocal images were acquired using a Leica TCS SP2 spectral confocal microscope. For images of cells exposed to HMBQ-Nap 1, samples were excited using the 458-nm line of an Ar/KrA laser (laser intensity = 72%), and the spectral emission was collected between 458 and 514 and 514 and 680 nm (Leica DD458/514); PMT voltage = 710 V. Similarly, cells exposed to DRAQ5 were excited using the 633-nm line of a HeNe laser (laser intensity = 35%), and the spectral emission was collected between 678 and 773 nm. All images were collected using a pinhole of 3.1 Airy units. Images were frame and line averaged 4 times. Image analysis was performed using ImageJ and Leica LAS AF lite software. As the control experiment to scavenge all the thiols in cells, H596 cells were pre–incubated with 10 mM *N*-ethylmaleimide (NEM) at 37 °C for 30 min. Then the cells were washed with 0.1 M, pH 7.4 PBS to remove any excess NEM, followed by incubation with 2×10^{-5} M HMBQ-Nap 1 prior to their being fixed as described previously.

3.3 Results and Discussion

3.3.1 Spectral Properties of HMBQ-Nap 1 / Nap 2 System

To demonstrate the off-on nature of the probe 1/reporter 2 system, the absorbance and fluorescence emission spectra of HMBQ-Nap 1 probe and pure Nap 2 reporter were obtained in aqueous phosphate buffer media at physiological pH (pH 7.4), Figure 3.2. HMBQ-Nap 1 probe shows absorbance maximum around 380 nm and very low (almost negligable) emission maximum around 460 nm Figure 3.2 (a). The free reporter Nap 2 (Figure 3.2 (b)) displays absorbance maximum at 432 nm with significantly large fluorescence enhancement at 540 nm.

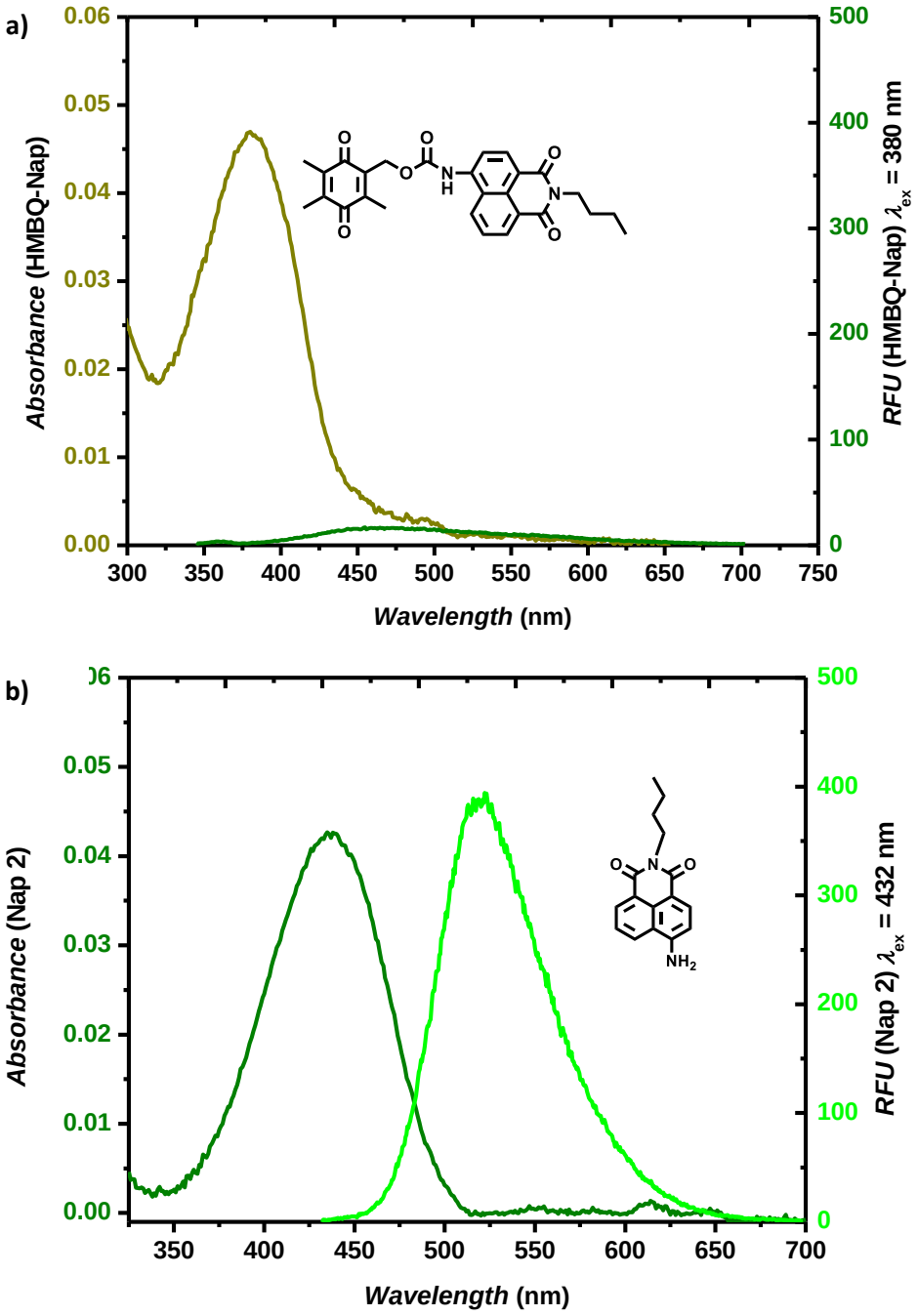

Figure 3.2 Absorption and emission spectra of 2×10^{-6} M (a) HMBQ-Nap 1 and (b) Nap 2 in 10% DMSO/90% 0.1 M, pH 7.4 phosphate-buffered saline (PBS) at 25 °C.

Nap 2 exhibits a strong Stokes shift between its absorption (λ_{abs} = 432 nm) and fluorescence emission (λ_{em}= 535 nm) maximum due to internal charge transfer, and the absorption maximum

of Nap 2 is red–shifted by ~70 nm from that of the HMBQ-Nap **1** probe making this set an excellent probe/reporter pair with minimum spectral overlap. To make sure efficient PeT quenching, quantum yields were also obtained in 90% aqueous buffered media with pH 7.4 phosphate buffered saline in 10% DMSO as co-solvent.

3.3.2 Calculation of Quantum Yield

Fluorescence quantum yields of Nap 2 dye and HMBQ-Nap 1 were determined with reference to two different standards, coumarin in EtOH ($\Phi = 0.54$) and quinine sulfate in 1 N H_2SO_4 ($\Phi = 0.51$).[27] Initially, a stock solution of Nap 2 was prepared in DMSO and diluted with 10% DMSO:90% 0.1 M, pH 7.4 phosphate–buffered saline to yield an absorbance between 0.02–0.08 absorbance units. Similarly, stock solutions of coumarin samples were also prepared in ethanol and diluted until the absorbance fell between 0.02–0.08 absorbance units. Then solutions were transferred to a 1-cm × 1-cm quartz cuvette and fluorescence measurements were taken by exciting the sample at the cross–over point of the absorbance spectra as shown in Figure 3.3 (a). In the same way as described above, fluorescence measurements were obtained for the HMBQ-Nap 1 probe and the quinine sulfate sample (Figure 3.3 b).

$$\Phi_{F(X)} = \left(\frac{A_S}{A_X}\right)\left(\frac{F_X}{F_S}\right)\left(\frac{n_X}{n_S}\right)^2 \Phi_{F(S)} \qquad \text{Equation 3.1}$$

The quantum yields were then calculated according to the Equation 3.1 where Φ_F is the fluorescence quantum yield, *A* is the absorbance at the excitation wavelength, *F* is the area under the corrected emission curve, and *n* is the refractive index of the solvents used. Subscripts S and X refer to the standard and to the unknown, respectively. Since the samples were excited at the cross over point of the two sample absorbances the values were canceled out. Similarly refractive indexes were canceled out due to the majority of the media being aqueous; simplifying the equation where area *F* accounts for the number of emitted photons. Calculated quantum yields for the probe HMBQ-Nap 1 and reporter Nap 2 were $\Phi_{\text{HMBQ-Nap 1}}$ =0.003 and $\Phi_{\text{Nap 2}}$ = 0.19. Based on its extremely low intensity emission spectrum (Figure 3.2 (a)) and miniscule quantum yield, the fluorescence of the HMBQ-Nap 1 probe is quenched in a highly effective manner in

stark contrast to the 65 times brighter Nap 2 reporter. This characteristic is attributed to HMBQ-Nap 1 being efficiently PeT quenched. Nap 2 reporter and HMBQ head group in HMBQ-Nap 1 act as a good donor and acceptor moiety making the probe efficiently PeT quenched. To further evaluate this possibility electrochemical measurements were carried out and are described in the following section.

3.3.3 Thermodynamic Feasibility of PeT quenching

To assess the thermodynamic feasibility of fluorescence quenching of HMBQ-Nap 1 by oxidative photo-induced electron transfer (OeT), voltammetric measurements of HMBQ-Nap 1 and its components (Figure 3.3, Figure 3.4 and, Figure 3.5) were used in conjunction with the Rehm-Weller equation (Equation 3.2) to calculate the free energy of the PeT process.

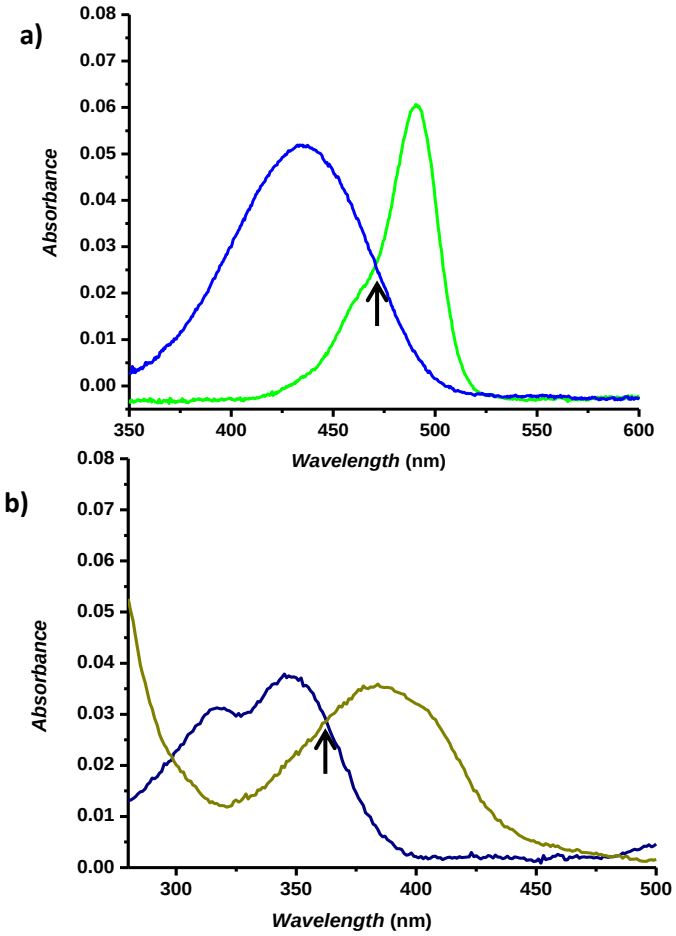

Figure 3.3 Absorbance overlap of a) Nap 2 (blue) in DMSO/0.1 M, pH 7.4 phosphate-buffered saline (PBS) with coumarin (green) in EtOH/0.1 M, pH7.4 PBS, and b) HMBQ-Nap (yellow) in DMSO/ 0.1 M, pH 7.4 PBS with quinine sulfate (blue) in 1 N H_2SO_4 at 25°C.

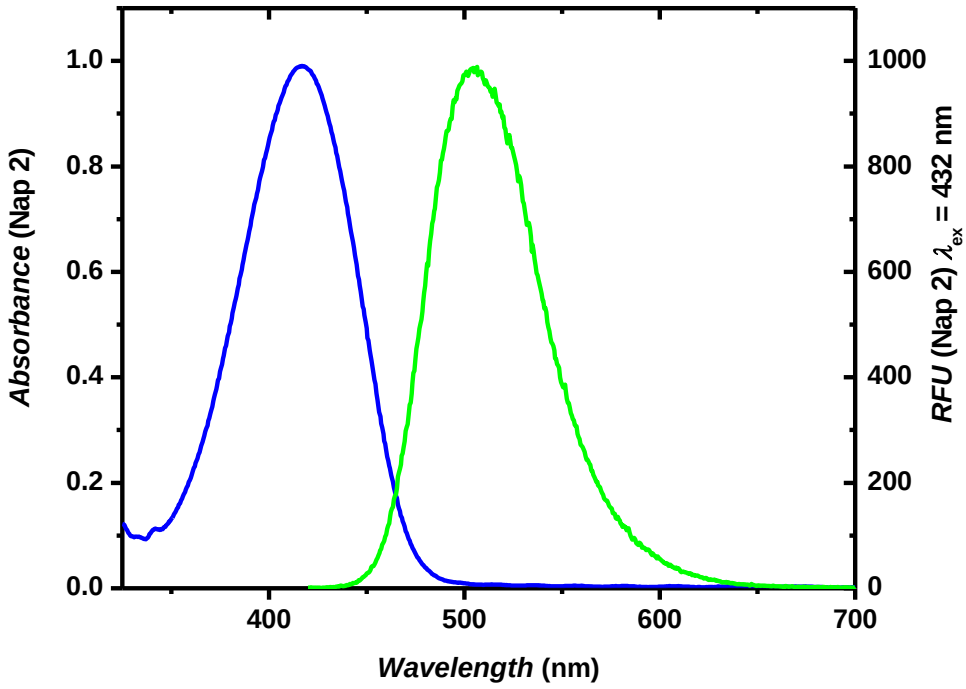

Figure 3.4 Absorption (blue) and emission (green) spectra of Nap 2 in acetonitrile at 25 °C.

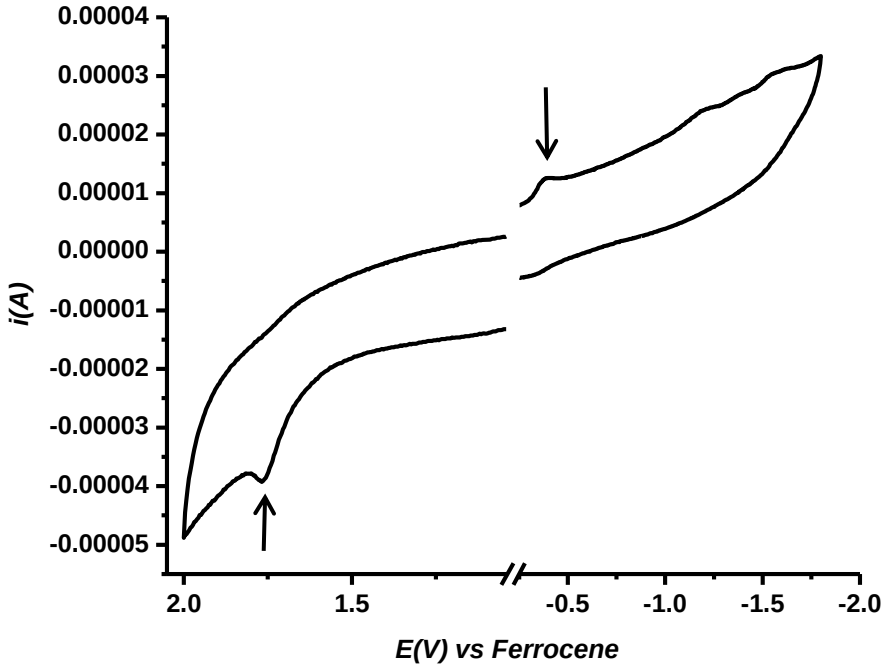

Figure 3.5 Cyclic voltammetry of HMBQ-Nap 1 at a 3-mm diameter glassy carbon working electrode using 0.1 M *tetra*–butylammonium perchlorate in acetonitrile. Scan rate was 0.1 V s^{-1}.

$$\Delta G_{PeT} = E_D - E_A - \Delta G_{00} - \frac{e^2}{\varepsilon d} \qquad \text{Equation 3.2}$$

From the cyclic voltammetric graphs (Figure 3.5) oxidation and reduction potentials of Nap 2 and head group HMBQ was determined. The OeT process, the redox potential (E_D) of the donor Nap 2 and the potential (E_A) of the acceptor HMBQ 3 were determined to be 1.24 V and −0.92 V, respectively. ΔG_{00}, the energy of the first excited singlet state of Nap 2, was found to be 2.67 eV and $e^2/\varepsilon d$ is the Coulombic interaction energy of the ion pair, known to be 0.06 eV. From these values, the energy change for OeT quenching, ΔG_{PeT}, is calculated to be −0.95 eV, indicating that electron transfer from the excited Nap 2 to the electron–poor HMBQ 3 is thermodynamically feasible.

3.3.4 Reduction Initiated Turn-on of HMBQ-Nap 1

As hypothesized, the reduction activation of the HMBQ-Nap 1 should initiate a cascade of reactions that would eliminate the reporter Nap 2, forming quinone methide and CO_2 as by products (Figure 3.6). Upon reduction the release of the Nap 2 reporter should turn on the bright fluorescence signal associated with it.

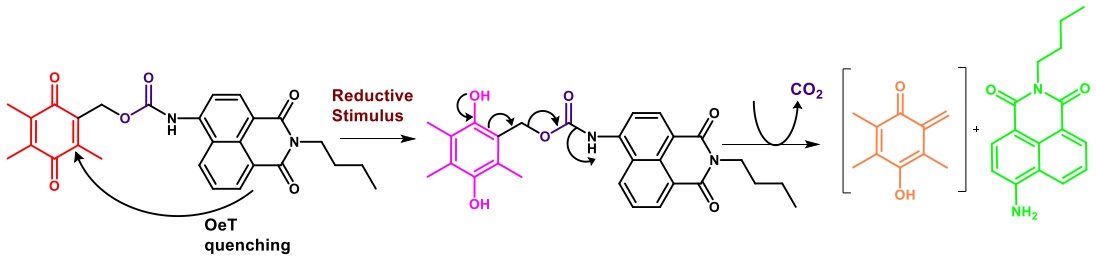

Figure 3.6 Schematic representation of reduction-activated elimination of HMBQ-Nap 1.

In order to determine the capability of HMBQ-Nap 1 to act as a turn-on probe upon reduction, aqueous solutions of HMBQ-Nap 1 were exposed to a solution of excess sodium dithionite (DT), and fluorescence was monitored at 540 nm while exciting the sample at 432 nm. As shown in the Figure 3.7, a rapid increase in fluorescence was observed both in the time-dependent fluorescence scan (excited at 432 nm and emission detection at 540 nm) and time-lapsed wavelength scan from 450 nm to 650 nm. Maximum release was achieved within about 250 s after addition of DT. Vigorous release of Nap 2 reporter after the initial reduction by dithionite was apparent by the appearance of the fluorescence band centered around 540 nm (Figure 3.7 inset), which matched exactly with the free Nap fluorescent band in 10%DMSO:

90% PBS at pH7.4. Invigorated by these results, I set out to find out the possible thiol–probing ability of HMBQ-Nap 1.

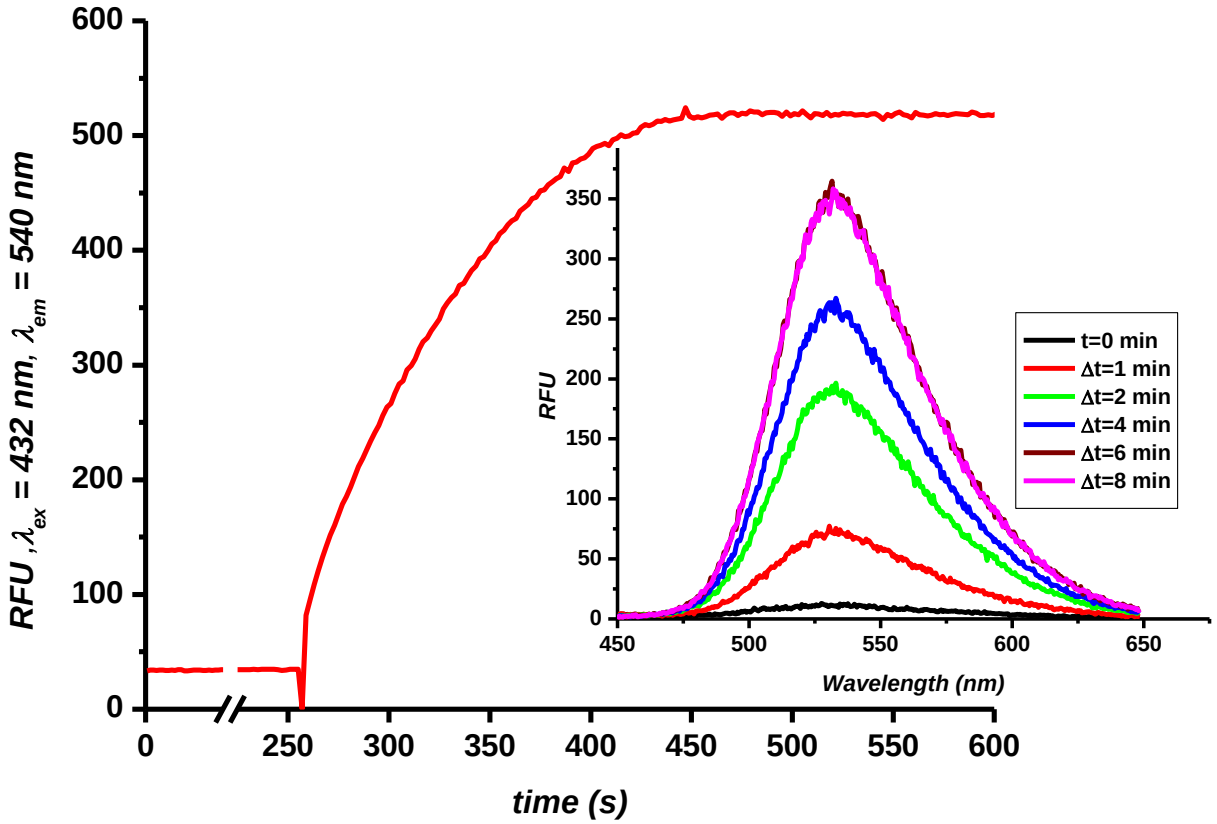

Figure 3.7 Time-dependent fluorescence of HMBQ-Nap 1 (10 μM), after addition of 50 μM $Na_2S_2O_4$ (DT) in 10% DMSO:90% pH = 7.4 PBS buffer at 25 °C. Inset: wavelength scan of 2 μM HMBQ-Nap 1 after DT addition from 450 nm–650 nm; $\Delta t = 2$ min.

3.3.5 In Vitro Response to Biological Thiols

The ability of HMBQ-Nap 1 to act as a turn-on thiol probe when in the presence of select biological thiols was determined by exposing aqueous, buffered solutions of HMBQ-Nap 1 to three physiologically significant non-protein thiols—GSH, Cys, and Hcy. As expected from previous DT reduction experiment (Figure 3.7) a rapid reaction response were observed with all three non-protein thiols. The rapid nature of the turn-on process was evidenced by the ~150 s time required to reach 90% of the maximum attainable signal, as shown in Figure 3.8. As expected for this group of biological thiols (similar thiol pK_a value) and the HMBQ trigger group, there is no significant difference in fluorescence signal profile. At this time, it is not known why the maximum achievable signal plateau is larger for GSH vs Cys and Hcy. The

temporal integrity of the fluorescence signal generated by production of Nap reporter was investigated so as to test for possible biological thiol-induced structural alterations of the Nap reporter. It was found that the fluorescence intensity of Nap was invariant when the reporter was treated with 100 equivalents of GSH (1 mM, Figure 3.8, green line) for up to 2000 s of incubation, the maximum time tested.

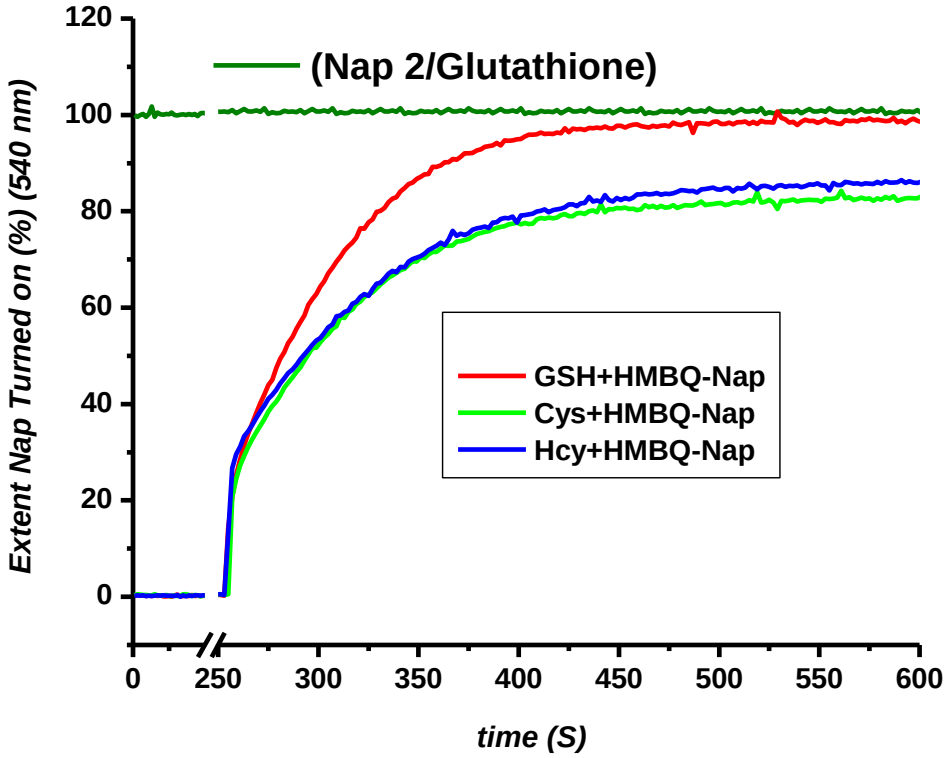

Figure 3.8 Time-dependent fluorescence (λ_{ex} = 432 nm, λ_{em}= 540 nm) from 10 μM HMBQ-Nap 1 incubated with 50 μM thiol-containing analyte in 0.1 M, pH 7.4 PBS/DMSO (9:1) at 25 $^{\circ}$C. Fluorescence signals were compared to that from a 10 μM solution of Nap 2. The stability of 10 μM Nap 2 with 1 mM GSH is demonstrated by the green line.

To determine whether the HMBQ-Nap 1 fluorescence turn-on response is a function of thiol concentration in the media, varying concentrations of all three thiols were incubated with 2 μM HMBQ-Nap 1 solution for 15 min (Figures 3.9–3.11), and then the turn-on response at 540 nm

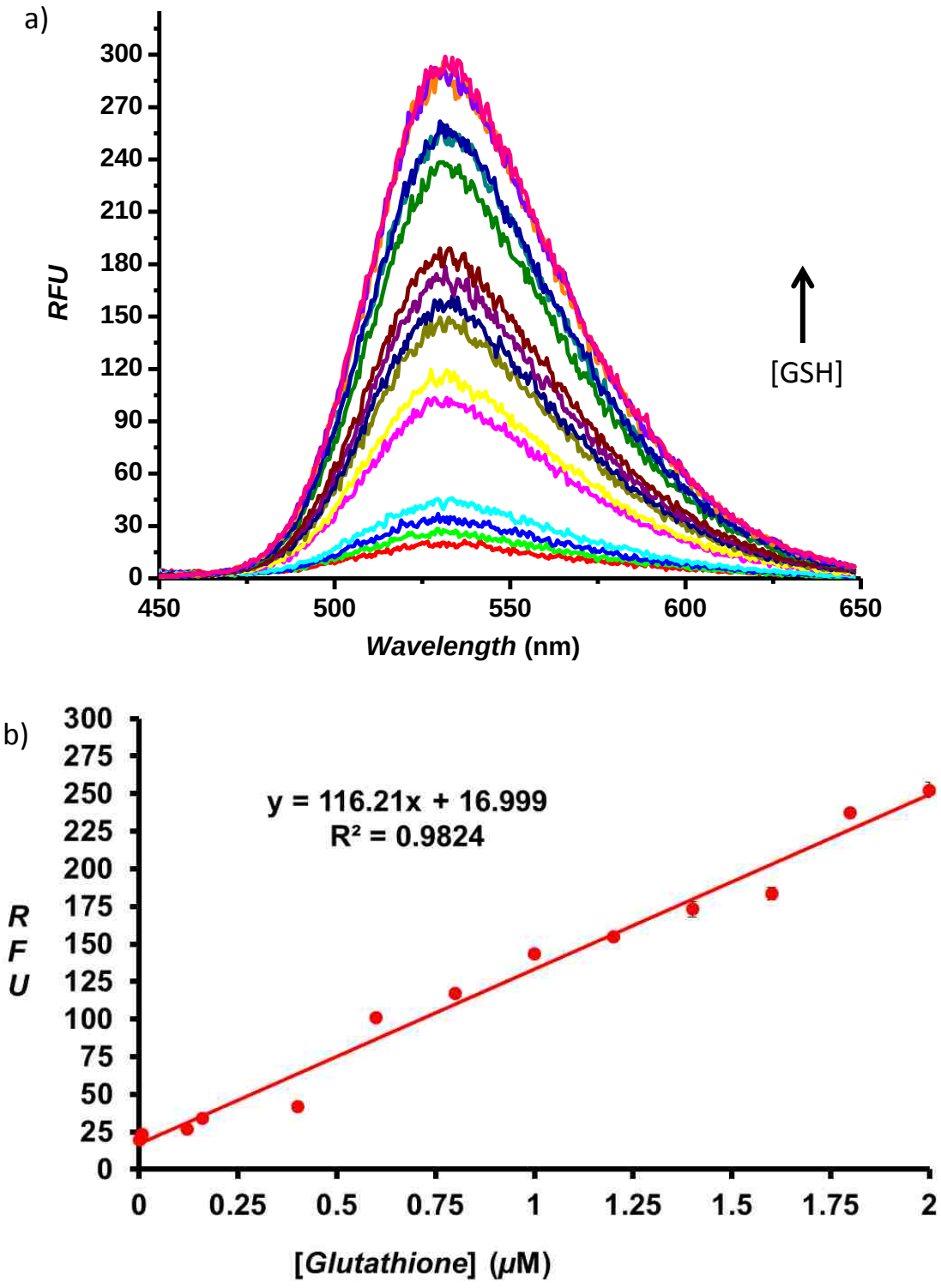

Figure 3.9 a) Fluorescence spectral changes of HMBQ-Nap 1 (2 μM) with a GSH (0–2 μM), b) the fluorescence intensity (λ_{ex} = 432 nm/λ_{em} = 540 nm) plot vs concentration of GSH. Error bars represent the standard deviation of the average data points for each concentration (n = 3).

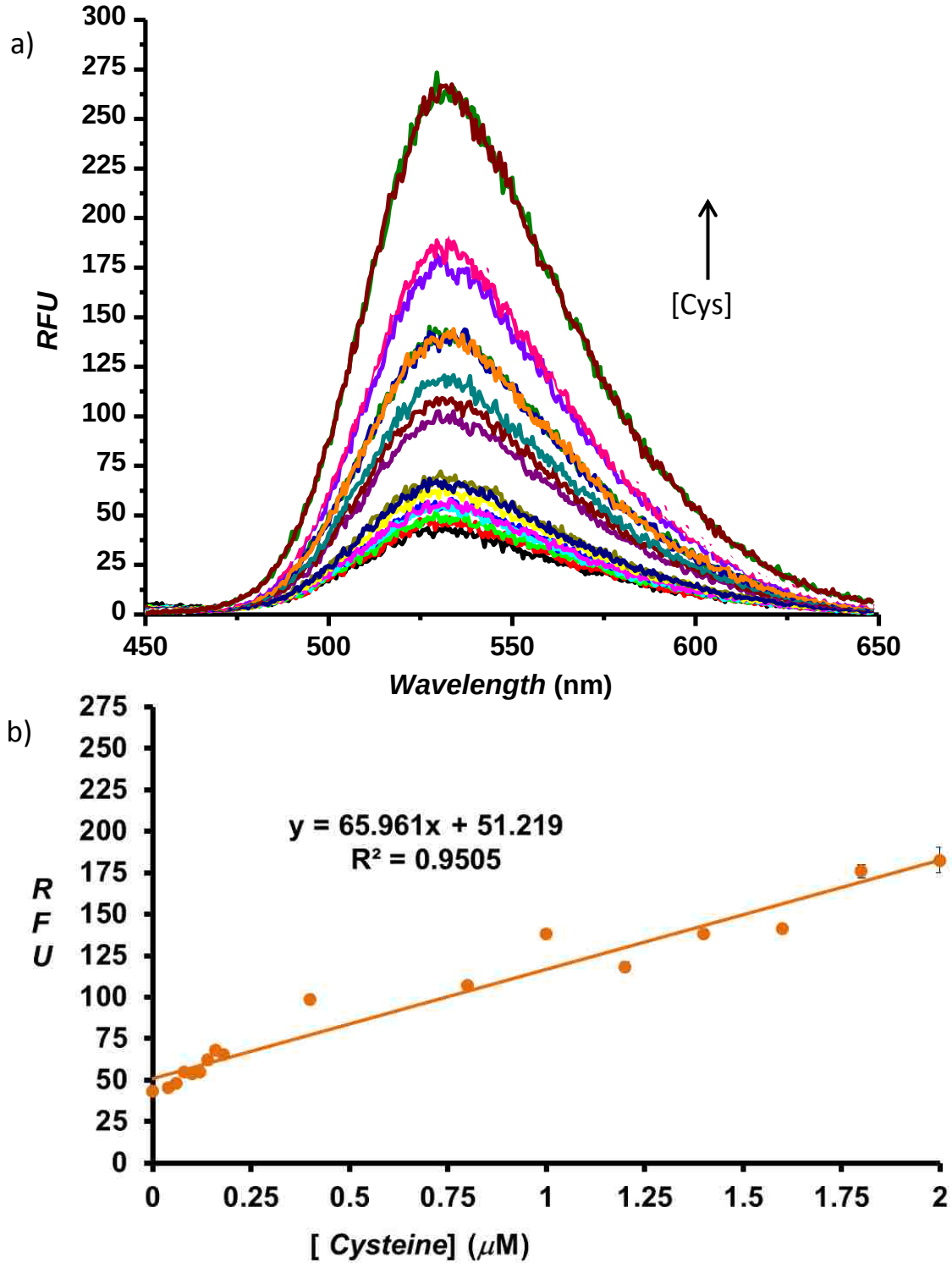

Figure 3.10 a) Fluorescence spectral changes of HMBQ-Nap 1 (2 μM) with Cys (0–2 μM), b) the fluorescence intensity (λ_{ex} = 432 nm/λ_{em} = 540 nm) plot vs concentration of Cys. Error bars represent the standard deviation of the average data points for each concentration (n = 3).

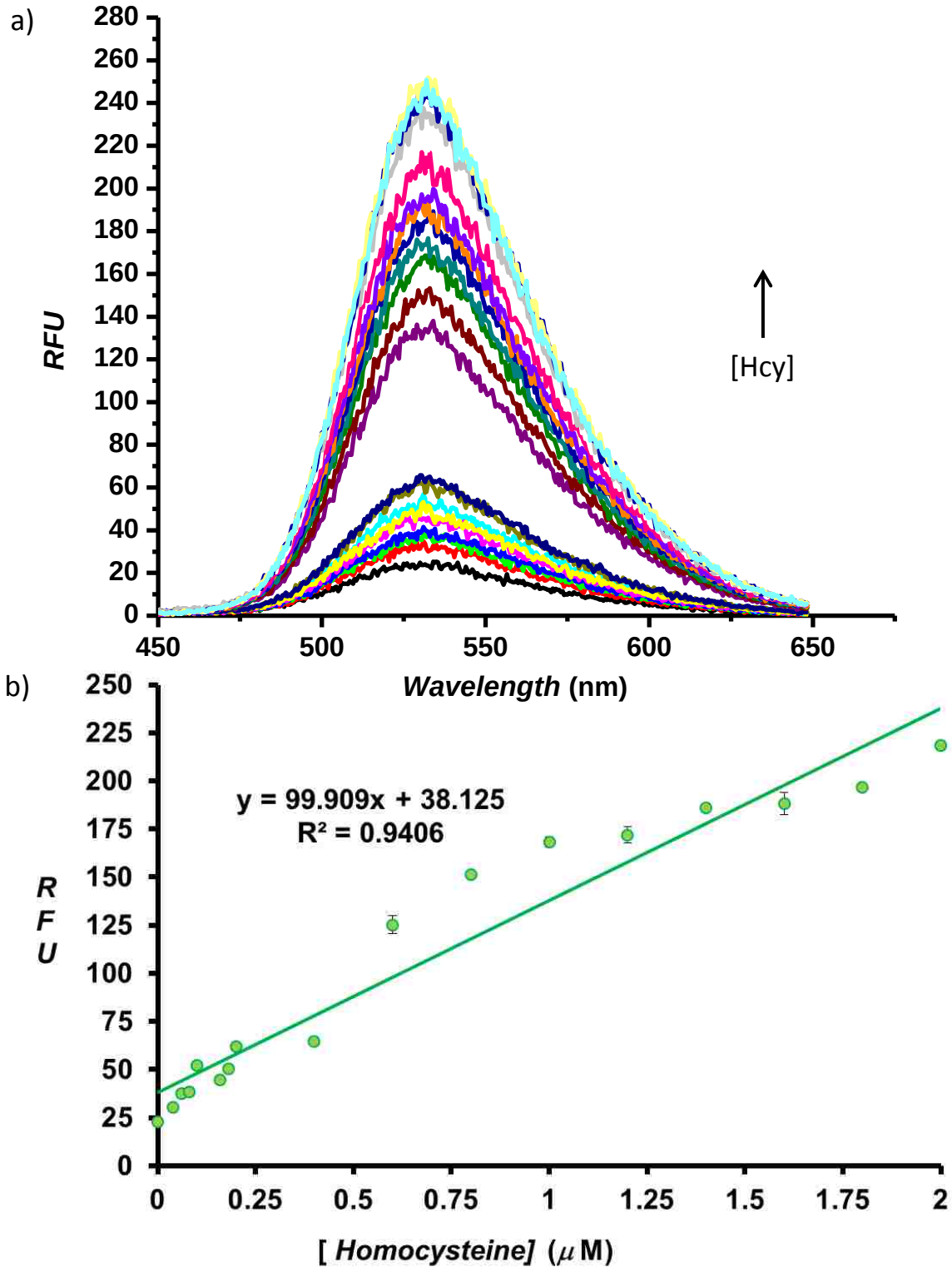

Figure 3.11 a) Fluorescence spectral changes of HMBQ-Nap 1 (2 μM) with Hcy (0–2 μM), b) the fluorescence intensity (λ_{ex} = 432 nm/λ_{em} = 540 nm) plot vs concentration of Hcy. Error bars represent the standard deviation of the average data points for each concentration (n = 3).

was measured. As shown by plots in Figures 3.9–3.11, the extent of the fluorescence increase was a function of the biological thiol: HMBQ-Nap 1 ratio. Upon evaluation of plots of the fluorescence intensity versus each biological thiol concentration it was found that there exists a linear relationship for bio-thiol concentrations up to 2 μM (Figure 3.9–3.11, b). From these calibration curves, it was determined that the concentration limit of detection for GSH, Hcy, and Cys was 33, 21, and 29 nM; and the concentration limit of quantification was 110, 70, and 98 nM respectively. These results indicate the potential use of HMBQ-Nap 1 probe for the rapid detection and quantification of lower nM range of thiols in physiological media.

As speculated by literature reports, possible turn-on mechanism of HMBQ-Nap 1 by thiols could be the result of either merely redox activation or a nucleophilic addition to the quinone moiety. Because there is no clear indication of the possible route, ^{1}H NMR and mass spectrometric studies were conducted to determine the products and then propose a plausible reaction mechanism for the release of the free reporter. NMR studies were carried out with mercaptoethanol, a thiol–containing small molecule as a mimic of cellular thiols in the media. As shown in Figure 3.12 (a and b), the initial NMR Spectrum of 2 mM HMBQ-Nap and 2 mM reporter Nap 2 in 9:1 DMSO:D_2O were recorded. Subsequently, 5 equivalents of mercaptoethanol were added to the HMBQ-Nap sample, and spectra were recorded every four seconds for about 4 hours. The rapid increase of peaks corresponding to Nap 2 reporter production was observed, and in addition, there were two sharp peaks around 6.12 ppm and 5.78 ppm that quickly appeared and then diminished as time progress. These peaks were speculated to be two alkene hydrogens in a quinone methide. To further evaluate this concept, the products formed by the added mercaptoethanol stimulus were further characterized by mass spectrometry analysis after vaccum drying the mercaptoethanol HMBQ-Nap sample. As shown in Figure 3.13, Nap 2 reporter was formed, as noted by the $[M-H]^-$ signal at *m/z* 267.1138 (expected *m/z* 267.1134; −1.50 ppm error) in panel a. Similarly, the mercapthoethanol product of the reactive quinone methide was observed in panel b, evidenced by the $[M-H]^-$ signal at *m/z* 239.0689 (expected *m/z* 239.0742; 22.2 ppm error). As seen in panel c, free HMBQ, resulting from water addition to the quinone methide, was also found to be present: $[M-H]^-$ signal at *m/z* 179.0688 (expected *m/z* 179.0708; 11.2 ppm error).

Outcomes from both ^{1}H NMR and mass spectrometry studies demonstrate that thiols undergo Michael addition to HMBQ-Nap in aqueous media to unleash Nap reporter and quinone methide

products; there is no indication of redox activation of HMBQ-Nap 1, as noted by the absence of spectroscopic signatures for reduced HMBQ (hydroquinone).

a)

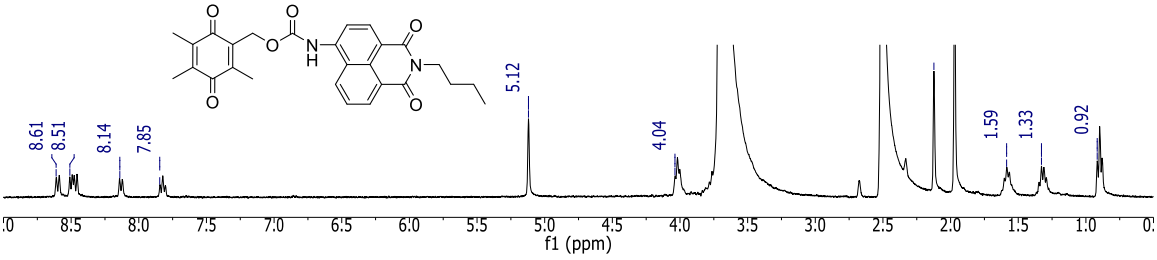

b)

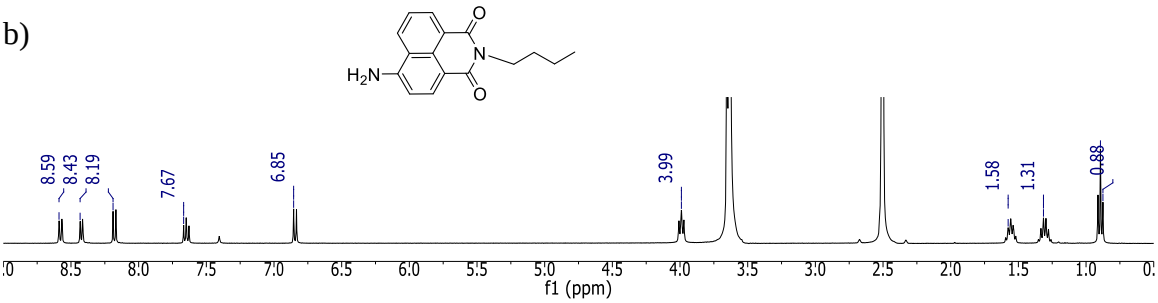

c) Mercapthoethanol added to **a**, Δt = 1 min

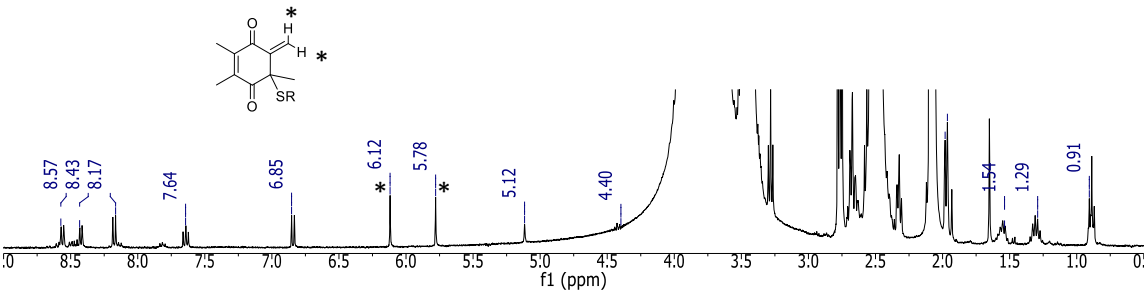

d) Same as c, Δt = 15 min

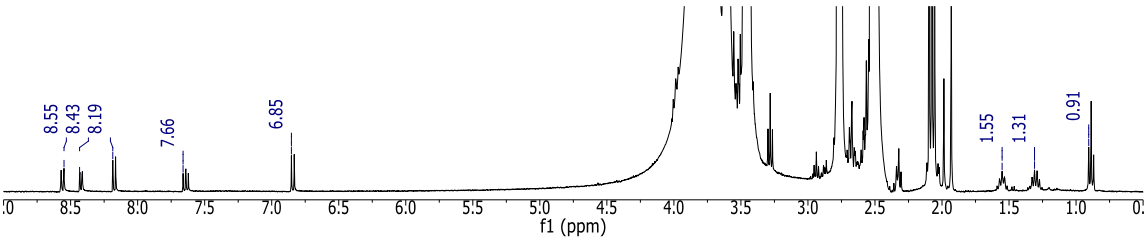

Figure 3.12 NMR spectra of: a) HMBQ-Nap 1 (2 mM) sample in 9:1 DMSO:D_2O; b) Pure Nap 2 sample in 9:1 DMSO:D_2O; c) upon addition of 5 equivalents of mercaptoethanol to a, spectrum

was recorded 1 min after addition; d) recorded spectrum of reaction mixture 15 min after addition.

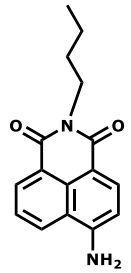

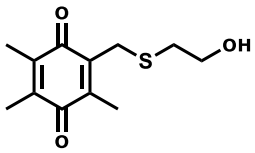

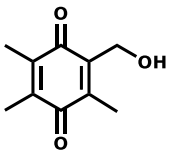

Figure 3.13 Negative-ion mass spectrum of HMBQ-Nap 1 upon reaction with mercaptoethanol to yield a) reporter 2 as observed by $[M-H]^-$ signal at *m/z* 267.1138 (expected *m/z* 267.1134,

−1.50 ppm error), b) mercaptoethanol product observed by $[M-H]^-$ signal at *m/z* 239.0689 (expected *m/z* 239.0742, 22.2 ppm error), c) HMBQ head group observed by $[M-H]^-$ signal at *m/z* 179.0688 (expected *m/z* 179.0708, 11.2 ppm error).

3.3.6 Selectivity of HMBQ-Nap to Biological Thiols

The potential sulfur-based, cross-reactive species H_2S and bovine serum albumin (BSA) were chosen for initial evaluation of HMBQ-Nap 1 selectivity. Hydrogen sulfide (H_2S), or more appropriately HS^- at physiological pH, has become an increasingly studied species in cells due to its link to cellular signaling pathways and a variety of inflammatory–associated diseases.[28] Even though its cellular concentration (nM) is estimated to be dwarfed by that of the more abundant biological thiols,[28] H_2S could possibly be an interferent because of the potential for it to undergo Michael addition to[29] or cause reduction of the HMBQ group. In addition, the protein content is roughly 20–25 wt% inside cells, with many of those proteins possessing free thiol groups.[30] Furthermore, over 90% of the extracellular thiols in blood are due to the presence of the most abundant protein (~60%), serum albumin.[31] Human serum albumin (HSA), like BSA, has only one free thiol (Cys 34);[32] this is a potential site of reaction with HMBQ-Nap. BSA was chosen for study here due to the known variability in the free thiol content of Cys 34 in HSA upon its storage.[32]

From the kinetic studies in Figure 3.14, it is found that in stark contrast to the rapid reaction of HMBQ-Nap with GSH, Cys, and Hcy, an exceedingly sluggish response is observed for HMBQ-Nap 1 in the presence of H_2S and BSA under equivalent conditions. At 150 s, the signal from GSH is 103-fold higher than that from H_2S and 17 times greater than for BSA. However, I have found that the fluorescence quantum yield of Nap 2 is roughly 25% higher in the presence of 50 μM BSA (Figure 3.15) under equivalent conditions to those in Figure 3.14, and the maximum absorbance of Nap 2 was also blue shifted about 10 nm (Figure 3.13); this is possibly due to viscosity and hydrophobic interaction effects. Thus, the selectivity of HMBQ-Nap activation by GSH, Cys, or Hcy versus BSA is certainly higher. The slow reaction of the thiol (Cys 34) in BSA with HMBQ-Nap 1 can be attributed to it being sterically hindered, as the thiol of Cys 34 is oriented toward the interior of the protein,[7] an observation that is consistent with the slow reactivity of Cys 34 in HSA with Ellman's reagent (5,5'-dithiobis-(2-nitrobenzoic acid)).[33] It is posited that the low reactivity of H_2S with HMBQ-Nap 1 is due to the lack of either HMBQ reduction by H_2S or its Michael addition to HMBQ. The reduction potential of HMBQ in probe

1 is −0.80 V vs SHE in comparison to 0.17 V[34] for H_2S, and successful Michael addition of H_2S requires a very electron deficient acceptor.[29, 35]

Figure 3.14 Time–dependent fluorescence (λ_{ex} = 432 nm, λ_{em} = 540 nm) of 10 μM HMBQ-Nap 1 incubated with 50 μM thiol–containing analytes in 0.1 M, pH 7.4 PBS/DMSO (9:1) at 25 $^{\circ}$C.

Figure 3.15 Fluorescence change for free Nap 2 reporter with BSA addition. Nap 2 (red line) in 10% DMSO: 90% PBS buffer pH 7.4 before BSA addition, and Nap 2 (green line) in 10% DMSO:90% PBS buffer pH 7.4 after BSA addition.

To further describe the selectivity of HMBQ-Nap activation by GSH, Cys, and Hcy, I examined HMBQ-Nap 1 stability under physiological solution conditions in the presence of select amino acids and reducing agents that might possibly activate HMBQ-Nap 1 so as to yield Nap 2 reporter. Upon inspection of Figure 3.16, it is clear that the three thiol-free amino acids (1 mM, 100 equivalents) and the other nucleophilic amino acids, such as serine and threonine, with the potential to undergo Michael addition to the HMBQ unit, do not interact with HMBQ-Nap 1. Furthermore, the biological reductants NADH ($E_{1/2} = -0.31$ V)[36]—present at mM levels within cells—and the ubiquitous ascorbic acid ($E_{1/2} = 0.051$ vs. SHE)[37] also did not induce the release of Nap 2 from HMBQ-Nap 1. The lack of redox-induced activation of HMBQ-Nap by these species is in agreement with the observations above with H_2S, as the reduction potentials of these possible interferents are not sufficient to allow reduction of the HMBQ unit in HMBQ-Nap probe (−0.80 V vs SHE).

Figure 3.16 Fluorescence response of HMBQ-Nap (10 μM) incubated at 25 $^{\circ}$C for 30 min with 1 mM amino acids and common reductants in 10% DMSO/90% 0.1 M, pH 7.4 PBS. Bars represent % release of free Nap 2 reporter with respect to that achieved for HMBQ-Nap 1 incubated with GSH for 30 min.

3.3.7 Reactivity of HMBQ-Nap with NADH Quinone Oxidoreductase

NAD(P)H:quinone oxidoreductase-1 (NQO1, DT-diaphorase, EC 1.6.99.2)[38-39] is a ubiquitous, homodimeric flavoprotein with one molecule of FAD non-covalently bound per monomer.[40] NQO1 is generally regarded as a detoxifying enzyme, where its major role has been considered to be its stability to catalyze the reduction of various quinones by direct two-electron reduction of quinone to hydroquinones.[41] Owing to its known function of reacting with quinones and its presence mainly in the cytosol, I speculated that it could be a possible interferent for HMBQ-Nap 1 in cellular media. To test if human NQO1 can initiate the reduction of HMBQ-Nap 1 and release of free Nap 2 reporter, enzyme kinetic assays were used to monitor the production of fluorescent reporter over time for a given fixed amount of enzyme. (Figure 3.17)

Figure 3.17 Kinetics of human NQO1 (2×10^{-6} g) with HMBQ-Nap ($0.5-11.5 \times 10^{-6}$ M) in pH 7.4, 0.1 M phosphate buffer. Values (n = 3) are the average ±1 sample standard deviation. The curve is the best fit to the average data. T = 25 $^{\circ}$C.

For quantitative evaluation of HMBQ-Nap 1 activation by human NQO1, I observed the rapid fluorescence intensity increase at 540 nm with different concentrations of HMBQ-Nap 1 (0.5–11.5 × 10^{-6} M) with a fixed amount of human NQO1 (2 × 10^{-6}g) and its cofactor NADH (1 × 10^{-4} M). All the fluorescence units were converted to concentration units using a calibration curve for free Nap 2 reporter. Control experiments with NADH alone did not yield significant changes in fluorescence. The initial rate of product formation, V (μmol $min^{-1}mg$.hNQO1^{-1}), was calculated and plotted as a function of HMBQ-Nap 1 concentration, Figure 3.15. Apparent kinetic parameters were then obtained by fitting the data in Figure 3.15 to the Michaelis-Menten equation, namely the Michaelis constant (K_m) = 9.959 ± 1.189 μM, maximum velocity (V_{max}) = 1.483 ± 0.096 μmol min^{-1}mg.hNQO1^{-1}, catalytic constant (k_{cat}) = 45.70 ± 0.01 min^{-1}, and catalytic efficiency (k_{cat}/K_m) = 4.37 × 10^6 ± 0.58 $M^{-1}s^{-1}$. These results indicate that the reduction of the quinone moiety of HMBQ-Nap 1 with human NQO1 is possible and quite rapid under physiological conditions. As a comparison between thiol reduction and NQO1 reduction, observed rate constants (k_{obs}) were calculated in the presence and absence of GSH; the most abundant non protein thiol along with NQO1. The experiment was designed such that a mixture of an equal concentration of (1 × 10^{-4} M) NADH and GSH were added to each well at the same time, and the fluorescent increase was monitored over time. Apparent kinetic parameters (k_{obs}) were then obtained (Figure 3.16 a and b) and compared with each other to understand if there is any significant difference between the observed rate constants.

The attempt to find out the Michalis–Menten enzyme kinetic parameters for the NQO1 catalysis of HMBQ-Nap 1 with the presence of thiols was not successful due to the reaction not approaching steady–state kinetics. The enzyme graph (i.e. fluorescence release) in the presence of thiol was completely linear (graph is not shown); whereas a typical Michaelis–Menten graph should adopt a hyperbolic shape as it approaches steady–state kinetics. I assumed that the reason for not approaching the steady–state kinetics was thiols being more efficient reducers of HMBQ-Nap 1 than NQO1. In order to further prove this concept and compare the efficiency of the two reductions, a comparison of observed rate constants (k_{obs} s^{-1}) was used. As shown in Figure 3.18a, the observed rate constant for fluorescence increase for the NQO1 without the GSH was 6.56 × 10^{-7} s^{-1}, and the observed rate constant for the fluorescence increase for NQO1 in the presence of the thiol GSH (Figure 3.18b) was 2.84 × 10^{-6} s^{-1}. When the two kinetic parameters

are compared, it is clear that in the presence of thiols the observed rate constant (k_{obs}) is about four times higher than that of NQO1 alone. From this observation and from the observations from previous sections of thiol kinetics, it is clear that the thiol reduction of HMBQ-Nap 1 is more rapid than NQO1 enzymatic reduction.

Figure 3.18 Kinetics (k_{obs} s^{-1}) of a) human NQO1 (2×10^{-6} g) with HMBQ-Nap 1 ($0.5–11.5 \times 10^{-6}$ M), b) human NQO1 (2×10^{-6} g) with HMBQ-Nap 1 ($0.5–11.5 \times 10^{-6}$ M) in the presence

of 100 μM GSH in pH 7.4, 0.1 M phosphate buffer. Values (n = 3) are the average ±1 sample standard deviation. The curve is the best fit to the average data T = 25 °C.

3.3.8 Imaging of Biological Thiol Presence in Human Cells

Upon demonstration that HMBQ-Nap 1 allows for class-selective detection of GSH, Cys, and Hcy under low probe:analyte conditions, an analysis was undertaken to examine the ability of HMBQ-Nap 1 to act as a possible imaging probe for the presence of these biological thiols in human cells.

The ability of HMBQ-Nap 1 to detect thiols in live cells was evaluated using the human lung cancer cell line H596, which is known to have a GSH content of 140±70 nmol mg^{-1} protein, and it lacks NQO1.[42] Two-dimensional cell cultures were incubated with 20 μM HMBQ-Nap 1 for 10 min at 37 °C and subsequently washed with pH 7.4 PBS (0.1 M); after staining the nuclei with DRAQ5, the cells were fixed using formaldehyde as fixing agent. As the negative-control/background experiment, H596 cells were pre-incubated with known thiol capping agent 10 mM *N*-ethylmaleimide (NEM) at 37 °C for 30 min to scavenge thiols in the cells, then the cells were washed with pH 7.4 PBS (0.1 M) to remove excess NEM, followed by incubation with 20 μM HMBQ-Nap 1 for 10 min, and then washed with pH 7.4 PBS prior to their being fixed as above. Fluorescence images were obtained using confocal laser microscopy via excitation at 458 nm and detection at 458–514/514–680 nm, with integrated cellular fluorescence intensity being obtained via software.

Unadulterated H596 cells that were exposed to HMBQ-Nap 1 exhibited strong fluorescence (Figure 3.19, without NEM), whereas there was little fluorescence in the negative control cells that were pretreated with thiol scavenger (Figure 3.19, with NEM). A signal-to-background ratio of 4.2 was obtained upon comparison of the integrated fluorescence intensities for the untreated and NEM-treated cells. Thus, electrically neutral HMBQ-Nap 1 is able to enter cells and report on the presence of intracellular biological thiols in a rapid and selective fashion (10 min).

3.4 Conclusions

I have designed, synthesized, and made feasible a new dual quenching/trigger group-based thiol probe whose PeT-quenched fluorescence signal is turned on selectively upon rapid reaction of quinone trigger group with biologically important thiols leading to probe shedding of the

thiol-activated trigger group. The probe HMBQ-Nap 1 exhibits high selectivity and rapid response toward the three biological thiols glutathione, cysteine, and homocysteine, when compared to protein-associated thiol or the simple gasotransmitter H_2S, as well as other potential interferents commonly found in mammalian systems. Rapid activation of HMBQ-Nap 1 by thiols

Figure 3.19 Microscopy images of human H596 lung cells A–C incubated for 10 min at 37 °C with 20 μM HMBQ-Nap 1, and D–F pre-incubated with 10 mM NEM thiol scavenger for 30 min at 37 °C, followed by incubation with 20 μM HMBQ-Nap 1 for 10 min at 37 °C. Confocal: A, B, D, E; and differential interference contrast: C and F image. Scale bar = 20 μm.

to yield the highly fluorescent reporter Nap 2 is attributed to thiol-addition-initiated elimination of the trigger group. Although quinone reductase enzyme NQO1 caused considerable activation of the trigger group, the NQO1 concentration in cells is far less than compared to mM thiol concentrations. Therefore, NQO1 is most likely a small interferent in comparison to the cellular thiols. Furthermore, it has been successfully demonstrated that HMBQ-Nap 1 can provide rapid and selective thiol detection in human cells, and with an exceedingly low limit of detection under in vitro conditions where there is no need for excessive amounts of probe, unlike previously reported probes that require probe:thiol ratios of 70:1 to 5000:1. Thus, HMBQ-Nap 1 diversifies the pool of biological thiol probes by offering rapid, class-selective detection and quantification with high figures of merit.

3.5 References

1. Sun, Y.-Q.; Chen, M.; Liu, J.; Lv, X.; Li, J.-f.; Guo, W., Nitroolefin-Based Coumarin as a Colorimetric and Fluorescent Dual Probe for Biothiols. *Chem. Commun.*, **2011**, *47*, 11029-11031.

2. Giustarini, D.; Dalle-Donne, I.; Lorenzini, S.; Milzani, A.; Rossi, R., Age-Related Influence on Thiol, Disulfide, and Protein-Mixed Disulfide Levels in Human Plasma. *J. Gerontol A. Biol Sci. Med. Sci.*, **2006**, *61*, 1030-8.

3. Jain, S. K.; Micinski, D.; Huning, L.; Kahlon, G.; Bass, P. F.; Levine, S. N., Vitamin D and L-Cysteine Levels Correlate Positively with Gsh and Negatively with Insulin Resistance Levels in the Blood of Type 2 Diabetic Patients. *Eur. J. Clin. Nutr.*, **2014**, *68*, 1148-53.

4. Giustarini, D.; Dalle-Donne, I.; Lorenzini, S.; Milzani, A.; Rossi, R., Age-Related Influence on Thiol, Disulfide, and Protein-Mixed Disulfide Levels in Human Plasma. *J. Gerontol., Ser. A*, **2006**, *61A*, 1030-1038.

5. Balendiran, G. K.; Dabur, R.; Fraser, D., The Role of Glutathione in Cancer. *Cell Biochemistry and Function*, **2004**, *22*, 343-352.

6. Refsum, H.; Ueland, P. M.; Nygard, O.; Vollset, S. E., Homocysteine and Cardiovascular Disease. *Annu. Rev. Med.*, **1998**, *49*, 31-62.

7. Turell, L.; Radi, R.; Alvarez, B., The Thiol Pool in Human Plasma: The Central Contribution of Albumin to Redox Processes. *Free Radical Biol. Med.*, **2013**, *65*, 244-253.

8. Nicholson, J. P.; Wolmarans, M. R.; Park, G. R., The Role of Albumin in Critical Illness. *Br. J. Anaesth.*, **2000**, *85*, 599-610.

9. Yonge, L.; Gracheva, S.; Wilkins, S. J.; Livingstone, C.; Davis, J., Potentiometric Differentiation of Mono- and Macromolecular Thiol within Human Plasma at Carbon Fiber Electrodes. *J. Am. Chem. Soc.*, **2004**, *126*, 7732-7733.

10. Tang, B.; Xing, Y.; Li, P.; Zhang, N.; Yu, F.; Yang, G., A Rhodamine-Based Fluorescent Probe Containing a Se-N Bond for Detecting Thiols and Its Application in Living Cells. *J. Am. Chem. Soc*, **2007**, *129*, 11666-11667.

11. Lee, J. H.; Lim, C. S.; Tian, Y. S.; Han, J. H.; Cho, B. R., A Two-Photon Fluorescent Probe for Thiols in Live Cells and Tissues. *J. Am. Chem. Soc.*, **2010**, *132*, 1216-1217.

12. Lin, W.; Long, L.; Yuan, L.; Cao, Z.; Chen, B.; Tan, W., A Ratiometric Fluorescent Probe for Cysteine and Homocysteine Displaying a Large Emission Shift. *Org. Lett.,* **2008**, *10*, 5577-5580.

13. Shao, N.; Jin, J. Y.; Cheung, S. M.; Yan, R. H.; Chan, W. H.; Mo, T., A Spiropyran-Based Ensemble for Visual Recognition and Quantification of Cysteine and Homocysteine at Physiological Levels. *Angew. Chem., Int. Ed.,* **2006**, *45*, 4944-4948.

14. Ros-Lis, J. V.; Garcia, B.; Jimenez, D.; Martinez-Manez, R.; Sancenon, F.; Soto, J.; Gonzalvo, F.; Valldecabres, M. C., Squaraines as Fluoro-Chromogenic Probes for Thiol-Containing Compounds and Their Application to the Detection of Biorelevant Thiols. *J. Am. Chem. Soc.,* **2004**, *126*, 4064-4065.

15. Hong, V.; Kislukhin, A. A.; Finn, M. G., Thiol-Selective Fluorogenic Probes for Labeling and Release. *J. Am. Chem. Soc.,* **2009**, *131*, 9986-9994.

16. Owen, T. C., Thiol Detection, Derivatization and Tagging at Micromole to Nanomole Levels Using Propiolates. *Bioorg. Chem.,* **2008**, *36*, 156-160.

17. Lee, J.-J.; Lee, S.-C.; Zhai, D.; Ahn, Y.-H.; Yeo, H. Y.; Tan, Y. L.; Chang, Y.-T., Bodipy-Diacrylate Imaging Probes for Targeted Proteins inside Live Cells. *Chem. Commun.,* **2011**, *47*, 4508-4510.

18. Guo, Y.; Yang, X.; Hakuna, L.; Barve, A.; Escobedo, J. O.; Lowry, M.; Strongin, R. M., A Fast Response Highly Selective Probe for the Detection of Glutathione in Human Blood Plasma. *Sensors*, **2012**, *12*, 5940-5950.

19. Yuan, L.; Lin, W.; Yang, Y., A Ratiometric Fluorescent Probe for Specific Detection of Cysteine over Homocysteine and Glutathione Based on the Drastic Distinction in the Kinetic Profiles. *Chem. Commun.,* **2011**, *47*, 6275-6277.

20. Lim, S.; Escobedo, J. O.; Lowry, M.; Xu, X.; Strongin, R., Selective Fluorescence Detection of Cysteine and N-Terminal Cysteine Peptide Residues. *Chem. Commun.,* **2010**, *46*, 5707-5709.

21. Lin, W.; Yuan, L.; Cao, Z.; Feng, Y.; Long, L., A Sensitive and Selective Fluorescent Thiol Probe in Water Based on the Conjugate 1,4-Addition of Thiols to A,B-Unsaturated Ketones. *Chem. Euro. J.,* **2009**, *15*, 5096-5103.

22. Kwon, H.; Lee, K.; Kim, H.-J., Coumarin-Malonitrile Conjugate as a Fluorescence Turn-on Probe for Biothiols and Its Cellular Expression. *Chem. Commun.,* **2011**, *47*, 1773-1775.

23. Zeng, Y.; Zhang, G.; Zhang, D.; Zhu, D., A Dual-Function Colorimetric Chemosensor for Thiols and Transition Metal Ions Based on Ict Mechanism. *Tetrahedron Lett.,* **2008**, *49*, 7391-7394.

24. Huang, S.-T.; Ting, K.-N.; Wang, K.-L., Development of a Long-Wavelength Fluorescent Probe Based on Quinone–Methide-Type Reaction to Detect Physiologically Significant Thiols. *Anal. Chim. Acta,* **2008**, *620*, 120-126.

25. Silvers, W. C.; Prasai, B.; Burk, D. H.; Brown, M. L.; McCarley, R. L., Profluorogenic Reductase Substrate for Rapid, Selective, and Sensitive Visualization and Detection of Human Cancer Cells That Overexpress Nqo1. *J. Am. Chem. Soc.,* **2013**, *135*, 309-14.

26. Giraud, L.; Giraud, A., Diels-Alder Trapping of Ortho-Quinone Methides. A New Entry to Substituted Xanthene-1,4-Diones. *Synthesis,* **1998**, 1153-1160.

27. Fery-Forgues, S.; Lavabre, D., Are Fluorescence Quantum Yields So Tricky to Measure? A Demonstration Using Familiar Stationery Products. *J. Chem. Educ.,* **1999**, *76*, 1260.

28. Li, L.; Rose, P.; Moore, P. K., Hydrogen Sulfide and Cell Signaling. *Annu. Rev. Pharmacol. Toxicol.,* **2011**, *51*, 169-187.

29. Perlinger, J. A.; Kalluri, V. M.; Venkatapathy, R.; Angst, W., Addition of Hydrogen Sulfide to Juglone. *Environ. Sci. Technol.,* **2002**, *36*, 2663-2669.

30. Ellis, R. J., Macromolecular Crowding: Obvious but Underappreciated. *Trends Biochem. Sci.,* **2001**, *26*, 597-604.

31. Nicholson, J. P.; Wolmarans, M. R.; Park, G. R., The Role of Albumin in Critical Illness. *Brit. J. Anaesth.,* **2000**, *85*, 599-610.

32. Tong, G. Characterization of Cysteine-34 in Serum Albumin Ph.D. thesis, Ohio State University, **2003**.

33. Torres, M. J.; Turell, L.; Botti, H.; Antmann, L.; Carballal, S.; Ferrer-Sueta, G.; Radi, R.; Alvarez, B., Modulation of the Reactivity of the Thiol of Human Serum Albumin and Its Sulfenic Derivative by Fatty Acids. *Arch. Biochem. Biophys.,* **2012**, *521*, 102-110.

34. Collman, J. P.; Ghosh, S.; Dey, A.; Decréau, R. A., Using a Functional Enzyme Model to Understand the Chemistry Behind Hydrogen Sulfide Induced Hibernation. *Proc. Natl. Acad. Sci.,* **2009**, *106*, 22090-22095.

35. Liu, C.; Peng, B.; Li, S.; Park, C.-M.; Whorton, A. R.; Xian, M., Reaction Based Fluorescent Probes for Hydrogen Sulfide. *Org. Lett.,* **2012**, *14*, 2184-2187.

36. Carlson, B. W.; Miller, L. L., Mechanism of the Oxidation of Nadh by Quinones - Energetics of One-Electron and Hydride Routes. *J. Am. Chem. Soc.,* **1985**, *107*, 479-485.

37. Ball, E. G., Studies on Oxidation-Reduction. Xxiii. Ascorbic Acid. *J. Biol. Chem.,* **1937**, *118*, 219-239.

38. Faig, M.; Bianchet, M. A.; Talalay, P.; Chen, S.; Winski, S.; Ross, D.; Amzel, L. M., Structures of Recombinant Human and Mouse Nad(P)H:Quinone Oxidoreductases: Species Comparison and Structural Changes with Substrate Binding and Release. *Proc. Natl. Acad. Sci.,* **2000**, *97*, 3177-3182.

39. Mendoza, M. F.; Hollabaugh, N. M.; Hettiarachchi, S. U.; McCarley, R. L., Human NAD(P)H:Quinone Oxidoreductase Type I (Hnqo1) Activation of Quinone Propionic Acid Trigger Groups. *Biochemistry,* **2012**, *51*, 8014-8026.

40. Nolan, K. A.; Scott, K. A.; Barnes, J.; Doncaster, J.; Whitehead, R. C.; Stratford, I. J., Pharmacological Inhibitors of Nad(P)H Quinone Oxidoreductase, Nqo1: Structure/Activity Relationships and Functional Activity in Tumour Cells. *Biochem. Pharmacol.,* **2010**, *80*, 977-981.

41. Talalay, P., Mechanisms of Induction of Enzymes That Protect against Chemical Carcinogenesis. *Adv. Enzyme Regul.,* **1989**, *28*, 237-50.

42. Carmichael, J.; Mitchell, J. B.; Friedman, N.; Gazdar, A. F.; Russo, A., Glutathione and Related Enzyme Activity in Human Lung Cancer Cell Lines. *Br. J. Cancer,* **1988**, *58*, 437-40.

CHAPTER 4
CASCADE REACTION-BASED NEAR-INFRARED FLUORESCENT PROBES FOR THE SELECTIVE DETECTION OF CYSTEINE

4.1 Introduction

Fluorescence-based small molecule probes have recently received much attention for their use in the tracking of important analytes in cellular environments and biological fluids, without affecting sample integrity. By making use of the intrinsically unique reactivities of select classes of organic molecules, these probes can be tailored to detect either broad classes of analytes or individual targets.[1] In recent literature, there are numerous reported fluorescent probes that claim to selectively detect various analytes, such as enzymes, metal ions, reactive-oxygen and nitrogen species, and thiols.[2-4]

The sulfur-containing small molecules glutathione (GSH), cysteine (Cys), and homocysteine (Hcy) are involved in a number of important biological processes, and they play an important role in the body.[5] Cys and Hcy are clearly prominent out of all the other naturally occurring amino acids, as they are the only amino acids with a free thiol (–SH) moiety. Hcy and Cys differ from each other by only a single methylene unit in their side chain, giving them similar structural and chemical characteristics. The thiol ionization state controls Cys/Hcy nucleophilicity and their redox susceptibility, facilitates unique functions of Cys/Hcy than other amino acids. For example, Cys partakes in several important biochemical functions, including bio-catalysis, allosteric regulation, metal binding, and structural stabilizations.[6] The sulfhydryl group in Cys can act as an ideal nucleophile in enzyme active sites that participate in enzymatic reactions; also by undergoing reversible oxidation and reduction, Cys helps to maintain the tertiary and quaternary structure of proteins. Another important property of Cys is its unique metal binding ability; the thiolate ligand binds to metal ions, such as $Fe^{2+/3+}$, Zn^{2+}, Cd^{2+}, and Cu^{+} , making Cys an important player in the detoxification of metal cations in cells. Furthermore, important post-translational modifications that regulate protein structure and function are found in cysteine-containing proteins and peptides.[6] Cys can also serve as an important intermediate in the glutathione biosynthetic pathway.[7] As a result, the availability of GSH is strongly dependent on the availability of reduced Cys in the cytosol.[8]

Alteration of cytosolic Cys levels can be an indicator of the functional state of the corresponding enzymes/proteins, or a breakdown in biochemical pathways, and this has been

correlated with several health complications. Cys has been linked as an indicator of delayed development in children, hair depigmentation, liver damage, muscle and fat loss, aging, and cancers.[9] Moreover, the plasma concentration of cysteine serves as an important factor in medical diagnosis. Downs syndrome, Parkinson's disease, obesity, and cardiovascular diseases have been associated with altered levels of plasma cysteine.[10-15] The traditional determination of plasma cysteine is greatly dependent on methods, such as HPLC and GC. However, these detection methods suffer from drawbacks, such as long sample processing time and low sensitivity or LOD.[16-17] Therefore, new, efficient and easy-to-operate routes need to be developed, and in that case, fluorescence-based probes are ideal candidates.

Owing to their similar chemical reactivity, the selective detection or quantification of a single thiol analyte by discriminating against other thiol-containing small molecules still remains a great challenge. When considering their selectivity toward cysteine, only very few reported probes have the ability to preferentially detect cysteine over Hcy and GSH. Furthermore, most of these reported probes have not had discussed their selectivity against possible cross reactants, such as H_2S.[18-20]

As I have mentioned before, the ability to distinguish between Cys and Hcy using a single probe is an enormous challenge, due to the structural similarity between the two amino acids. Out of several reported strategies used, one of the commonly used methods for Cys/Hcy discrimination versus GSH is thiazolidine formation resulting from aldehydes.[21] Because the aldehyde functional group can possibly form 5- or 6- membered rings rapidly with 1,3–or 1,2–amino thiols where GSH cannot, such a ring structure can be used to distinguish Hcy and Cys from GSH.[22] Another successful strategy reported is conjugate addition, followed by cyclization with α,β unsaturated esters. This method involves thio-ether formation, followed by cyclization that releases the fluorophore and a lactam. This has been successfully shown to be able to differentiate Cys from Hcy as a result of the difference in ring formation kinetics.[22]

Most of the early reported fluorescence probes for biological thiols were based on dyes, such as coumarin,[23-24] 1,8-napthalimide,[25-27] xanthene,[28-30] and fluorescein.[31-32] These probes and their fluorescent counterparts suffer from short-wavelength emission, giving rise to a high background signal, especially in biological sample analysis.[33] NIR fluorescent dyes (650–900 nm) possess unique advantages for tracing molecular processes in vitro and in vivo with less background interference.[34] High tissue auto-fluorescence taking place from native biomolecules in living

systems rarely interfere with NIR emission of probes/reporters. Furthermore, most abundant biomolecules found in the body such as hemoglobin, water, and lipids—the principal absorbers of red/green light—have their lowest absorption coefficient in the NIR region.[4] Therefore, NIR dyes increase tissue penetration depth, thereby facilitating deep-tissue imaging with minimum damage to biological samples. The photostability of the NIR fluorophore is another crucial parameter in designing fluorescence sensors for real-time analyte detection. Although long-wavelength cyanine dyes are widely used in designing NIR sensors for bio-imaging, they typically suffer from poor photostability in aqueous solutions.[35] Indocyanine green (ICG), for example, the only FDA-approved NIR dye for biomedical imaging, has shown very low photostability in the body, making its prolonged detection rather impossible.[36] Therefore, novel NIR-active fluorophores with exceptional photostability and photophysical properties are desired for designing biomedical sensors. Dicyanomethylene-4*H*-pyran (DCM) dyes and their derivatives have long been used for non-linear optical materials, logic gates,[37] and photovoltaic sensitizers.[38-39] Recently, they have received much attention as a possible candidate for fluorescence-based bio-sensors.[33] As a donor–π–acceptor type chromophore, dicyanomethylene-4*H*-pyran (DCM) derivatives has attractive photophysical properties,[37] such as a tunable emission wavelength in the red or NIR region via controling the electron donor ability, a large Stokes-shift explained by ICT, and a high photostability. These properties make them a good candidate for the design of biosensors.[40] The capability of two-photon excitation is another added advantage of DCM dyes. Compared with other traditional one-photon microscopy (OPM), two-photon microscopy (TPM) utilizes lower energy photons to obtain the excited state of a fluorophore, resulting in deeper penetration into tissue and less photo-toxicity. Also, TPM has a higher microscopic resolution (800 μm) than confocal (500 μm) and epi (20 μm) microscopic techniques.[4] However, most of the traditionally known TP dyes have their emission in the short wavelength region (< 600 nm); therefore, it is important to develop new TP fluorophores with emission in the red and NIR regions.[41]

The work here presents the design, synthesis and evaluation of two different fluorescent probes, Nap-Cys and DCM-Cys, for the selective detection of cysteine in biological fluids and cellular environments. Out of these two probes investigated here, DCM-Cys offers a rapid and selective detection of cysteine at sub-nanomolar levels, and it yields a quick (<12 min) response with good selectivity. The general design rationale of the cysteine-activated,

DCM-Cys fluorescent probe is shown in Figure 4.1, and is described as follows. The cysteine-selective probes contain a reporter dye attached to a cysteine-reactive acrylate moiety via a linker. Initially, in the presence of cysteine, the sulfhydryl group will undergo a Michael addition to α,β-unsaturated double bonds in the reactive acrylate moiety to form a thio-ether. The second step utilizes the amine group in the cysteine amino acid and will undergoes a nucleophilic attack on the carbonyl carbon of the linker, thereby, forming cyclized lactam products. Lactam formation will induce a cascade of downstream processes involving quinone methide formation resulting in release of the linker and free fluorophore. As a result of these fluorophores being ICT dyes, release of the linker will result in bright fluorescence enhancement. The probe DCM-Cys has successfully demonstrated to function as a cysteine selective thiol probe, and has been applied to the in vitro and in cyto detection of cysteine.

Figure 4.1 Schematic representation of the design rationale for the Cys–selective fluorescent probe.

4.2 Experimental

4.2.1 Synthetic Materials and Methods

All the column purifications were performed using SNAP silica columns on a Flashmaster Personal from Biotage. Chemicals were purchased from Sigma-Aldrich or Fisher Scientific. Thin-layer chromatography was performed on aluminum-backed 60 F_{254} silica plates from EMD Chemicals, Incorporated. All the ^{1}H NMR and ^{13}C NMR spectra were collected in chloroform, D_2O or DMSO-d_6 at 25 $^{\circ}C$ on a Bruker AV-400 Spectrometer. Chemical shifts are reported in the standard δ notation of parts per million, using tetramethylsilane (TMS) as an internal reference. Absorption bands in NMR spectra are listed as singlet (s), doublet (d), triplet (t),

or multiplet (m), and the coupling constants *J* are expressed in hertz (Hz). Mass spectral analyses were carried out using an Agilent 6210 ESI-TOFMS. All the solutions were prepared using Nanopure water from a Barnstead Diamond Nanopure water System (18 MΩ-cm).

4.2.2 Synthesis

The syntheses of two probes, Nap-Cys and DCM-Cys, were performed by adopting literature reported methods. The synthesis plan for Nap-Cys[42-46] is shown in Scheme 4.1, The synthesis plan for the NIR dye DCM is shown in Scheme 4.2[41, 46] with that for synthesis of DCM-Cys in Scheme 4.3[44-45, 47-48].

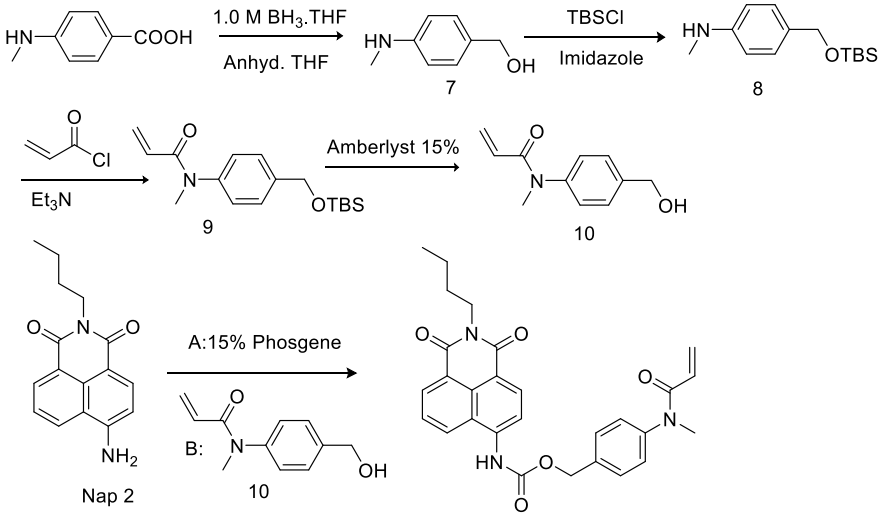

Scheme 4.1 Synthesis of probe Nap-Cys

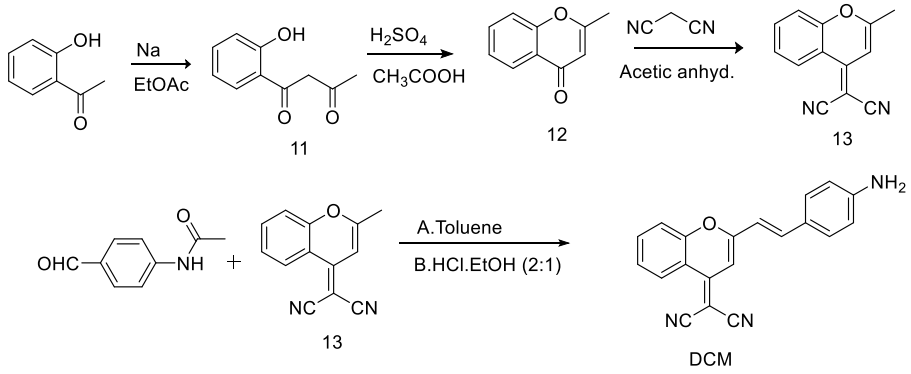

Scheme 4.2 Synthesis of the DCM dye

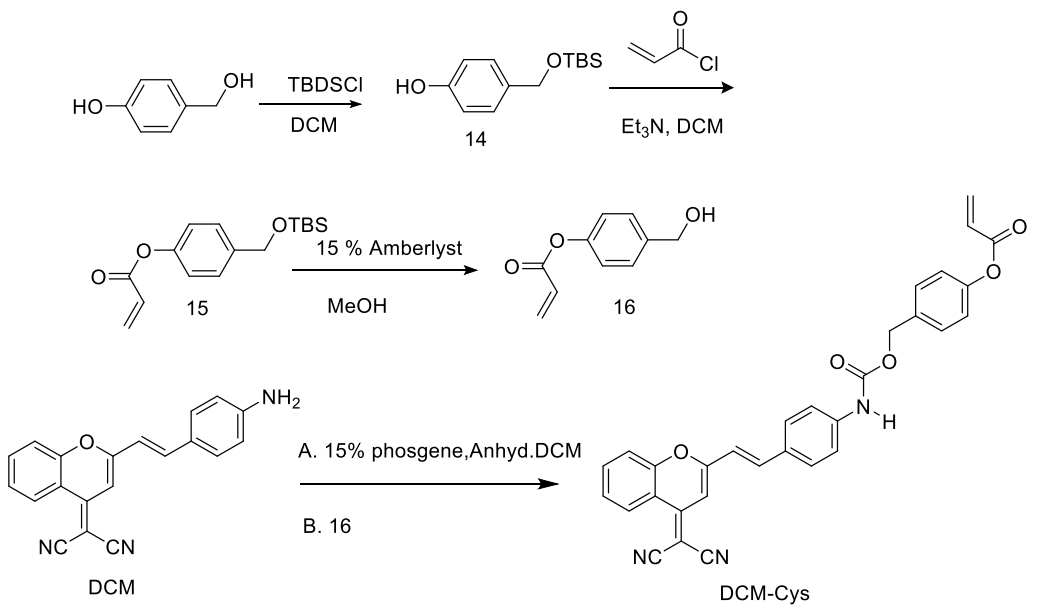

Scheme 4.3 Synthesis of probe DCM-Cys.

Synthesis of 4-(*N*-methylamino)benzyl alcohol (7)

To a cold solution (0 °C) of 4-(*N*-methylamino)benzoic acid (10.0 g, 66.0 mmol) in THF (35 mL) under N_2 , 1.0 M borane-THF complex (200 mL, 200.0 mmol) in THF was added dropwise over a period of 1 h using an addition funnel. The resulting solution was stirred for an additional 6 h at room temperature (RT), and then, cooled to 0 °C. NaOH solution (3 M, 25 mL) was added to the solution to consume excess hydride and to hydrolyze the amine-borane complex. The resulting mixture was stirred at RT for an additional 12 h. Then, the aqueous phase was saturated with potassium carbonate, and the organic layer was collected. The aqueous phase was extracted with diethyl ether (3 × 50 mL); the combined organic layers were dried over anhydrous $MgSO_4$. After filtration, the filtrate was evaporated under vacuum to obtain 7 as a light brown solid (87 % yield). This material was used in the next step without further purification. ^{1}H NMR (400 MHz, methanol-d_4) δ 7.22–7.01 (m, 2H), 6.69–6.48 (m, 2H), 4.44 (s, 2H), 2.73 (s, 3H).

Synthesis of 4-[[(*tert*-butyldimethylsilanyl)oxy]methyl]-*N*-methylaniline (8)

Imidazole (4.27 g, 62.3 mmol) and *tert*–butyldimethylsilyl chloride (9.45 g, 62.75 mmol) were added to a cooled (0 °C) solution of 7 (8.6 g, 62.75 mmol) dissolved in DMF (25 mL). The reaction mixture was stirred at RT for 6 h and then diluted with brine solution. The mixture was extracted with ethyl acetate (3 × 20 mL) and the organic layer was dried over anhydrous $MgSO_4$.

A light brown colored oil was obtained after evaporating the solvent under vacuum. The compound was purified by a flash column using CH_2Cl_2/Hex (2:1, v/v) to obtain product 8 as a yellowish oil (85 % yield). ^{1}H NMR (400 MHz, chloroform-*d*) δ 7.49–7.14 (m, 1H), 6.78–6.51 (m, 1H), 4.70 (s, 1H), 2.87 (d, *J* = 1.8 Hz, 1H), 1.00 (d, *J* = 1.7 Hz, 3H), 0.15 (d, *J* = 1.9 Hz, 2H). ESI-MS: for $C_{14}H_{25}NOSi$: expected *m/z* = 252.1785 $[M+H]^+$; found *m/z* =252.1768 $[M+H]^+$; 6.0 ppm error.

Synthesis of *N*-(4-[[(*tert*-butyldimethylsilyl)oxy]methyl]phenyl)-*N*-methylprop-2-enamide (9)

To a stirred solution of 8 (5.0 g, 0.019 mmol) and triethylamine (2.65 mL, 0.019 mmol) in 35 mL of CH_2Cl_2 at 0 $^\circ$C was added acryloyl chloride (1.54 mL, 0.019 mmol) in 10 mL CH_2Cl_2. The reaction mixture was stirred overnight at RT. The mixture was then washed with 5% $NaHCO_3$ and brine. After drying over $MgSO_4$, the solvent was removed under vacuum to yield the crude product 9 as brown oil. The compound was used directly for the next step without further purification (70% yield). ^{1}H NMR (400 MHz, chloroform-*d*) δ 7.36 (d, *J* = 7.9 Hz, 2H), 7.13 (d, *J* = 7.5 Hz, 2H), 6.31 (d, *J* = 16.4 Hz, 1H), 6.07 (m, 1H), 5.48 (d, *J* = 12.9 Hz, 1H), 4.75 (s, 2H), 3.32 (s, 3H), 0.94 (s, 9H), 0.11 (s, 6H). ESI-MS: for $C_{17}H_{27}NO_2Si$: expected *m/z* = 306.1891 $[M+H]^+$; found *m/z* =306.1879 $[M+H]^+$; 3.3 ppm error.

Synthesis of *N*-[4-(hydroxymethyl)phenyl]-*N*-methylprop-2-enamide (10)

Compound 9 (1.5 g, 4.90 mmol) was dissolved in THF (15 mL), and a solution of TBAF (7.84 mL, 1 M in THF) was added dropwise. The solution was stirred at RT for 3 h, and upon completion; the solvent was removed under vacuum. The remaining residue was dissolved in CH_2Cl_2, washed with brine and dried over $MgSO_4$. The solvent was removed under vacuum, and the crude material was purified on a flash column using a gradient elution of Hex/EtOAc (4:1, v/v) and EtOAc/Hex (5:2, v/v). Final product 10 was obtained as colorless oil with 60% yield. ^{1}H NMR (400 MHz, chloroform-*d*) δ 7.36 (d, *J* = 8.0 Hz, 2H), 7.06 (d, *J* = 8.1 Hz, 2H), 6.22 (dd, *J* = 16.8, 2.0 Hz, 1H), 5.98 (dd, *J* = 16.8, 10.3 Hz, 1H), 5.39 (d, *J* = 10.3 Hz, 1H), 4.64 (s, 2H), 4.33–4.11 (m, 1H), 3.23 (s, 3H). ESI-MS: for $C_{11}H_{13}NO_2$: expected *m/z* = 192.1026 $[M+H]^+$; found *m/z* =192.1020 $[M+H]^+$; 2.6 ppm error

Synthesis of Nap-Cys

The detailed description of the synthesis of Nap 2 is given in the chapter 2 under "synthesis". To a solution of Nap 2 (26.8 mg, 0.1 mmol) in anhydrous DCM under argon at −15 °C, 4-dimethylaminopyridine (DMAP, 24.24 mg, 0.2 mmol) was added, and the solution was stirred for a few minutes. Then, a solution of phosgene (15% toluene, 0.7 mL) was added drop wise, and stirred under argon for 6 h. The excess phosgene was then removed by bubbling argon gas through the solution for 30 min. To the resulting solution, compound 10 (57.43 mg, 0.3 mmol) was added, and the reaction was stirred overnight at 0 °C. Then, the reaction mixture was quenched with water (20 mL) and extracted with CH_2Cl_2 (2 × 25 mL). The organic layer was dried over $MgSO_4$, filtered, and concentrated under vacuum. The crude product was purified by a flash column using CH_2Cl_2/EtOAc (20:1, v/v) to yield the product as a yellow solid. (35% yield). ^{1}H NMR (400 MHz, chloroform-*d*) δ 8.67 (t, *J* = 8.1 Hz, 2H), 8.42 (d, *J* = 9.7 Hz, 1H), 8.21 (d, *J* = 9.1 Hz, 1H), 7.81 (t, *J* = 7.9 Hz, 1H), 7.54 (t, *J* = 9.1 Hz, 2H), 7.24 (t, *J* = 6.3 Hz, 2H), 6.43 (d, *J* = 18.5 Hz, 1H), 6.15 (m, 1H), 5.57 (d, *J* = 18.5 Hz, 1H), 5.35 (s, 3H), 4.19 (t, *J* = 7.5 Hz, 2H), 3.39 (s, 3H), 1.75 (quint, *J* = 7.8 Hz, 2H), 1.62 (sext, *J* = 7.5 Hz, 2H), 1.00 (t, *J* = 7.3 Hz, 3H). ^{13}C NMR (126 MHz, chloroform-*d*) δ 165.71, 164.11, 163.63, 152.90, 143.73, 138.61, 134.85, 132.47, 131.30, 129.80, 128.93, 128.35, 127.87, 127.56, 126.72, 125.70, 123.57, 122.90, 118.12, 116.81, 67.11, 40.28, 37.45, 30.22, 20.41, 13.88. ESI-MS: for $C_{28}H_{27}N_3O_5$ expected: *m/z* = 486.2031 $[M+H]^+$; found *m/z* = 486.2030 $[M+H]^+$; 0.2 ppm error.

Synthesis of 1-(2-hydroxyphenyl)butane-1,3-dione (11)

The starting material, 1-(2-hydroxyphenyl)ethanone (10.0 g, 73.50 mmol) was dissolved in 200 mL ethyl acetate, and solid sodium chunks (8.00 g, 0.34 mmol) were slowly added to the solution. The reaction was left overnight, and a grayish-green solid was isolated by filtration. The solid was then dissolved in 100 mL of deionized water, followed by adjustment of the pH to neutral using a few drops of concentrated H_2SO_4. The aqueous solution was extracted with 200 mL EtOAc, and the organic layer was dried over $MgSO_4$. Then the solution was filtered, and concentrated under vacuum to yield the final crude product 11 as a brown solid (80% yield). The product was used directly in the next step without further purification. ESI-MS: for $C_{10}H_{10}O_3$: expected *m/z* = 201.0529 $[M+Na]^+$; found *m/z* = 201.0529 $[M+Na]^+$; 0.0 ppm error.

Synthesis of 2-methyl-4*H*-chromen-4-one (12)

Compound 11 (7.0 g, 38.9 mmol) was dissolved in acetic acid (70 mL) and Concentrated sulfuric acid (5.0 mL) was slowly added to the mixture. The resulting solution was refluxed for about 2 h and then poured into 800 mL of ice water. The pH of the water was adjusted to neutral using solid Na_2CO_3. The aqueous solution was extracted with CH_2Cl_2 twice (2 × 30 mL), and the organic layer was dried over $MgSO_4$. The solvent was evaporated under vacuum to afford 12 as a dark brown solid. (70% yield). The crude product was used directly in the next step without further purification. ESI-MS: for $C_{10}H_8O_2$: expected *m/z* = 161.0604 $[M+H]^+$; found *m/z* = 161.0599 $[M+H]^+$; 3.1 ppm error.

Synthesis of 2-(2-methyl-4H-chromen-4-ylidene)malononitrile (13)

Crude product 12 (2.48 g, 15.50 mmol) and malononitrile (1.23 g, 7.70 mmol) were dissolved in 15 mL acetic anhydride, and the solution was refluxed for 14 h. The solvents were evaporated under vacuum, and the dark brown residue was refluxed in deionized water for another 30 min. The mixture was extracted with CH_2Cl_2 and the organic layer was dried over $MgSO_4$. The crude product was crystalized from ethanol to obtain pure product 13 as bright orange solid (40% yield). ^{1}H NMR (400 MHz, chloroform-*d*) δ 8.91 (d, *J* = 8.8 Hz, 1H), 7.71 (t, *J* = 7.6 Hz, 1H), 7.45 (d, *J* = 8.4 Hz, 2H), 6.72 (s, 1H), 2.44 (s, 3H). ^{13}C NMR (126 MHz, chloroform-*d*) δ 161.72 , 153.24 , 152.89 , 134.59 , 126.03 , 125.78 , 118.65 , 117.54 , 116.58 , 115.46 , 105.47 , 76.79 , 62.32 , 20.49. ESI-MS: for $C_{13}H_8N_2O$: expected *m/z* = 209.0717 $[M+H]^+$; found *m/z* = 209.0709 $[M+H]^+$; 3.8 ppm error.

Synthesis of free dye DCM

Step A) Compound 13 (2.03 g, 9.75 mmol) and commercially purchased *N*-(4-formyl phenyl)acetamide (1.5 g, 8.97 mmol) were dissolved in toluene (200 mL) and mixed with piperidine (5.0 mL) and acetic acid (5.0 mL) under nitrogen at RT. After a Dean Stark trap was fitted, the mixture was heated and then refluxed overnight to yield an orange precipitate. Then the mixture was cooled to RT and placed in a refrigerator for another 3 h to let the reaction mixture get cooled. An orange precipitate (DCM-acetamide, 15 A) was obtained after filtration, and this was used directly in the next step without further purification. ^{1}H NMR (400 MHz, DMSO-d_6) δ 10.20 (s, 1H), 8.76 (d, *J* = 7.65 Hz, 1H), 7.94 (t, *J* = 9.8 Hz, 1H), 7.82 (d, *J* = 8.8

Hz, 1H), 7.77–7.67 (m, 3H), 7.63 (t, *J*= 7.7 Hz, 1H), 7.38 (d, *J*= 15.0 Hz, 1H), 7.01 (s, 1H), 2.09 (s, 3H). ESI-MS: for $C_{22}H_{15}N_3O_2$: expected m/z = 354.1241 $[M+H]^+$; found *m/z* = 354.1242 $[M+H]^+$; 0.28 ppm error.

Step B) The orange solid obtained (15A) was dissolved in a concentrated HCl:ethanol (2:1, v/v, 30 mL) mixture , and the mixture was refluxed overnight. After cooling to room temperature, the pH of the solution was adjusted to neutral using solid Na_2CO_3. The aqueous solution was extracted with EtOAc (3 × 20 mL), and the extracts were dried over $MgSO_4$. After filtering, the solvent was evaporated under vacuum to afford a purple solid which was then recrystallized from ethanol to afford pure DCM dye as a deep-purple solid. (40% yield). ^{1}H NMR (400 MHz, DMSO-d_6) δ 8.74 (d, *J* = 8.6 Hz, 1H), 7.90 (t, *J* = 7.7 Hz, 1H), 7.79 (d, *J* = 7.7 Hz, 1H), 7.67 (s, 1H), 7.59 (m, 1H), 7.50 (d, *J* = 8.5 Hz, 2H), 7.11 (d, *J* = 15.4 Hz, 1H), 6.87 (s, 1H), 6.63 (d, *J* = 7.6 Hz, 2H), 6.02 (s, 2H). ^{13}C NMR (126 MHz, DMSO-d_6) δ 160.26, 153.08, 152.59, 152.54, 141.14, 135.49, 131.15, 126.37, 125.02, 122.76, 119.37, 118.27, 117.70, 116.91, 114.25, 112.88, 105.18, 57.82. ESI-MS: for $C_{20}H_{13}N_3O$: expected *m/z* = 312.1139 $[M+H]^+$, found *m/z* = 312.1127 $[M+H]^+$; 3.8 ppm error.

Synthesis of 4-[[(*tert*-butyldimethylsilyl)oxy]methyl]phenol (14)

To a solution of 4-hydroxybenzyl alcohol (5 g, 40.30 mmol) and imidazole (2.74 g, 40.3 mmol) cooled to 0 $^\circ$C in 40 mL DMF, *tert*-butyldimethylsilyl chloride (TBSCl, 6.0 g, 40.3 mmol) was added and stirred at the RT overnight. The reaction mixture was diluted with brine solution and extracted with ethyl acetate (3 × 20 mL). The organic layer was dried over anhydrous $MgSO_4$, filtered and a light brown-colored oil was obtained after evaporating the solvent under vacuum. The compound was purified using a flash column with EtOAc/Hex (1:3) to obtain product 16 as a yellowish oil. (86% yield). ^{1}H NMR (400 MHz, chloroform-*d*) δ 7.22 (d, *J* = 8.4 Hz, 2H), 6.78 (d, *J* = 7.9 Hz, 2H), 6.58 (bs, 1H), 4.73 (s, 2H), 1.01 (s, 9H), 0.17 (s, 6H). ESI-MS: for $C_{13}H_{22}O_2Si$: expected *m/z* = 261.1289 $[M+Na]^+$; found *m/z* = 261.1280 $[M+Na]^+$; 3.4 ppm error.

Synthesis of 4-[*tert*-butyldimethlsilyl]oxy]methyl]phenylprop-2-enoate (15)

To a stirred solution of 14 (5.0 g, 0.021 mmol) and trimethylamine (2.90 mL, 0.021 mmol) in 35 mL of CH_2Cl_2 at 0 °C, acryloyl chloride (1.70 mL, 0.019 mmol) was added dropwise in 10 mL CH_2Cl_2. The reaction mixture was stirred overnight at RT, and was then washed with 5% $NaHCO_3$ and brine. After drying over $MgSO_4$, the solvent was removed under vacuum to yield crude product 15 as a light brown oil. The compound was purified on a flash column using EtOAc:Hex (1:10. v/v) to yield compound 15 as a brown solid (70% yield). ^{1}H NMR (400 MHz, chloroform-*d*) δ 7.36 (d, J = 7.4 Hz, 2H), 7.11 (d, J = 8.1 Hz, 2H), 6.65 (d, J = 17.1 Hz, 1H), 6.38 (m, 1H), 6.04 (d, J = 10.1 Hz, 1H), 4.76 (s, 2H), 0.97 (s, 9H), 0.13 (s, 6H). ^{13}C NMR (126 MHz, chloroform-*d*) δ 164.65, 149.41, 139.08, 134.61, 132.43, 128.00, 127.01, 121.22, 64.43, 25.95, 18.41, −5.25. ESI-MS: for $C_{16}H_{24}O_3Si$: expected m/z = 315.1395 $[M+Na]^+$; found m/z = 315.1390 $[M+Na]^+$; 1.6 ppm error.

Synthesis of 4-(hydroxymethyl)phenylprop-2-enoate (16)

To a solution of compound 15 (1.0 g, 3.4 mmol) in methanol (20 mL), amberlyst-15 (150.0 mg, 15% by weight) was added. The reaction was stirred at RT for 6 h. The solid was filtered, and the filtrate solvent was removed under vacuum to offer a brown oil. The compound was purified in a flash column with CH_2Cl_2/Hex (5:1) to afford compound 16 as light yellow oil (80% yield). ^{1}H NMR (400 MHz, chloroform-*d*) δ 7.39 (d, J = 8.9 Hz, 2H), 7.13 (d, J = 11.0 Hz, 2H), 6.60 (d, J = 17.6 Hz, 1H), 6.34 (m, 1H), 6.05 (d, J = 10.9 Hz, 1H), 4.65 (s, 2H), 2.33 (s, 1H). ESI-MS: for $C_{10}H_{10}O_3$: expected *m/z* = 179.0710 $[M+H]^+$; found *m/z* = 179.0705 $[M+H]^+$; 2.8 ppm error.

Synthesis of DCM-Cys probe

To a solution of DCM (23.45 mg, 0.075 mmol) in anhydrous CH_2Cl_2 under argon at −15 °C, 4-dimethylaminopyridine (DMAP, 18.30 mg, 0.15 mmol) was added, and the solution was stirred for 10 minutes. Then a solution of phosgene (15% toluene, 1.0 mL) was added drop wise, and the reaction was stirred under argon for 12 h; then excess phosgene was removed by bubbling argon gas through the solution for 30 min. To the resulting solution, alcohol 16 (40.0 mg, 0.23 mmol) was added, and it was stirred overnight at 0 °C. Then the reaction mixture was quenched with water (20 mL) and extracted with CH_2Cl_2 (2 × 25 mL). The organic layer was

dried over $MgSO_4$, filtered, and concentrated under the vacuum. The crude product was purified by flash column chromatography with a gradient elution of CH_2Cl_2 (100%) to remove starting materials and, followed by EtOAc/petether (1:2, v/v). The pure DCM-Cys product was isolated as a yellow solid (10% yield). ^{1}H NMR (400 MHz, chloroform-*d*) δ 9.91 (s, 1H), 8.93 (d, J = 7.8 Hz, 1H), 7.85 (d, J = 5.5 Hz, 2H), 7.74 (t, J = 8.3 Hz, 1H), 7.55 (d, J = 8.5 Hz, 2H), 7.44 (m, 4H), 7.15 (d, J = 7.5 Hz, 3H), 6.98–6.69 (m, 3H), 6.59 (d, J = 17.5 Hz, 1H), 6.33 (m, 1H), 6.02 (d, J = 10.9 Hz, 1H), 5.22 (s, 2H). ^{13}C NMR (126 MHz, chloroform-*d*) δ 190.88, 164.44, 157.64, 152.85, 152.62, 152.35, 150.73, 150.68, 143.35, 138.26, 134.59, 133.39, 133.21, 132.86, 131.84, 131.29, 129.76, 129.72, 129.09, 127.76, 125.93, 125.86, 121.85, 121.83, 118.74, 118.57, 118.07, 117.89, 117.39, 106.61, 66.83. ESI-MS: for $C_{31}H_{21}N_3O_5$: expected m/z = 516.1561 $[M+H]^+$; found m/z = 516.1562 $[M+H]^+$; 0.2 ppm error.

4.2.3 Spectroscopic Methods

All spectroscopic measurements were performed in 0.1 M, pH 7.4 phosphate-buffered saline solution. Fluorescence data were collected using a Perkin Elmer LS-55 spectrometer, and absorption spectra were recorded using a Varian Cary-50 spectrophotometer. Samples for absorption and emission measurements were obtained in 1-cm × 1-cm quartz cuvettes (1.5-mL volume, Sigma-Aldrich).

4.2.4 Procedure for Solution-phase Thiol Sensing

Stock solutions of 2×10^{-4} M probes (Nap-Cys or DCM-Cys) were prepared in 100% DMSO and were subsequently diluted to prepare preferred concentration solutions in pH 7.4 PBS/DMSO buffer. Stock solutions of thiol were freshly prepared prior to each experiment. For the calibration curve of cysteine, a fixed concentration solution of DCM-Cys was incubated with different concentrations of cysteine at 37 $^\circ$C for 15 min, and spectral data were recorded. For the Nap-Cys probe, excitation was performed at 432 nm, and emission was detected at 540 nm (for the detection of the free dye Nap 2). For the detection of Nap-Cys probe emission, the sample was excited at 380 nm and detected at 480 nm. The excitation and emission slit widths were set at 2.5 nm for Nap-Cys sample. For the DCM-Cys probe (detect the release of the free dye), samples were excited at 520 nm, and emission was detected at 640 nm. The excitation and emission slit widths were 5 nm and 10 nm respectively.

4.2.5 Mass-spectrometric Studies for Cysteine End-product

Aqueous solution of cysteine (4×10^{-4} M) was added to a 2×10^{-4} M solution of DCM-Cys probe in 40% DMSO:60% 0.1 M, pH 7.4 PBS, 10 μL and the sample was incubated at 37 $^{\circ}$C for 30 min. The solvent was evaporated and vacuum dried until a dry powder was obtained. The dry powder was re-dissolved in methanol and ESI-MS was obtained both in negative and positive ion mode.

4.2.6 Cell Culture

Human non-small cell lung cancer cells H596, cell culture base media, and fetal bovine serum (FBS) were purchased from American Type Cell Culture (ATCC, Manassas, VA). All cell culture procedures were performed as suggested by ATCC. H596 cells were cultured in RPMI-1640 with 10% FBS and 100 IU/ml penicillin-streptomycin. Cells were incubated at 37 $^{\circ}$C in a humidified incubator containing 5% wt/vol CO_2.

4.2.7 Imaging of cysteine in cells via Scanning Laser Confocal Microscopy

H596 cells were cultured overnight on 22-mm × 22-mm glass cover slips on a treated tissue culture 6-well plate purchased from Fisher Scientific. The existing growth medium was replaced with 2 mL of fresh cysteine free medium and then incubated at 37 $^{\circ}$C. Solutions of DCM-Cys was dissolved in DMSO were added to the cells to give final concentration of 3×10^{-5} M of DCM-Cys, keeping the DMSO concentration at < 1%. Then cells were incubated with DCM-Cys at 37 $^{\circ}$C for 10 min. Next, the medium was removed, and the cells were fixed in 2 mL of 4% paraformaldehyde for 15 min with shaking. After fixing, the cells were rinsed with Nanopure water, and the cover slips were mounted to glass slides with Immumount (obtained from Fisher Scientific). Glass slides were left in the dark overnight to allow the Immumount to dry. Confocal images were acquired using a Leica TCS SP2 spectral confocal microscope. For images of cells exposed to DCM-Cys samples were excited using the 488-nm line of an Ar/KrA laser (laser intensity = 45.32%), and the spectral emission was collected between 625 and 750 nm (Leica DD458/514); PMT voltage = 710 V. All images were collected using a pinhole of 1.0 Airy units. Images were frame and line averaged 4 times with zoom factor 0f 3.25. Image analysis was performed using ImageJ and Leica LAS AF lite software. As the control experiment to scavenge all the thiols in cells, H596 cells were pre–incubated with 10 mM *N*-ethylmaleimide (NEM)

temperature at 37 °C for 30 min. Then the cells were washed with 0.1 M, pH 7.4 PBS to remove any excess NEM, followed by incubation with 3×10^{-5} M DCM-Cys prior to their being fixed as described previously.

4.3 Results and Discussion

4.3.1 Spectral Properties of Nap-Cys/Nap 2 System

To determine the spectroscopic properties of the Nap-Cys/Nap 2 system, absorption and fluorescence spectra of the Nap-Cys probe were obtained in the aqueous phosphate-buffered media under physiological pH (7.4). As demonstrated by its highly intense fluorescence with λ_{max} at 470 nm (Figure 4.2, blue line), the Nap-Cys probe could be used as a dual-wavelength ratiometric fluorescent probe. The distinct difference in the spectroscopic properties of the free Nap 2 reporter (Figure 3.2 b, Chapter 3) and Nap-Cys probe can be attributed to the disruption of the electron donating ability of the nitrogen by the carbamate bond, making the fluorescence of the Nap-Cys blue shifted. Also, as an added advantage, the emission of the Nap-Cys probe is Stokes-shifted (Figure 4.2, blue line) from its maximum absorbance (Figure 4.2, red line) by ~100 nm, providing less background interference for fluorescence measurements.

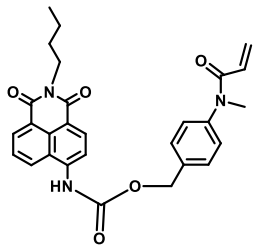

Figure 4.2 Absorption and emission spectra of 2×10^{-6} M Nap-Cys in 10% DMSO/90% 0.1 M, pH 7.4 phosphate-buffered saline (PBS) at T = 37 °C.

When reacted with cysteine, the fluorescence band that corresponds to λ_{max} = 470 nm (fluorescence of Nap-Cys) was expected to decrease, with a concomitant rise in fluorescence of Nap 2 reporter (λ_{max} = 540 nm).

4.3.2 Cysteine Selective Ability of Nap-Cys and Proposed Reaction Mechanism

In order to determine the Nap-Cys ability to act as a fluorescence sensor for cysteine an aqueous buffered sample of Nap-Cys (2 μM) in 10% DMSO/90% 0.1 M, pH 7.4 PBS was incubated with 100 μM cysteine for 2 h at 37 $^{\circ}$C (Figure 4.3). The sample was excited at λ_{ex} = 380 nm, and emission (λ_{em} = 470 nm) was observed to check the disappearance of probe fluorescence. To detect the formation of free Nap 2 reporter, the sample was excited at λ_{ex} = 440 nm, and emission was detected at λ_{em} = 540 nm. Surprisingly, probe disappearance at 470 nm (Figure 4.3, dashed black line and red line) or appearance of a new free Nap 2 dye at 540 nm (Figure 4.3, orange line and dashed green line) was not observed, even after several hours of incubation. If the Nap-Cys probe reacted with cysteine as proposed, the band (λ_{em} = 470 nm) that corresponds to the Nap-Cys probe should decrease gradually, and the band that corresponds to free Nap 2 reporter (λ_{em} = 540 nm) should increase over time. These observations suggested that the probe did not work according to the proposed design mechanism. The details of the proposed reaction mechanism are given below and are depicted in Scheme 4.4.

According to the illustrated reaction mechanism in Scheme 4.4, the release of Nap 2 reporter consists of three major events—thio-ether formation, subsequent cyclization to yield the lactam (a) and aza-quinone methide (b), followed by release of the Nap 2 reporter. Previously published work by our group and that of others supports the concept of rapid aza-quinone methide formation to eliminate the Nap 2 reporter upon production of CO_2 (g).[48-49] Considering these reported outcomes, I assumed that the formation of b and elimination of CO_2 (g) would act as the driving force to move the reaction toward its end product, Nap 2, assuming that the first step has occurred.

However in this probe system, the reason for not observing the expected product formation may be due to the nitrogen atom being both the leaving group and the nucleophile attack species during the cyclization process, and therefore the downstream quinone methide formation did not occur. A similar type of result observed with a previously reported probe in the McCarley group

Figure 4.3 Emission spectra of 2×10^{-6} M Nap-Cys in 10% DMSO/90% 0.1 M, pH 7.4 PBS before and after incubated with 1×10^{-4} M cysteine for t = 2 h. All data were recorded at temperature T = 37 °C. Dashed black line = initial Nap-Cys spectra at t = 0 h, red colored line = Nap-Cys at t = 2 h, orange colored line = detection of Nap 2 at t = 0 h, dashed green colored line = detection of Nap 2 at t = 2 h.

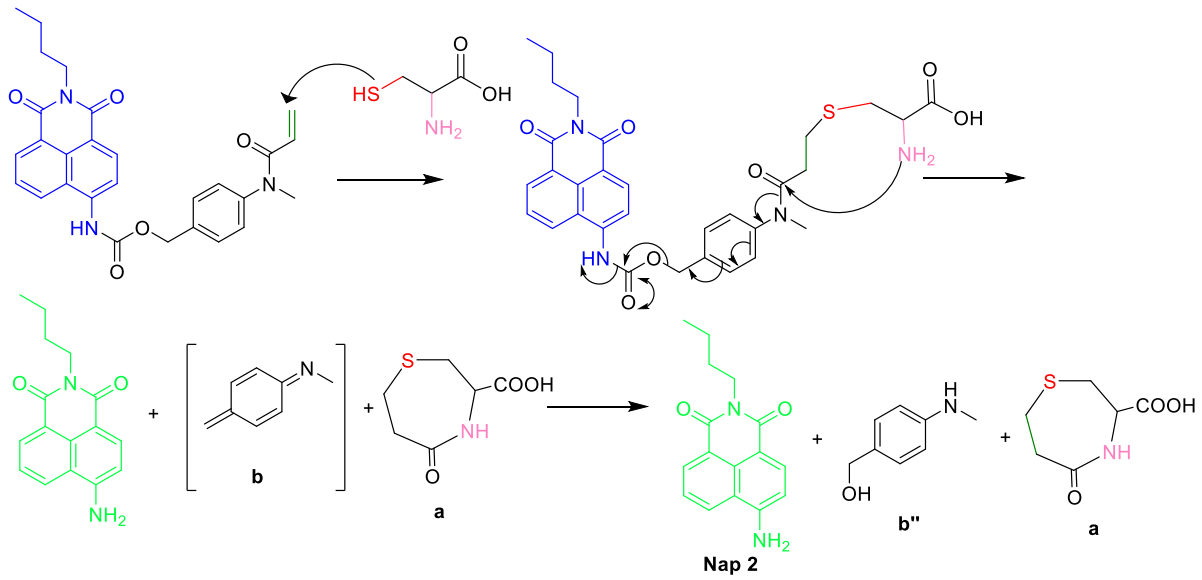

Scheme 4.4 Proposed mechanism for reaction of Nap-Cys probe with cysteine to eliminate the reporter Nap 2.

supports this hypothesis.[50] Therefore, a new strategy to design a cysteine-selective probe was carried out by changing the linker from an aminobenzyl alcohol to benzyl alcohol in the DCM-Cys probe system. The ability of the DCM-Cys probe to detect cysteine is further discussed in the following sections.

4.3.3 Spectral Properties of the DCM-Cys/DCM System

In order to determine the spectral properties of the probe/reporter system, absorption and fluorescence spectra of DCM-Cys and free DCM reporter dye were obtained in aqueous DMSO/PBS solution. As shown in Figure 4.4, the DCM-Cys probe shows a weak absorbance band possessing a maximum absorbance (λ_{abs}) centered around 440 nm (Figure 4.4, green line); when the sample was excited at its maximum absorbance wavelength, a fluorescence spectrum was obtained with a maximum fluorescence (λ_{em}) centered around 550 nm (Figure 4.4, blue line).

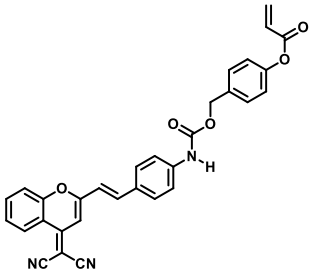

Figure 4.4 Absorption spectrum (green line) and fluorescence spectrum (blue line) of 30 μM DCM-Cys probe in 40%:60% DMSO:0.1 M, pH 7.4 phosphate-buffered saline (PBS) at 37 $^{\circ}$C.

The spectral properties of free DCM reporter shown in Figure 4.5 are described follows. The DCM has a very strong absorbance band when compared to the DCM-Cys probe with a

maximum absorbance centered around λ_{abs} = 490 nm and a large Stokes-shifted emission having a maximum emission wavelength (λ_{em}) around 640 nm. The remarkable ~ 150 nm spectral difference between the absorption and emission spectra of DCM is an added advantage, as it will facilitate the efficient monitoring of free dye release in biological samples with less background interference. However, as noted by the two absorption spectra of the DCM-Cys probe and free DCM reporter, a spectral overlap was observed between the probe and the reporter making it difficult to follow reaction of the probe with cysteine using UV-vis spectroscopy.

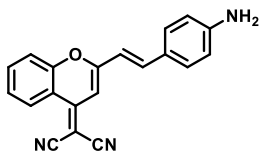

Figure 4.5 Absorption spectrum (blue line) and fluorescence spectrum (red line) of 10 μM free DCM reporter dye in 40%:60% DMSO:0.1 M, pH 7.4 phosphate-buffered saline (PBS) at, T = 37 $^{\circ}$C.

4.3.4 Colorimetric Determination of Cysteine Reactivity

As shown in Figure 4.6, an attempt was made using UV-Vis spectroscopy to determine the ability of the DCM-Cys probe to react with cysteine and provide the expected outcome of release of the free DCM reporter. The initial spectrum of 30 μM aqueous DCM-Cys (Figure 4.6, green line) was recorded and then the sample was exposed to 60 μM cysteine. The solution was then left in the dark for about 20 minutes at 37 $^{\circ}$C, and the final absorption spectrum was obtained. As seen in Figure 4.6 (red line), a new absorption band that corresponds to free DCM reporter is present at λ_{abs} = 490 nm, and the absorption band of DCM-Cys at λ_{abs} = 440 nm is effectively reduced. However, as mentioned earlier, the absorption overlap of the DCM-Cys probe and

DCM reporter make it difficult to monitor whether the reaction has reached completion (complete disappearance of the probe). However, as an added advantage, the color change of the aqueous system could clearly be monitored by the naked eye thereby allowing for visual inspection of the reaction progress. As shown in Figure 4.6a, the initial yellow color of the solution changed to a red color (Figure 4.6b) as the reaction progressed, making this a promising approach towards visual detection of cysteine.

Figure 4.6 Monitoring the progress of the reaction using UV-Vis spectra of 30 μM DCM-Cys in 40%:60% DMSO:0.1 M, pH 7.4 phosphate-buffered saline (PBS). The initial absorption spectrum of the solution before 60 μM cysteine was added (green line) and the final absorption spectrum of the sample incubated at T = 37 $^{\circ}$C for 20 min after cysteine was added (red line) are shown. Image depicts the a) color of the solution before cysteine was added, and b) the color of the solution 20 min after cysteine was added.

4.3.5 Fluorescence Spectroscopic Determination of Cysteine Reactivity

The differences that exist between both the absorption and emission spectra of the DCM-Cys probe and the reporter DCM dye prompted me to investigate the possibility of DCM-Cys being used as a ratiometric probe for cysteine. The absorption maximum of the probe (λ_{abs} = 440 nm) is blue shifted by about 50 nm in comparison to the absorption maximum (λ_{abs} = 490 nm) of the free reporter; also the emission maximum of the probe (λ_{em} = 540 nm) is blue shifted ~100 nm

versus that of the free reporter (λ_{em} = 640 nm). In order to test this possibility DCM-Cys was excited at different wavelengths (Figure 4.7–Figure 4.9), and the fluorescence signal outcome was monitored.

Figure 4.7 Fluorescence spectral changes of 30 μM DCM-Cys in 40%:60% DMSO:0.1 M, pH 7.4 phosphate-buffered saline (PBS) after adding 60 μM cysteine at T = 37 $^{\circ}$C. λ_{ex} = 440 nm (the maximum absorbance of DCM-Cys probe).

Figure 4.8 Fluorescence spectral changes of 30 μM DCM-Cys in 40%:60% DMSO:0.1 M, pH 7.4 phosphate-buffered saline (PBS) after adding 60 μM cysteine at T = 37 $^{\circ}$C. λ_{ex} = 490 nm (the absorbance maximum of DCM free reporter dye).

Figure 4.9 Fluorescence spectral changes of 30 μM DCM-Cys in 40%:60% DMSO:0.1 M, pH 7.4 phosphate-buffered saline (PBS) after adding 60 μM cysteine at T = 37 $^{\circ}$C. λ_{ex} = 520 nm (the absorbance of DCM dye without interference from DCM-Cys probe).

After addition of 60 μM cysteine, the fluorescence spectra were recorded every 2 min intervals. In Figure 4.7 is shown the spectral change when the sample was excited at the maximum absorbance of DCM-Cys probe (λ_{ex} = 440 nm). In Figure 4.8 is shown the spectral change when the sample was excited at the maximum absorbance of the DCM reporter (λ_{ex} = 490 nm). And in Figure 4.9 is shown the spectral change when the sample was excited at λ_{ex} = 520 nm, the absorbance wavelength that was selected to avoid emission interference from the DCM-Cys probe. Upon inspecting the outcomes of each graph it was clear that DCM-Cys acts as a turn on probe in contrast to the ratiometric response with maximum turn on response showing at λ_{ex} = 520 nm with λ_{em} = 640 without interference from the probe fluorescence. Because the decrease of the fluorescence response of the DCM-Cys probe at λ_{em} = 540 nm was not very prominent (Figure 4.7) when compared to turn on fluorescence response of release of free DCM reporter, all the analysis for cysteine reactivity was monitored considering DCM-Cys as a turn on probe at λ_{em} = 640 nm.

In order to determine the capability of DCM-Cys to act as a turn-on probe upon reaction with cysteine, an aqueous solution of 30 μM DCM-Cys was reacted with 60 μM cysteine, and the fluorescence increase was monitored at 640 nm upon exciting the sample at 520 nm.

Figure 4.10 Time-dependent fluorescence (λ_{ex} = 520 nm, λ_{em} = 640 nm) of 30 μM DCM-Cys incubated with 60 μM cysteine in 40%:60% DMSO:0.1 M, pH 7.4 phosphate-buffered saline (PBS) at T = 37 $^{\circ}$C. Inset: a) emission spectra of 30 μM DCM-Cys after cysteine addition, 550 nm–750 nm Δt = 2 min; b) visualization of the fluorescence change of the aqueous sample under UV lamp (λ =~365 nm) before and 10 min after cysteine was added, T = 37 $^{\circ}$C.

As revealed in Figure 4.10, a rapid increase in fluorescence was observed in both the time-dependent fluorescence scan and the time-lapse wavelength scans from 550 nm to 750 nm. Maximum release was achieved within about 700 s (~12 min) after cysteine was added. The fluorescent band centered around 640 nm (Figure 4.10 inset) is consistent with the free DCM fluorescent band obtained by excitation at 520 nm in 40%:60% DMSO:0.1 M, pH 7.4 phosphate-buffered saline, further verifying release of the free reporter.

To determine whether the DCM-Cys fluorescence turn-on response is a function of cysteine concentration in the media, varying concentrations of cysteine were incubated with 30 μM DCM-Cys solution for 20 min at 37 $^{\circ}$C. The turn-on response at 640 nm was measured. As shown in Figure 4.11a, it is clear that the florescence response increased with the increasing concentration of cysteine in the media, and after plotting the maximum fluorescence as a function of concentration, (Figure 4.11b) it was concluded that there exists a linear relationship

between cysteine concentration and fluorescence response of the DCM-Cys probe up to 30 μM cysteine (1 equivalent), with the concentration limit of detection of 21 nM and the concentration limit of quantification of 70 nM.

Figure 4.11 a) Fluorescence spectral changes of probe DCM-Cys (30 μM) with added cysteine (0–30 μM); b) the resulting fluorescence intensity (λ_{ex} = 520 nm/λ_{em} = 640 nm) vs concentration of cysteine plot. Error bars represent the standard deviation of the average data for each concentration (n = 3).

4.3.6 Mechanism of Cysteine Selectivity

The proposed mechanism of DCM-Cys reaction with cysteine (highlighted in Scheme 4.5) to yield free DCM reporter is described as follows. Initially, the double bond of acrylate moiety undergoes a nucleophilic attack by the sulfhydryl group of cysteine to yield a thio-ether compound. Then, the amino group of cysteine makes a subsequent nucleophilic attack on the adjacent carbonyl carbon to yield the tetrahedral intermediate that then collapses to yield the lactam (b). Quinone methide (c) elimination from the benzyl alcohol linker results in free DCM reporter dye production. The unstable quinone methide intermediate will undergo further reaction in the water medium to yield benzyl alcohol (c"). The release of the free reporter to give the expected fluorescence enhancement provides evidence that the initial steps have occurred as suggested.

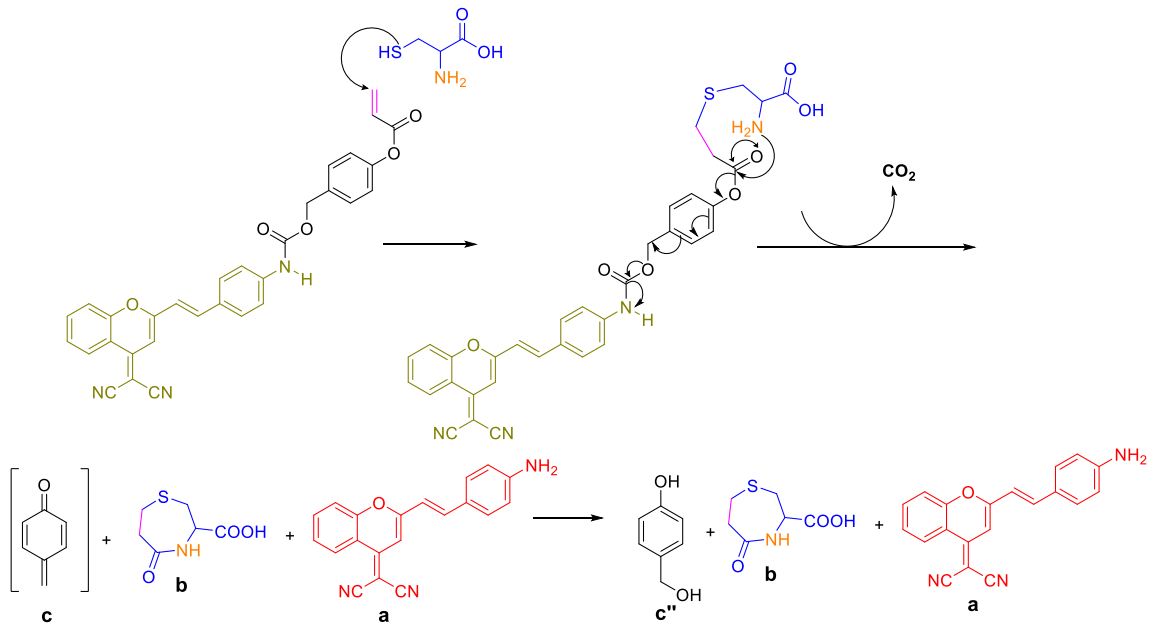

Scheme 4.5 Proposed reaction mechanism of DCM-Cys probe with cysteine to produce the free DCM reporter.

As another strategy for evaluating the expected end-product during the cysteine reaction with DCM-Cys, mass-spectrometry studies were conducted. A concentrated sample of DCM-Cys (200 μM) was reacted with excess cysteine in aqueous media at 37 $^{\circ}$C for 30 min. Then the sample was vacuum dried until a dry powder was obtained and then dissolved in methanol to

obtain mass spectral data. Studies were conducted both in negative and positive ion mode to obtain the best possible ionization. As shown in Figure 4.12, free reporter DCM release (Scheme 4.5, compound a) was noted by the $[M-H]^-$ signal at *m*/*z* = 310.0978 (expected *m*/*z* = 310.0979, 0.32 ppm error) in panel I and the expected cyclized product b was observed by the $[M+H]^+$ signal at *m*/*z* = 176.0371 (expected *m*/*z* = 176.0383, 6.8 ppm error) in panel ii. These successful outcomes further provided evidence for the products shown in Scheme 4.5.

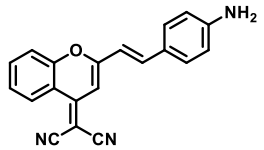

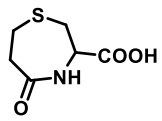

Figure 4.12 Mass spectrometric analysis of end-product of DCM-Cys upon reaction with cysteine. i) free DCM reporter (a) observed by $[M-H]^-$ signal at *m*/*z* = 310.0978 (expected *m*/*z* = 310.0979, 0.32 ppm error), ii) cyclized lactam product (b) observed by $[M+H]^+$ signal at *m*/*z* = 176.0371 (expected *m*/*z* = 176.0383, 6.80 ppm error).

In addition to free reporter a and cyclized product b, another expected product the benzyl alcohol linker c" was not observed in mass-spectral data. The reason for not observing the expected product c'' was may be due to the low ionization efficiency of benzyl alcohol linker.

However, the observation of the peaks corresponding to free DCM reporter and lactam provided adequate evidence in support of the mechanism proposed in Scheme 4.5.

4.3.7 Reactivity of DCM-Cys with Other Thiols

GSH, Hcy and H_2S—the other commonly found thiols in the body with similar reactivity to cysteine—have the probability to act as cross-reactive species with the DCM-Cys probe. The pK_a of GSH and Hcy are very similar (8.72, 8.25, respectively) to that of cysteine (8.10),[51] implying similar reactivity. H_2S on the other hand, which is considered more acidic (pK_a 6.9) than other three thiols could act as a stronger nucleophile. In addition, proteins with free cysteine residues could also act as possible reactive species with the DCM-Cys probe. As described in the previous chapter, the protein content is roughly 20–25 wt% inside cells, with many of those proteins possessing free cysteine residues.[52] Furthermore, over 90% of the extracellular thiols in blood are due to the presence of the most abundant protein (~60%), serum albumin.[53] Human serum albumin (HSA), like BSA, has only one free cysteine (Cys 34);[54] this is a potential site of reaction for DCM-Cys. The protein BSA was chosen for study here due to the known variability in the free thiol content of Cys 34 in HSA upon its storage.[54] As shown in Figure 4.13, these components were tested (60μM) by incubating them with aqueous 30 μM DCM-Cys. The fluorescence turn-on signal was examined over ~20 min.

As demonstrated by outcomes of Figure 4.13, none of the potential cross-reactive thiol components tested exhibits the ability to act as an interferent in the time frame tested, in comparison to the response for cysteine. The selectivity toward cysteine versus GSH and Hcy may be due to differences in ring-formation kinetics. As demonstrated by Strongin and coworkers in 2011,[55] the size of the lactam ring formed can offer a selective process, thereby allowing for discrimination cysteine from GSH and Hcy. According to Scheme 4.6, formation of the smaller sized 7-membered lactam ring is kinetically favored over the larger sized 8- and 12-membered ring formation with Hcy and GSH. Therefore, as demonstrated in Figure 4.13, the potential turn-on ability of DCM-Cys corresponds to the size of the ring formed. Cysteine was the fastest reacting species, exhibiting a rapid turn-on response (< 12 min), followed by Hcy (> 30 min), and GSH being the least reactive species. As mentioned in chapter 3, the potentially lower reactivity of cysteine residues (Cys-34) in BSA may be due to steric hindrance of the Cys

residue as it oriented more toward the interior of the protein.[5] The reason for the lack of observing any reaction with H_2S is due to its inability to undergo ring formation.

Figure 4.13 Time-dependent fluorescence (λ_{ex} = 520 nm, λ_{em} = 640 nm) from 30 μM DCM-Cys probe incubated with 60 μM thiol-containing analytes in 0.1 M, pH 7.4 PBS/DMSO (60%:40%) at 37 $^{\circ}$C.

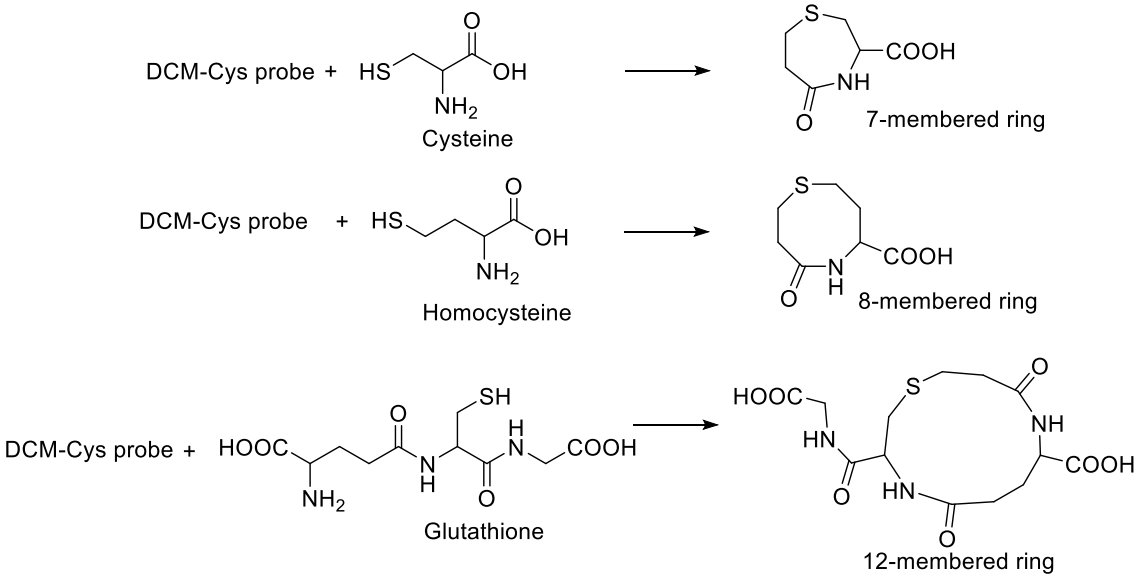

Scheme 4.6 Lactam ring formation resulting from reaction of DCM-Cys probe with cysteine.

4.3.8 Reactivity of DCM-Cys with other Biological Analytes

The results discussed in the previous section demonstrated the selectivity of DCM-Cys toward cysteine versus other bio-thiols (GSH, Hcy, H_2S). In order to further evaluate selectivity, the response of DCM-Cys with a few select naturally-occurring amino acids, such as glycine (Gly), methionine (Met), serine (Ser), and threonine (Thr), was investigated. In addition, other commonly abundant biomolecules in biological milieu, such as the ubiquitous ascorbic acid and NADH, were also tested as possible interferents. A 30 μM aqueous solution of DCM-Cys was incubated with 150 μM of each analyte at 37 $^{\circ}$C for 20 min. The fluorescence response was measured by exciting the sample at λ_{ex} = 520 nm and measuring the intensity of the emission maximum at λ_{em} = 640 nm. As shown in Figure 4.14, both non-thiol nucleophilic amino acids (Gly, Ser, and Thr) or the thiol-containing amino acid methionine did not cause any significant increase in fluorescence. The biological reductant NADH, which is present at mM levels within cells, and the common antioxidant ascorbic acid also did not cause release of the free reporter from the DCM-Cys probe.

Figure 4.14 Fluorescence response of DCM-Cys (30 μM) incubated at 37 $^{\circ}$C for 20 min with 150 μM amino acids and other common interferents in 40% DMSO:60% 0.1 M, pH 7.4 PBS. Bars represent % release of free DCM reporter with respect to that achieved for DCM-Cys incubated with 60 μM Cys for 20 min.

A significant increase in fluorescence was observed only upon addition of 60 μM cysteine, providing further evidence for the feasibility of the cysteine reaction. The visual color change under white light (Figure 4.15a) and the fluorescence color change under UV lamp exposure (Figure 4.15b) of the solutions upon addtion of each analyte is demonstrated as follows. Upon inspecting the solutions. it is clear that the significant color change from yellow to red occurs only when the cysteine is present in the media.

Figure 4.15 Visual observation of solutions of DCM-Cys (30 μM) in 0.1 M, pH 7.4 PBS/DMSO 60%:40% in the presence of 150 μM various other analytes and 60 μM cysteine: a) visual color under white light illumination and b) fluorescence emission under UV-lamp irradiation (λ =~365 nm). Each sample was incubated 20 min at 37 $^{\circ}$C after addition of each analyte.

4.3.9 Imaging of Cysteine Presence in Human Cells

Upon demonstration that DCM-Cys allows selective detection of cysteine under low probe: analyte conditions with relatively short incubation time (<12 min), an analysis was undertaken to examine the ability of DCM-Cys to act as a possible cysteine detecting probe in thiol upregulated human cancer cells.

The ability of DCM-Cys to detect cysteine in live cells was evaluated using the human lung cancer cell line H596. The H596 cell line was chosen due to its known thiol content as mentioned in Chapter 3.[56] Two-dimensional cell cultures were incubated with 30 μM DCM-Cys

for 10 min at 37 °C and subsequently washed with pH 7.4 PBS; then the cells were fixed using formaldehyde, and the slides were left in the dark in a refrigerator for 24 hours prior to being imaged. As the negative control experiment, H596 cells were pre-incubated with the known thiol capping agent *N*-ethylmaleimide (10 mM NEM) for 30 min at 37 °C and subsequently washed with PBS buffer to remove any excess NEM. Then the cells were incubated with 30 μM DCM-Cys for 10 min followed by washing with pH 7.4 PBS buffer. Slides were then fixed as mentioned above. Fluorescence images were obtained using confocal scanning laser microscopy via excitation at the laser line λ = 488 nm and detection at λ = 625–750 nm.

As demonstrated by Figure 4.16 (Panel B), unadulterated H596 cells that were exposed to the DCM-Cys probe exhibited strong red fluorescence when compared to the cells that were first incubated with NEM (Figure 4.16, Panel C). In Figure 4.16 A is shown untreated H596 cells

Figure 4.16 Microscopy images of human H596 lung cells a) A–C confocal images b) D–F differential interference contrast images; image A-control experiment without probe, image B-incubated with 30 μM DCM-Cys for 10 min at T = 37 °C, image C-pre-incubated with 10 mM NEM thiol scavenger for 30 min at 37 °C, followed by incubation with 30 μM DCM-Cys for 10 min at T = 37 °C. Scale bar = 20 μM

that were used as a background control to make sure that there was no other background interferences contributing to the observed fluorescence. The clear fluorescent contrast observed between image B and image C indicated the presence of cysteine in cells. The electrically neutral DCM-Cys can enter cells (similar to the observation with HMBQ-Nap 1 probe for thiols), and has the potential ability to report intracellular cysteine presence in a rapid and selective manner.

4.4 Conclusions

I have successfully designed and synthesized two fluorescent probes possessing a reactive acrylate moiety; Nap-Cys and DCM-Cys, with the intention of selectively detecting cysteine both in cellular and aqueous media. Out of these two probes, DCM-Cys possesses the ability to provide detection of cysteine in aqueous buffered media in a relatively short time period (< 20 min). The rapid activation of the DCM-Cys by cysteine is attributed to the acrylate moiety undergoing nucleophilic attack by the thiol group of cysteine, followed by a rapid cyclization and elimination reaction to release the free DCM reporter that was detected at λ_{max} = 640 nm. In addition to the fluorescence change in the media, a strong change in the color of the solution from yellow to red upon reaction with cysteine facilitated the visual and colorimetric monitoring of cysteine at micromolar concentration levels. The feasibility of the smaller sized ring formation kinetics of cysteine (7-membered) when compared to glutathione (12-membered) and homocysteine (8-membered) make the DCM-Cys probe highly selective. In addition, any significant cross reactivity of DCM-Cys with other nucleophilic amino acids and strong reducing agents in biological media was not observed. This further substantiates the success of DCM-Cys as a cysteine-selective fluorescent probe. In regards to its high selectivity and rapid response, this probe has the potential ability to be used as a cysteine detecting probe in actual cellular environments. This was demonstrated by the successful outcome of cellular images that were obtained with and without thiol capping agents.

4.5 References

1. Lee, M. H., Kim, J.S., Sessler, J.L., Small Molecule-Based Ratiometric Fluorescence Probes for Cations, Anions, and Biomolecules. *Chem. Soc. Rev., Ahead of print*, **2015**.

2. Chen, X.; Tian, X.; Shin, I.; Yoon, J., Fluorescent and Luminescent Probes for Detection of Reactive Oxygen and Nitrogen Species. *Chem. Soc. Rev.*, **2011**, *40*, 4783-4804.

3. Kobayashi, H.; Choyke, P. L., Target-Cancer-Cell-Specific Activatable Fluorescence Imaging Probes: Rational Design and in Vivo Applications. *Acc. Chem. Res.,* **2011**, *44*, 83-90.

4. Weissleder, R.; Ntziachristos, V., Shedding Light onto Live Molecular Targets. *Nat. Med.,* **2003**, *9*, 123-128.

5. Turell, L.; Radi, R.; Alvarez, B., The Thiol Pool in Human Plasma: The Central Contribution of Albumin to Redox Processes. *Free Radical Biol. Med.,* **2013**, *65*, 244-253.

6. Pace, N. J.; Weerapana, E., Diverse Functional Roles of Reactive Cysteines. *ACS Chem. Biol.,* **2013**, *8*, 283-96.

7. Miller, A. L., The Methionine-Homocysteine Cycle and Its Effects on Cognitive Diseases. *Altern. Med. Rev.,* **2003**, *8*, 7-19.

8. Paulsen, C. E.; Carroll, K. S., Cysteine-Mediated Redox Signaling: Chemistry, Biology, and Tools for Discovery. *Chem. Rev.,* **2013**, *113*, 4633-4679.

9. Hanjing P., W. C., Yunfeng C.,Lovemore H., Strongin R., Wang B., Thiol Reactive Probes and Chemosensors. *Sensors,* **2012**, *12*, 15907-15946.

10. Refsum, H.; Ueland, P. M.; Nygard, O.; Vollset, S. E., Homocysteine and Cardiovascular Disease. *Annu. Rev. Med.,* **1998**, *49*, 31-62.

11. Müller, T.; Muhlack, S., Cysteine Decrease Following Acute Levodopa Intake in Patients with Parkinson's Disease. *Neurosci. Lett.,* **2012**, *521*, 37-39.

12. De Chiara, B.; Sedda, V.; Parolini, M.; Campolo, J.; De Maria, R.; Caruso, R.; Pizzi, G.; Disoteo, O.; Dellanoce, C.; Corno, A. R.; Cighetti, G.; Parodi, O., Plasma Total Cysteine and Cardiovascular Risk Burden: Action and Interaction. *Sci. World J.,* **2012**, 303654, 7 pp.

13. Brosnan, J. T.; Brosnan, M. E., The Sulfur-Containing Amino Acids: An Overview. *J. Nutr.,* **2006**, *136*, 1636S-1640S.

14. El-Khairy, L.; Ueland, P. M.; Nygard, O.; Refsum, H.; Vollset, S. E., Lifestyle and Cardiovascular Disease Risk Factors as Determinants of Total Cysteine in Plasma: The Hordaland Homocysteine Study. *Am. J. Clin. Nutr.,* **1999**, *70*, 1016-1024.

15. Heafield, M. T.; Fearn, S.; Steventon, G. B.; Waring, R. H.; Williams, A. C.; Sturman, S. G., Plasma Cysteine and Sulphate Levels in Patients with Motor Neurone, Parkinson's and Alzheimer's Disease. *Neurosci. Lett.,* **1990**, *110*, 216-220.

16. Chwatko, G.; Bald, E., Determination of Cysteine in Human Plasma by High-Performance Liquid Chromatography and Ultraviolet Detection after Pre-Column Derivatization with 2-Chloro-1-Methylpyridinium Iodide. *Talanta,* **2000**, *52*, 509-515.

17. Spãtaru, N.; Sarada, B. V.; Popa, E.; Tryk, D. A.; Fujishima, A., Voltammetric Determination of L-Cysteine at Conductive Diamond Electrodes. *Anal. Chem.,* **2001**, *73*, 514-519.

18. Liu, Y.; Yu, D.; Ding, S.; Xiao, Q.; Guo, J.; Feng, G., Rapid and Ratiometric Fluorescent Detection of Cysteine with High Selectivity and Sensitivity by a Simple and Readily Available Probe. *ACS Appl. Mater. Interfaces,* **2014**, *6*, 17543-17550.

19. G, U. R.; Agarwalla, H.; Taye, N.; Ghorai, S.; Chattopadhyay, S.; Das, A., A Novel Fluorescence Probe for Estimation of Cysteine/Histidine in Human Blood Plasma and Recognition of Endogenous Cysteine in Live Hct116 Cells. *Chem. Commun.,* **2014**, *50,* 9899-9902.

20. Niu, L.-Y.; Guan, Y.-S.; Chen, Y.-Z.; Wu, L.-Z.; Tung, C.-H.; Yang, Q.-Z., A Turn-on Fluorescent Sensor for the Discrimination of Cystein from Homocystein and Glutathione. *Chem. Commun.,* **2013**, *49*, 1294-1296.

21. Jung, H. S.; Chen, X.; Kim, J. S.; Yoon, J., Recent Progress in Luminescent and Colorimetric Chemosensors for Detection of Thiols. *Chem. Soc. Rev.,* **2013**, *42*, 6019-6031.

22. Jung, H. S.; Chen, X.; Kim, J. S.; Yoon, J., Recent Progress in Luminescent and Colorimetric Chemosensors for Detection of Thiols. *Chem. Soc. Rev.,* **2013**, *42*, 6019-31.

23. Lim, N. C.; Schuster, J. V.; Porto, M. C.; Tanudra, M. A.; Yao, L.; Freake, H. C.; Brückner, C., Coumarin-Based Chemosensors for Zinc(Ii): Toward the Determination of the Design Algorithm for Chef-Type and Ratiometric Probes. *Inorg. Chem.,* **2005**, *44*, 2018-2030.

24. Zhao, Y.; Zheng, Q.; Dakin, K.; Xu, K.; Martinez, M. L.; Li, W.-H., New Caged Coumarin Fluorophores with Extraordinary Uncaging Cross Sections Suitable for Biological Imaging Applications. *J. Am. Chem. Soc.,* **2004**, *126*, 4653-4663.

25. Duke, R. M.; Veale, E. B.; Pfeffer, F. M.; Kruger, P. E.; Gunnlaugsson, T., Colorimetric and Fluorescent Anion Sensors: An Overview of Recent Developments in the Use of 1,8-Naphthalimide-Based Chemosensors. *Chem. Soc. Rev.,* **2010**, *39*, 3936-3953.

26. Grabchev, I.; Chovelon, J.-M., New Blue Fluorescent Sensors for Metal Cations and Protons Based on 1,8-Naphthalimide. *Dyes. Pigments.,* **2008**, *77*, 1-6.

27. Chen, Z.; Wu, D.; Han, X.; Nie, Y.; Yin, J.; Yu, G.-A.; Liu, S. H., 1,8-Naphthalimide-Based Highly Blue-Emissive Fluorophore Induced by a Bromine Atom: Reversible Thermochromism and Vapochromism Characteristics. *RSC. Adv.,* **2014**, *4*, 63985-63988.

28. Chen, X.; Pradhan, T.; Wang, F.; Kim, J. S.; Yoon, J., Fluorescent Chemosensors Based on Spiroring-Opening of Xanthenes and Related Derivatives. *Chem. Rev.,* **2011**, *112*, 1910-1956.

29. Kobayashi, H.; Ogawa, M.; Alford, R.; Choyke, P. L.; Urano, Y., New Strategies for Fluorescent Probe Design in Medical Diagnostic Imaging. *Chem. Rev.,* **2010**, *110*, 2620-2640.

30. Li, J.; Hu, M.; Yao, S. Q., Rapid Synthesis, Screening, and Identification of Xanthone- and Xanthene-Based Fluorophores Using Click Chemistry. *Org. Lett.,* **2009**, *11*, 3008-3011.

31. Tanaka, K.; Miura, T.; Umezawa, N.; Urano, Y.; Kikuchi, K.; Higuchi, T.; Nagano, T., Rational Design of Fluorescein-Based Fluorescence Probes. Mechanism-Based Design of a Maximum Fluorescence Probe for Singlet Oxygen. *J. Am. Chem. Soc.,* **2001**, *123*, 2530-2536.

32. Zheng, H.; Zhan, X. Q.; Bian, Q. N.; Zhang, X. J., Advances in Modifying Fluorescein and Rhodamine Fluorophores as Fluorescent Chemosensors. *Chem. Commun.,* **2013**, *49*, 429-47.

33. Wu, X.; Sun, X.; Guo, Z.; Tang, J.; Shen, Y.; James, T. D.; Tian, H.; Zhu, W., In Vivo and in Situ Tracking Cancer Chemotherapy by Highly Photostable Nir Fluorescent Theranostic Prodrug. *J. Am. Chem. Soc.,* **2014**, *136*, 3579-3588.

34. Guo, Z.; Park, S.; Yoon, J.; Shin, I., Recent Progress in the Development of near-Infrared Fluorescent Probes for Bioimaging Applications. *Chem. Soc. Rev.,* **2014**, *43*, 16-29.

35. Altman, R. B.; Terry, D. S.; Zhou, Z.; Zheng, Q.; Geggier, P.; Kolster, R. A.; Zhao, Y.; Javitch, J. A.; Warren, J. D.; Blanchard, S. C., Cyanine Fluorophore Derivatives with Enhanced Photostability. *Nat. Methods,* **2012**, *9*, 68-71.

36. Luo, S.; Zhang, E.; Su, Y.; Cheng, T.; Shi, C., A Review of Nir Dyes in Cancer Targeting and Imaging. *Biomaterials,* **2011**, *32*, 7127-7138.

37. Guo, Z.; Zhu, W.; Tian, H., Dicyanomethylene-4h-Pyran Chromophores for Oled Emitters, Logic Gates and Optical Chemosensors. *Chem. Commun.,* **2012**, *48*, 6073-84.

38. Liu, B.; Li, X.; Liu, M.; Ning, Z.; Zhang, Q.; Li, C.; Müllen, K.; Zhu, W., Photovoltaic Performance of Solid-State Dsscs Sensitized with Organic Isophorone Dyes: Effect of Dye-Loaded Amount and Dipole Moment. *Dyes. Pigments.,* **2012**, *94*, 23-27.

39. Liu, B.; Zhu, W.; Zhang, Q.; Wu, W.; Xu, M.; Ning, Z.; Xie, Y.; Tian, H., Conveniently Synthesized Isophorone Dyes for High Efficiency Dye-Sensitized Solar Cells: Tuning Photovoltaic Performance by Structural Modification of Donor Group in Donor-Pi-Acceptor System. *Chem. Commun.,* **2009**, 1766-8.

40. Tong, H.; Hong, Y.; Dong, Y.; Ren, Y.; Haussler, M.; Lam, J. W.; Wong, K. S.; Tang, B. Z., Color-Tunable, Aggregation-Induced Emission of a Butterfly-Shaped Molecule Comprising a Pyran Skeleton and Two Cholesteryl Wings. *J. Phys. Chem. B.,* **2007**, *111*, 2000-7.

41. Sun, W.; Fan, J.; Hu, C.; Cao, J.; Zhang, H.; Xiong, X.; Wang, J.; Cui, S.; Sun, S.; Peng, X., A Two-Photon Fluorescent Probe with near-Infrared Emission for Hydrogen Sulfide Imaging in Biosystems. *Chem. Commun.,* **2013**, *49*, 3890-3892.

42. Nawimanage, R. R.; Prasai, B.; Hettiarachchi, S. U.; McCarley, R. L., Rapid, Photoinduced Electron Transfer-Modulated, Turn-on Fluorescent Probe for Detection and Cellular Imaging of Biologically Significant Thiols. *Anal. Chem.,* **2014**, *86*, 12266-12271.

43. Cieslak, J.; Kauffman, J. S.; Kolodziejski, M. J.; Lloyd, J. R.; Beaucage, S. L., Assessment of 4-Nitrogenated Benzyloxymethyl Groups for 2'-Hydroxyl Protection in Solid-Phase Rna Synthesis. *Org. Lett.,* **2007**, *9*, 671-674.

44. Erez, R.; Shabat, D., The Azaquinone-Methide Elimination: Comparison Study of 1,6- and 1,4-Eliminations under Physiological Conditions. *Org. Biomol. Chem.,* **2008**, *6*, 2669-2672.

45. Jia, J.; Sarker, M.; Steinmetz, M. G.; Shukla, R.; Rathore, R., Photochemical Elimination of Leaving Groups from Zwitterionic Intermediates Generated Via Electrocyclic Ring Closure of A,B-Unsaturated Anilides. *J. Org. Chem.,* **2008**, *73*, 8867-8879.

46. Yu, D.; Huang, F.; Ding, S.; Feng, G., Near-Infrared Fluorescent Probe for Detection of Thiophenols in Water Samples and Living Cells. *Anal. Chem.,* **2014**, *86*, 8835-8841.

47. Jin, H.-j.; Lu, J.; Wu, X., Development of a New Enzyme-Responsive Self-Immolative Spacer Conjugate Applicable to the Controlled Drug Release. *Bioorg. Med. Chem.,* **2012**, *20*, 3465-3469.

48. Hettiarachchi, S. U.; Prasai, B.; McCarley, R. L., Detection and Cellular Imaging of Human Cancer Enzyme Using a Turn-on, Wavelength-Shiftable, Self-Immolative Profluorophore. *J.Am. Chem. Soc.,* **2014**, *136*, 7575-7578.

49. Avital-Shmilovici, M.; Shabat, D., Self-Immolative Dendrimers: A Distinctive Approach to Molecular Amplification. *Soft. Matt.,* **2010**, *6*, 1073-1080.

50. Silvers, W. C.; Prasai, B.; Burk, D. H.; Brown, M. L.; McCarley, R. L., Profluorogenic Reductase Substrate for Rapid, Selective, and Sensitive Visualization and Detection of Human Cancer Cells That Overexpress Nqo1. *J. Am. Chem. Soc.*, **2013**, *135*, 309-14.

51. Montoya, L. A.; Pluth, M. D., Hydrogen Sulfide Deactivates Common Nitrobenzofurazan-Based Fluorescent Thiol Labeling Reagents. *Anal. Chem.*, **2014**, *86*, 6032-6039.

52. Ellis, R. J., Macromolecular Crowding: Obvious but Underappreciated. *Trends Biochem. Sci.*, **2001**, *26*, 597-604.

53. Nicholson, J. P.; Wolmarans, M. R.; Park, G. R., The Role of Albumin in Critical Illness. *Brit. J. Anaesth.*, **2000**, *85*, 599-610.

54. Tong, G. Characterization of Cysteine-34 in Serum Albumin Ph.D. thesis, Ohio State University, **2003**.

55. Yang, X.; Guo, Y.; Strongin, R. M., Conjugate Addition/Cyclization Sequence Enables Selective and Simultaneous Fluorescence Detection of Cysteine and Homocysteine. *Angew. Chem. Int. Ed.*, **2011**, *50*, 10690-3.

56. Carmichael, J.; Mitchell, J. B.; Friedman, N.; Gazdar, A. F.; Russo, A., Glutathione and Related Enzyme Activity in Human Lung Cancer Cell Lines. *Br. J. Cancer*, **1988**, *58*, 437-40.

CHAPTER 5
SUMMARY, CONCLUSIONS, AND OUTLOOK: NIR FLUORESCENT PROBE FOR THE SELECTIVE DETECTION OF HYDROGEN SULFIDE

5.1 Summary and Conclusions

The overall goal of this research was design, synthesis, and characterization of small molecule-based fluorescent probes for the detection of thiols in biological environments, especially in cells. Fluorescence detection methods have several advantages over other traditional methods. Their great simplicity and low cost of operational requirements, combined with high sensitivity and less invasiveness, offer up fluorescence methods as a potentially indispensable tool for biomedical diagnosis. On the other hand, thiols in bodily fluids and cellular environments are biomarkers of several health complications and altered biochemical pathways. Therefore, accurate determination of thiol content inside cells has a great importance. However, drawbacks in currently reported methods, such as slow response time and less selectivity in biological environments motivated me to develop a new set of thiol probes to perform detection more efficiently with relatively short time.

As the first part of my project, I have investigated the potential ability of a redox-active hydroxymethyl benzoquinone (HMBQ) group to act as a trigger motif in self-immolative delivery systems. Inspired by previously published work by the McCarley group and others, I successfully synthesized and characterized novel redox-active HMBQ–DOPE-based liposomes as encapsulated drug delivery agents. According to spectroscopic and light scattering data, calcein-encapsulated large unilamellar vesicles (LUVs), with an average diameter of 150 nm, were obtained using the lipid hand-extrusion method. However, in stark contrast to what was expected, contents release upon HMBQ reduction by the strong reducing agent sodium dithionite (DT) was not achieved. The reason for this observation was attributed to two possible outcomes. It could be either the inability of the lipid group to leave the reduced hydroquinone head group, or it could be the result of nucleophilic attack of the electron-rich amine group of DOPE on the quinone methide moiety to form a stable hydroquinone species. In order to further understand the release mechanism, and as a simple method to detect released end products, the nitroaniline-based probe HMBQ-Npc was synthesized and characterized using NMR and absorption spectroscopies. Both absorption and NMR data confirmed rapid release of the *para*-nitroaniline reporter upon HMBQ reduction. According to kinetic parameters obtained by absorption

spectroscopy data, the purported rate-limiting step of the reaction leading to quinone methide formation was fitted to first-order kinetics. The linear natural logarithm graph of extent of product disappearance versus time yielded a highly correlated relationship; thereby demonstrating disappearance of HMBQ-Npc follows first-order kinetics. The calculated pseudo first-order rate constant (k_1) for the product disappearance was 0.0303 min^{-1}. However, *para*-nitroaniline product formation did not follow simple first-order kinetics, which was evidenced by the hyperbolic shape of the product formation (*para*-nitroaniline) graph rather than the expected linear response. At this moment, there are not enough data to calculate the order of the product formation reaction. However, rapid elimination of *para*-nitroaniline was further evidenced by NMR; the decrease in peak intensity corresponding to probe (HMBQ-Npc), and appearance of aromatic hydrogen peaks corresponding to product (*para*-nitroaniline) formation was observed about 15 min after addition of dithionite. Interestingly, quinone methide elimination was also observed by NMR experiment; the two peaks that were assumed to correspond to the alkene hydrogens of the quinone methide appeared shortly after dithionite addition, and they diminished in intensity when the reaction reached completion. Combining the results observed for both absorption and NMR spectroscopies, it was concluded that quinone methide formation and elimination of Nap 2 reporter upon reduction of the HMBQ head group of HMBQ-Npc is a rapid process. Thus, a possible reason for not observing release of HMBQ-DOPE liposomes could be the attack of the amine group of the DOPE lipid on the quinone methide to form the hydroquinone-coupled DOPE species. Due to its rapid elimination kinetics, the HMBQ group has the potential to be used as a good trigger group in self-immolative delivery systems.

In the third chapter, a novel thiol imaging probe, HMBQ-Nap 1, was successfully synthesized and characterized, taking advantage of the outcomes observed in the HMBQ-Npc system in Chapter 2. HMBQ-Nap 1 consists of the HMBQ head group attached to the Nap 2 reporter dye via a carbamate linkage. The HMBQ trigger group can acts as a potential reaction site for thiols, and the trigger group can function as a PeT quencher of the Nap 2 reporter dye. Initially, the fluorescence of the Nap 2 reporter dye is efficiently PeT quenched in the probe, as indicated by the very low quantum yield of the probe ($\Phi_{\text{HMBQ-Nap1}}$ = 0.003). The calculated quantum yield of Nap 2 was 65 times brighter ($\Phi_{\text{Nap 2}}$ = 0.19) than the probe, giving rise to good signal contrast when the free reporter Nap 2 was released from the probe. This vast difference in quantum yields between probe and reporter makes HMBQ-Nap 1 a good turn-on probe. As an

added advantage of this probe/reporter system, Nap 2 exhibits a strong Stokes-shift between its absorption (432 nm) and fluorescence emission maxima (540 nm), as a result of internal charge transfer taking place in the dye. The absorption maximum of Nap 2 was red shifted about 70 nm versus that of HMBQ-Nap 1, making the HMBQ-Nap 1/Nap 2 pair an excellent probe/reporter system with less background interferences. The HMBQ-Nap 1 probe was first tested with dithionite reductant in order to determine its potential ability to release the Nap 2 reporter upon reduction. Encouraged by the observed rapid fluorescence after dithionite reduction, fluorescence studies with thiols were carried out in a similar way. Glutathione, cysteine, and homocysteine were chosen for the studies, due to their abundance in cellular media, and due to the significant role they play in physiological systems. As anticipated, a rapid fluorescence increase was observed, indicating a very strong affinity of thiols for the HMBQ head group. The rapid nature of the turn-on process was evidenced by the ~150 s time required to reach 90% of the maximum attainable signal. To determine the concentration dependence of the thiol on the HMBQ-Nap 1 probe system, varying concentrations of thiols were incubated with the probe for 15 min, and the fluorescence increase was measured. According to the data obtained, it was found that a linear relationship exists between fluorescence intensity and their concentration between 0–2 μM. From the calibration curve obtained for each thiol, the concentration limit of detection was determined as 33 nM for GSH, 21 nM for Hcy, and 29 nM for Cys; the limit of quantification was obtained as 110, 70, and 98 nM respectively. These low limits indicate the potential ability of HMBQ-Nap 1 to be used to quantify a low concentration range (nM) of thiols in bodily fluids, such as plasma thiols.[1] Next, in order to determine the activation mechanism of HMBQ-Nap 1 by thiols, NMR and mass spectrometry studies were conducted. As speculated in literature reports and studies in Chapter 2, the turn-on mechanism of HMBQ-Nap 1 upon reaction with thiols could be the result of either merely redox activation of, or a nucleophilic addition to, the quinone moiety. When HMBQ-Nap 1 was treated with 5 equivalents of biological thiol analogue (mercaptoethanol), a rapid appearance (< 1 min) of NMR spectral peaks corresponding to Nap 2 reporter were observed, with concomitant reduction of peak intensities corresponding to HMBQ-Nap 1. In addition, two other signals in the alkene hydrogen region (5–6 ppm) quickly appeared after reduction, and they diminished in intensity as time progressed; these were assigned as quinone methide hydrogen signals. These observations were comparable to what was observed in the HMBQ-Npc NMR experiment (Chapter 2) and further confirmed that the reaction

mechanism progressed through quinone methide formation. The final products of the NMR experiment were characterized by mass spectrometry to identify the end product formed. Results from the mass spectrometry experiment demonstrated release of free Nap 2 reporter dye, as noted by the $[M-H]^-$ signal at *m/z* 267.1138 (expected *m/z* 267.1134; −1.50 ppm error) and signals corresponding to the reporter produced with the mercapthoethanol addition to quinone methide as evidenced by the $[M-H]^-$ signal at *m/z* 239.0689 (expected *m/z* 239.0742; 22.2 ppm error), and free HMBQ resulting from water addition to the quinone methide; $[M-H]^-$ signal at *m/z* 179.0688 (expected *m/z* 179.0708; 11.2 ppm error). However, the absence of the hydroquinone product of HMBQ provided evidence that the reaction progressed through nucleophilic addition rather than redox activation by thiols. Furthermore, to determine the selectivity of the HMBQ-Nap 1 probe in biological media, selectivity studies were carried out by incubating the HMBQ-Nap 1 probe with other commonly found interferents in biological systems, such as NADH, amino acids, ascorbic acid, H_2S, and the reductase enzyme NQO1. The results obtained suggest a remarkable stability of HMBQ-Nap 1 in the presence of other analytes and further reinforce the successful ability of HMBQ-Nap 1 to accurately detect thiols in biological media without any cross reactivity. Finally, successful outcomes of the biological evaluation of HMBQ-Nap 1 with the H596 cancer cell line demonstrated the ability of HMBQ-Nap 1 to act as a thiol imaging agent in mammalian cells.

Further extending my scope toward developing thiol-detecting probes, and given the important role cysteine plays in physiological systems, the two probes Nap-Cys and DCM-Cys were designed, synthesized, and examined for their ability to detect cysteine. The Nap-Cys probe consisted of an acrylate moiety as the potential reactive site for cysteine, and this was attached to the fluorescent reporter Nap 2 via an amino benzyl alcohol linker. The probe was designed, such that upon reacting with cysteine, it should give rise to a ratiometric response by diminishing the probe fluorescence band at λ_{max} = 470 nm, while giving rise to a reporter fluorescence band (Nap 2) at λ_{max} = 540 nm. However, the expected band increases at 540 nm and decrease at 470 nm were not observed, even in the presence of 100 equivalents of added cysteine. According to literature reports, as lactam ring formation was proven to be a feasible process,[2] it was concluded that the downstream process of aza-quinone methide formation upon cyclization was not a feasible mechanism due to nitrogen being both the leaving and nucleophilic attacking group. Therefore, in the next approach, DCM-Cys was synthesized using a benzyl alcohol linker instead

of the amino-benzyl alcohol linker in the Nap-Cys probe. The DCM-Cys probe contains an acrylate moiety attached to the benzyl alcohol linker between the DCM reporter dye and the reactive acrylate moiety. The DCM-Cys probe exhibited weak absorbance and fluorescence bands centered around λ_{abs} = 440 nm and λ_{em} = 550 nm. In contrast, the free DCM reporter showed a large Stokes-shift between its absorbance (λ_{abs} = 490 nm) and fluorescence (λ_{em} = 640 nm) maxima, offering less background interferences. DCM-Cys was successfully used as a turn on response probe at 640 nm to monitor the release of free reporter DCM dye. Upon exposure to cysteine, DCM-Cys exhibited a rapid turn-on response, indicating the release of the free DCM dye. The rapidness of the reaction is evidenced by the relative short time period (< 12 min) required to acquire the maximum attainable fluorescence signal with a low thiol:reporter ratio. In addition, the prominent color change of the system from yellow to red allowed the visual detection of the reaction progress. The concentration dependency of DCM-Cys toward cysteine was monitored by varying the concentration of cysteine and measuring the fluorescence response at each concentration. By evaluating the data obtained from the calibration plot, it is clear that DCM-Cys exhibits a linear response up to 30 μM of cysteine (1 equivalent) with a concentration limit of detection of 21 nM and concentration limit of quantification of 70 nM. These recorded values were well below the lowest known plasma cysteine concentrations, indicating the successful ability of DCM-Cys to measure lower cysteine content in biological fluids.[1] As a method to detect the end product of the cysteine reaction, mass spectrometric studies were carried out. Results from the mass spectrometry experiment proved the release of free DCM reporter as noted by a peak at *m*/*z* = 310.0978 ($[M-H]^-$, expected *m*/*z* = 310.0979, 0.32 ppm error). Release of the cyclized lactam product was evidenced by the signal *m*/*z* = 176.0371 ($[M+H]^+$, expected *m*/*z* = 176.0383, 6.8 ppm error). Although the benzyl alcohol linker was not observed in the mass spectra, the data were sufficient to allow me to conclude that the reaction progressed through the proposed mechanism. Solution-phase analysis of DCM-Cys reactivity toward other commonly found bio-thiols in the body, such as GSH, Hcy, and H_2S, demonstrated the probe has remarkably good selectivity. The feasibility of smaller size ring formation of cysteine (7-membered), when compared to the larger sized ring structures of Hcy (8-membered) and GSH (12-membered), provided good discrimination between these similar bio-thiols. Interestingly, DCM-Cys shows a strong affinity for non-protein free thiols in comparison to the cysteine residues in protein thiols, as seen by the sluggish reaction rate observed for the Cys 34

residue in bovine serum albumin. The slow reaction rate observed for protein bound cysteines was attributed to the steric interactions of these reaction sites compared to free cysteines in the media. Furthermore, the DCM-Cys probe demonstrated its successful ability to be a selective probe by being remarkably stable in the presence of other commonly found analytes, such as amino acids, NADH, and ascorbic acid. Finally, the ultimate goal of biological evaluation of cysteine presence in a living cellular environment was successfully achieved as evidenced by data obtained by the fluorescence studies of human lung cancer cell line H596.

5.2 Outlook

5.2.1 NIR Fluorescent Probe for the Selective Detection of Hydrogen Sulfide

In a parallel project I was carrying out, I was working on the targeted development of an NIR fluorescent probe for the selective detection of H_2S in cells, due to a rising concern about the physiological role of this small but important molecule. Hydrogen sulfide (H_2S), the smallest member of the thiol family, despite its traditional consideration as a toxic substance, is undergoing reclassification as an important endogenously produced molecule for maintaining normal physiology in the body. H_2S, together with NO and CO, belongs to a family of important gasotransmitters, and it has the ability to freely travel through cell membranes without specific transporters.[3-5] H_2S is synthesized in cells via both enzymatic and non-enzymatic pathways. The enzymatic synthesis is catalyzed by cystathionine-β-synthase (CBS), cystathionine-γ-lyase (CSE), cysteine-aminotransferase (CAT), and mercaptopyruvate-sulfurtransferase (MST) in the presence of the thiol-containing biomolecules cysteine and homocysteine.[6-7] Non-enzymatic production of H_2S occurs by release from sulfur stores and in the metabolism of polysulfides.[8] A unique aspect of H_2S compared to other gasotransmitters, is its different protonation states. In aqueous solutions, H_2S is considerably more acidic ($pK_a = 6.9$) than Cys ($pK_a = 8.10$), GSH ($pK_a = 8.72$) or Hcy ($pK_a = 8.25$), resulting in about 80% of H_2S existing in the reactive anionic form (HS^-).[9] H_2S has been shown to contribute to several important functions in the body, such as modulating potassium ion channels and acting as a relaxant of smooth muscle, as well as being a regulator of cardiovascular and gastrointestinal systems.[10] Alteration of H_2S production in cells is linked to several disease conditions, including diabetes, liver damage, Alzheimer's disease, and Down syndrome.[10]

Concentration levels of H_2S have been reported to span a broad range in the literature.[11] To monitor these concentration fluctuations in the body and cellular sites, it is required to have probes with high H_2S sensitivity, selectivity, and real-time detection capability. There are several major challenges that are needed to address when designing an efficient probe for H_2S. Due to the transient nature of H_2S and its relatively low abundance in most tissues,[11] the probes need to provide a fast response toward analyte, and also, they should be selective toward H_2S without giving premature triggers in the presence of other thiols that are usually present in milimolar concentrations inside cells.[11]

The design strategies for fluorescent probes for H_2S are based on specific chemical reactions that take advantage of the nucleophilic properties of H_2S (HS^-) or the strong reducing properties of H_2S. The ability of H_2S to reduce azides and other oxidized nitrogen species much faster than other thiols has been exploited as a very promising route for H_2S detection. Upon reduction, the electron withdrawing azido or nitro groups are converted to a more electron donating amine group that will result in alterations in the fluorescence properties of the probe being used.[12-15] The strong di-nucleophilic property, when compare to other thiols, has also been explored as a successful strategy to develop selective probes for H_2S. Hydrogen sulfide can react with the more electrophilic moiety of the probe first to form an intermediate with a free sulfhydryl group, and when another electrophilic center is positioned at a suitable position, it can undergo Michael addition with the nearby sulfhydryl to cause a spontaneous cyclization that triggers the fluorescence change.[11, 16-18] Sulfide precipitation is another popular route used for the design of fluorescence probes. This approach utilizes the displacement of Cu^{2+} from the fluorophore's environment to produce fluorescence turn-on changes via H_2S-mediated precipitation of CuS from Cu^{2+}. At the beginning, the emission of the fluorophore is quenched by the presence of paramagnetic Cu^{2+} in the center. However, in the presence of H_2S, precipitation of the bound Cu^{2+} as CuS allows the fluorescence turn on, thereby facilitating the detection of H_2S.[19-22]

The proposed fluorescent probe (DCM-HS) contains dicyanomethylene-4*H*-pyran (DCM) as the NIR fluorescent reporter and an aldehyde and an ester moiety in close proximity to each other as potential reactive electrophilic centers for hydrogen sulfide. The reactive electrophilic centers are attached to the DCM fluorophore, via a benzyl alcohol linker. As shown in Figure 5.1 the proposed mechanism for this reporter system is based on the tandem nucleophilic addition and cyclization strategy for the selective detection of H_2S versus other biological thiols. Initially,

HS^- attacks the carbonyl carbon of the aldehyde moiety, reducing it to a secondary alcohol and in the next step, due to the double nucleophilic property of H_2S, it further reacts with the carbonyl carbon of the neighboring ester moeity. The second addition to the ester moiety will result in cyclization, eliminating the 1,2-benzenedicarbothioic acid (c) and quinone methide (b). Formation of the reactive quinone methide and CO_2 production is anticipated to facilitate the cascade of downstream processes that eliminate the linker group, with release of the free DCM reporter. As expected from my previous outcomes with DCM-Cys, the elimination of the free reporter should result in the turn-on response at λ_{em} = 640 nm providing an efficient method to monitor H_2S both in solution and cellular environments.

Taken together, the concept presented in this dissertation facilitated the fluorescent monitoring of biological relevant thiols both in solution phase and cellular environment with good selectivity and sensitivity. With a good understanding of the cellular mechanism of action, in the future, these types of probe systems could possibly make significant contribution to disease-targeted analyte detection in the biomedical field.

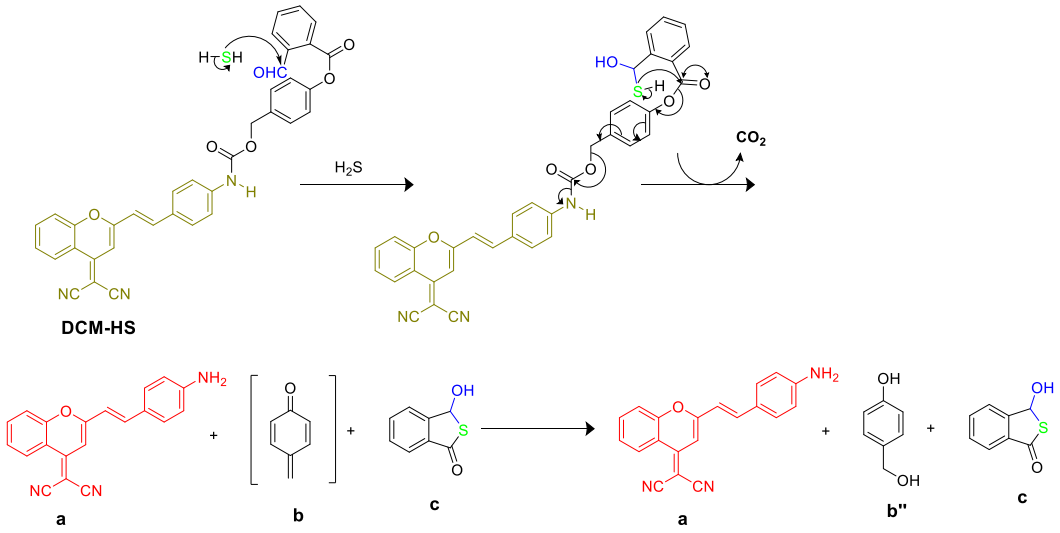

Figure 5.1 Schematic representation of the proposed mechanism of the DCM-HS probe.

5.3 Experimental

5.3.1 Synthetic Materials and Methods

The synthesis plan of the H_2S-selective probe, DCM-HS is shown in Scheme 5.1, and the partially completed synthesis (compound 18 and 19) is described as follows.

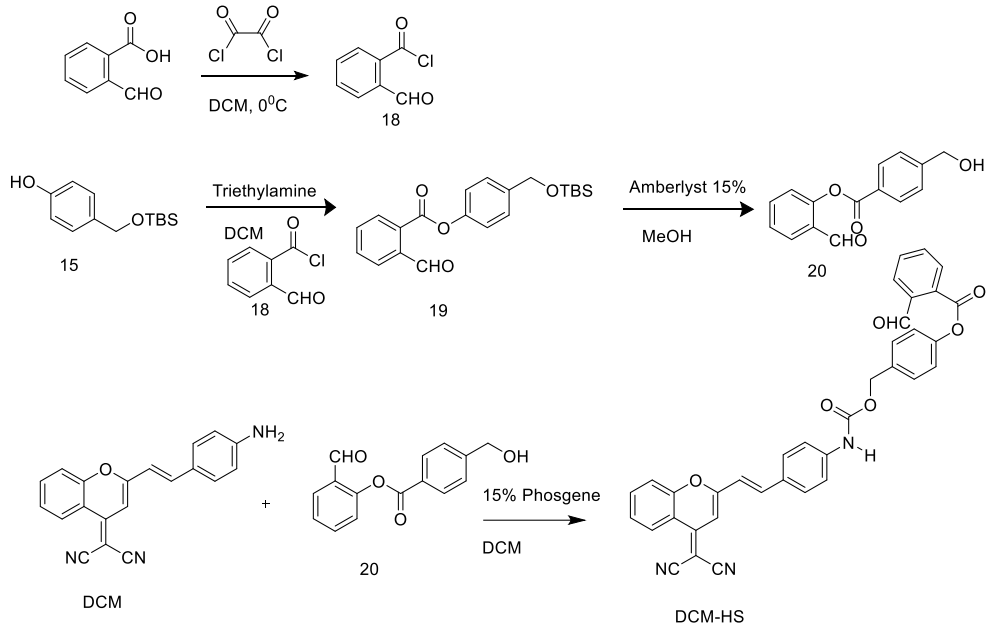

Scheme 5.1 Synthesis of probe DCM-HS

Synthesis of 2-formylbenzoyl chloride (18)

To a cooled (0 °C) suspension of 2-carboxybenzaldehyde (2.25 g, 15.0 mmol) in dry CH_2Cl_2 (50 mL), oxalyl chloride (2.85 mL, 30.0 mmol) and DMF (22.5 μL) were slowly added. The reaction mixture was stirred at RT for 8 h, and then the mixture was evaporated under vacuum to remove solvents. The oily material obtained was subsequently dried under vacuum to yield crude compound 18 as an off-white powder. The product was used in the next step without further purification.

Synthesis of 4-{[(*tert*-butyldimethylsilyl)oxy]methyl}phenyl 2-formylbenzoate (19)

To a solution of 15 (47.68 mg, 0.20 mmol) in dry CH_2Cl_2 (30 mL) at 0 °C, trimethylamine (0.28 mL, 0.6 mmol) was added, and this was allowed to stir for about 5 minutes. Then the crude compound 18 was dissolved in small amount of dry CH_2Cl_2, and the solution was slowly added into the reaction mixture; the mixture was warmed to RT and stirred overnight. Finally, the reaction mixture was diluted with distilled water, and then this was extracted into CH_2Cl_2 (50 mL). The solvent was evaporated, and compound 19 was isolated as a white solid. The

compound was characterized by ESI-MS: for $C_{21}H_{26}O_4Si$: expected *m/z* = 371.1680 $[M+H]^+$; found *m/z* = 371.1663 $[M+H]^+$; −4.5 ppm error.

5.4 References

1. Turell, L.; Radi, R.; Alvarez, B., The Thiol Pool in Human Plasma: The Central Contribution of Albumin to Redox Processes. *Free Radical Biol. Med.,* **2013**, *65*, 244-253.

2. Yang, X.; Guo, Y.; Strongin, R. M., Conjugate Addition/Cyclization Sequence Enables Selective and Simultaneous Fluorescence Detection of Cysteine and Homocysteine. *Angew.Chem. Int. Ed.,* **2011**, *50*, 10690-10693.

3. Mustafa, A. K.; Gadalla, M. M.; Snyder, S. H., *Signaling by Gasotransmitters*. 2009; Vol. 2, p re2-re2.

4. Szabo, C., Hydrogen Sulphide and Its Therapeutic Potential. *Nat. Rev.Drug Discov.,* **2007**, *6*, 917-935.

5. Kim, H. P.; Ryter, S. W.; Choi, A. M. K., Co as a Cellular Signaling Molecule. *Annu. Rev. Pharmacol. Toxicol.,* **2006**, *46*, 411-449.

6. Hanjing P., W. C., Yunfeng C.,Lovemore H., Strongin R., Wang B., Thiol Reactive Probes and Chemosensors. *Sensors,* **2012**, *12*, 15907-15946.

7. Olas, B., Hydrogen Sulfide in Signaling Pathways. *Clinica. Chimica. Acta.,* **2015**, *439*, 212-218.

8. Lin, V. S.; Chang, C. J., Fluorescent Probes for Sensing and Imaging Biological Hydrogen Sulfide. *Curr. Opin. Chem. Biol.,* **2012**, *16*, 595-601.

9. Montoya, L. A.; Pluth, M. D., Hydrogen Sulfide Deactivates Common Nitrobenzofurazan-Based Fluorescent Thiol Labeling Reagents. *Anal. Chem.,* **2014**, *86*, 6032-6039.

10. Chen, Z. J.; Ai, H. W., A Highly Responsive and Selective Fluorescent Probe for Imaging Physiological Hydrogen Sulfide. *Biochemistry,* **2014**, *53*, 5966-74.

11. Qian, Y.; Zhang, L.; Ding, S.; Deng, X.; He, C.; Zheng, X. E.; Zhu, H.-L.; Zhao, J., A Fluorescent Probe for Rapid Detection of Hydrogen Sulfide in Blood Plasma and Brain Tissues in Mice. *Chem. Sci.,* **2012**, *3*, 2920-2923.

12. Peng, H.; Cheng, Y.; Dai, C.; King, A. L.; Predmore, B. L.; Lefer, D. J.; Wang, B., A Fluorescent Probe for Fast and Quantitative Detection of Hydrogen Sulfide in Blood. *Angew. Chem. Int. Ed.,* **2011**, *50*, 9672-9675.

13. Yu, F.; Li, P.; Song, P.; Wang, B.; Zhao, J.; Han, K., An Ict-Based Strategy to a Colorimetric and Ratiometric Fluorescence Probe for Hydrogen Sulfide in Living Cells. *Chem. Commun.,* **2012**, *48*, 2852-2854.

14. Montoya, L. A.; Pluth, M. D., Selective Turn-on Fluorescent Probes for Imaging Hydrogen Sulfide in Living Cells. *Chem. Commun.,* **2012**, *48*, 4767-4769.

15. Wu, Z.; Li, Z.; Yang, L.; Han, J.; Han, S., Fluorogenic Detection of Hydrogen Sulfide Via Reductive Unmasking of O-Azidomethylbenzoyl-Coumarin Conjugate. *Chem. Commun.,* **2012**, *48*, 10120-10122.

16. Yu, F.; Han, X.; Chen, L., Fluorescent Probes for Hydrogen Sulfide Detection and Bioimaging. *Chem. Commun.,* **2014**, *50*, 12234-12249.

17. Qian, Y.; Karpus, J.; Kabil, O.; Zhang, S.-Y.; Zhu, H.-L.; Banerjee, R.; Zhao, J.; He, C., Selective Fluorescent Probes for Live-Cell Monitoring of Sulphide. *Nat. Commun.,* **2011**, *2*, 495.

18. Liu, C.; Peng, B.; Li, S.; Park, C.-M.; Whorton, A. R.; Xian, M., Reaction Based Fluorescent Probes for Hydrogen Sulfide. *Org. Lett.,* **2012**, *14*, 2184-2187.

19. Kumar, N.; Bhalla, V.; Kumar, M., Recent Developments of Fluorescent Probes for the Detection of Gasotransmitters (No, Co and H_2s). *Coord. Chem. Rev.,* **2013**, *257*, 2335-2347.

20. Sasakura, K.; Hanaoka, K.; Shibuya, N.; Mikami, Y.; Kimura, Y.; Komatsu, T.; Ueno, T.; Terai, T.; Kimura, H.; Nagano, T., Development of a Highly Selective Fluorescence Probe for Hydrogen Sulfide. *J. Am. Chem. Soc.,* **2011**, *133*, 18003-18005.

21. Choi, M. G.; Cha, S.; Lee, H.; Jeon, H. L.; Chang, S.-K., Sulfide-Selective Chemosignaling by a Cu2+ Complex of Dipicolylamine Appended Fluorescein. *Chem. Commun.,* **2009**, 7390-7392.

22. Hou, F.; Cheng, J.; Xi, P.; Chen, F.; Huang, L.; Xie, G.; Shi, Y.; Liu, H.; Bai, D.; Zeng, Z., Recognition of Copper and Hydrogen Sulfide in Vitro Using a Fluorescein Derivative Indicator. *Dalton. Trans.,* **2012**, *41*, 5799-5804.

APPENDIX A: SUPPORTING INFORMATION

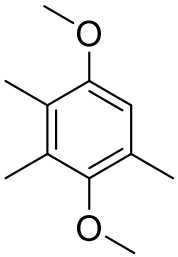

^{1}H NMR spectrum of 1,4-Dimethoxy-3,5,6-trimethyl benzene (1) in chloroform-*d* at 400 MHz

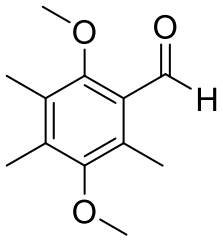

^{1}H NMR spectrum of 2,5-Dimethoxy-3,4,6-trimethylbenzaldehyde (2) in chloroform-*d* at 400 MHz

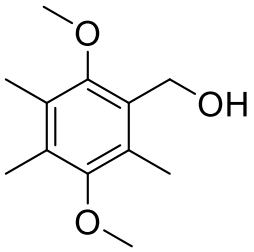

^{1}H NMR spectrum of 1-Hydroxymethyl-2,5-dimethoxy-3,4,6-trimethylbenzene (3) in chloroform-*d* at 400 MHz

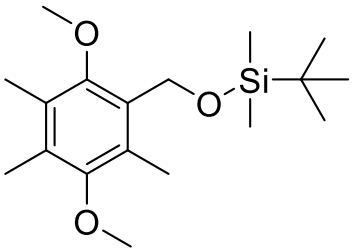

^{1}H NMR spectrum of 2,5-Dimethoxy-3,4,6-trimethylsilyl ether (4) chloroform-*d* at 400 MHz

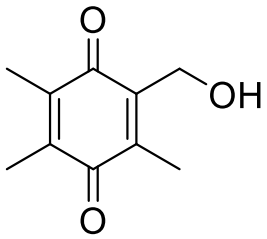

^{1}H NMR spectrum of 2-Hydroxymethyl-3,5,6-trimethyl-1,4-benzoquinone (5, HMBQ) in chloroform-*d* at 400 MHz

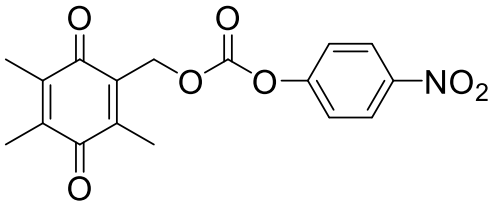

^{1}H NMR spectrum of 4-nitrophenyl (2,4,5-trimethyl-3,6-*di*oxocyclohexa-1,4-*di*en-1-yl)methyl carbonate (6) in chloroform-*d* at 400 MHz

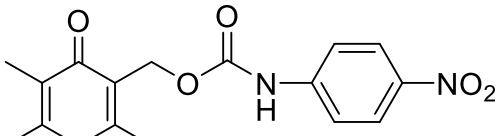

^{1}H NMR spectrum of HMBQ-Npc in chloroform-*d* at 400 MHz

^{1}H NMR spectrum of Nap reporter in chloroform-*d* at 400 MHz

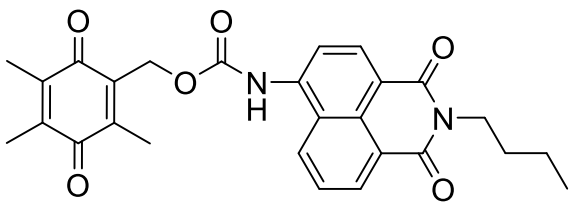

^{1}H NMR spectrum of HMBQ-Nap 1 in DMSO-d_6 at 400 MHz

^{1}H NMR spectrum of 4-(*N*-methylamino) benzyl alcohol (7) in methanol-d_4 at 400 MHz

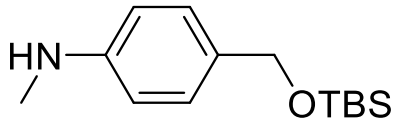

[1]H NMR spectrum of 4-[[(*tert*-butyldimethylsilanyl)oxy]methyl]-*N*-methylaniline (8) in chloroform-*d* at 400 MHz

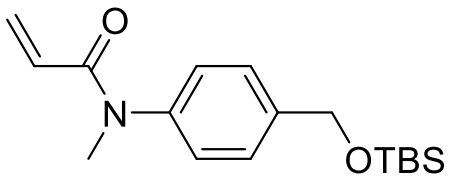

^{1}H NMR spectrum of *N*-(4-[[(*tert*-butyldimethylsilyl)oxy]methyl]phenyl)-*N*-methylprop-2-enamide (9) in chloroform-*d* at 400 MHz

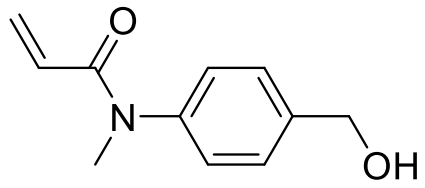

^{1}H NMR spectrum of *N*-[4-(hydroxymethyl)phenyl]-*N*-methylprop-2-enamide (10) in chloroform-*d* at 400 MHz

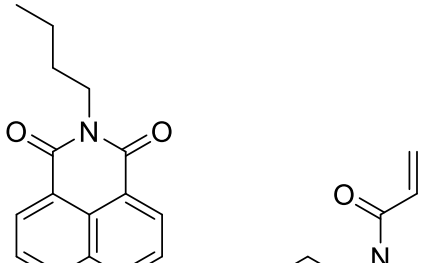

^{1}H NMR spectrum of Nap-Cys in chloroform-*d* at 400 MHz

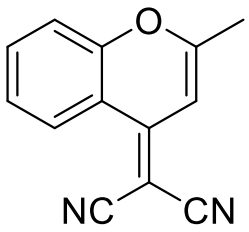

^{1}H NMR spectrum of 2-(2-methyl-4*H*-chromen-4-ylidene)malononitrile (13) in chloroform-*d* at 400 MHz

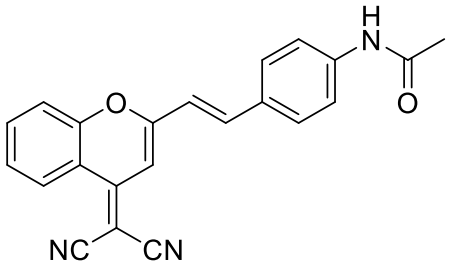

^{1}H NMR spectrum of DCM-acetamide (15 A) in DMSO-d_6 at 400 MHz

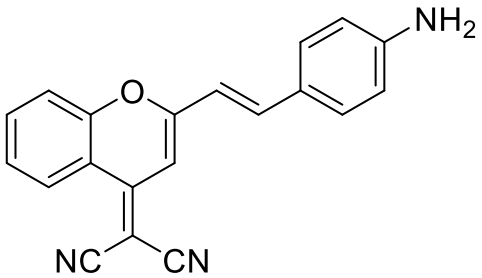

^{1}H NMR spectrum of DCM in DMSO-d_6 at 400 MHz

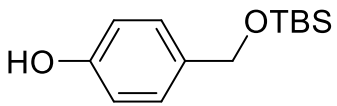

^{1}H NMR spectrum of 4-[[(*tert*-butyldimethylsilyl)oxy]methyl]phenol (14) in chloroform-*d* at 400 MHz

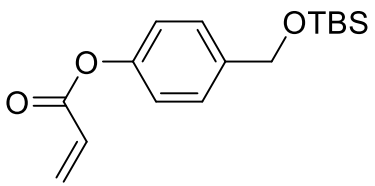

^{1}H NMR spectrum of 4-[*tert*-butyldimethlsilyl]oxy]methyl]phenyl prop-2-enoate (15) in chloroform-*d* at 400 MHz

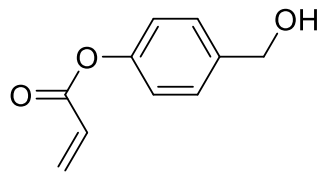

^{1}H NMR spectrum of 4-(hydroxymethyl)phenyl prop-2-enoate (16) in chloroform-*d* at 400 MHz

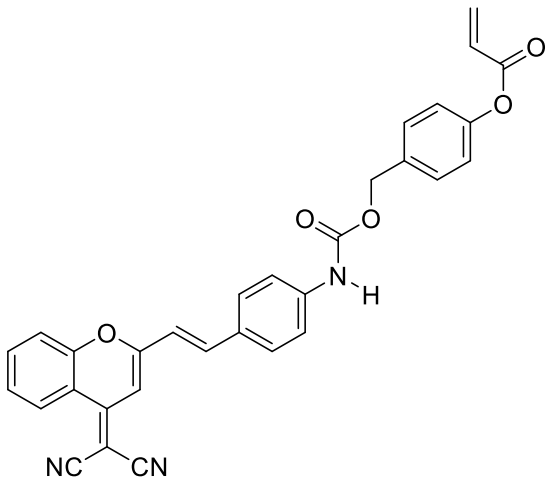

^{1}H NMR spectrum of DCM-Cys in chloroform-*d* at 400 MHz

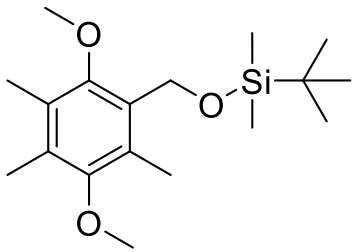

^{13}C NMR spectrum of 2,5-Dimethoxy-3,4,6-trimethylsilyl ether (4) in chloroform-*d* at 100 MHz

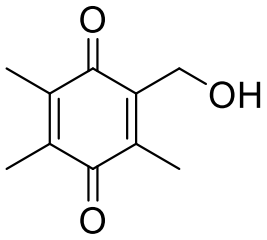

^{13}C NMR spectrum of 2-Hydroxymethyl-3,5,6-trimethyl-1,4-benzoquinone (5, HMBQ) in chloroform-*d* at 100 MHz

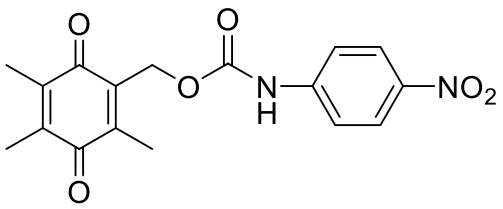

^{13}C NMR spectrum of HMBQ-Npc in chloroform-*d* at 100 MHz

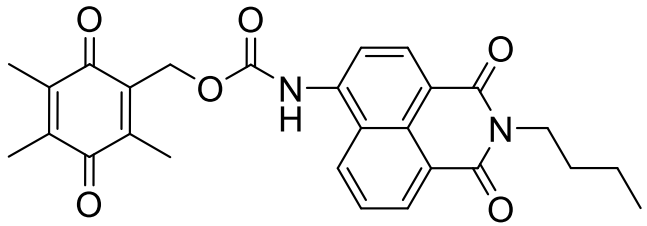

^{13}C NMR spectrum of HMBQ-Nap 1 in DMSO-d_6 at 100 MHz

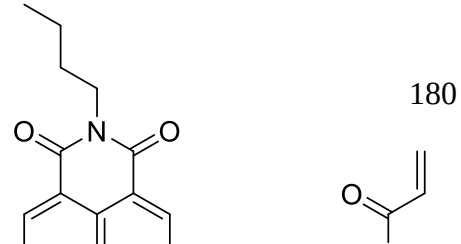

^{13}C NMR spectrum of Nap-Cys in chloroform-*d* at 100 MHz

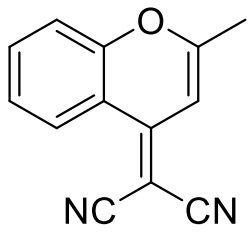

^{13}C NMR spectrum of 2-(2-methyl-4H-chromen-4-ylidene)malononitrile (13) in chloroform-*d* at 100 MHz

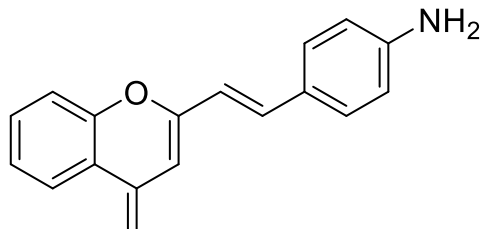

^{13}C NMR spectrum of DCM in DMSO-d_6 at 100 MHz

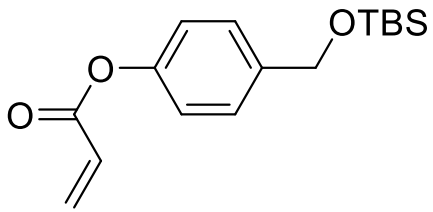

^{13}C NMR spectrum of 4-[*tert*-butyldimethlsilyl]oxy]methyl]phenyl prop-2-enoate (15) in chloroform-*d* at 100 MHz

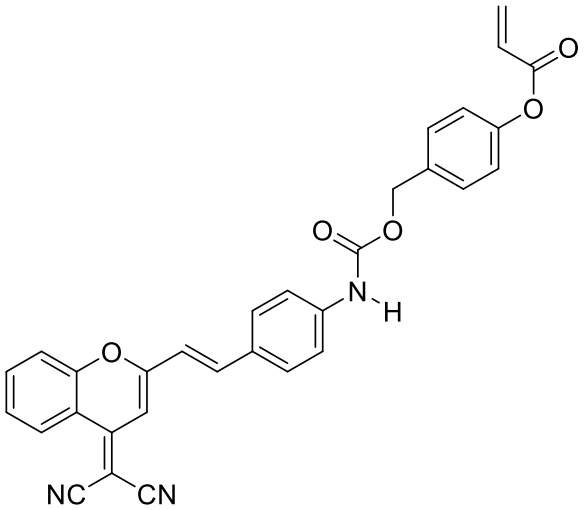

^{13}C NMR spectrum of DCM-Cys in chloroform-*d* at 100 MHz

APPENDIX B: LETTERS OF PERMISSION

F

VITA

Rasika Ranatunga Nawimanage was born and raised in Colombo, Sri Lanka. She had her primary and secondary education at Presbyterian Girls School and Anula Vidyalaya respectively. She entered the University of Colombo in year 2004 and graduated with Honors Degree in chemistry in 2008.

After serving for a few months as a teaching assistant at the Department of Chemistry, University of Colombo, she was accepted to Graduate School Doctoral program at Louisiana State University in the Department of Chemistry in 2009.

She joined the laboratory of Prof. Robin L. McCarley in January 2010 where she carried out her doctoral research work on small molecule-based fluorogenic probes for the detection of cellular thiols. She is a candidate for the degree of Doctor of Philosophy in the Spring Commencement 2015.